The Significance of Human Papillomavirus E6 PDZ Binding Motif on the Transformation and Immortalization of Human Neonatal Keratinocytes.

by

Kerry Ann Nichol Dust

A Thesis submitted to the Faculty of Graduate Studies of
The University of Manitoba
in partial fulfillment of the requirements of the degree of

Doctor of Philosophy

Department of Medical Microbiology and Infectious Diseases
Rady College of Medicine, Rady Faculty of Health Sciences
University of Manitoba
Winnipeg, Manitoba, Canada

Abstract

Of the over two hundred types of human papillomavirus (HPV), there is a small group, termed "high-risk HPV," which is highly associated with cervical, oral, and genital cancers. Although there are vaccines which can protect against some HPV types, there are only harsh surgical therapies for persistently infected individuals. Therefore, it is imperative to identify oncogenic molecular signatures which may uncover potential therapeutic targets or biomarkers to facilitate more efficient prognoses.

The E6 oncoproteins of the high-risk HPV types possess a PDZ protein binding motif on their carboxyl-termini that is absent from the E6 proteins in all the low-risk HPV types. Several *in vitro* studies have previously demonstrated that this E6 PDZ binding motif allows the virus to bind and degrade PDZ proteins including those of the tight junction and polarity complexes, suggesting that the PDZ binding motif promotes the loss of tight junctions and subsequent epithelial to mesenchymal transition of cells. The necessity of the PDZ binding motif for the transformation of keratinocytes by high-risk HPV is not confirmed but notably, PDZ proteins are targeted by other oncogenic viruses and are dysregulated in several epithelial cancers.

To study the significance of the HPV16 E6 PDZ binding motif on immortalization, transformation, and changes to the host proteome, human neonatal keratinocytes were transduced using lentiviruses encoding the full-length E6 gene in addition to the HPV16 E7 gene or a truncated E6 gene lacking the PDZ binding motif and the E7 gene. The transduced cells continued to replicate for over twice as long as the control cells regardless of whether the full-length or truncated E6 gene was expressed, indicating that the PDZ binding motif was not crucial for extending the proliferative capacity of keratinocytes. However, the E6 PDZ binding motif was associated with significantly lower levels of the tumor suppressor protein p53. Similarly, both cell lines expressing HPV oncoproteins had increased levels of hTERT expression, relative

to the control cells, but the E6 PDZ binding motif was associated with significantly higher levels of hTERT. The association between the PDZ binding motif, which is considered a marker of carcinogenic potential and enhanced carcinogenic phenotypes (p53 degradation and hTERT expression) is significant as it demonstrates that the carboxyl-termini of HPV16 E6 enhances transformation-associated traits. The enhanced p53 degradation and hTERT expression, however, were not sufficient to induce anchorage-independent growth in soft agar.

Quantitative tandem mass spectrometry measured the global protein dysregulation associated with the presence of the HPV16 E6 PDZ binding motif, and pathway and gene ontology enrichment analyses predicted that cellular organization and immune responses are influenced by this protein binding motif.

The HPV16 E6 PDZ binding motif was found to enhance the degradation or mislocalization of PDZ tight junction and polarity proteins in keratinocytes. The levels and or location of the PDZ proteins PAR3 and MAGI1 were found to be altered in cell junctions in the cells expressing HPV16 E6 and E7 compared to the cells lacking an E6 PDZ binding motif. ZO1 and JAM1 levels were not changed in association with the HPV16 E6 PDZ binding motif.

We additionally assessed the overall protein dysregulation induced by the HPV16 E6 and E7 oncoproteins in keratinocytes. These proteomic investigations catalogued several host proteins dysregulated by the expression of HPV16 oncoproteins. Pathway and gene ontology enrichment analyses indicate that the HPV16 E6 and E7 proteins modulate proteins involved in replication, DNA damage repair, and innate immune signaling pathways, as well as proteins associated with cell organization and differentiation. LAMP3 and midkine, potential biomarkers for the prognosis of persistent HPV, were upregulated in association with HPV16 E6+E7 expression.

Acknowledgements

Dr. Alberto Severini of the Public Health Agency of Canada was very kind to take me on as a graduate student. I appreciate that he was always so generous with his time and knowledge. I am so grateful that he allowed me to participate in this project with him.

I would like to thank the members of my advisory committee, Dr. Kevin Coombs and Dr. Brian Mark for their support, guidance and constructive feedback.

Dr. Michael Carpenter also guided me and assisted me greatly in the planning and execution of this project. He shared his extensive expertise for the construction of the lentiviruses used in this project and taught me how to use the proteomic analysis software.

I am extremely grateful for the support and encouragement of Dr. Paul Van Caeseele, Medical Director of Cadham Provincial Laboratory. Additionally, I would like to extend a huge thank you to my colleagues at Cadham Lab for supporting me while I worked on this project.

Thank you to the lab members and fellow students at the National Microbiology Lab Viral Exanthemata and STD section and Hepatitis C lab for sharing your knowledge, lab space and equipment with me. Getting to know all of you was my favorite part of this whole adventure!

Above all, I thank my family for encouraging me to complete this degree and for their unwavering love and encouragement.

Table of Contents

List of Tables

List of Figures

Copyright Permissions

Figure 1. Adapted with permission from Portland Press. Clinical Science Aug 10, 2017, 131 (17) 2201-2221; DOI: 10.1042/CS20160786

Figure 2. Adapted with permission Frontiers in Bioscience 16, 1069-1083, January 1, 2011; DOI: 10.2741/3736

Figure 3. Adapted with permission from Lentivector Expression Systems: Guide to Packaging and Transduction of Target Cells; www.systembio.com

Figure 4. Adapted with permission from Lentivector Expression Systems: Guide to Packaging and Transduction of Target Cells; www.systembio.com

List of Abbreviations

2DIGE	two-dimensional Difference In Gel Electrophoresis
AINX	Alpha internexin (INA)
AKT	protein kinase B
aPKC	atypical protein kinase
BAK	BCL2-antagnoist killer 1
BRCA1	Breast cancer type 1 susceptibility protein
BST2	Bone marrow stromal antigen 2
CaSki	HPV16 transformed cervical cell line
CBP	CRE-binding protein
Cdc42	Cell division control protein 42
CO6A2	Collagen alpha-2 VI chain
DAPI	4′,6-diamidino-2-phenylindole
DLG	Disks Large
DSC1	Desmocollin 1
DSC2	Desmocollin 2
DTT	Dithiothreitol
E1	HPV early protein 1
E2	HPV early protein 2
E4	HPV early protein 3
E5	HPV early protein 4
E6	HPV early protein 5
E7	HPV early protein 6
EBV	Epstein Barr Virus
EGF	Epidermal growth factor
ELAF	Elafin
EMT	epithelial to mesenchymal transition
ERBB2	Erb-B2 Receptor Tyrosine Kinase 2
FDR	False discovery rate
FIJI	Fiji is just image J software
GAG	GAG lentiviral protein
GAPDH	Glyceraldehyde 3-phosphate dehydrogenase
GFP	Green Fluoresent protein
GIPC	GAIP Interacting Protein carboxyl-terminus PDZ motif containing family, member 1
GO	Gene Ontology
GOPC	Golgi-associated PDZ and coiled-coil motif-containing protein
HCD	High energy collision dissociation
HEKn	Human neonatal keratinocytes
HeLa	HPV18 transformed cervical cell line
HEPES	4-(2-hydroxyethyl)-1-piperazineethanesulfonic acid
HERC	E3 ISG15-protein ligase
HPV	Human papillomavirus
HSPA2	Heat shock-related protein 2
hTERT	catalytic subunit of telomerase
HTLV	Human T cell leukemia virus

IAA	Iodoacetamide
IB44	HLA class I histocompatibility antigen IB-44 alpha chain
ICAM1	Intercellular cell adhesion molecule 1
IDT	Integrated DNA technologies
INVOL	Involucrin
IPA	Ingenuity Pathway analyses
IRF	Interferon Regulatory Factor
JAM	Junctional adhesion molecule
KSHV	Kaposi's Sarcoma-associated herpesvirus
K2C6B	keratin 6B
L1	HPV late protein 1, major capsid protein
L2	HPV late protein 2, minor capsid protein
LAMP3	Lysosome-associated membrane glycoprotein 3
LC/LC	Two-dimensional Liquid chromatography
LCR	Long control region
LIMMA	Linear models for microarray data in R
MAGI	Membrane-associated guanylate kinase WW and PDZ motif-containing protein
MAGUK	Membrane-associated guanylate kinases
MAPK/ERK	Mitogen-activated protein kinases / extracellular signal-regulated kinases
MARE1	Microtubule-associated protein RP/EB family member 1
MCM	Minichromosome maintenance complex
MDCK	Madin-Darby Canine Kidney cells
MK	Midkine
MOI	Multiplicity of infection
mRNA	Messenger Ribonucleic Acid
MS/MS	Tandem Mass Spectrometry
mTOR	mammalian Target of Rapamycin
MUPP1	Multi-PDZ motif protein 1
MX2	Interferon-induced GTP-binding protein MX2
NET1	Neuroepithelial Cell Transforming 1
NFH	neurofilament heavy
NFkB	Nuclear Factor kappa-light-chain-enhancer of activated B cells
NFL	neurofilament light
NFM	neurofilament medium
NHREF1	Na (+)/H (+) exchange regulatory cofactor NHE-RF1
NML	National Microbiology Lab, Winnipeg, MB.
ORF	open reading frame
PALS1	protein-associated with Lin seven
PAR3	partitioning-defective protein 3
PAR6	partitioning-defective protein 6
PATJ	PALS-1-associated tight junction protein
PBM	PDZ binding motif
PBS	Phosphate buffered saline
PCR	Polymerase Chain Reaction
PDZ	Post-synaptic 95, Disks Large, Zonula Occuludens type protein interaction region
PDZRN3	PDZ Domain Containing Ring Finger 3

PI3K/AKT	phosphatidylinositol-3 kinase / protein kinase B
pPACKH1-GAG	GAG lentiviral packaging plasmid encoding structural and polymerase genes
pPACKH1-REV	Rev lentiviral packaging plasmid encoding a regulatory gene required for replication
pVSV-G	Vesicular stomatitis virus packaging plasmid encoding a VSV envelope gene
PTEN	Phosphatase and tensin homolog
PTPN13	Protein Tyrosine Phosphatase Non-Receptor Type 13
PTPN3	Protein Tyrosine Phosphatase Non-Receptor Type 3
Revigo	Reduce visualize gene ontology
RPTN	repetin
RT-PCR	Reverse transcriptase Polymerase Chain Reaction
SARS	Severe acute respiratory syndrome virus
SDS	Sodium dodecyl sulfate
SH3	SRC Homology 3 Domain
SiHa	HPV16 transformed cervical cell line
SIRT1	Sirtuin-1
SP100	nuclear autoantigen Sp-100
SPRR3	Small proline rich protein 3
STRING	Search Tool for the Retrieval of Interacting Genes/Proteins
SUMO	Small ubiquitin-related modifier 3
SV40	Simian virus 40
TAX	HTLV Oncoprotein
TAZ	Transcriptional coactivator with PDZ-binding motif
TBS	Tris buffer
TBST	Tris buffer plus Tween 20
TGFβ	transforming growth factor-β
Tiam1	T-cell lymphoma invasion, and metastasis-inducing protein 1
TIPC	Tax interacting protein
TLR	Toll-like Receptor
TMT	Tandem Mass Tagged
TNF	Tissue Necrosis Factor
TOP2A	Topoisomerase 2-alpha
UCHL1	Ubiquitin carboxyl-terminal hydrolase L1
UEB	Urea Exchange buffer
YAP	Yes-associated protein 1
ZO	Zonula occludens

Chapter 1: Introduction

1.1 Human Papillomaviruses (HPV)

1.1.1 HPV Infection

HPV is one of the most common sexually transmitted infections in the world. It is estimated that approximately 80% of sexually active adults will acquire Human Papillomavirus (HPV) by 45 years of age (1). These viruses can cause a spectrum of disease ranging from benign warts and lesions to oral and anogenital cancers. Globally, 4.5% of new cancer cases each year are associated with HPV, although the rates of HPV-associated cancers are higher in the inhabitants of developing regions of the world such as Sub-Saharan Africa, which often lack cancer screening programs (2).

As of 2015, five genera (alpha, beta, gamma, mu, and nu), 49 species and 202 types of HPV have been recognized by the International Committee on Taxonomy of Viruses Papilloma study group (3). The nucleotide sequences of the capsid gene, L1, are highly conserved among genotypes and are used for HPV taxonomic classification (4). In addition to molecular classification, these viruses may be categorized based on their tissue tropism (mucosal or cutaneous epithelial cells) or by their oncogenic potential (high-risk or low-risk) (5). There are around forty types of HPV that infect the anogenital or oral mucosal epithelium, and among these, there are fourteen HPV types designated as being high-risk for cancer, with the *Alphapapillomavirus* HPV16 being the most prevalent high-risk type (3).

1.1.2 Prevention and Treatment

There are three prophylactic HPV vaccines. These vaccines target the low-risk HPV types 6 and 11, which cause *condyloma acuminata* (genital warts), as well as some of the high-risk HPV

types. The quadrivalent HPV vaccine targets HPV type 6, 11, 16, and 18, while the more recently available nonavalent vaccine additionally protects against HPV types 31, 33, 45, 52, and 58. The bivalent and quadrivalent vaccines have been available for over a decade and appear to be very effective based on declining rates of vaccine-associated HPV types being reported among vaccinated populations in several countries (6-8). Because its introduction was so recent, the impacts of the nonavalent vaccine on HPV rates in the general population are not yet determined.

Most HPV infections are cleared by the host within two years; however, infections that persist can lead to cancer (9-11). Smoking, sexual practices, other concurrent sexually transmitted infections, and exposure to hormonal birth control have been associated with increased duration of HPV infections (9-11). Early identification of precancerous lesions is key to preventing HPV-associated cancer. For example, regular cervical cancer screening, using cytological or molecular methods, is very effective for the early identification of persistent HPV-associated pre-cancerous lesions and early treatment can prevent most invasive cervical cancers. Unfortunately, current therapies are limited to harsh chemotherapies and or surgical approaches to remove the infected tissues. There is a need for therapeutics, and the development of these therapeutics can be fostered by increasing our knowledge of the proteomic dysregulation and cellular changes induced in the host cells by HPV oncoproteins.

1.1.3 HPV Life Cycle

Infection with HPV is a multi-step process which commences when the viruses access mitotically active basal keratinocytes through micro-abrasions in the upper epithelium. There, the L1 viral capsid protein interacts with an initial receptor on the cell surface or in the extracellular matrix. The host receptors required for HPV infection are not definitively identified but, Lamellin-

332, serine proteases, and heparan sulfate proteoglycans have all been proposed as initial receptors for HPV infection (12). Upon attachment to the host, the virus enters the cell via macro-pinocytosis (13). These interactions induce a conformational change in the capsid and allow L2 to interact with an unconfirmed receptor. Next, HPV moves from the endosome to the nucleus via the trans-Golgi network (14).

The viral life cycle is closely linked to the host cell's differentiation status. HPV infects undifferentiated basal cells and initially produces 50 to 100 genomic copies, which are maintained as episomes (14). As the infected cells begin to differentiate and migrate upward through the epidermal layers, the virus increases its replication, producing and packaging new viruses which are released as the host cells are sloughed off at the surface of the epidermis.

1.1.4 HPV Virology

HPV's small, 55nm diameter, capsid encloses an 8 kb circular double-stranded DNA genome. The genome can be divided into three regions: early, late, and long control region (LCR), separated by two polyadenylation sites (Figure 1) (14). The compact HPV genome yields polycistronic mRNA and relies on both constitutive and alternative splicing to express its proteins.

The LCR, is a highly variable region of the HPV genome. It does not code for any HPV genes but does contain the early promoter p97, part of the late promoter p670 sequence (p670 also requires sequences in E6 and E7 regions of the genome), as well as the late poly A signal. These cis-acting sequences regulate polyadenylation and the origin of replication.

The origin of replication is activated when bound by the E2 protein. The early proteins E1 and E2 stimulate and commandeer the host cell's DNA damage response proteins, initiating the viral replication process (15). The E1 protein acts as a DNA helicase, unwinding viral DNA during

replication and is recruited by E2 to the origin of replication to initiate DNA replication (16). Remarkably the E2 protein can also simultaneously bind to both the viral and host DNA during mitosis, ensuring that the viral genome is transferred to both daughter cells (17). Accumulation of E2 leads to the repression of E6 and E7 transcription as the E2 can bind to the p97 promoter and promote the switch from early to late gene expression stages of the HPV life cycle.

The expression of the early proteins relies on the p97 promoter. Despite encoding only seven open reading frames (E1, E2, E4, E5, E6, E7 and E8), there are close to twenty different mRNAs that can be expressed via alternative splicing of the polycistronic mRNA (18). In fact, the HPV16 E6 and E7 region can give rise to a full-length transcript which includes both E6 and E7 ORFs, as well as several shorter transcripts. The most common of the spliced transcripts is commonly referred to as E6*I and employs a splice site at nucleotide 226, eliminating nucleotides 227 to 408 (18, 19). The type of mRNA transcribed, either spliced or full-length, can vary depending upon the stage of the cell cycle. For example, the E6*I transcript is more abundant than full-length E6 at the G2/M phase of the cell cycle in HPV18 infected cells (20). One of the proposed functions of E6*I is to prevent E6-mediated degradation of p53, indicating an opposing role to the full-length E6 protein (21).

The E6 and E7 proteins are vital to the HPV life cycle and are among the first, and most abundant early proteins generated. Through the binding and degradation of the host tumor suppressor retinoblastoma family of proteins (pRb, p107, and p130), E7 prevents the repression of the E2F transcription factors, encouraging DNA replication (22). Meanwhile, the E6 protein binds the pro-apoptotic protein p53, interfering with the apoptotic processes initiated by the host in response to the aberrant transcription activity caused by E7 binding to pRb (23). Notably, the E6 protein from high-risk types of HPV can bind and promote proteasomal degradation of p53, but

low-risk E6 proteins only bind p53 (23). Additionally, HPV can interrupt apoptosis through the binding and degradation of the pro-apoptotic protein BAK (BCL2-antagonist killer 1) (24). BAK regulates caspases via the release of cytochrome C, and when bound by E6, it is unable to trigger apoptosis (25). HPV E6 and E7 proteins also influence several biological processes in addition to transcription and apoptotic signaling, including the inhibition of the interferon pathway, activation of telomerase, promotion of NFkB (nuclear factor kappa-light-chain-enhancer of activated B cells) signaling and disruption of keratinocyte differentiation and organization (26-31). Several of these interactions are restricted to the E6 and E7 proteins of the high-risk HPV types and will be discussed in more detail later.

The E8 ORF is not well described as it does not encode a protein, but instead can fuse to the terminus of the E2 protein in a spliced mRNA product. Although more study is required, there is some evidence that the E8^E2 product antagonizes viral replication promoted by the un-spliced E2 product to regulate viral genome copy numbers (32, 33).

Despite being categorized as an early protein, E5 protein production commences in the intermediate stages of infection. The E5 early proteins have several roles in the HPV life cycle. Purported to have an oncogenic role, E5 proteins can contribute to anti-apoptotic signaling by downregulating the FAS receptor, impairing Tumor necrosis factor ligand-mediated apoptosis (34). Also, E5 proteins have been shown to downregulate the levels of major histocompatibility complex class one proteins on the host cells, which helps avoid immune detection (35). And finally, the E5 proteins interact with epidermal growth factor receptors and are thought to play a role in genome amplification (36). Although the E5 protein may augment HPV-associated transformation, it is not essential for transformation (37-39).

The E4 protein is most abundant toward the final stages of HPV infection. The E4 gene products are derived from E1^E4 spliced mRNA (40). While not as well characterized as the other early proteins, E1^E4 proteins are known to enhance genome amplification and viral synthesis (40). E1^E4 can also bind with keratin and affect the cytokeratin organization, suggesting a role in viral release (40). The E1^E4 proteins can also affect viral maturation as recently demonstrated by Biryukov *et al.*, who found that mutations in E1^E4 proteins result in impaired capsid formation and stability (41).

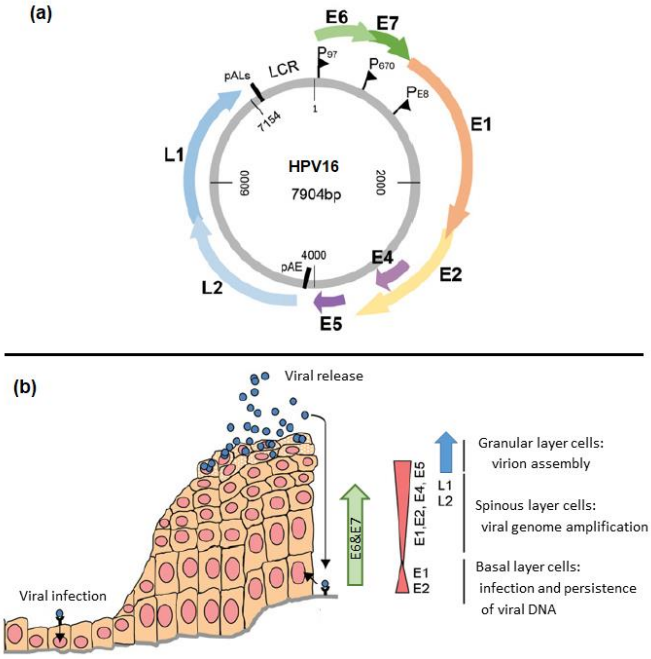

Figure 1. a) Schematic diagram of the HPV16 circular double-stranded DNA genome encoding two structural capsid proteins, L1 and L2 and six early proteins, E1, E2, E4, E5, E6, and E7. The E8 ORF does not encode a protein and is not labeled on the diagram, but it is located adjacent to the E8 promoter (PE8) between E7 and E1. b) The HPV lifecycle begins with the infection of basal keratinocytes. First, early proteins are expressed to establish and maintain the viral genome. As the infected basal cells differentiate and move upward through the layers of epithelial cells, levels of E6 and E7 proteins increase. Subsequently, the expression of the other early proteins is stimulated, and the viral genome is amplified. As the infected cells reach the upper layers of the epithelium, the structural proteins, L1 and L2 are required for viral assembly and release. Modified from Graham 2017 (42). Copyright Portland Press.

L1 and L2 encode the major and minor capsid proteins and the activation of a second promoter, P670, is required for their expression. The viral capsid is made up of 360 copies of the major capsid protein, L1 organized into 72 capsomeres. The number of copies of the minor capsid protein, L2, is undetermined because they are obscured by the L1 protein in cryo-electron microscopy images (43). The nucleotide sequence of the L1 ORF is highly conserved among genotypes and is therefore, used for molecular typing of HPV.

1.1.5 HPV-associated Cellular Transformation

Immortalization is a state of indefinite cell proliferation and is an essential first step in the development of cell transformation; a process which requires specific physiological changes including aberrant cell cycle progression, abrogation of apoptosis, compromised DNA damage repair mechanisms, and accumulation of genetic mutations (44). The expression of telomerase, an enzyme which prevents the natural shortening of telomeres that occurs with each cell division cycle, is regarded as one of the hallmarks of cell immortalization (29).

The discovery of HPV DNA in cervical tumors supported Dr. Harold Zur Hausen's hypothesis that these members of the *Papillomaviridae* family are the etiological agents of cervical cancer (45). Since then, a great deal of research has been dedicated to understanding the mechanisms of HPV tumorigenesis. Experimental studies have established that the high-risk HPV E6 and E7 oncoproteins are essential for efficient HPV-associated immortalization and transformation of keratinocytes (46). However, the mechanisms by which E6 and E7 induce these changes are not entirely understood. Co-expression of high-risk E6 and E7 may not be sufficient to induce the transformation of keratinocytes as the expression of other oncogenes or stimuli may be required. For example, the addition of an oncogene such as ras or fos, or the extensive passaging of

high-risk HPV immortalized cells have previously been used to prime cells for transformation *in vitro* (47-49).

HPV E6 and E7 stimulate changes associated with transformation. For example, the progression of the cell cycle is dysregulated by E7 binding to pRb, p107, and p130, alleviating the repression of E2F and S phase genes (50, 51). Both low-risk and high-risk E7 can bind pRb; however, the low-risk types bind pRb with less affinity than high-risk types (52). Similarly, the E6 proteins of high-risk and low-risk HPV can dysregulate apoptosis via their interactions with p53; however, the ability to promote the degradation of p53 is restricted to the high-risk E6 proteins (23, 24). Both high-risk and low-risk HPV E6 proteins can degrade BAK, but the high-risk E6 proteins are more effective (23, 24).

High-risk HPV oncoproteins also contribute to cell immortalization and transformation of their hosts by the induction of hTERT expression (29). hTERT is the catalytic subunit of telomerase, a protein that is typically repressed in primary cells but often overexpressed in cancers (53, 54). hTERT expression extends the replicative capacity of cells by preventing the erosion of telomeres that naturally occurs with each round of cell division (54, 55). The E6 proteins of all high-risk HPV types induce hTERT expression, but low-risk HPV types do not induce hTERT expression (56, 57). High-risk E7 proteins cannot independently induce hTERT, but they do augment high-risk HPV E6-induced hTERT expression (30).

The high-risk E6 proteins modulate immune responses and inflammation, encouraging the survival of the host cell and persistence of the virus. HPV16 E6 proteins interact with members of the toll-like receptor pathways and dysregulate Toll-like receptor 9 to modulate the host cell's immune response (58, 59). Additionally, high-risk HPV E6 proteins activate the NFkB cell survival

signaling pathway which may contribute to HPV-associated transformation (59). Increased NFkB signaling is associated with the initiation and progression of several types of cancer (60, 61).

As previously mentioned, the expression of the HPV E5 protein is associated with overexpression of epidermal growth factor receptors, immune evasion and the impairment of apoptotic signaling, however this protein is not essential for transformation (37-39). Additionally, the other early proteins: E1, E2, and E4, are not required for transformation; however, mutations to E1 or E2 genes may compromise the regulation of the E6/E7 promoter and have been associated with an increase in the immortalization of keratinocytes (62). E2 represses the transcription of the E6 and E7 genes. In cervical tumours E2 may be inactivated, either by mutations or via integration of the HPV DNA into the host genome, relieving the repression of the E6 and E7 transcription.

1.1.6 High-risk HPV E6 PDZ Binding Motif

There is a molecular structure that is unique to the high-risk types of HPV: a Class I PDZ binding motif, which is located at the carboxyl-terminus of the HPV E6 protein. A Class I PDZ binding motif is comprised of four amino acids in a specific arrangement: X[T/S]XΘ, where X is any amino acid, and Θ is any hydrophobic amino acid (63). A list of the carboxyl-termini of several high-risk HPV types, including their PDZ binding motifs, two low-risk mucosal HPV types and three cutaneous types of HPV are listed in Table 1.

Because the E6 PDZ binding motif is present in all known high-risk HPV types and is absent in all currently known low-risk HPV types, it is regarded as a marker of carcinogenic potential. The E6 PDZ binding motif allows the virus to interact with PDZ proteins and leads to their degradation (64, 65). While some studies have concluded that immortalization and or transformation of cells by high-risk HPV E6 is not possible without the PDZ binding motif,

others have had contradicting results (66-69). For example, immortalization of tonsil epithelial cells required the expression of a full-length HPV16 E6 with an intact PDZ binding motif, while human epithelial keratinocytes became immortalized in cells expressing E6 proteins with or without a PDZ binding motif (66-68, 70). Difference in experimental models used are likely responsible for the discrepant results.

Similarly, the high-risk HPV E6 PDZ binding motif may not be necessary, but appears to enhance the epithelial to mesenchymal transition (EMT) of cells expressing full-length HPV E6. EMT the process whereby a polarized epithelial cell changes into a mesenchymal cell phenotype with an enhanced migratory capacity, increased invasiveness, and elevated resistance to apoptosis (71). EMT is a key event which precedes the acquisition of malignant phenotypes by epithelial cancer cells and is marked by disrupted tight junctions, loss of cell to cell contact, loss of polarity and cytoskeletal changes (72). Watson *et al.* observed that the disruption of the actin cytoskeleton and adherens junctions were more pronounced in SV40-immortalized keratinocytes expressing wild type HPV18 E6 compared to those expressing HPV18 E6 lacking a PDZ binding motif (31).

The fact that several viruses have PDZ binding motifs supports the idea that the ability to interact with host PDZ proteins is advantageous for those viruses, yet the PDZ protein targets, their fates, and the downstream biological consequences of these interactions are not necessarily identical for the various viruses (73-77). For example, the carboxyl-terminus of the Adenovirus type 9 E4 protein is essential for the transformation of rat mammary cells, suggesting that the PDZ binding motif is a marker of carcinogenic potential (78). Binding of the PDZ protein DLG1 by Adenovirus type 9 E4-ORF1 promotes viral replication by activating c-Myc expression which can contribute to transformation (79). Additionally, the E4-ORF1 causes the mislocalization of

MAGI1, ZO2, PAT-J, and MUPP1 in cell culture (80, 81). Another viral oncoprotein with a PDZ binding motif is the HTLV1 TAX protein. TAX can dysregulate the tight junction protein, MAGI1, and mislocalize Scribble and DLG (82, 83). Additionally, the TAX protein's PDZ binding motif is essential for AKT activation (84).

Some non-oncogenic viruses such as rabies and avian influenza also encode proteins with PDZ binding motifs. The rabies virus relies on the survival of infected neurons for its virulence, and interactions with host PDZ proteins assist the rabies virus in preventing neuronal apoptosis (85). The avian influenza NS1 protein's ability to bind with PDZ proteins results in damage to the host cell's tight junctions and has been attributed to the higher level of virulence associated with avian influenza (86).

Table 1. The carboxyl-terminus of all currently known high-risk mucosal HPV types each has a PDZ binding motif (highlighted in red font). Notably, there are also similarities among the two or three amino acids upstream of the PDZ binding motif. The carboxyl-termini of a few low-risk mucosal and cutaneous HPV types are included in this table for comparison.

HPV16E6	CCRSSRTRRETQL	High-Risk mucosal types
HPV18E6	CCNRARQERLQRRRETQV	
HPV31E6	CWRRPRTETQV	
HPV33E6	CWRSRRRETAL	
HPV35E6	CWKPTRRETEV	
HPV39E6	CWTTKREDRRLARRETQV	
HPV45E6	CCDQARQERLRRRRETQV	
HPV52E6	CSECWRPRPVTQV	
HPV56E6	CWRQTSREPRESTV	
HPV58E6	CWRPRRRQTQV	
HPV59E6	CRTRARHLRQQRQARSETLV	
HPV68E6	CWTSKREDRRRTRQETQV	
HPV73E6	CWRPSATVV	
HPV82E6	CRTAARQRSETQV	
HPV6E6	CWTTCMEDMLP	Low-Risk mucosal types
HPV11E6	CWTTCMEDLLP	
HPV2E6	CGSSCTATDPASRTLH	Cutaneous types
HPV5E6	CKHFYHDW	
HPV7E6	CWKKCMEKGQRSETSC	

1.2 HPV16 E6 Interactions with PDZ proteins

Several of the high-risk HPV E6 PDZ protein binding partners have been catalogued, and include tight junction and polarity proteins (87-89). A higher number of binding partners is associated with increased carcinogenic potential, as HPV16 and HPV18 interact with the highest number of PDZ proteins (90). These two types of HPV are associated with over 70% of cervical cancers (91). Differences in PDZ binding among the HPV types are due to variations in the amino acid sequences of their PDZ binding motifs (92, 93). Phosphorylation at the phosphoreceptor site within the E6 PDZ binding motif has also been shown to affect the ability of the PDZ binding motif to interact with ligands (94, 95). Phosphorylation of the E6 PDZ binding motif may occur at different stages of the viral life cycle, suggesting that the E6-PDZ interactions are regulated at various stages of the viral life cycle (94, 95).

1.2.1 Tight Junction PDZ Proteins and High-risk HPV E6

Many of the PDZ proteins targeted by HPV E6 proteins are multifunctional scaffolding proteins associated with tight junctions and or polarity complexes, and these PDZ proteins regulate cellular organization, signaling, and proliferation; cellular properties which are notably disrupted during EMT (87, 89, 92, 96). Tight junctions are structures which regulate the paracellular diffusion of ions and solutes and are comprised of several proteins including the integral membrane proteins: claudins, occludins, tricellins, and junctional adhesion molecules (JAM). Additionally, tight junctions include the cytoplasmic plaque proteins: membrane-associated guanylate kinase with an inverted repeat (MAGI), multi-PDZ motif protein (MUPP1), and zonula occludens (ZO) (97). (Figure 2). Many of the tight junction PDZ proteins possess

multiple PDZ motifs as well as other protein interaction motifs that enable them to interact with a variety of proteins at once, including the proteins of the polarity complexes and signaling pathways (98, 99).

The three members of the ZO family of tight junction adaptor proteins, ZO1, ZO2, and ZO3, all possess multiple PDZ regions as well as SH3 and GUK protein interaction motifs, which allow simultaneous interactions with the tight junction transmembrane proteins and the actin cytoskeleton. In contact-inhibited cells ZO proteins complex with the transcription factor ZONAB (ZO1 associated nucleic acid binding proteins) and are located at tight junctions, however, in proliferating cells this complex moves to the nucleus where it promotes cell proliferation (100-102). Previous studies, using Madin-Darby canine kidney cells (MDCK), found that HPV16 E6 influences the distribution of ZO1 and ZO2, relocating the ZO proteins from the cell junctions to the nucleus, promoting cell proliferation in infected cells (65, 103).

MAGI1, MAGI2, and MAGI3 are part of the MAGUK family of tight junction PDZ proteins that can be bound by HPV16 E6 (104, 105). Normally, MAGI1 proteins bind to the PDZ binding motif of Phosphatase and tensin homolog (PTEN) enhancing its ability to regulate the phosphatidylinositol-3 kinase/protein kinase B (PI3K/AKT) signaling pathway and prevent cell proliferation (106, 107). However, targeting of MAGI1 by HPV E6 disrupts the MAGI-PTEN interaction, promotes AKT activation and ultimately, cell proliferation (99).

Another tight junction scaffolding protein is MUPP1, which has thirteen PDZ regions. Previous studies have determined that the dysregulation of MUPP1 leads to disruption of Rho A signaling and ultimately results in aberrant cell division, morphology, and migration (108). Interestingly, MUPP1 is targeted by Adenovirus type 9 E4-ORF1 and high-risk HPV E6 proteins in a PDZ binding motif-dependent manner (81). As a result of these interactions, Adenovirus

type 9 causes the mislocalization of MUPP1 from the membrane to the cytoplasm, while HPV E6 leads to the degradation of MUPP1 (81, 92).

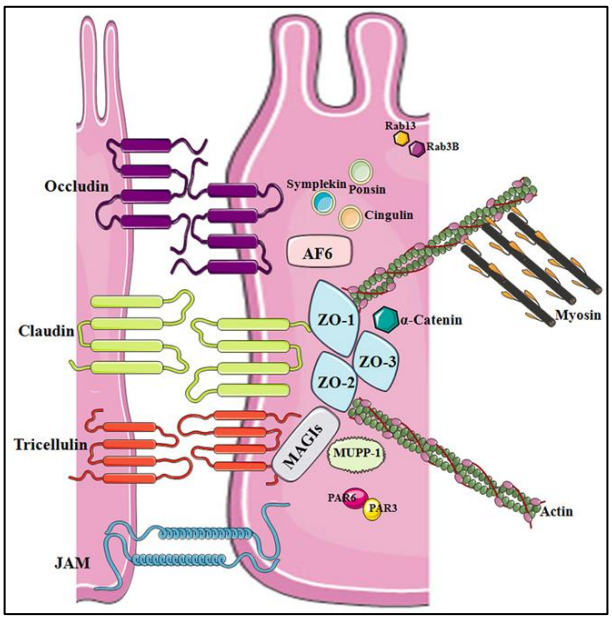

Figure 2. Proteins of the cellular tight junctions. Tight junctions include integral membrane proteins: claudins, occludins, tricellins, and junctional adhesion molecules (JAM) as well as cytoplasmic proteins: membrane-associated guanylate kinase with an inverted repeat (MAGI), multi-PDZ motif protein (MUPP1), and zonula occludens (ZO). Although categorized as part of the polarity complex, PAR3 and PAR6 are PDZ proteins that modulate cellular polarity and interact with junctional proteins. From Escudero-Esparza *et al*. (109). Copyright Frontiers in Bioscience.

1.2.2 Polarity Complex PDZ Proteins and High-risk HPV E6

There are three polarity complexes, Crumbs, PAR, and Scribble, which regulate the apical and basal orientation of epidermal cells. The polarity complexes are integral to epithelial cell organization and regulation of signaling pathways, and each of these includes one or more PDZ proteins. In addition to their roles in polarity, several of the PDZ proteins that belong to these complexes also serve as adaptor proteins in tight junctions and are involved in the regulation of signaling pathways required for cell growth and proliferation; (110-115). Although each

complex is spatially distinct from the others, these proteins participate in reciprocal antagonistic interactions with each other and with junctional-associated proteins to ensure the maintenance of apical-basal polarity.

The PAR complex includes the partitioning-defective proteins, PAR3 and PAR6, the cell division control protein 42 homolog (Cdc42) and the atypical protein kinase C (aPKC) (116, 117). As adaptor proteins, the PDZ proteins PAR3 and PAR6 are vital in tight junction formation and maintenance, interacting with signaling proteins such as Rho GTPases to ensure their spatial-temporal regulation (118).

PAR3 is a scaffolding protein that has several protein interaction motifs, including three PDZ regions. HPV18 E6 causes the mislocalization of PAR3 in a PDZ-dependent manner (119). The effects of HPV16 E6 on PAR3 levels or localization have yet to be determined.

PAR3 can influence the cellular location of some of its binding partners leading to the modulation of cell proliferation. For example, in sub-confluent MDCK cells, PAR3 binds the transcriptional regulator Yes-associated protein, (YAP), alters YAP's subcellular location, phosphorylation and promotes its activation (120). PAR3 expression can also alter cell proliferation via epidermal growth factor (EGF) signaling (121). The Rac exchange factor, T-cell lymphoma invasion, and metastasis-inducing protein 1 (Tiam1) are sequestered by PAR3, and the loss of either of Tiam1 or PAR3 leads to disruption of the tight junctions and cell proliferation in pancreatic cancer (121).

The other PDZ protein of the PAR complex is PAR6. Dysregulation of PAR6 has not been linked to HPV-associated cancers, although PAR6 proteins are known to be tumorigenic in epithelial cells and overexpression of PAR6 in cancer cells disrupts cell polarity and promotes cell proliferation enhancing capacity for migration and invasiveness (122, 123). Pathway and

gene ontology enrichment analyses of tissue microarrays have provided evidence that overexpression of PAR6 is associated with metastatic invasive breast cancers, and other studies have linked overexpression of PAR6 to aggressive lung, breast, and prostate cancers (124-126). In addition to the effects on polarity, overexpression of PAR6 can stimulate cell proliferation as it binds and activates aPKC (127). When in complex with both aPKC and Cdc42, overexpression of PAR6 can activate MAPK/ERK signaling (123). Aberrant aPKC activity has been associated with epithelial tumors, and inhibiting the phosphorylation of PAR6-aPKC can prevent migration and invasion of prostate cancer cells or breast cancer cells (124, 125).

The Scribble polarity complex regulates basolateral polarity, and it is comprised of three proteins: Scribble, Discs-Large (DLG) and Lethal giant larvae (LgL1). Both Scribble and DLG are MAGUK proteins and possess multiple interaction sites, including one or more PDZ regions as well as SH3 and GUK motifs. Like PDZ proteins found in the other polarity complexes, Scribble and DLG also influence signaling pathways in addition to regulating cell polarity (111, 112, 128). Both Scribble and DLG are targeted by high-risk HPV E6 for proteasomal degradation *in vitro* (129).

The expression of Scribble in cancers is tissue and context-dependent, and expression varies with tumor type and stage of cancer (130, 131). In cervical cancers, HPV E6 may be responsible for the mislocalization of Scribble. For example, a recent immunohistochemical evaluation found that Scribble was mislocalized in 100% of cervical tumors evaluated (132). Like MAGI1, Scribble also affects PI3K/AKT signaling through interactions with PTEN and when PTEN is bound to cytoplasmic Scribble, it is unable to prevent AKT activation; thus the loss of Scribble would be expected to promote cell proliferation (130). Scribble also regulates epidermal growth factor signaling through interactions with ERK. When Scribble is lost from

cells, ras/MAPK signaling is hyper-activated, indicating a tumor suppressive role for Scribble (133, 134). Like PAR3, Scribble can also influence the Hippo signaling pathway through interactions with YAP (Yes-associated protein 1) and TAZ (Transcriptional coactivator with PDZ-binding motif). In breast cancer cells, Scribble can bind TAZ and sequester it in the cell cortex to regulate the Hippo pathway (135).

The human DLG family of proteins (DLG1, DLG2, DLG3, DLG4, and DLG5) are part of the Scribble polarity complex. DLG proteins influence several signaling pathways, including PI3K/AKT, Rho GTPase and Wnt/ β-catenin (112, 128, 136-138). Like Scribble, DLG1 is also targeted by high-risk HPV, and loss of DLG1 has been reported in the late stages of several types of cancer (139).

The Crumbs complex is made up of three proteins: Crumbs, protein-associated with Lin seven (PALS1) and PALS-1-associated tight junction protein (PATJ). These proteins regulate the apical membrane of epithelial cells and directly interact with PAR complex proteins to establish and maintain polarity (121). Both PALS1 and PATJ have PDZ motifs.

Although altered levels of PALS1 and PATJ proteins have not been described in cancers, PATJ is known to be targeted by HPV18 E6 protein (140). Interestingly, MUPP1 is a homolog of the PATJ protein of the Crumbs polarity complex, and both PATJ and MUPP1 bind several of the same tight junction proteins (141). Functional studies suggest that the dysregulation of PATJ could lead to tumor proliferation. As part of normal cell function, PATJ binds the Tuberous sclerosis complex protein, a regulator of the mammalian target of rapamycin (mTOR) pathway. The mTOR protein belongs to the PI3K family and is involved in regulating cell metabolism, proliferation, and survival, and there is evidence that the loss of PATJ may facilitate tumor progression because its loss leads to an increase in mTOR signaling (142, 143).

There are several PDZ proteins targeted by high-risk HPV which are not part of the junctions or polarity complexes. These include Protein Tyrosine Phosphatase Non-Receptor Type 3 (PTPN3), Protein Tyrosine Phosphatase Non-Receptor Type 13 (PTPN13), Tax interacting protein (TIPC), Golgi-associated PDZ and coiled-coil motif-containing protein (GOPC), ubiquitin ligase PDZ Domain Containing Ring Finger 3 (PDZRN3), and the scaffolding protein Na^+/H^+ exchange regulatory factor 1 (NHREF1) (144-150).

PTPN3 and PTPN13 are non-receptor phosphatases which contain multiple PDZ motifs. PTPN13 mediates FAS-induced apoptosis and pro-apoptotic signaling, and its loss promotes carcinogenesis in HPV-associated cancers as well as non-small cell lung carcinoma, (68, 145). High-risk HPV E6 proteins interact with PTPN13 in a PDZ binding motif-dependent manner, and loss of PTPN13 in cells expressing ras or ERBB2 (Erb-B2 Receptor Tyrosine Kinase 2) enhances epidermal growth factor signaling (68). The binding and degradation of PTPN3 by high-risk HPV E6 also results in lower levels of this non-receptor phosphatase and enhances cell proliferation (146).

1.2.3 Other PDZ proteins targeted by high-risk E6

GIPC (GAIP Interacting Protein carboxyl-terminus PDZ motif containing family, member 1) is a trafficking protein that is dysregulated in several cancers (151). GIPC is bound and degraded by high-risk HPV E6 in a PDZ-dependent manner, and its loss results in the dysregulation of transforming growth factor-β (TGFβ) signaling and increased cell proliferation (148). Similarly, HPV E6 targets GOPC, a vesicle trafficking PDZ protein associated with cystic fibrosis, to the proteasome for degradation; however the biological consequences of this interaction in HPV infected cells are not clear (149, 152).

Another PDZ protein that is degraded by high-risk HPV in a PDZ binding motif-dependent manner is NHREF1 (Na(+)/H(+) exchange regulatory cofactor NHE-RF1), a scaffolding protein that regulates Wnt–β-catenin signaling in cervical cancer (150, 153). Dysregulation of NHREF1 by high-risk HPV enhances PI3K/AKT signaling in CaSki and SiHa cells (150).

Finally, high-risk HPV E6 proteins are known to target the ubiquitin ligase, PDZRN3 (PDZ Domain Containing Ring Finger 3) for degradation (154). PDZRN3 in known to inhibit cell differentiation, an event required for HPV replication, via Wnt–β-catenin or STAT5 signaling, (155, 156).

1.3 HPV Dysregulation of Host Gene Expression

Mass spectrometry is an excellent tool for the investigation of global proteomic changes associated with viral infections. Using mass spectrometry to investigate how the host's proteome is altered by HPV may identify biologically significant proteins or pathways targeted by the virus, revealing potential therapeutics for treating or diagnosing persistent HPV infections. Several proteomic studies investigating the effects of HPV have been published, but there is still a lot of work to be done.

Gel-based methods such as Two-dimensional Difference In Gel Electrophoresis mass spectrometry (2DIGE-MS) has been used by Bae *et al.* to investigate proteomic dysregulation in cervical lesions while Merkley *et al*. used 2DIGE-MS to investigate the specific effects of HPV16 E6 and E7 expression in keratinocytes (157, 158). One of the disadvantages of 2DIGE methods is the limited sensitivity, which affects the number of proteins that can be resolved.

Modern quantitative two dimensional Liquid Chromatography and Tandem Mass spectrometry (LC/LC-MS/MS) techniques coupled with sophisticated pathway analysis software promise greater sensitivity for an unparalleled exploration of the global dysregulation of the host proteome by HPV16 E6 and E7 proteins (159). LC/LC-MS/MS offers improved sensitivity over gel-based methods, and these types of studies have become more prevalent (160-162). iTRAQ quantitative LC-MS was used to compare the protein abundances in cervical cancers to that of healthy tissues (160). Pappa *et al.* used LC-MS/MS to investigate the proteomic changes in various HPV infected and non-infected transformed cell lines (161). While LC-MS/MS methods are more sensitive than the gel-based techniques, experiments using naturally infected tissues are not able to discern the proteomic changes specifically related to HPV16 E6 and E7 expression. Also, the use of heterogeneous populations of cells dampens the power of a study. Despite their limitations, these earlier studies are still valuable and provide some insight into how HPV manipulates host cells.

Trends uncovered by these early proteomic and expression investigations point to HPV16 E6's propensity for targeting immune signaling, cell cycle, transcription, cell junctions, and DNA repair signaling and provide an excellent starting point for further analyses (160-162). Experiments using quantitative LC/LC-MS/MS to investigate the global proteomic dysregulation in keratinocytes associated with the HPV16 E6 PDZ binding motif have not been previously undertaken.

1.4 Gaps in Knowledge

- The PDZ binding motif on the E6 carboxyl-terminus of all high-risk HPV types is considered a sign of carcinogenic potential; however, it is not clear whether this protein binding motif is essential for immortalization and transformation of HEKn.

- Several studies have shown that the HPV16 E6 PDZ binding motif can target PDZ proteins, leading to their degradation or mislocalization; this is expected to disrupt tight junctions and cell polarity and contribute to EMT. The effects of the HPV16 E6 PDZ binding motif on tight junction integrity in primary keratinocyte cultures have not been well documented.

- High-risk HPV can induce hTERT expression, but it is not clear whether the PDZ binding motif is required for this.

- The effects of the HPV16 E6 PDZ binding motif on the global dysregulation of the human neonatal keratinocyte proteome has not been documented.

- Although gene expression and proteomic changes associated with HPV infections in cervical tissues have been documented, the use of a sensitive, quantitative LC/LC-MS/MS to explore the global protein dysregulation in keratinocytes expressing HPV16 E6+E7 proteins will increase our understanding of their roles in HEKn cells.

- Prognostic biomarkers or potential therapeutic targets suitable for the management of persistent HPV infections are lacking.

1.5 Rationale and Hypothesis

The dysregulation of PDZ proteins by high-risk HPV E6 proteins can disrupt cell polarity, junctional proteins and impair cell signaling pathways; however, it remains to be determined whether the existence of the HPV16 E6 PDZ binding motif is essential for immortalization and transformation of HEKn. Some previous studies support the idea that the HPV E6 PDZ binding motif is essential for immortalization and transformation while others had contradicting results (31, 67, 68). Examining the changes incurred by the host proteome due to the HPV16 E6 PDZ binding motif may bring us closer to clarifying the biological significance of the PDZ binding motif regarding the immortalization and transformation of keratinocytes and may identify therapeutic candidates.

I hypothesize that the HPV16 E6 PDZ binding motif is required for the immortalization of human neonatal keratinocytes (HEKn). Furthermore, I predict that the HPV16 E6 PDZ binding motif will cause alterations to keratinocyte tight junctions.

The specific objectives for this study are:

1. Evaluate the influence of the HPV16 E6 PDZ binding motif on human neonatal foreskin keratinocytes' growth, immortalization, and transformation.
2. Assess the effects of HPV16 E6 PDZ binding motif on the host cell proteome, using quantitative mass spectrometry coupled with pathway and gene ontology enrichment analyses.
3. Visualize the repercussions of the PDZ binding motif on the level and localization of tight junction proteins using immunofluorescence microscopy.

Chapter 2: Materials and Methods

2.1 General Laboratory Techniques

2.1.1 Cell Culture

HEKn Cells

Human neonatal keratinocytes (HEKn) (Thermofisher Scientific, cat# C0015C) were grown in Epilife media (Life technologies cat# M-EPI-500-CA) supplemented with human keratinocyte growth serum (HKGS) (Life technologies cat# S-001_5). Cultures were maintained in 75 cm^2 flasks (Corning cat# 430725U) at 37°C in a humidified incubator with 5% CO_2. HEKn were split 1:10 when they reached 80 to 90% confluence. To split the HEKn cells, they were rinsed once with trypsin/EDTA solution (Thermofisher Scientific, cat# R-001-100) and then incubated with trypsin for 10 minutes at room temperature. Intermittent tapping on the side of the flasks was necessary for dislodging the cells. Once trypsinization was complete, trypsin neutralizer (Thermofisher Scientific, cat# R-002-100) was added to the cells. The cells were pipetted to a centrifuge tube and pelleted by centrifugation at 500 x g for 5 minutes. The supernatant was removed, and the pelleted cells were resuspended in Epilife media.

Cells were resuspended 1:1 in 0.4% trypan blue stain and viable cells were counted using the Countess automated cell counter (Thermofisher Scientific, cat#1754B) as per the manufacturer's instructions.

To measure the growth rate of HEKn, cells were plated into 150 cm^2 barcoded flasks to yield a 10% confluence. These flasks were loaded onto the CompacT SelecT cell culture robot (Tap Biosystems, Hertfordshire, UK). The robot changed the medium every 48 hours and

measured the cell confluence every four hours until 85% confluence was reached. Logistic growth rates for each cell line was calculated by the following equation:

$F(x) = L/ 1+e^{-k(x-x0)}$

F=cell density
L=maximum cell density
k=slope factor of the tangent at half point
X0= time at half confluence
X= time

293TN Cells

293TN cells (SBI, cat# LV900A-1), which are derived from HEK293 human embryonic kidney cell line and carry an SV40 large T antigen ORF, were used for lentivirus construction. $2.5x10^5$ 293TN cells were plated in a 10 cm dish producing a 70% monolayer the following day. 293TN were cultured in complete DMEM: Dulbecco's modified Eagle's medium (DMEM, Gibco, cat# 11995-065) supplemented with 10% fetal bovine serum (FBS) (Gibco, cat# 10082-147), 1X penicillin-streptomycin-glutamine (Gibco, cat#15070-063) and 1X MEM non-essential amino acids (Gibco, cat# 11140076). These cells were maintained in a humidified 37°C incubator with 5% CO_2.

SiHa Cells

SiHa cells (ATCC, cat# HTB35), were used as a positive control in the soft agar assays. These cells were grown in complete DMEM with 10% FBS. Cultures were maintained in 75 cm^2 flasks (Corning cat# 430725U) at 37°C in a humidified incubator with 5% CO_2. When these cells reached 80-90% confluence, they were split 1:10 to a new 75 cm^2 flask.

2.1.2 Molecular analyses

Polymerase chain reaction (PCR)

Polymerase chain reaction (PCR) was used to amplify the HPV16 E6 and E7 genes prior to cloning, as well as to verify the presence of E6 and E7 lentivectors in transduced cells. The primers and their sequences used for this study are listed in Table 2.

To verify transduction success, the transduced cells were washed twice with PBS and then harvested from the 75 cm^2 flask by scraping and aspirating into a 1.5 mL mini centrifuge tube. The cells were then homogenized by spinning them through a Qiashredder column for 2 minutes at 20,000 x g. DNA was extracted using Qiagen QIAamp Mini DNA kit (Qiagen, cat# 51304) as per the manufacturer's instructions.

For amplification of HPV16 E6 or E7, 5 µL of DNA from the transduced cells was added to 40 µL of Invitrogen Platinum PCR Supermix (Invitrogen, cat# 11306-016), 3 µM forward and 3 µM reverse primers, and 2 µL nuclease-free water. PCR was run on a Veriti thermal cycler (Thermofisher Scientific, cat# 4375786) using the following thermal profile: 2 minutes at 94°C, followed by 40 cycles of 30 seconds at 94°C, 30 seconds at 55°C and 30 seconds at 72°C and one final extension cycle at 72°C for 3 minutes. Amplified DNA was visualized using a Qiaxcel High Resolution DNA kit (Qiagen, cat# 929002) as per the manufacturer's instructions.

Reverse Transcription PCR (RT-PCR)

RT-PCR targeting HPV16 E6 and E7 mRNA was performed to verify gene expression. Cells in 75 cm^2 flasks were washed twice with PBS and then harvested by scraping and transferring them to a 1.5 mL mini centrifuge tube. The cells were homogenized by spinning

them through a Qiashredder column for 2 minutes at 20,000 x g. Next, RNA was extracted using Qiagen's RNeasy kit (Qiagen, cat# 74104) as per the manufacturer's instructions.

To verify the presence of E6 mRNA, a 359 bp region was amplified using HPV16 E6SM&NT_F and HPV16 E6_R primers. Similarly, E7 mRNA was identified using HPV16E7_F_bamK forward and HPV16E7_R _not reverse primers to yield a 326 bp amplicon. Each 20 µL RT-PCR reaction consisted of 5 µL of TaqMan® Fast Virus 1-Step Master Mix (TFV) (Thermofisher Scientific, cat# 4444432), 6 µL of water and 1.0 nM each of HPV16 E6SM&NT_F forward primer and HPV16 E6SM&NT_R reverse primer and 5 µL of RNA. RT-PCR used the following thermal profile: 50°C for 5 min, 95°C for 20 sec followed by 40 cycles of 95°C for 3 sec and 55°C for 30 seconds. Amplified products were visualized using a Qiaxcel High Resolution DNA kit (Qiagen, cat# 929002) as per the manufacturer's instructions.

Table 2. Primers used for PCR and RT-PCR reactions in this project were synthesized at either Integrated DNA technologies (IDT), (Skokie, Illinois, USA) or the National Microbiology Lab's DNA Core (NML), (Winnipeg, MB, Canada).

Target	**ID**	**5' to 3' Sequence**	**Source**
HPV16 E6 splice site, full-length	HPV16 E6SM-F	ATCGCAGGATCCATGCACCAAAAGAGAACTG	NML
	HPV16 E6SM-R	GTACTAGCGGCCGCTTACAGCTGGGTTTCTCTA CG	NML
HPV16 E6 splice site, truncated	HPV16 E6NT-F	ATCGCAGGATCCATGCACCAAAAGAGAACTG	NML
	HPV16 E6NT-R	GTACTAGCGGCCGCTTAACAAGACATACATCGACCGGT	NML
HPV16 E6	HPV16 E6SM&NT_F	CCATGCACCAAAAGAGAACTG	IDT
	HPV16 E6SM&NT_R	TCAAAAGCCACTGTGTCCTGA	IDT
HPV16 E7	HPV16E7_F_	ACATGGATCCGCCACCATGCATGGAG	NML
	HPV16E7_R_	ATCTGCGGCCGCTTATGGTTTCTGAGAACA	NML
Lentivector	CMV_lenti F	CACGCTGTTTTGACCTCCATAGA	NML
WPRE	WPRE 909F	CGCTGCTTTAATGCCTTTGTAT	NML
	WPRE 910R	GGGCCACAACTCCTCATAAA	NML
GAPDH	GAPDH_F	ACATCGCTCAGACACCATG	NML
	GAPDH_R	TGTAGTTGAGGTCAATGAAGGG	NML

2.1.3 Western Blotting

Twenty μg of protein was added to each well of a 4–20% polyacrylamide Mini-PROTEAN® TGX™ Precast Gel (Biorad, cat# 4561093EDU) and electrophoresed at 95 volts for 5 minutes followed by 200 volts for 30 minutes. For size reference, 5 μL of BenchMark™ Pre-stained Protein Ladder (Invitrogen, cat# 10748010) and 2 μL of Magic Mark™ XP standard (Invitrogen, cat# LC5602) were loaded on the gel. Proteins were transferred to a nitrocellulose membrane using the iBlot2 transfer stacks (Invitrogen, cat#IB23001) and Invitrogen's iBlot system. LI-COR TBS Odyssey buffer (LI-COR, cat#927-50100) was used to block the membranes for 1 hour at room temperature. The membranes were incubated at 4°C with primary antibodies overnight. The primary antibodies used for Western blotting are listed in Table 3. The next day the membranes were washed 3 times in 1xTBST (1L of 1xTBS (Tris-buffered saline) + 1 mL Tween 20) for 5 minutes before incubation with secondary antibodies for 1 hour at room temperature. Secondary antibodies included IRDye® 680LT Goat anti-Mouse IgG (LI-COR, cat# 925-68020) and IRDye 800LT Goat anti-Rabbit IgG (LI-COR, cat# 925-68021) at 1:20,000 in a 1:1 solution of LI-COR Odyssey buffer and TBST. Subsequently, three washes in TBST for 5 minutes were followed by two 5-minute washes in TBS. Finally, the membranes were blotted dry on a Kimwipe® tissue and imaged on the Odyssey FC imager (LI-COR Biosciences, Mandel Scientific, cat# LIC-9201-00). Estimation of protein quantification was performed using Image Studio Lite software (version 3.1) from LI-COR by comparing the pixel intensity measured for the protein of interest to the pixel intensity for the load control protein (GAPDH, cofilin, or vinculin).

Table 3. List of primary antibodies used for Western blot and or Immunofluorescence Microscopy.

Protein Target	Descrip-tion	Host	kDa	Western blot dilution	Immuno-fluorescence Microscopy dilution	Vendor	Cat #
AINX	monoclonal	Rabbit	55	1:1000	N/A	AbCam	Ab40758
BST2	monoclonal	Mouse	34	1:200	N/A	SantaCruz	sc-390719
cofilin	monoclonal	Rabbit	20	1:2000	N/A	AbCam	ab124979
ICAM1	monoclonal	Mouse	85-110	1:200	N/A	SantaCruz	sc-8439
GAPDH	monoclonal	Mouse	36	1 :1000	N/A	Invitrogen	MA5-15738
Involucrin	Polyclonal	Rabbit	68	1 :200	N/A	AbCam	ab53112
JAM1	polyclonal	Rabbit	32	N/A	1:100	AbCam	ab180821
MAGI1	Polyclonal	Rabbit	N/A	N/A	1:40	AbCam	ab222082
MARE1	monoclonal	Mouse	30-38	1:250	N/A	SantaCruz	sc-47704
NFL	monoclonal	Mouse	68	1:250	N/A	SantaCruz	sc71678
p53	monoclonal	Mouse	53	1 :250	N/A	SantaCruz	sc-125
PAR3	monoclonal	Rabbit	150	N/A	1:100	AbCam	ab40769
Telomerase	Polyclonal	Rabbit	120	1:500	N/A	AbCam	ab183105
Vinculin	Polyclonal	Rabbit	130	1:2000	N/A	AbCam	ab73412
ZO1	monoclonal	Mouse	225	N/A	1:200	Invitrogen	339188

2.2 Lentivirus Construction

2.2.1 HPV16 E6 and E7 Plasmid Cloning

To create a full-length HPV16 E6 gene of interest, our lab synthesized a HPV16 E6 gene (GenBank Accession# NC_001526.4) with a point mutation (nt 226 G→A) that abolishes the 5' splice site, resulting in a V to I amino acid substitution and promoting the transcription of the full-length E6 protein (19). The splice site was abolished using the QuickChange Lightning Site-Directed Mutagenesis kit as per the manufacturer's instructions (Agilent, cat# 210518). Similarly, a truncated version of the HPV16 E6 gene product including the splice site mutation but lacking the PDZ binding motif was created by omitting the last twelve amino acids from the carboxyl-terminus. We named this truncated E6 product: E6ΔPBM. Finally, the full-length

HPV16 E7 gene (GenBank Accession# NC_001526.4) was ligated into a pCDH-CMV-MCS-EF1-Hygro lentivector. The DNA sequences for the HPV genes in the lentiviruses created for this study are listed in Table 4.

The desired HPV16 E6, E6ΔPBM, or E7 DNA sequences were amplified by PCR using primers listed in Table 2. Each of the forward primers included a Kozak sequence and a BAMHI restriction site while each of the reverse primers included a NOTI restriction sequence. Kozak sequences are recommended to enhance translation from the correct initiation codon (163). The restriction sites were utilized to prepare the target sequence for ligation to the lentivector. A 50 µL PCR reaction including 40 µL of Invitrogen Platinum PCR Supermix (Invitrogen, cat# 11306-016), 3 µM of forward and 3 µM reverse primers, 2 µL nuclease-free water was run on a Veriti thermal cycler using the following thermal profile: 2 minutes at 94°C, followed by 40 cycles of 30 seconds at 94°C, 30 seconds at 55°C and 30 seconds at 72°C. There was a single final extension cycle at 72°C for 3 minutes.

The DNA amplicons, (HPV16 E6, HPV16 E6ΔPBM, or HPV16E7), were purified and verified by DNA sequencing at the NML DNA core facility. Next, the amplicons were cut with BamHI and NotI restriction enzymes and then ligated into pCDH-CMV-MCS-EF1-Neo (Systems Biosciences, cat# CD514B-1) lentivectors or pCDH-CMV-MCS-EF1-Hygro (Systems Biosciences, cat# CD515B-1) lentivectors using New England Biosystems' Quick Ligation kit (New England Biosystems cat# M2200S) following the manufacturer's instructions. The vector maps are shown in Figure 3. The ligation products were then cloned into One Shot TOP10 *Escherichia coli* cells (Invitrogen cat# C4040-03) following the manufacturer's protocol. The transformed cells were grown on a Luria-Bertani (LB) agar plate containing 50 µg/mL ampicillin at 37°C overnight. Colonies were selected, and the gene insertion was verified by PCR and

DNA sequencing at the NML DNA core facility. Once the gene inserts were verified, colonies were grown up in 500 mL flasks containing 200 mL of LB broth on a 37°C shaking incubator overnight. Qiagen Endo-free Plasmid Midi-prep kit (Qiagen cat#12145) was used to harvest and purify the plasmids following the manufacturer's instructions.

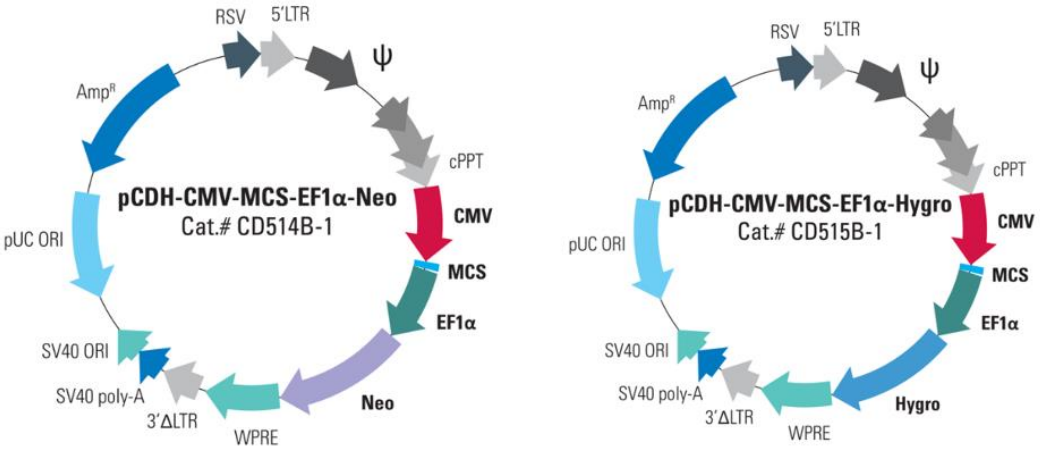

Figure 3. Vector maps of pCDH-CMV-MCS-EF1-Neo (Systems Biosciences, cat# CD514B-1) and pCDH-CMV-MCS-EF1-Hygro (Systems Biosciences, cat# CD515B-1) cloning and expression lentivectors used in this study. These lentivectors drive expression of the gene-of-interest from the CMV promoter, and expression of an antibiotic resistance marker (Neomycin or Hygromycin) from the EF1α promoter. In our study, the HPV16 E6 genes were inserted into the pCDH-CMV-MCS-EF1α-Neo lentivectors, and the E7 genes were inserted into the pCDH-CMV-MCS-EF1α-Hygro lentivector.

Table 4. List of the HPV lentiviruses made for this study including the associated DNA sequences of HPV genes and translated amino acid sequences. The underlined DNA sequence and amino acid sequences represent the portion of the E6 carboxyl-terminal tail missing in the truncated E6ΔPBM gene. The Four amino acids in red constitute the PDZ binding motif.

Name of Pseudo Lentivirus	**Description**	**Lenti-vector**	**DNA Sequence of HPV gene in plasmid**	**Amino acid sequence of HPV protein**
HPV16 E6	Full-length HPV16 E6	pCDH-CMV-MCS-EF1-Neo	**pHPV16 E6**: ATGCACCAAAAGAGAACTGCAATGTTTCAGGACCCACAGGAGCGACCCAG AAAGTTACCACAGTTATGCACAGAGCTGCAAACAACTATACATGATATAAT ATTAGAATGTGTGTACTGCAAGCAACAGTTACTGCGACGTGAGATATATGA CTTTGCTTTTCGGGATTTATGCATAGTATATAGAGATGGGAATCCATATGCT GTATGTGATAAATGTTTAAAGTTTTATTCTAAAATTAGTGAGTATAGACATT ATTGTTATAGTTTGTATGGAACAACATTAGAACAGCAATACAACAAACCGT TGTGTGATTTGTTAATTAGGTGTATTAACTGTCAAAAGCCACTGTGTCCTGA AGAAAAGCAAAGACATCTGGACAAAAAGCAAAGATTCCATAATATAAGGG GTCGGTGGACCGGTCGATGTATGTCTTGTTGCAGATCATCAAGAACACGTA GAGAAACCCAGCTGTAA	MHQKRTAMFQDPQERPRKLPQL CTELQTTIHDIILECVYCKQQLLR REIYDFAFRDLCIVYRDGNPYAV CDKCLKFYSKISEYRHYCYSLYG TTLEQQYNKPLCDLLIRCINCQK PLCPEEKQRHLDKKQRFHNIRGR WTGRCMSCCRSSRTRRETQL
HPV16 E6ΔPBM	Truncated HPV16 E6 lacking 7 amino acids at the carboxyl-terminus	pCDH-CMV-MCS-EF1-Neo	**pHPV16 E6ΔPBM:** ATGCACCAAAAGAGAACTGCAATGTTTCAGGACCCACAGGAGCGACCCAG AAAGTTACCACAGTTATGCACAGAGCTGCAAACAACTATACATGATATAAT ATTAGAATGTGTGTACTGCAAGCAACAGTTACTGCGACGTGAGATATATGA CTTTGCTTTTCGGGATTTATGCATAGTATATAGAGATGGGAATCCATATGCT GTATGTGATAAATGTTTAAAGTTTTATTCTAAAATTAGTGAGTATAGACATT ATTGTTATAGTTTGTATGGAACAACATTAGAACAGCAATACAACAAACCGT TGTGTGATTTGTTAATTAGGTGTATTAACTGTCAAAAGCCACTGTGTCCTGA AGAAAAGCAAAGACATCTGGACAAAAAGCAAAGATTCCATAATATAAGGG GTCGGTGGACCGGTCGATGTATGTCTTGTTAA	MHQKRTAMFQDPQERPRKLPQL CTELQTTIHDIILECVYCKQQLLR REIYDFAFRDLCIVYRDGNPYAV CDKCLKFYSKISEYRHYCYSLYG TTLEQQYNKPLCDLLIRCINCQK PLCPEEKQRHLDKKQRFHNIRGR WTGRCMSC
HPV16E7	HPV16 E7	pCDH-CMV-MCS-EF1-Hygro	**pHPV16E7:** ATGCATGGAGATACACCTACATTGCATGAATATATGTTAGATTTGCAACCA GAGACAACTGATCTCTACTGTTATGAGCAATTAAATGACAGCTCAGAGGAG GAGGATGAAATAGATGGTCCAGCTGGACAAGCAGAACCGGACAGAGCCCA TTACAATATTGTAACCTTTTGTTGCAAGTGTGACTCTACGCTTCGGTTGTGC GTACAAAGCACACACGTAGACATTCGTACTTTGGAAGACCTGTTAATGGGC ACACTAGGAATTGTGTGCCCCATCTGTTCTCAGAAACCATAA	MHGDTPTLHEYMLDLQPETTDL YCYEQLNDSSEEEDEIDGPAGQA EPDRAHYNIVTFCCKCDSTLRLC VQSTHVDIRTLEDLLMGTLGIVC PICSQKP

2.2.2 Lentivirus production

The lentiviral expression vectors from Systems Biosciences used in this project (pCDH-CMV-MCS-EF1α-Neo or pCDH-CMV-MCS-EF1α-Hygro) are part of a third generation, self-inactivating recombinant lentiviral system. This system was chosen for its enhanced safety features. The lentiviral particles produced by this system can infect target cells and express effector or reporter molecules but cannot replicate within target cells due to a lack of the viral structural genes. Additionally, a deletion in the LTR ensures that it is self-inactivating upon transduction. The genetic elements for transcription and packaging of an RNA copy of the expression construct into recombinant viral particles (pPACKH1-GAG, pPACKH1-REV, pVSV-G) are delivered as individual plasmids which ensures that the lentiviral particles are replication incompetent and only contain the expression construct of interest (i.e. E6 or E7) (Figure 4). The pPACKH1-GAG plasmid contains the structural (*gag*), and replication (*pol*) genes required to produce the lentivirus as well as the viral *env* gene, which encodes the envelope protein. pPACKH1-REV is a plasmid that contains the regulatory protein rev, required for replication. Finally, the pVSV-G plasmid yields the envelope glycoprotein of vesicular stomatitis virus from the CMV promoter and important to mediate entry of the lentiviral particles (i.e. E6 or E7 lentiviruses) into the host cells.

293TN cells were used for lentiviral production. These cells were grown to 70-80% confluence in DMEM as described above. For transfection of 293TN cells, 1 mL DMEM, 1.7 µg of the E6 or E7 lentivirus expression vector plasmids (described in Table 4) and 2.8 µg of each of pPACKH1-GAG, pPACKH1-REV, pVSV-G lentiviral plasmids, (donated by Dr. Michael Carpenter's lab, NML), were combined with 30 µL of Roche Xtreme gene HP (Roche cat# 06 366 236 001). This mixture was incubated for 15 minutes at room temperature, and then

it was added dropwise to 293TN cells in freshly changed media. The transfected cells were returned to the incubator for 48 hours. Lentiviruses were harvested from the supernatant. All the tissue culture fluid (approximately 10 mL) was added to a 15 mL tube containing 2.5 mL PEG-IT (System Biosciences cat# LV810A-1), a commercial polyethylene glycol solution. The PEG-IT and virus mixture was pipetted gently to mix and then stored at 4°C overnight to concentrate the virus. The next day the PEG-IT and virus mixture was centrifuged at 1500xg for 40 minutes at 4°C to pellet the virus. The supernatant was removed, and the virus pellet was resuspended in 1 mL DMEM with 2% FBS.

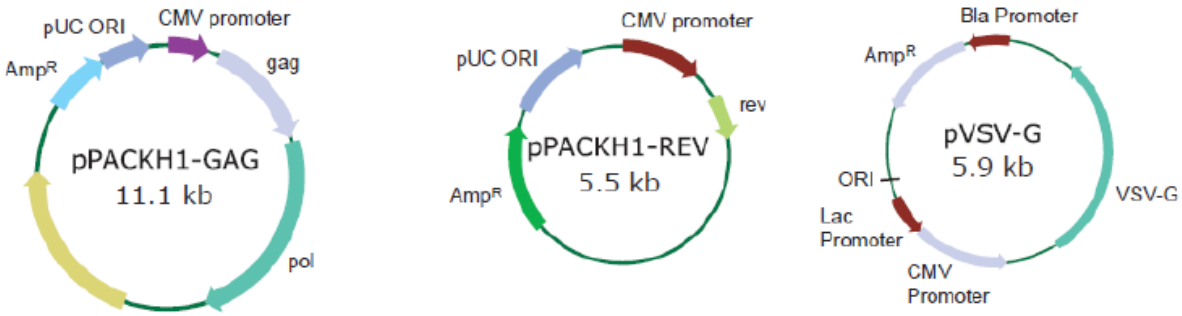

Figure 4. Packaging plasmids used for lentiviral construction. The pPACKH1-GAG plasmid encodes gag, pol, and env genes required to produce the lentiviruses. The pPACKH1-REV is a plasmid that contains the regulatory protein rev and is necessary for replication. The pVSV-G plasmid expresses the envelope glycoprotein of vesicular stomatitis virus (VSV-G). Figure is modified from Lentivector Expression Systems: Guide to Packaging and Transduction of Target Cells; systembio.com.

The lentiviruses were titrated using a quantitative PCR (qPCR) test to measure the copy number of lentivirus specific Woodchuck Hepatitis Virus Post-Transcriptional Regulatory Element (WPRE) following infections of HEKn cells. The WPRE is incorporated in the lentivector to enhance the stability and translation of lentivector driven transcripts. The WPRE

can also be used for lentiviral titration as it is a lentiviral element that is integrated into the genome of transduced cells. WPRE DNA was normalized to GAPDH DNA.

First, DNA was extracted from HEKn cells infected with lentivirus at 48 hours post-infection using the Qiagen QIAamp DNA mini kit (Qiagen, cat# 51304) as per the manufacturer's instructions. Next, the number of functional lentiviral particles was measured by targeting the WPRE by PCR (164). In each 20 µL reaction, 0.4 µM of each primer, WPRE 909F, and WPRE 910R, was added to 10 µL of SYBR green master mix (Biotool.com, cat# B21203). Using the Roche Lightcycler 480 system the reactions were subjected to one cycle at 50°C for 2 minutes, one cycle at 95°C for 2 minutes, 40 cycles at 95°C for 3 seconds and then 60°C for 30 seconds. GAPDH DNA was amplified for normalization using 0.4 µM of each primer (GAPDH_F and GAPDH_R), and 10 µL of SYBR green was used in each 20 µL reaction and employed identical thermal conditions as described above. The titer of each sample is then determined by calculating the amount of WPRE element normalized to GAPDH DNA against a standard curve. The standard curve was generated from GAPDH DNA quantified standards created at the NML.

2.3 HEKn Transduction

HEKn cells at 25 population doublings were seeded into 24 well culture plates (Corning cat#3524) at 25000 cells per well. Two days later HPV16 E6, HPV16 E6ΔPBM, and E7 lentiviruses were used to transduce the HEKn at an MOI of one. HEKn cells transduced with empty lentivectors were used as controls. HEKn cells transduced with a lentivirus expressing green fluorescent protein (GFP) were used as transduction and selection controls. The lentiviruses adsorbed on the cells for 4 hours, and then 800 µL of Epilife media was added to

each well. Transduced cells were incubated at 37°C in 5% CO_2 for 48 hours. After 48 hours, the success of the transduction was assessed by visualization of fluorescence in the GFP control. Antibiotic selection was initiated at the first media change; 48 hours post-transduction. 15 µg/µL Gibco Geneticin G418 Sulfate (Thermofisher Scientific, cat # 10131035) and 15 µg/µL Hygromycin B (Thermofisher Scientific, cat # 10687010) were used for 5 days, then each antibiotic was reduced to 5 µg/µL for 10 days to ensure the elimination of cells not containing a lentivirus insertion.

2.4 Soft Agar Assays

Cells from each experimental cell line were plated in a soft agar suspension to determine if they had transformed and could grow in an anchorage-independent manner. The cells were trypsinized, counted and added to 0.5% agar (BD Agar cat# 214220). Each cell suspension was pipetted on top of a 1% agar base in a well, in a six-well culture plate (Corning cat# C3516) and incubated at 37°C in a humidified incubator at 5% CO_2. Colony formation was assessed visually for three weeks or until colonies formed. 500 µL of Epilife medium was added on top of the soft agar every seven days to replenish nutrients and moisture. Soft agar analysis was performed using cells transduced with HPV16 E6 and E7 lentiviruses as well as cells transduced with HPV16 E6ΔPBM and E7 lentiviruses, at 50 and 95 population doublings. HPV positive SiHa cells were used as a positive control and LV-HEKn cells (<45 population doublings) were used as negative controls.

2.5 Quantitative Mass Spectrometry LC/LC-MS/MS

2.5.1 Peptide Preparation

Transduced cells at 45 population doublings were grown to confluence in 75 cm^2 flasks. Epilife medium was removed, and the cells were washed twice with ice-cold PBS. The cells were then manually scraped from the flask and collected in 2% SDS (sodium dodecyl sulfate) in phosphate-buffered saline (PBS). Cells in 2% SDS were heated for 5 minutes at 99°C and then homogenized using Qiashredder column as per the manufacturer's instructions (Qiagen cat#79656). Proteins were quantified using Pierce Bicinchoninic acid (BCA) kit as per the manufacturer's instructions (Thermofisher Scientific, cat #23227). The Pierce BCA kit is based on the chelation of copper ions in an alkaline solution with proteins followed by a colorimetric change due to their reaction with bicinchoninic acid. This colorimetric change was measured at an absorbance of 562 nm. The level of absorbance for the samples were measured against a bovine serum albumin protein standard dilution series.

100 µg of proteins were diluted 10 times with 1M DTT (Dithiothreitol) (Sigma cat# DO632) and heated for 5 minutes at 99°C to reduce disulfide bonds. Once cooled to room temperature, the sample was incubated with an equal volume of Urea exchange Buffer (UEB) at room temperature for 10 minutes. UEB= 8M Urea (GE Healthcare cat#17-1319-01) in 50 mM HEPES buffer (Thermofisher Scientific, cat # 5630106). The protein/DTT/UEB mixture was then passed through a Pall Omega Nanosep 10K cartridge filter (Thermofisher Scientific, cat# NC0361262) by centrifugation at 10000 x g for 10 minutes and flow through was discarded. The filter was washed with 100 µL UEB three times. 100 µL of 50 mM Iodoacetamide (IAA) in UEB was added to alkylate the proteins. Samples were incubated in the dark for 20 minutes at room temperature followed by centrifugation 10000 x g for 10 minutes. The filter was washed with 100 µL UEB three times. 150 µL of 50 mM HEPES was passed through the filter by centrifugation at 10000 x g for 10 minutes. To degrade any DNA or RNA, 50 µL of Benzonase

(Sigma cat# E1014) was added to the filter and incubated with shaking at 600 rpm for 2 minutes at room temperature followed by 30 minutes of incubation without shaking at room temperature. The filter was washed 3 times with 100 µL 50 mM HEPES followed by centrifugation at 10000 x g for 10 minutes. 1.5 µg of Trypsin in 50 mM HEPES was added to the filter and incubated overnight at 37°C in a humidified chamber. The next day 50 µL of 50 mM HEPES was added to the filter, and it was shaken at 600 rpm for 2 minutes at room temperature. Next, the filter was inverted into a low bind 1.5 mL tube and centrifuged 10000 x g for 3 minutes to collect the peptides from the filter into the 1.5 mL tube.

Peptides were labeled with tandem mass tagged (TMT) six-plex Isobaric Label Reagent Set (Thermofisher Scientific cat# 90061) as per the manufacturer's protocol. These low mass isobaric reporter ions are used to report relative protein abundances during peptide fragmentation. Briefly, TMT labels dissolved in ethanol were added to the peptide tube and incubated at room temperature overnight. The next day 8 µL of hydroxylamine quenching reagent was added to the peptide tube and incubated for 30 minutes at room temperature. The samples were then lyophilized in a Speed Vac. Before use, the dehydrated peptides were reconstituted in 40 µL of MS-grade water.

2.5.2 Quantitative LC/LC-MS/MS

Samples were fractionated into 12 fractions by high-pH C18 reversed-phase liquid chromatography using an Agilent 1200 micro-flow liquid chromatography system (Agilent Technologies, Santa Clara, CA). Each fraction was concentrated to near-dryness using vacuum centrifugation, resuspended in 80 µL of buffer A (2% acetonitrile, 0.1% formic acid) and loaded (2 µL) onto a on a low-pH C18 reversed-phase Easy-Spray column (Thermofisher Scientific, 50

cm x 100 µm) using an Easy nLC 1000 coupled to a Q-Exactive Plus mass spectrometer (Thermofisher Scientific). Peptides were eluted off the column using linear gradients from 5% to 32% buffer B (98% acetonitrile, 0.1% formic acid) over 120 min at a constant flow of 200 nL/min. Total LC/LC-MS/MS run-time per fraction was 160 minutes.

Two TMT runs were performed on a total of four biological replicates for each cell line: HPV16 E6+E7, HPV16 E6ΔPBM+E7, and LV-HEKn control cells (HEKn transduced with empty lentivectors. The first LC/LC-MS/MS run included biological replicates 1 and 2 of HPV16 E6+E7, HPV16 E6ΔPBM+E7, and LV-HEKn. The second LC/LC-MS/MS run included the biological replicates 3 and 4 of each of these cell lines. Isobaric tags were shuffled between replicate runs for each of the three transduced lines to avoid bias.

2.5.3 Data Analyses

A data-dependent acquisition method was used; dynamically choosing the top 15 abundant precursor ions for fragmentation by high energy collision dissociation (HCD). The peptide sequence data were searched against a database containing the SwissProt database (2015_04) restricted to Human (20,216 entries) and HPV (4 entries) using Mascot v2.5 (Matrix Science). Mascot search results were imported into Scaffold Q+ v4.4 (Proteome Software) and filtered using 0.1% FDR (false discovery rate) for peptides, 1.0% FDR for proteins, and at least two peptides per protein. Median normalization, inter-run, intra-run, and peptide spectrum normalization was generated using Scaffold Q+ v4.4 software.

Further data processing included removing proteins that were not detected in any of the TMT experiments as well as any proteins that were detected in one TMT run but not the other. Principal component analyses were used for data exploration of log2 protein intensity while a

heat map was generated to evaluate hierarchical clustering (165). Statistical analyses for differential protein abundance were conducted using LIMMA (Linear Models for Microarray Data in R) on log2 normalized protein intensity generated by Scaffold (166). P-values were adjusted by the Benjamini-Hochberg (BH) method to correct for multiple hypothesis testing (167). The threshold for significance was set at an adjusted p-value of ≤ 0.05.

2.5.4 Pathway Analyses

We employed Qiagen's Ingenuity Pathway analyses (IPA) (QIAGEN Inc., https://www.qiagenbioinformatics.com/products/ingenuitypathway-analysis), STRING v10.5 (Search Tool for the Retrieval of Interacting Genes/Proteins) to identify the protein networks and biological functions associated with the dysregulated proteins in our data (168, 169). Using both IPA and STRING allowed us to increase the robustness of our analyses.

The Core Analysis program in IPA uses Qiagen's proprietary algorithms to identify relationships, biological functions, and pathways relevant to our dataset based on the information in Qiagen's manually curated Ingenuity Knowledge Base. The Core Analysis predicted which canonical pathways were associated with our data and which protein networks and associated biological effects might be altered in our cells.

The STRING software is open-access and is part of the Swiss Institute of Bioinformatics. STRING's algorithms use manually curated databases, Kyoto Encyclopedia of Genes and Genomes (KEGG) pathway maps, as well as automated text mining of Med-line abstracts to uncover statistical and/or semantic links between proteins that are predicted to contribute to a common biological outcome (169). STRING can be useful for visualizing clusters of protein-protein networks.

Revigo (Reduce visualize gene ontology) software simplifies large numbers of biological gene ontology (GO) terms derived by the STRING analysis, and graphically represents the related biological trends affected by the dysregulated proteins.

First, to assess the enriched GO terms, protein networks and dysregulated canonical pathways associated with the PDZ binding motif we uploaded the list of 142 proteins found to be significantly differentially expressed (adjusted p-value ≤0.05) by ±1.3-fold (0.4 log2) change between cells transduced with HPV16 E6+E7 and cells transduced with HPV16 E6ΔPBM +E7 into IPA and STRING software. We chose to use a ±1.3-fold (0.4 log2) change cut off for our analyses because increasing the stringency of our analyses to ±1.5-fold (0.6 log2) meant that only 48 proteins would be included in the IPA and STRING analyses and this small dataset did not allow the software to make predictions regarding the enrichment of protein networks, pathways or biological functions.

In addition to investigating the dysregulated proteins associated with the PDZ binding motif, we also chose to examine the global proteomic changes related to the expression of the E6 and E7 oncoproteins in HEKn. For this uploaded the list of 678 proteins significantly differentially expressed (adjusted p-value ≤0.05) by ±1.5-fold (0.6 log2) change between the cells transduced with HPV16 E6+E7 and the LV-HEKn control into IPA and performed a Core Analysis. We also uploaded the 678 proteins dysregulated by ±1.5-fold (0.6 log2) change into STRING software. This large number of proteins resulted in an overcrowded protein-protein network figure and rendered it impossible to identify clusters of protein networks. Therefore, we restricted the STRING analysis to the 155 proteins significantly dysregulated by ±2-fold (1 log2) as this smaller dataset enhanced the visualization of the protein interaction network clusters.

2.6 Immunofluorescence Microscopy

2.6.1 Slide Preparation

Each well of an eight-well chamber slide (Life Technologies, cat# 154534) was seeded with 21,000 cells in 300 µL (70 cells/µL). The cells were grown in Epilife medium supplemented with human keratinocyte growth serum (HKGS) in a 37°C humidified incubator at 5% CO_2. The medium was changed every 36 hours until the cells reached confluence. Once confluent, the medium was removed and then the cells were rinsed twice with PBS. The cells were fixed with 300 µL of 4% paraformaldehyde (Alpha Aesar, cat# J61899) for 10 minutes at room temperature and then washed with 300 µL of PBS.

To permeabilize the cells, the PBS was removed, and 300 µL of 0.5% Triton X in PBS was added to each well. The slides were incubated at room temperature for 10 minutes. Next, the cells were washed twice with 0.1% Triton X in PBS. The cells were blocked for 1 hour with 300 µL of 5% donkey serum.

Two biological replicates of each of the three cell lines were prepared for each protein. To limit bias due to sample preparation, all three cell lines were prepared at the same time and stained with the same preparation of primary and secondary antibodies. The antibodies used in this study are listed in Table 3.

The MAGI1, JAM1, and PAR3 primary antibodies were not conjugated to fluorophores. The primary antibody was added to the permeabilized cells and incubated at 4°C overnight. The next day the cells were washed twice with 0.1% Triton X in PBS. 300 µL of secondary antibody: (Goat Anti-Mouse IgG H&L (Alexa Fluor® 647) Abcam cat# ab150115) or Goat Anti-Mouse IgG H&L (Alexa Fluor® 488) Abcam cat#ab150113) was added, and the cells were

incubated in the dark at room temperature. After 1 hour, the cells were washed twice with 0.1% Triton X in PBS and twice with PBS.

The ZO1 antibody was conjugated to Alexa Fluor® 488 and was added to the permeabilized cells, and then the slide was incubated in the dark at room temperature for 1 hour. Next, the cells were washed twice with 0.1% Triton X in PBS and twice with PBS.

To mount the coverslip, the plastic chambers were removed and the entire slide was rinsed with Milli-Q water. The slides were air dried for 5 minutes. Next, four drops of Prolong Gold with DAPI (Thermofisher Scientific, cat# P36935) were added directly on top of the cells and then a number 1.5 coverslip (Thermofisher Scientific, cat #3322) was gently pressed into place to extrude excess mounting media and eliminate bubbles. The slides were placed in the dark to harden for 24 to 72 hours until imaged.

2.6.2 Immunofluorescence Imaging and Analyses

To visualize the proteins of interest, we used an LSM510 confocal microscope coupled with an Axiovert 200M inverted microscope and a Plan-Apochromat 20x/0.8M27 objective (Carl Zeiss). Digital images were captured at 364nm excitation/454nm emission (blue), 488nm excitation/519nm emission (green) and 647nm excitation/668nm emission (red) and processed using Zeiss Zen image software. Channels were acquired sequentially. Images for each of the antigens were captured using identical microscope and camera settings. To verify antibody specificity secondary antibody-only controls were used. This control was also used to set the threshold for subsequent acquisitions and avoid false-positive signals.

To measure fluorescence intensity and estimate the abundance of the junctional or polarity complex proteins in the cells we employed the particle measurement function of FIJI

(Fiji is Just Image J -win64) software (NIH). First, the raw, unprocessed digital fluorescence file was opened in FIJI as a 16-bit file; the channels were split into "image slices" based in their excitation wavelengths (647/red, 488/green and 364/blue). Next, the brightness and contrast were optimized to ensure cells and background were distinguishable for the purpose of selecting the region of interest; this does not alter the intensity value of the pixels. In the slice of the image containing the channel of interest, the free-hand draw tool was used to select an area of background, avoiding any cell-associated fluorescent signals, to determine the level of background fluorescence. Next, under the "Analysis" drop-down menu, the "Measure" option was selected. FIJI provided values for the area measured as well as the mean, minimum and maximum intensity values, integrated density and raw integrated density. We took three background readings for each image and averaged the mean intensity values of these three readings.

Similarly, to measure cell-associated fluorescence we outlined individual cells with the freehand drawing tool. Again, we selected "Measure" from the "Analysis" drop- down menu. This was repeated three times and averaged for each cell. We measured twelve cells per protein of interest in two biological replicates. To calculate the Corrected Total Cell Fluorescence for the cells in an image we used the formula from Gordan *et al.* (170):

Corrected Total Cell Fluorescence =
Integrated density- (Area of cell x Mean fluorescence of background)

The two-tailed, Student's T-test was used to determine if the corrected total cell fluorescence was significantly different between cell lines. ANOVA was used for comparing the

variation in corrected total cell fluorescence among the three cell lines: HPV16 E6+E7, HPV16 E6ΔPBM +E7, and LV-HEKn.

Additionally, to assess colocalization of the tight junction proteins MAGI1 and JAM1, we captured images of the cells probed with both JAM1 and MAGI1 antibodies as described above. The raw, unprocessed digital images were opened with FIJI software and analyzed with the Colocalization Threshold and Colocalization Test programs. This software uses Costes' thresholding to determine the Pearson's correlation and Mander's coefficients of colocalization. Costes' method determines the minimum intensity above which both channels are colocalized (171). Pearson's correlation coefficient describes the intensity distribution between the two channels of interest and can range from -1.0 to 1.0. A Pearson's correlation coefficient of 1.0 means that there is 100% colocalization while a result of -1.0 indicates complete negative correlation and thus an absence of colocalization. Alternatively, Mander's coefficient of overlap indicates the actual overlap of signals and can range from 0 to 1. A value of 1 indicates that 100% of both channels colocalize (172). Three biological replicates were performed. ANOVA was used to determine if the calculated Mander's coefficients or the Pearson's correlation coefficients were significantly different among cell lines.

Chapter 3: Significance of the HPV16 E6 PDZ Binding Motif on Human Neonatal Keratinocyte Immortalization and Transformation

3.1 Introduction and Rationale

The role of the HPV E6 PDZ binding motif in cell immortalization and transformation is unclear. Some studies have concluded that immortalization of cells by high-risk HPV E6 is not possible without the PDZ binding motif while others have contradicting results (64, 66-69). As previously described, these opposing conclusions are likely due to the different experimental models used. A HEKn primary cell line was used in our study, as this is a physiologically appropriate model for studying the early stages of HPV infections and transformation (173).

First, we created three types of cell lines by transducing HEKn cells with lentiviruses carrying either the full-length HPV16 E6 gene or a truncated HPV16 E6ΔPBM gene as well as lentiviruses carrying E7 genes. The two experimental cell lines transduced with HPV genes are named HPV16 E6+E7 and HPV16 E6ΔPBM+E7. The control HEKn were transduced with lentiviruses carrying empty lentivectors (no HPV genes) and are named LV-HEKn. The differences in amino acid sequence and protein structure between the two HPV16 E6 genes employed in these experiments are illustrated in Figure 5. Both HPV16 E6 and HPV16 E6ΔPBM genes carry mutations at nucleotide 226 which abolish the 5' splice site and ensures the full-length E6 protein is expressed. The difference between the two E6 genes employed here is that the HPV16 E6ΔPBM construct is missing the last twelve amino acids, including the four which make up the canonical PDZ binding motif (ETQL) at the carboxyl-terminus (64, 174).

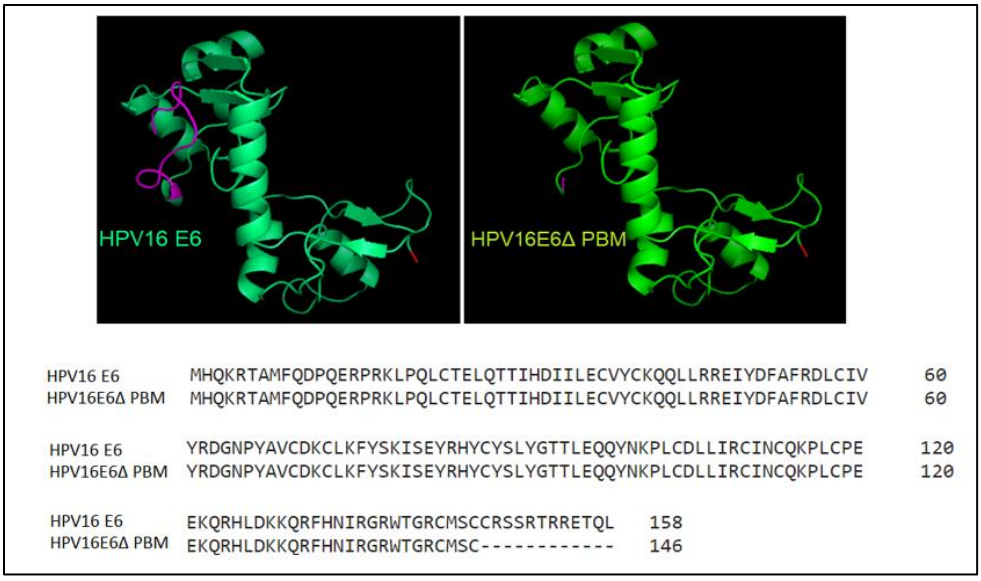

Figure 5. Ribbon diagram of the predicted structures and amino acid sequences of high-risk HPV16 E6 (amino acids 1-158) and truncated high-risk HPV16 E6ΔPBM (amino acids 1-146). Note in the aligned sequence the last 12 amino acids at the carboxyl-terminus are missing from the truncated protein HPV16 E6ΔPBM. The images of the E6 structures were created using Edu PyMOL (v1.74). The N-termini are red, and the carboxyl-termini are colored purple.

Antibiotic selection was used to verify the successful transduction of HEKn. All non-transduced control cells did not survive beyond five days when the culture media was supplemented with antibiotics. Once antibiotic selection was complete, we verified the expression of the HPV16 E6 and E7 genes in the transduced cells using RT-PCR. Thirteen biological replicate transductions were performed for each cell line and the longevity of these transduced cells was monitored until they achieved 100 population doublings or entered a senescent state. Senescence was defined as not achieving 80% confluence within three weeks.

The levels of hTERT and p53 were assessed by Western blot in three biological replicates of the three cell lines. Subsequently, we investigated the ability of the transduced cells to grow in soft agar as evidence of transformation.

3.2 Results

3.2.1 Longevity and Growth Rates

HEKn is a primary cell line capable of a finite number of population doublings. According to the manufacturer, HEKn cells can undergo approximately 30 population doublings before entering senescence. In our study the HEKn transduced with either HPV16 E6+E7 or HPV16 E6ΔPBM + E7 could continue to proliferate beyond 100 population doublings but all of the LV-HEKn control cells, transduced with empty lentivectors, entered senescence by 50±5 population doublings (Figure 6). 100% of the biological replicates transduced with full length E6+E7 continued to replicate beyond 100 population doublings. Only 85% (11/13) of the biological replicates of transductions with E6ΔPBM+E7 transductions continued to replicate beyond 100 population doublings, suggesting that the immortalization efficiency is lower in the E6ΔPBM+E7 cells.

Using the time to confluence to estimate growth rate, we determined that the HPV16 E6 PDZ binding motif was not observed to impact the growth rate of immortalized HEKn cells. Remarkably, the expression of the full-length HPV16 E6+E7 did not confer an increased rate of growth over that of controls cells or cells expressing the truncated HPV16 E6ΔPBM+E7. Control cells, (LV-HEKn), grew at a similar rate as the transduced cells carrying either the truncated or the full-length HPV16 E6 and E7 genes. The logistic growth rates (k) for non-senescent control cells (LV-HEKn), cells expressing full-length HPV16 E6+E7, and cells transfected with HPV16 E6ΔPBM+E7 were $1.77x10^{-2}$ ($1.62x10^{-2}$ – $1.84\ x10^{-2}$, 95% CI), $1.80x10^{-2}$ ($1.45\ x10^{-2}$ – $2.17\ x10^{-2}$ 95% CI) and $1.94x10^{-2}$ ($1.80\ x10^{-2}$ – $2.10\ x10^{-2}$ 95% CI), respectively.

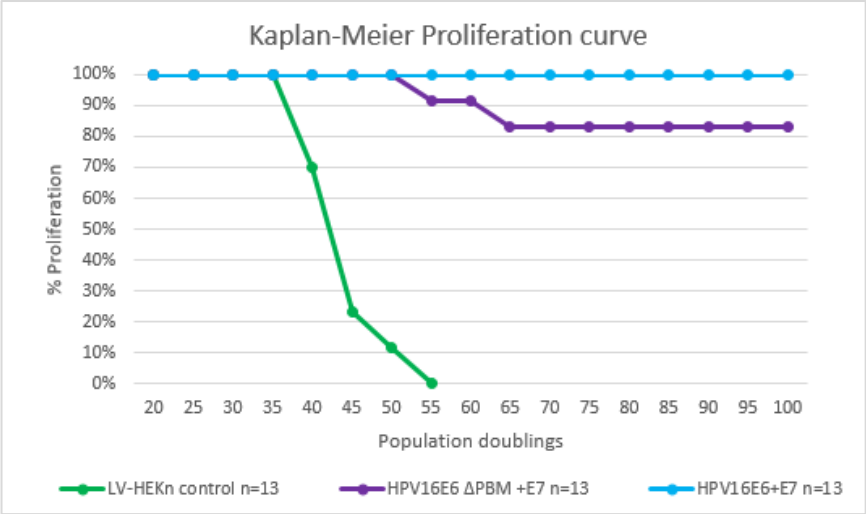

Figure 6. Kaplan-Meier proliferation curve depicting the number of population doublings during which transduced cells remained in a replicative state. The cell transduced with full-length HPV16 E6+E7 cells all continued to proliferate beyond 100 population doublings. Most of the cells transduced with the truncated HPV16 E6+E7 continued to proliferate for at least 100 population doublings. All lentivector transduced control cells (LV-HEKn) were senescent by 50 population doublings.

3.2.2 p53 degradation

The degradation of p53 by high-risk HPV has been well documented. Fittingly, we observed that the levels of p53 on a Western blot were much lower in cells expressing HPV16 E6+E7 compared to the LV-HEKn controls. (Figure 7). Interestingly, p53 levels were also reduced in the HPV16 E6ΔPBM+E7 cells; although not by as much as the cells expressing the full-length E6 protein. These experiments verified that the PDZ binding motif is not strictly required for p53 degradation but certainly enhances the degradation of this pro-apoptotic protein.

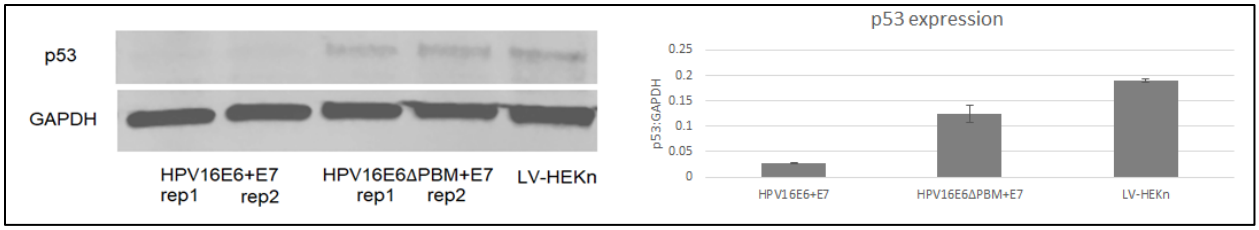

Figure 7. Western blot depicting p53 levels among the three transduced cell lines. p53 was lower in cells expressing HPV16 E6ΔPBM than in the control cells, indicating that the PDZ binding motif is not required for p53 degradation. Significantly, p53 levels were lowest in cells expressing full-length HPV16 E6+E7 proving that the PDZ binding motif enhances the degradation of p53. The bar chart data is representative of data from three biological replicate cell lines.

3.2.3 Telomerase expression

The activation of the catalytic subunit of human telomerase, hTERT, extends the replicative life span of cells by extending the length of telomeres, and HPV16 E6 proteins are known to induce hTERT expression (53, 54). The expression of hTERT in the transduced cells was evaluated by Western blot. As expected, the control cells had very low hTERT protein levels. Cells transduced with lentiviruses carrying the full-length HPV16 E6 and E7 genes exhibited the highest expression of hTERT, followed by the cells transduced with lentiviruses carrying HPV16 E6ΔPBM and E7 genes. As seen in Figure 8, the amount of hTERT protein in the cells expressing the truncated HPV16 E6ΔPBM and E7 proteins was around 20% lower than in the cells transduced with the full-length E6+E7. This indicates that the HPV16 E6 PDZ binding motif enhances hTERT expression.

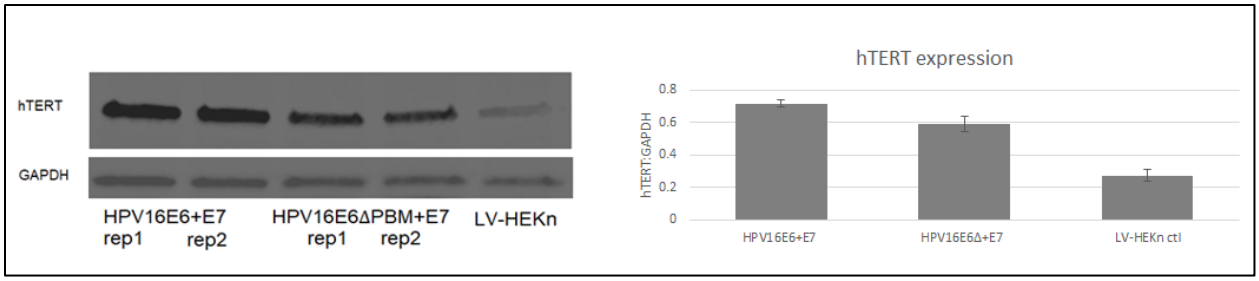

Figure 8. hTERT levels among the three transduced cell lines measured by Western blot. The presence of the E6 PDZ binding motif was not required for the expression of hTERT enhanced its expression. The highest levels of hTERT were measured in cells expressing HPV16 E6+E7. Cells expressing HPV16 E6ΔPBM+E7 also had higher levels of hTERT than the LV-HEKn control cells. Bar chart data is representative of data from three biological replicate cell lines.

3.2.4 Anchorage-independent Growth

Anchorage-independent growth is a phenotypic hallmark of transformed cells. Although the cells expressing E6+E7 or E6ΔPBM+E7 proteins displayed increased longevity and were expressing hTERT, none of the transduced cell lines displayed evidence of transformation in soft agar assays. (Figure 9). Cells transduced with lentiviruses carrying HPV16 E6+E7 or HPV16 E6ΔPBM+E7 failed to yield colonies in the soft agar assays at both 50 and 95 population doublings. These results are significant because these experiments show that HPV16 E6+E7 or HPV16 E6ΔPBM+ E7, expression is not capable of inducing anchorage-independent growth of HEKn in culture. It is possible that a secondary factor, perhaps an activated oncogene, estrogen exposure, or accumulation of oncogenic mutations during lengthy passaging in culture, may be required in addition to HPV16 E6+E7 expression to promote transformation.

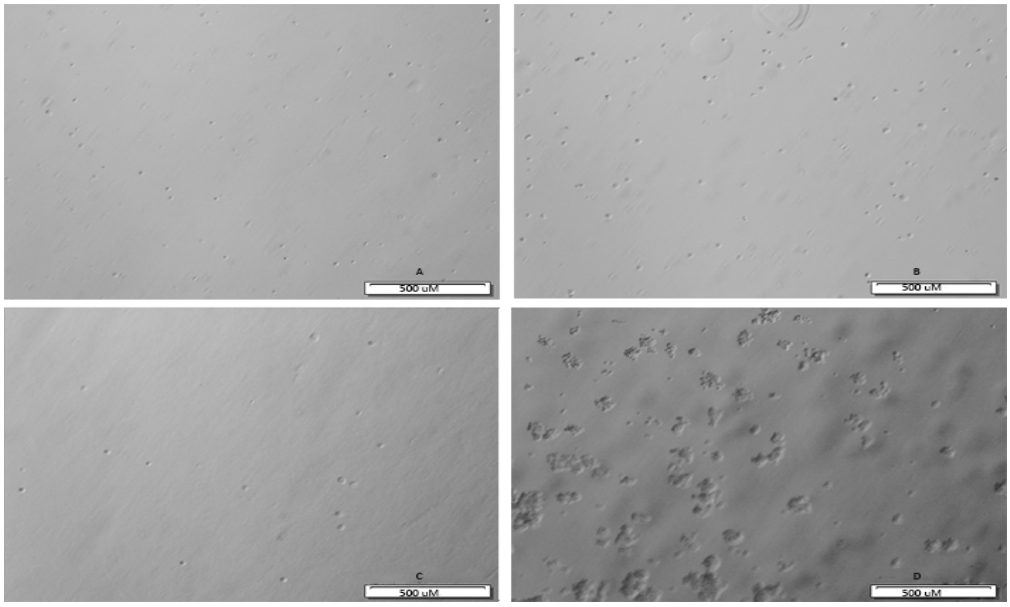

Figure 9. Soft Agar assay to determine capacity for anchorage-independent growth. After two weeks at 37°C, soft agar suspensions of cells transduced with HPV16 E6+E7 at 95PD (panel A), HPV16 E6ΔPBM+E7 at 95PD (Panel B) or control LV-HEKn at 30PD (panel C) did not exhibit anchorage-independent growth. SiHa cells (panel D), are an HPV16 transformed cell line, capable of growing in soft agar in an anchorage-independent manner. Scale bar 500μM.

3.3 Summary

The cells transduced with the truncated HPV16 E6 lacking PDZ binding motif and E7 continued to proliferate equally as long as the cells which were transduced with lentiviruses carrying the full-length E6 and E7 genes confirming that the HPV16 E6 PDZ binding motif is not required for immortalization. Similarly, the carboxyl-terminus of the E6 proteins expressed in our cell lines did not alter the growth rate of the transduced cells.

Western blot experiments established that the HPV16 E6 PDZ binding motif significantly increases the high-risk E6 oncoprotein's ability to promoted p53 degradation, and to promote hTERT over expression. These findings are significant because this proves that the PDZ binding motif, does contribute to pro-oncogenic processes associated with high-risk HPV. The influence of the E6 PDZ binding motif on p53 and hTERT may be key to high-risk HPV's ability to

transform cells. The mechanisms by which the E6 PDZ binding motif contributes to these biological processes warrant further exploration.

We were unable to determine whether the HPV16 E6 PDZ binding motif was required for HEKn transformation because none of the transduced cells showed evidence of anchorage-independent growth despite increased hTERT expression in cells expressing the HPV oncoproteins. These results prove that the expression of HPV16 E6+E7 or HPV16 E6ΔPBM+ E7 are insufficient to induce keratinocyte transformation in culture.

Chapter 4: Quantitative Mass spectrometry LC/LC-MS/MS

4.1 Introduction and Rationale

While the expression of high-risk HPV E6 and E7 proteins has previously been recognized to promote cellular transformation, the influence of these oncoproteins on the keratinocyte proteome is not well described. Likewise, the presence of a PDZ binding motif at the carboxyl-terminus of high-risk HPV E6 proteins is considered a marker of carcinogenic potential, but its effect on global protein abundances in keratinocytes has not been well characterized. Here we sought to catalogue the effects of the HPV16 oncoproteins, and specifically the influence of the E6 PDZ binding motif, on the host proteome.

Quantitative mass spectrometry is a powerful tool capable of measuring global proteomic changes among different cell lines. The successful detection of proteins is dependent upon several factors including, but not limited to, adequate specimen preparation, resolution, ionization, detection, and identification. The sensitivity of two-dimensional Liquid Chromatography and Tandem Mass spectrometry (LC/LC-MS/MS) is very good, however false negative results cannot be ruled out.

A bottom-up approach using LC/LC-MS/MS and TMT labeled peptides was undertaken to quantify the changes in protein abundance among our three cell lines. The resulting lists of dysregulated proteins were analysed using gene ontology enrichment and pathway and gene ontology enrichment software to identify cellular pathways and networks altered by the expression of HPV16 E6+E7 or HPV16 E6ΔPBM+E7 in HEKn cells.

4.2 Results

4.2.1 Quantitative LC/LC-MS/MS

Two six-plex TMT quantitative LC/LC-MS/MS runs on a total of four biological replicates for each of the three transduced cell lines were performed. The first LC/LC-MS/MS run included biological replicates 1 and 2 of HPV16 E6+E7, HPV16 E6ΔPBM+E7, and LV-HEKn. The second LC/LC-MS/MS run included the biological replicates 3 and 4 of each of these cell lines.

The spectral data underwent pre-processing and data exploration steps prior to statistical analyses by Dr. Chih-yu Chen, at the NML proteomic core. Data processing included removing proteins that were not detected in any of the TMT experiments as well as any proteins that were detected in one TMT run but not the other. Principal component analyses were used for data exploration of log2 protein intensity, and a heat map was generated to evaluate hierarchical clustering (165). Statistical analyses for differential protein abundance were conducted using LIMMA on log2 normalized protein intensity generated by Scaffold (166). P-values reported here are adjusted by Benjamini-Hochberg (BH) method to correct for multiple hypothesis testing (167). In total 5837 proteins were identified by LC/LC-MS/MS.

To verify the results from the proteomic experiments, the levels of several significantly differentially abundant proteins identified in LC/LC-MS/MS analyses were assessed by Western blot (Figure 10). In agreement with our mass spectrometry data, higher levels of Alpha-internexin (AINX p=1.92e-04), Bone marrow stromal antigen 2 (BST p=1.83e-04), Intercellular adhesion molecule 1 (ICAM1 p=2.35e-03), and Neurofilament light polypeptide (NFL p=2.6e-03) were observed in cells transduced with HPV16 E6+E7 compared to those transduced with HPV16 E6ΔPBM+E7. Similarly, microtubule-associated protein RP/EB family member 1 (MARE1 p=2.13e-03) was expressed at lower levels in cells transduced with HPV16 E6+E7 than

in those transduced with HPV16 E6ΔPBM+E7 in agreement with the LC/LC-MS/MS data. Finally, involucrin (INVOL p=1.51e-04) was found by Western blot to be expressed at similar levels in all three cell lines although it was found by mass spectrometry to be reduced in the oncoprotein expressing cell lines compared to the control cells.

Figure 10. Western Blot analyses of protein abundance for six proteins found to be differentially expressed in LC/LC-MS/MS data. Grey bars indicate the average of four replicates of proteins measured by LICOR Western Blots. The red line represents the LC/LC-MS/MS measurements. GAPDH, vinculin, or cofilin were used as load controls.

4.2.3 Proteins Differentially expressed between HPV16 E6+E7 vs. HPV16 E6ΔPBM+E7 cells

Of the 5837 proteins identified by LC/LC-MS/MS, 5% (280 proteins) were significantly differentially expressed ($p \leq 0.05$) between cell lines expressing full-length HPV16 E6+E7 and HPV16 E6ΔPBM +E7. From the volcano plot shown in Figure 11, one can see that the fold change differences measured for the 280 proteins were small. The protein with the largest fold change observed between cells expressing the full-length HPV16 E6 and truncated E6ΔPBM was neurofilament heavy (NFH) protein (4.7-fold change, p=1.33E-02). The top ten significantly up and downregulated proteins between the HEKn expressing full-length HPV16 E6+E7 compared to truncated HPV16 E6ΔPBM +E7 are listed in Tables 5 and 6 while the complete list of significantly regulated proteins can be found in Appendix 1. Notably, there weren't any PDZ proteins found to be significantly differentially expressed between HPV16 E6+E7 and HPV16 E6ΔPBM+E7.

Table 5. List of the top ten proteins most increased in abundance as measured by quantitative tandem mass spectrometry in HEKn cells expressing HPV16 E6+E7 compared to the truncated HPV16 E6ΔPBM+E7.

Protein Name	**UNIPROT_ID**	**Fold Change**	**Adjusted p-value**
Neurofilament heavy polypeptide	NFH_HUMAN	4.77	1.33E-02
Alpha-internexin	AINX_HUMAN	4.73	1.92E-04
Bone marrow stromal antigen 2	BST2_HUMAN	3.05	1.83E-04
Reticulocalbin-3	RCN3_HUMAN	2.11	2.31E-02
Collagen alpha-2 (VI) chain	CO6A2_HUMAN	2.11	2.13E-03
Neurofilament light polypeptide	NFL_HUMAN	2.08	2.60E-03
Ubiquitin carboxyl-terminal hydrolase isozyme L1	UCHL1_HUMAN	2.05	3.31E-04
Peptidyl-prolyl cis-trans isomerase FKBP10	FKB10_HUMAN	1.87	1.69E-04
Radical S-adenosyl methionine motif-containing protein 2	RSAD2_HUMAN	1.78	1.15E-03
Histone H1x	H1X_HUMAN	1.77	3.16E-02

Table 6. List of the top ten proteins most decreased in abundance as measured by quantitative tandem mass spectrometry in HEKn cells expressing HPV16 E6+E7 compared to the truncated HPV16 E6ΔPBM+E7.

Protein Name	UNIPROT_ ID	Fold Change	Adjusted p-value
Aldo-keto reductase family 1 member C3	AK1C3_HUMAN	-2.53	4.28E-02
Ganglioside GM2 activator	SAP3_HUMAN	-1.73	3.42E-02
Protein S100-A2	S10A2_HUMAN	-1.71	4.56E-02
Solute carrier family 2, facilitated glucose transporter member 1	GTR1_HUMAN	-1.67	1.69E-04
Adipogenesis regulatory factor	ADIRF_HUMAN	-1.59	4.23E-02
Neuron-specific protein family member 1	NSG1_HUMAN	-1.57	2.60E-03
RNA-binding protein 3	RBM3_HUMAN	-1.54	1.36E-02
Carbonic anhydrase 12	CAH12_HUMAN	-1.53	4.94E-02
Teneurin-2	TEN2_HUMAN	-1.53	4.15E-03
Xanthine dehydrogenase/oxidase	XDH_HUMAN	-1.49	7.02E-03

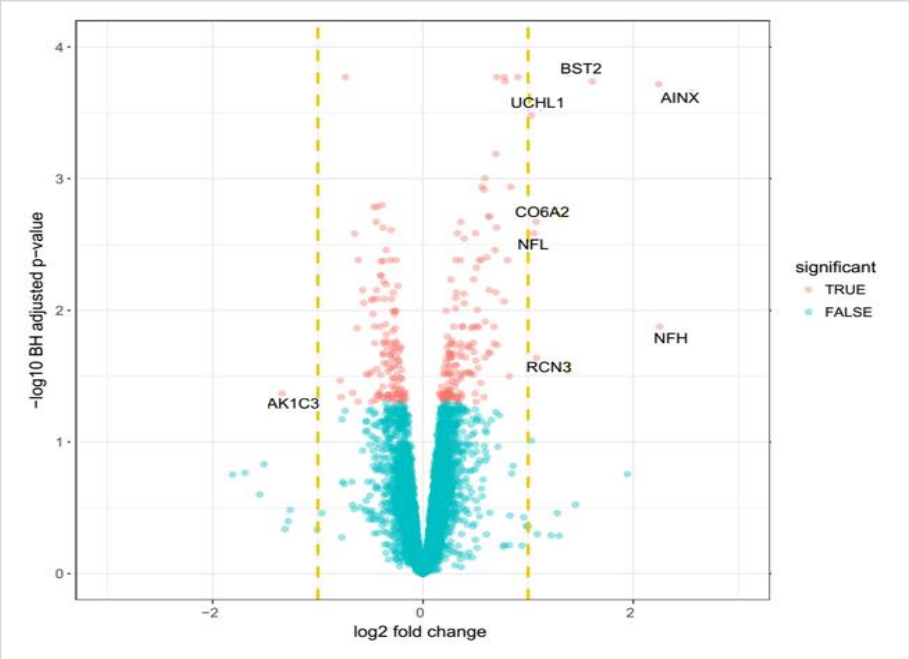

Figure 11. Volcano plot of differentially abundant proteins in cells expressing HPV16 E6+E7 compared to the truncated HPV16 E6ΔPBM+E7. The 280 proteins which were significantly differentially abundant ($p \geq 0.05$) are represented by pink dots. Only eight proteins were significantly differentially abundant by more than 2-fold (1 log2) change (yellow dashed lines) in HPV16 E6+E7 compared to the truncated HPV16 E6ΔPBM+E7.

4.2.4 Pathway Analyses: proteins dysregulated in HPV16 E6+E7 vs. HPV16 E6ΔPBM+E7 cells

Qiagen's Ingenuity Pathway Analysis software (IPA) and STRING software were used for the evaluation of canonical pathways, protein interaction networks and downstream biological effects related to the significantly differentially abundant proteins in our cell lines. There were only 48 proteins significantly differentially abundant by ≥1.5-fold (0.6 log2). Qiagen IPA core analyses and STRING protein analyses of this small dataset were unable to reveal conclusive enriched GO terms or pathways. Therefore we reduced the stringency of our dataset to include the 142 proteins significantly differentially abundant ($p \leq 0.05$) between cells expressing full-length HPV16 E6+E7 and HPV16 E6ΔPBM+E7 by at least ≥1.3-fold (0.4 log2) in order to identify the most meaningful biological effects associated with the HPV16 E6 PDZ binding motif while still retaining sufficient data for analyses.

Canonical Pathways

Canonical pathways are established biochemical processes preceding biological functions or effects. IPA ranks the canonical pathways associated with significantly differentially abundant proteins in a dataset based on their p-value (Fisher's exact test) and using information from Qiagen's extensive curated database, the Ingenuity Knowledge Base. IPA also calculates a z-score for each canonical pathway associated with significantly differentially abundant proteins in the dataset, to predict whether it is activated or inhibited.

There were 61 canonical pathways predicted to be significantly ($p \leq 0.05$ (-1.3-log10) affected by the 142 proteins differentially abundant between HPV16 E6+E7 and HPV16 E6ΔPBM +E7 cells by ≥±1.3-fold (0.32 log2) change. Notably, canonical pathways predicted to be affected by the presence of the HPV16 E6 PDZ binding motif included p53 signaling, remodeling of epithelial adherens junctions, actin nucleation by ARP-WASP complex, neuro-

inflammation signaling pathway, and the antigen presentation pathway. However, as seen in Table 7, most of the canonical pathways were linked to fewer than five proteins from our dataset, precluding IPA from providing an estimation of activity.

Protein-Protein Networks and Downstream effects

A useful tool for the visualization of the overall protein-protein networks among the significantly differentially abundant proteins is STRING software. The results of these analyses illustrate that there were only a handful of inter-connected proteins among the significantly differentially abundant proteins. (Figure 12). IPA network analyses also found only a small number of protein-protein networks among the 142 proteins significantly differentially abundant by ≥±1.3-fold change between HPV16 E6+E7 and HPV16 E6ΔPBM +E7 cells. The scarcity of protein-protein relationships makes it difficult to discern the biological implications of the HPV16 E6 PDZ binding motif. However, there were two main themes which stood out among the biological effects predicted to be enriched in our dataset.

Foremost, cellular processes related to inflammation and immune response signaling were clearly predicted to be associated with the protein interaction networks calculated by STRING and IPA analyses. For example, “Immune response”, “Type I interferon signaling pathway”, “Defense response to virus”, “Negative regulation of viral life cycle”, and “Response to stress”, were some of the biological GO terms predicted by STRING. Additionally, “Organismal Injury and Abnormalities”, “Inflammatory Response” and “Inflammatory Disease” were predicted by IPA and are summarized in Table 8. The protein-protein network analyses revealed linkages between several proteins related to immune signaling and inflammatory responses including 2'-5'-oligoadenylate synthase-like protein (OASL), 2'-5'-oligoadenylate synthase 2 (OAS2), BST2,

Interferon-induced protein with tetratricopeptide repeats 2 (IFIT2), Heat shock-related 70 kDa protein 2 (HSPA2), Small ubiquitin-related modifier 3 (SUMO3), Intercellular adhesion molecule 1 (ICAM1), and Nuclear autoantigen Sp-100 (SP100). Many of these proteins were also grouped by IPA in the fourth ranked network that was associated with "Inflammatory Response" and "Inflammatory Disease" downstream effects. Each protein in this network was upregulated in the HPV16 E6+E7 cells.

The second biological trend highlighted by network analyses was cellular organization and signaling. Four of the top ten upregulated proteins in our dataset, neurofilament light (NFL), neurofilament heavy (NFH), alpha internexin (AINX or INA) and collagen alpha-2 VI chain (CO6A2) led to the prediction that "Neurofilament cytoskeleton organization" "Cell-To-Cell Signaling and Interaction", "Cellular Assembly and Organization", and "Cellular Growth and Proliferation" are affected by the proteins dysregulated in cells transduced with full-length HPV16 E6+E7 compared to HPV16 E6ΔPBM+E7 cells.

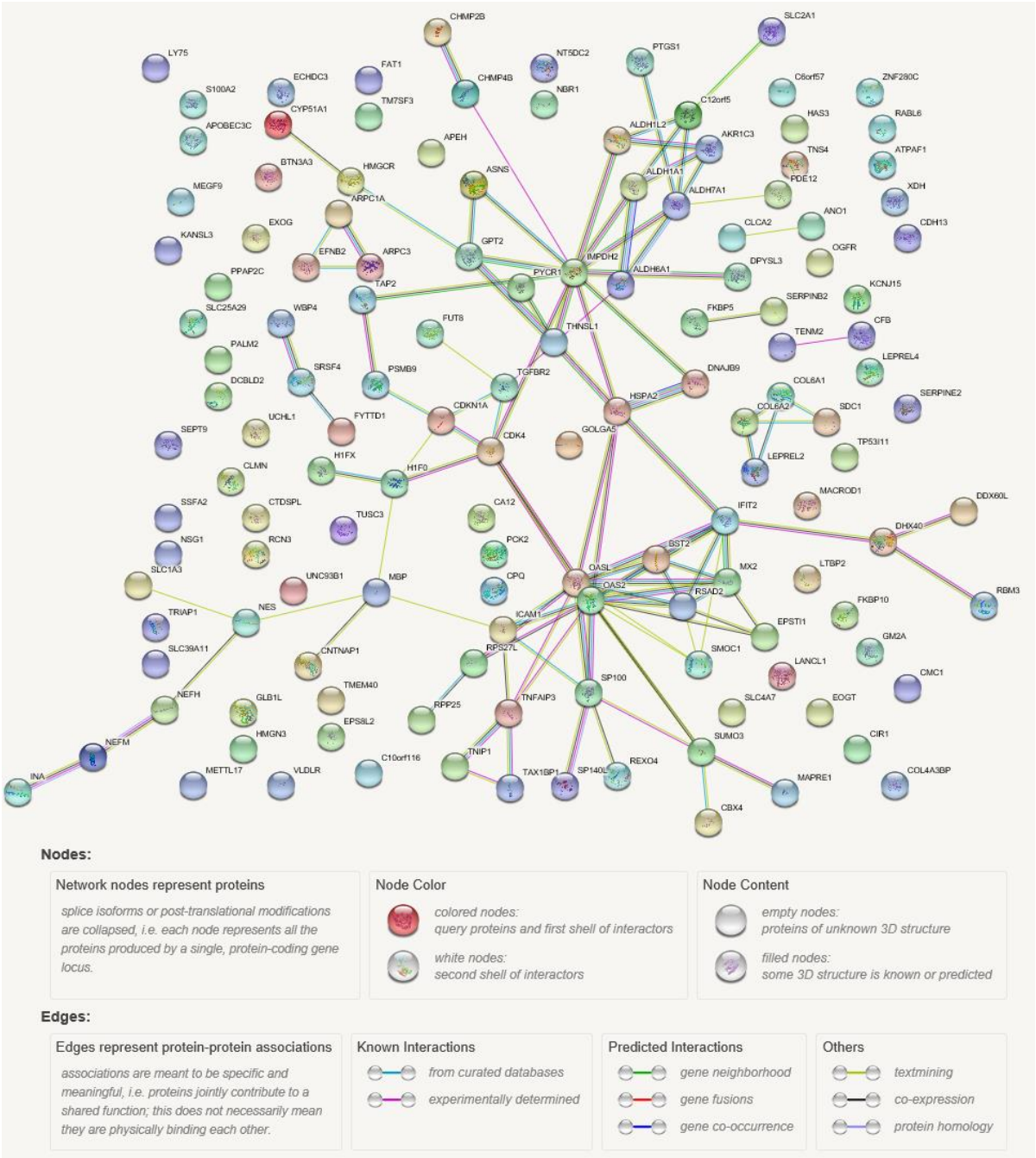

Figure 12. STRING protein-protein interaction networks among proteins significantly differentially abundant by ≥±1.3-fold change between cells expressing full-length HPV16 E6+E7 or the truncated HPV16 E6ΔPBM+E7 proteins. From the STRING analysis, there are only a few protein-protein interactions evident among these proteins as most of the proteins have no direct connection to other proteins in the dataset. Color is not significant.

Table 7. Sixty-one canonical pathways which are predicted to be affected by the presence of the HPV16 E6 PDZ binding motif. Predictions were made by IPA software based on the proteins significantly differentially abundant by ≥±1.3-fold (0.32 log2) change in cells expressing HPV16 E6 and E7 compared to cells expressing HPV16 E6ΔPBM+E7.

Canonical Pathways	-log (p-value)	Molecules
Antigen Presentation Pathway	4.03	HLA-A, TAP2, HLA-B, PSMB9
Histamine Degradation	3.66	ALDH1A1, ALDH7A1, ALDH1L2
Aryl Hydrocarbon Receptor Signaling	3.57	CDK4, ALDH1A1, ALDH7A1, ALDH6A1, ALDH1L2, CDKN1A
Oxidative Ethanol Degradation III	3.53	ALDH1A1, ALDH7A1, ALDH1L2
Fatty Acid α-oxidation	3.46	ALDH1A1, ALDH7A1, ALDH1L2
Putrescine Degradation III	3.41	ALDH1A1, ALDH7A1, ALDH1L2
Ethanol Degradation IV	3.3	ALDH1A1, ALDH7A1, ALDH1L2
Tryptophan Degradation X (Mammalian, via Tryptamine)	3.3	ALDH1A1, ALDH7A1, ALDH1L2
Protein Ubiquitination Pathway	2.83	HSPA2, HLA-A, TAP2, UCHL1, HLA-B, PSMB9, DNAJB9
Dopamine Degradation	2.79	ALDH1A1, ALDH7A1, ALDH1L2
Ethanol Degradation II	2.79	ALDH1A1, ALDH7A1, ALDH1L2
Noradrenaline and Adrenaline Degradation	2.69	ALDH1A1, ALDH7A1, ALDH1L2
Urate Biosynthesis/Inosine 5'-phosphate Degradation	2.53	IMPDH2, XDH
p53 Signaling	2.27	CDK4, SERPINE2, CDKN1A, TIGAR
Asparagine Biosynthesis I	2.2	ASNS
GADD45 Signaling	2.2	CDK4, CDKN1A

Purine Nucleotides Degradation II (Aerobic)	2.2	IMPDH2, XDH
Hepatic Fibrosis / Hepatic Stellate Cell Activation	2.18	TGFBR2, COL4A3BP, COL6A1, COL6A2, ICAM1
Granzyme A Signaling	2.16	H1F0, H1FX
Remodeling of Epithelial Adherens Junctions	2.03	ARPC3, MAPRE1, ARPC1A
CD28 Signaling in T Helper Cells	2.01	HLA-A, ARPC3, HLA-B, ARPC1A
T Helper Cell Differentiation	1.96	TGFBR2, HLA-A, HLA-B
Estrogen-mediated S-phase Entry	1.94	CDK4, CDKN1A
Alanine Biosynthesis II	1.9	GPT2,
Alanine Degradation III	1.9	GPT2,
Choline Degradation I	1.9	ALDH7A1,
Serotonin Degradation	1.9	ALDH1A1, ALDH7A1, ALDH1L2
β-alanine Degradation I	1.9	ALDH6A1,
Super pathway of Cholesterol Biosynthesis	1.88	HMGCR, CYP51A1
CD40 Signaling	1.87	TNFAIP3, ICAM1, PTGS1
Th2 Pathway	1.82	TGFBR2, HLA-A, HLA-B, ICAM1
Cytotoxic T Lymphocyte-mediated Apoptosis of Target Cells	1.76	HLA-A, HLA-B
Inhibition of Angiogenesis by TSP1	1.71	TGFBR2, SDC1
Retinoate Biosynthesis I	1.71	AKR1C3, ALDH1A1
Glucocorticoid Receptor Signaling	1.69	HSPA2, PCK2, TGFBR2, FKBP5, CDKN1A, ICAM1
Cdc42 Signaling	1.67	HLA-A, ARPC3, HLA-B, ARPC1A

B Cell Development	1.67	HLA-A, HLA-B
Sumoylation Pathway	1.64	SP100, CBX4, SUMO3
Proline Biosynthesis I	1.6	PYCR1
Estrogen Biosynthesis	1.56	AKR1C3, CYP51A1
Mechanisms of Viral Exit from Host Cells	1.56	CHMP2B, CHMP4B
Th1 and Th2 Activation Pathway	1.53	TGFBR2, HLA-A, HLA-B, ICAM1
Chronic Myeloid Leukemia Signaling	1.53	TGFBR2, CDK4, CDKN1A
Lysine Degradation II	1.51	ALDH7A1,
Lysine Degradation V	1.51	ALDH7A1,
Amyotrophic Lateral Sclerosis Signaling	1.48	NEFH, NEFM, NEFL
Dendritic Cell Maturation	1.46	HLA-A, HLA-B, LY75, ICAM1
Autoimmune Thyroid Disease Signaling	1.44	HLA-A, HLA-B
Graft-versus-Host Disease Signaling	1.44	HLA-A, HLA-B
Arginine Degradation VI (Arginase 2 Pathway)	1.43	PYCR1
Proline Biosynthesis II (from Arginine)	1.43	PYCR1
Rapoport-Luebering Glycolytic Shunt	1.43	TIGAR
Zymosterol Biosynthesis	1.43	CYP51A1
Pancreatic Adenocarcinoma Signaling	1.4	TGFBR2, CDK4, CDKN1A
RhoA Signaling	1.36	ARPC3, SEPT9, ARPC1A
FXR/RXR Activation	1.34	PCK2, VLDLR, SDC1

Melanoma Signaling	1.33	CDK4, CDKN1A
Neuroinflammation Signaling Pathway	1.33	TGFBR2, HLA-A, HLA-B, SLC1A3, ICAM1
Unfolded protein response	1.33	HSPA2, DNAJB9
AMPK Signaling	1.32	PCK2, HMGCR, CDKN1A, SLC2A1
Actin Nucleation by ARP-WASP Complex	1.31	ARPC3, ARPC1A

Table 8. Top protein networks identified by IPA to be modulated by proteins significantly ($p \leq 0.05$) differentially abundant by $\geq \pm 1.3$-fold change (0.32 log2), in cells expressing HPV16 E6 and E7 compared to cells expressing HPV16 E6ΔPBM+E7. Proteins listed in red or green font were up or downregulated respectively in our data. The proteins in black font were predicted to by IPA to participate in that network but were not among the proteins identified in our experiments. The networks are ranked based on scores calculated by IPA which reflects the probability of finding the observed proteins in a given network by random chance, i.e. a higher score reflects a lower probability. The number of focus molecules is a count of the number of network proteins that were among the significantly differentially abundant proteins in our data. The top diseases and functions are ranked based on the number of associated proteins in a given network. Multiple networks may have similar biological functions or disease predictions.

ID	Molecules in Network	Score	Focus Molecules	Top Diseases and Functions
1	**AKR1C3**, ALDH, **ALDH1A1, ALDH1L2, ALDH6A1**, **ALDH7A1**, Aldose Reductase, **CFB**, **COL4A3BP**, **COL6A1**, **COL6A2**, Collagen type IV, **GPT2**, Growth hormone, **HAS3**, HDL-cholesterol, **IMPDH2**, **INA**, Laminin1, Mmp, **NEFH**, **NEFL**, **NEFM**, **NES**, NFkB (complex), **P3H3**, **P3H4**, **SERPINE2**, Tgf beta, Tnf (family), **VLDLR**, **XDH**, aldehyde dehydrogenase (NAD), collagen, trypsin	43	22	Cell-To-Cell Signaling and Interaction, Cellular Assembly and Organization, Nervous System Development and Function
2	**ANO1**, AURK, Actin, Alpha tubulin, **CDK4**, **CDKN1A**, **CLCA2**, **CLMN**, Cg, Creb, **EPS8L2**, ERK, **GM2A**, **H1F0**, **H1FX**, Histone H1, Histone h3, Integrin, Laminin (complex), Mek, **OGFR**, P-TEFb, **PYCR1**, Pdgf (complex), Pkc(s), **RPS27L**, **SDC1**, **SERPINB2**, **SSFA2**, Sos, **TGFBR2**, **THNSL1**, **TIGAR**, **TRIAP1**, caspase	36	19	Cellular Growth and Proliferation, Hair and Skin Development and Function, Cancer
3	26s Proteasome, ADRB, AMPK, Akt, **CBX4**, **CDH13**, **CNTNAP1**, **CYP51A1**, **DCBLD2**, **DDX60L**, **DHX40**, EGLN, HDL, **HMGCR**, Ikb, LDL, **LY75**, Ldh (complex), MTORC1, **NBR1**, PDGF BB, PI3K (family), PP2A, **PTGS1**, Pde4, **RBM3**, **SLC1A3**, SLC2A1, **SLC4A7**, **SUMO**, **SUMO3**, Secretase gamma, **UCHL1**, Ubiquitin, Vegf	30	17	Cancer, Organismal Injury and Abnormalities, Carbohydrate Metabolism
4	20s proteasome, **BST2**, **EPSTI1**, ERK1/2, **FUT8**, Fc gamma receptor, HLA Class I, **HLA-A**, **HLA-B**, **IFIT2**, IFN Beta, IFN alpha/beta, IFN type 1, IL12 (complex), Ifn, Ifnar, IgG, IgG1, Immunoglobulin, Interferon alpha, JAK1/2, MHC, MHC Class I (complex), MHC Class II (complex), **MX2**, **OAS2**, **OASL**, **PSMB9**, **RSAD2**, **SP100**, **TAP2**, **TAX1BP1**, **TNFAIP3**, Tlr, **UNC93B1**	29	16	Antimicrobial Response, Inflammatory Response, Cancer

5	**ASNS**, **CA12**, CD3, **CTDSPL**, Calmodulin, **DNAJB9**, **EFNB2**, **FKBP5**, Focal adhesion kinase, **HSPA2**, Histone h4, **Hsp70**, Hsp90, **ICAM1**, IL1, Igm, Insulin, Jnk, **KCNJ15**, **LTBP2**, **MBP**, P38 MAPK, **PALM2**, PCK2, PI3K (complex), Pka, RNA polymerase II, Ras, **SEPT9**, SRC (family), TCR, **TM7SF3**, cytokine, estrogen receptor	26	15	Connective Tissue Disorders, Developmental Disorder, Hereditary Disorder
6	ADCY9, AHR, ASPN, Alpha catenin, **BST2**, CDH5, CDIP1, **CIR1**, **COL6A1**, **COL6A2**, COL6A3, **CPQ**, **DPYSL3**, **EXOG**, FCF1, FSTL3, GATA1, **KANSL3**, KLK14, **LANCL1**, **MACROD1**, MAN2B2, **MEGF9**, MOB3C, MRPS6, NUPR1, PI4K2B, SAMD4A, SLC39A8, **SRSF4**, TCEANC2, TGFB1, **TNIP1**, TRIM25, UBN2	22	13	Dermatological Diseases and Conditions, Inflammatory Disease, Organismal Injury and Abnormalities
7	ADCYAP1, **ADIRF**, **APEH**, BICD1, **BTN3A3**, **CA12**, CCDC80, CCNI, CD33, CPD, CRLF1, **HMGN3**, KLF7, LGR5, **NSG1**, **NT5DC2**, NT5DC3, NTRK1, **PDE12**, PON2, RDH11, **S100A2**, SERPINF1, **SLC39A11**, **SMOC1**, SMPDL3B, TCIM, **TENM2**, **TMEM40**, TNF, TNFSF8, ZFP36L2, androstenedione, beta-estradiol, lipid peroxide	22	13	Cell-To-Cell Signaling and Interaction, Small Molecule Biochemistry, Drug Metabolism
8	**APOBEC3C**, APP, **ATPAF1**, CASZ1, **CMC1**, **COX6A2**, CSN3, Calcineurin B, DRAM1, DYNLL2, ENO3, EOGT, FAM171A1, FKBP10, FN1, GLB1L, HTT, **INA**, **MAPRE1**, MDK, NDRG3, **NEFH**, PPP1CA, PVALB, RAF1, RASGRP2, RPP25, **SP140L**, TMCC2, TUSC3, WBP4, ZFYVE16, ZNF706, methylamine, taurine	20	13	Cellular Compromise, Neurological Disease, Organismal Injury and Abnormalities
9	ADCY9, **ARPC1A**, **ARPC3**, **BST2**, **CHMP2B**, **CHMP4B**, CRHR2, CRYM, CYFIP2, CYP2J2, ERBB2, Exoc7, **FAT1**, FSH, FSTL3, **GOLGA5**, GPR132, Gsk3, IL17B, IL6, LAG3, Lh, MAPK6, **METTL17**, NPC2, POP5, PTGER1, RAB1A, **RABL6**, THNSL2, **TNS4**, **TP53I11**, **ZNF280C**, androstenedione, taurine	20	12	Infectious Diseases, Cell Morphology, Cellular Assembly and Organization

4.2.5 Proteins Differentially abundant between HPV16 E6+E7 and LV-HEKn

The results of the LC/LC-MS/MS experiments revealed that 3014 proteins were significantly differentially abundant ($p \leq 0.05$) between the HPV16 E6+E7 cells and the LV-HEKn control cells. Of these 3014 proteins, 1733 proteins were upregulated, and 1281 proteins were downregulated. (Figure 13). The complete list is available in Appendix 2. The top ten upregulated, and the top ten downregulated proteins are listed in Tables 9 and 10, respectively.

At 19.6-fold change, LAMP3 was the protein with the largest differential expression between the LV-HEKn and cells expressing HPV16 E6+E7 (p =1.17e-02). LAMP3, also known as DC-LAMP, is an integral membrane lysosomal-associated membrane protein whose function is not well defined but may be involved in cell survival during proteasomal inhibition (175, 176).

Several proteins related to interferon signaling and host immune response were among the top ten upregulated proteins including, bone marrow stromal antigen 2 (BST2 p=4.91e-07), HLA class I histocompatibility antigen IB-44 alpha chain (IB44 p=0.02), Tumor necrosis factor ligand superfamily member 10 (TNF10 *p*=3.46e-06) and Interferon-induced GTP-binding protein MX2 (MX2 p=2.68e-07).

Other notable proteins found to be upregulated in the E6+E7 transduced cells were those associated with DNA replication including members of the minichromosome maintenance complex (MCM 2-7), sirtuin-1 (SIRT1) and midkine (MK).

The protein downregulated by the largest margin was proline rich protein 9 (PRR9) with a -12.8-fold change (p = 0.002). PRR9 is involved in cell organization and differentiation as are several of the other most substantially downregulated proteins: elafin (ELAF), repetin (RPTN), keratin 6B (K2C6B) small proline rich protein 3 (SPRR3), involucrin (INVO) and filamin (FILA).

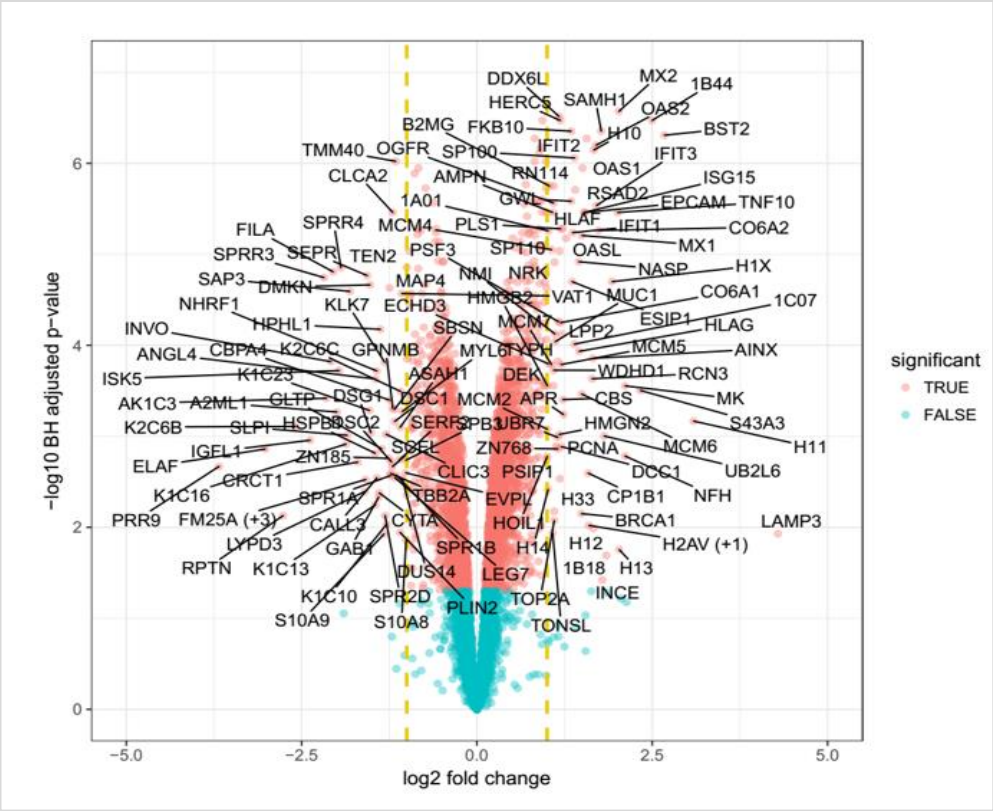

Figure 13. Volcano plot of 3014 differentially abundant proteins in HPV16 E6+E7 cells compared to the LV-HEKn control cells. The proteins which are significantly differentially abundant ($p \geq 0.05$) are represented by pink dots. Many proteins were significantly differentially abundant by more than 2-fold change (1 log2 (yellow dashed lines) in HPV16 E6+E7 compared to the control cells.

Interestingly, p53 was not among the proteins determined to be dysregulated by LC/LC-MS/MS, although it was observed to be downregulated by Western blot in cells expressing HPV16 E6+E7. It is possible that p53 levels were not detected by LC/LC-MS/MS because they were below the method's limit of detection. In unstressed cells levels of p53 are maintained at low levels by the Mdm2 E3 ubiquitin ligase and when high-risk HPV E6 proteins are present p53 is degraded (177). Alternatively, it is possible that the absence of p53 in the LC/LC-MS/MS data was due to the limited number of trypsin cleavage sites in p53 that yield usable spectra (178). One caveat of MS is that the absence of detection may mean either the protein is truly not present or that it is present, but simply not detected. Notably, p53 signaling was among the canonical

pathways predicted to be affected by the presence of the HPV16 E6 PDZ binding motif, as documented below (Table 9).

While there weren't any significantly differentially abundant PDZ proteins among the top ten most downregulated proteins between HPV16 E6+E7 and control cells, several of the Disks Large (DLG) proteins, DLG1, DLG4, and DLG5, were found to be significantly downregulated by 1.2, 1.2- and 1.1-fold change respectively in cells expressing HPV16 E6+E7 compared to the controls. DLG3, on the other hand, was upregulated by 1.2-fold change in HPV16 E6+E7 compared to controls. The DLG proteins possess multiple PDZ motifs and have roles in cell polarity.

It is interesting that DLG1 was also found to be downregulated by 1.2-fold change in HPV16 E6ΔPBM+E7 cells compared to controls, because this truncated E6 protein does not have a PDZ binding motif. Like HPV16 E6+E7 expressing cells, DLG3 was also upregulated by 1.3-fold change in HPV16 E6ΔPBM+E7 expressing cells compared to controls.

Other PDZ proteins dysregulated in HPV16 E6+E7 cells compared to LV-HEKn controls included Scribble, ZO1 and ZO2, GOPC and GIPC1. The E6 PDZ binding motif was not required for the reduction in GOPC, as it was also downregulated in HPV16 E6ΔPBM+E7 cells compared to the HEKn controls. Conversely, GIPC, ZO1, and ZO2 proteins were not dysregulated in in HPV16 E6ΔPBM+E7 cells compared to the HEKn controls.

Table 9. List of the top ten proteins most increased in abundance as measured by quantitative tandem mass spectrometry in HEKn cells expressing HPV16 E6 and E7 compared to control cells.

Protein Name	UNIPROT_ID	Fold Change	Adjusted p-value
Lysosome-associated membrane glycoprotein 3	LAMP3_HUMAN	19.6	1.17E-02
Histone H1.1	H11_HUMAN	8.5	6.80E-04
Bone marrow stromal antigen 2	BST2_HUMAN	6.4	4.91E-07
HLA class I histocompatibility antigen, B-44 alpha chain	1B44_HUMAN	5.6	3.38E-07
Solute carrier family 43 member 3	S43A3_HUMAN	5.0	3.13E-04
Midkine	MK_HUMAN	4.3	1.65E-03
Neurofilament heavy polypeptide	NFH_HUMAN	4.3	2.79E-04
Histone H1.3	H13_HUMAN	4.1	1.76E-02
Interferon-induced GTP-binding protein Mx2	MX2_HUMAN	4.1	2.68E-07
Tumor necrosis factor ligand superfamily member 10	TNF10_HUMAN	4.0	3.46E-06

Table 10. List of the top ten proteins most decreased in abundance as measured by quantitative tandem mass spectrometry in HEKn cells expressing HPV16 E6 and E7 compared to control cells.

Protein Name	UNIPROT_ ID	Fold Change	Adjusted p-value
Proline-rich protein 9	PRR9_HUMAN	-12.8	2.14E-03
Elafin	ELAF_HUMAN	-8.1	1.38E-03
Repetin	RPTN_HUMAN	-6.8	7.44E-03
Keratin, type II cytoskeletal 6B	K2C6B_HUMAN	-6.0	7.78E-04
Insulin growth factor-like family member 1	IGFL1_HUMAN	-5.2	1.10E-03
Small proline-rich protein 3	SPRR3_HUMAN	-4.5	1.80E-05
Aldo-keto reductase family 1 member C3	AK1C3_HUMAN	-4.4	3.82E-04
Involucrin	INVO_HUMAN	-4.2	1.51E-04
Filaggrin	FILA_HUMAN	-4.1	1.56E-05
Alpha-2-macroglobulin-like protein 1	A2ML1_HUMAN	-4.0	5.40E-04

4.2.6 Pathway Analyses: proteins dysregulated in HPV16 E6+E7 vs. LV-HEKn cells

Next, we used the pathway ontology software to examine relationships among proteins significantly differentially abundant between cells expressing the HPV16 E6+E7 oncoproteins and control cells. The IPA analyses were restricted to include the 395 proteins significantly upregulated by ≥1.5-fold (0.6 log2) change and the 283 proteins significantly downregulated by ≥1.5-fold (0.6 log2) change.

We elected to use a more restrictive cut-off for the STRING analysis, only including proteins differentially abundant by a minimum of ± 2.0-fold (1.0 log2) change because this smaller dataset of proteins was more conducive to visualizing the protein-protein interaction network groups.

Canonical Pathways

IPA identified 52 canonical pathways predicted to be affected by the proteins significantly differentially abundant in HEKn cells transduced with HPV16 E6+E7 (Figure 14). Understanding which pathways are significantly affected by HPV oncoproteins may elucidate key host processes that are modulated by E6 and E7.

The canonical pathways affected by HPV16 E6+E7 oncoproteins were related to cell cycle control, replication, DNA damage response, the antigen presentation pathway, interferon signaling, and apoptotic signaling. For six of these pathways, IPA was able to calculate a z-score and make a prediction of decreased activity. Cdc42 signaling, Sumoylation Pathway, Cell Cycle: G2/M DNA Damage Checkpoint Regulation, Neuroprotective Role of THOP1 in Alzheimer's Disease, Protein kinase A signaling and ILK Signaling canonical pathways are all predicted to be decreased in cells expressing HPV16 E6+E7.

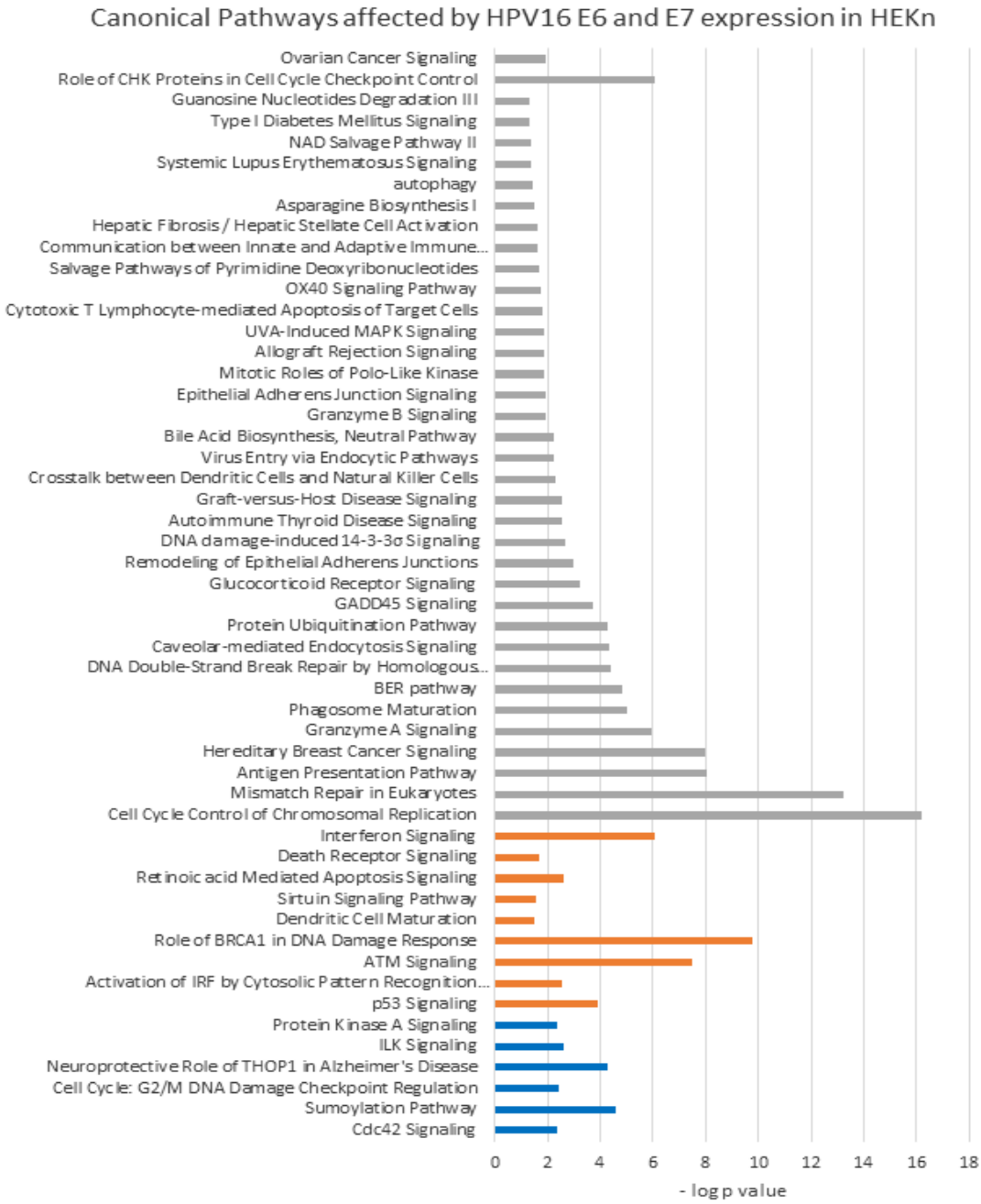

Figure 14. Fifty-two canonical pathways predicted by IPA to be significantly (p-value≤0.05 (-1.3 log10) affected in HEKn expressing HPV16 E6+E7 oncoproteins compared to LV-HEKn control cells. Included in this analysis were proteins significantly differentially abundant by ≥±1.5-fold change. Blue shading indicates a predicted inhibition of canonical pathway, orange shading indicates a predicted increase in activity and grey shading indicates that information regarding the activation of the canonical pathway is not available based on current evidence in the Qiagen Ingenuity Pathway database.

Similarly, there was enough evidence for IPA to predict the increased activation of nine canonical pathways in cells expressing HPV16 E6+E7: The Role of BRCA1 in Damage response, Antigen presentation pathway, ATM signaling, Interferon signaling, Retinoic-mediated apoptosis signaling, Death receptor signaling, Sirtuin Signaling pathway, p53 signaling and activation of Interferon Regulatory Factors (IRF) by cytosolic pattern recognition receptors.

The activation or inhibition of the other 37 canonical pathways could not be predicted based on the current data in the IPA ingenuity database, but included pathways related to DNA damage, antiviral responses, cell survival and proliferation.

Protein Networks and Downstream Effects

The IPA Core Analysis identified 25 dysregulated protein networks from the 678 proteins significantly dysregulated by ≥1.5-fold change in cells expressing HPV16 E6+E7 compared to controls. The predicted biological functions associated with these protein networks include: Cell Cycle, DNA Replication, Recombination and Repair, Cell Morphology, Cellular Movement, Cellular Assembly and Organization; Cell Death and Survival; Antimicrobial Response, Inflammatory Response, Immunological Disease; Cancer; and Dermatological Diseases and Conditions. These are summarized in Table 11.

As shown in Figure 15, STRING analysis of the proteins significantly differentially abundant by ± >2.0-fold change reveals three distinct clusters or groups of multiple protein-protein interactions. The largest protein-protein interaction cluster includes proteins known to be involved in interferon response and inflammation, such as 2'-5'-oligoadenylate synthase 1 (OAS1), Signal transducer and activator of transcription 1 (STAT1) and E3 ISG15-protein ligase (HERC5). The medium sized cluster which includes minichromosome maintenance (MCM)

proteins, also contains proteins involved in mediating cell cycle progression and DNA transcription, and DNA damage response including Breast cancer type 1 susceptibility protein (BRCA1), DNA topoisomerase 2-alpha (TOP2A) and several histones (H1X, H10 H11, H12, H13). The least dense cluster includes several keratins, small proline rich proteins (SPR1A, SPR1B, SPRR2D, SPRR3, SPRR4), and desmocollins (DSC1, DSC2); proteins that are related to the epidermal differentiation. The biological function GO terms assigned to our data by STRING software, and summarized by Revigo, corroborated many of the biological functions identified by IPA network analyses such as cytoskeletal organization, type I interferon signaling pathway and DNA replication (Figure 16).

Table 11. Twenty-five protein networks were identified by IPA based on the proteins differentially abundant by ≥±1.5-fold (0.6 log2) change in cells expressing HPV16 E6 and E7 compared to controls. Proteins listed in red or green font were up or downregulated respectively in our data. The proteins in black font were predicted by IPA to participate in that network but were not among the proteins identified by our experiments. The networks are ranked based on scores calculated for each network. The score reflects the probability of finding the observed proteins in a given network by random chance. A higher score reflects a lower probability. The number of focus molecules is a count of the number of network proteins that were among the significantly differentially abundant proteins in our data. The top diseases and functions are those associated with proteins in a given network. Multiple networks may have similar biological functions or disease predictions.

ID	Molecules in Network	Score	Focus Molecules	Top Diseases and Functions
1	**ACTN1**, **BAG2** ,**BAG3**, **BRCA1**, **DDX21**, **EEF1B2, EEF1G**, **FANCD2**, **FKBP10, FKBP5, FLNC**, **GAN**, **H2AFX, HNRNPC, HNRNPU**, **HSPB1**, **IRF2BPL, LSM8, MCM2, NUMA1, OSBPL9**, PARP, **PPM1G, PRPF19, RBM39, RNPS1, RRS1**, **SDK2**, **SURF6**, **TUBA4A, UBE2E3, USP11**, **YWHAG**, p85 (pik3r), snRNP	48	32	Cell Cycle, DNA Replication, Recombination, and Repair, RNA Post-Transcriptional Modification
2	**APP**, **ARGLU1**, C1orf116, **C1orf174, CCDC137, CFDP1**, **CLIC3**, **DDX49**, **EOGT**, **EXOSC2, EXOSC3**, **EXOSC5, EXOSC6, EXOSC8, EXOSC9, GLB1L, HERC6**, Irp, **KIAA0930, LAD1**, **LAP3, MASTL, MPHOSPH6, POLE3**, **RETSAT**, **SCEL**, **SH3BGRL3**, **SNRNP70, SP140L**, **SPG11**, **SPRR4, TOM1L2, ZCCHC8, ZNF740**, plasminogen activator	47	33	Developmental Disorder, Hereditary Disorder, Neurological Disease
3	**CLN5, DCBLD2**, **DHRS13, DHX40**, **EGLN**, **FBXO6**, **FLG2, FTL**, FXR ligand-FXR-Retinoic acid-RXRα,**GBP1, GMPS, GUSB, HNRNPR**, **IGSF3**, Ifn gamma, **KDELC2, LGALS9**, **MAN2B1, MAN2B2, MANBA**, **MYEF2**, Mannosidase Alpha, P38MAPK, **PAM**, **PHGDH**, **RNASET2, RPS27L, SGSH, SIAE**, **SLC29A1**,**SRSF9, TNFSF9, TP53I3,VLD**L, **VLDLR**	43	29	Carbohydrate Metabolism, Small Molecule Biochemistry, Metabolic Disease
4	**ACTN4, ANLN**, **ARPC3**, Actin, **CALML3, CAP1, CRCT1**, Cofilin,F Actin, **FBLIM1, FLNA, FLNB**, Filamin, **GSN**, LIN54, **MAP4, MYH9, MYL12A, MYL6, MYO5A, MYO6, PALLD, PSTPIP2**, Pka, **RACGAP1**, Rab11, **SLC1A3**, **SLC1A5**, **SSFA2**, **TLK1, TPM1, TPM3, TPM4, TRIAP1**, Talin	41	28	Cell Morphology, Cellular Movement, Cellular Assembly and Organization

5	**BARD1**, BRCA1 complex B, BRCA1-BARD1, BRCA1-BRCA2-FANCD2-FANCN-RAD51, **BRCA2**, **CAMK2G**, **CHTF18, CMPK2**, Cdk, **DSCC1, FANCI, FEN1**, Fanc, **MACROD1, MLH1, MSH2,NBN, PARP2, PCNA, PLEKHA4, RAVER1, RFC1, RFC4, RFC5, RIF1, RNF169, RPA1, RPA2**, **SPRR1A, STAT1, TDRD7**, **TMEM159, TPRG1L**, **TYMP**, pentosyltransferase	41	29	Cancer, Endocrine System Disorders, Hereditary Disorder
6	**A2ML1, ACTR1A, AHNAK, AHNAK2**, Alpha tubulin, Beta Tubulin, **CIT**, **CLIP1, DCTN1, DCTN2, DCTN3, DMKN, DYNC1I2, DYSF**, Dynein,ERK, Hspg, **ING2, KIF14, KIF23, KIF2C, KIF4A**, **MAPRE3, NDEL1**, **PRC1**, S100, **S100A10, S100A2, S100A4**,**SLC43A3**, Sec23, **TRIM29**, **VEZF1, WARS**, tubulin (family)	39	27	Cell Cycle, Cellular Assembly and Organization, Cellular Function and Maintenance
7	Ap2, **BRIX1**, **CSDE1**, Cdc2, Cytokeratin, **DDX27, EBNA1BP2**, **ENAH**, Erm, **FAT1, FTSJ3, H1F0, H1FX**, **HAS3**, **HIST1H1A, HIST1H1C, HIST1H1D, HIST1H1E**, **HOMER3**, Histone H1, Importin beta, **LACTB**, **LYAR, MCAM, MSLN, MTHFD2, NBR1, NUB1**, PI3K (complex), **PLBD2**, **PPAN, PTMA, REXO4, UHRF1**, gelatinase	39	27	Cellular Assembly and Organization, DNA Replication, Recombination, and Repair, Developmental Disorder
8	**ARID5B**, ATM/ATR, **CALML5, CORO1A, CORO1B**, Caspase 3/7, **DSN1**, **EXOC7**, Fgfr, **HMGN2, KIFC1**, L-type Calcium Channel, **MGME1, MIS12**, MLH1-MSH2-MSH6-PMS2, **MSH6, NCAPG2, NCAPH2, NT5C3A, PDIA4, PDS5B, PLCD1**, **PMF1/PMF1-BGLAP, PYGB,** Pde4, Pkc(s), **RSL1D1**, SMC, **SMC1A, SMC2, SMC3, SMC4, UTP23, ZC3H4, ZNF768**	39	27	Cell Cycle, Cellular Assembly and Organization, DNA Replication, Recombination, and Repair
9	**ANPEP,** APC (complex), **ATP6V0A1, ATP6V1B2, ATP6V1G1**, **BAZ1B, CBX1, CBX3, CBX5, CD3EAP, CHAF1A, CHAF1B, DDX50**, HP1, **HP1BP3, INCENP, LBR, LY75, MDC1**, **MPV17L2**, MutS alpha, **NOLC1, NRCAM, NUSAP1, PSIP1, RFC2**, RNA polymerase I, Rnr, SL1, **SP100, TCOF1**, TFIIH, **TMPO, UBTF**, Vegf	37	27	Cellular Assembly and Organization, DNA Replication, Recombination, and Repair, Gene Expression
10	**ADAR, DDX58, EIF2AK2, HELZ2, HERC5, IFI16, IFI35, IFIH1, IFIT1, IFIT2, IFIT3**, IFN Beta, IFN alpha/beta, IFN type 1, IRF, **IRF9, ISG15**, ISGF3, Ifn, Interferon alpha, Interferon-α Induced, JAK, **MX1, MX2, N4BP1, NMI, OASL**, **RPLP1**, **RSAD2, SAMHD1, TNFSF10, TREX1, UBE2L6, UNC93B1,** cytokine	34	25	Antimicrobial Response, Inflammatory Response, Infectious Diseases

11	**ACAA1, ALDH1A3**, AP-3, **BUD13**, **CAMSAP3, CNN2**, **EPSTI1**, **FAM160A1**, Fascin, Ferritin, **HOOK3**, JUN/JUNB/JUND, NCOR-LXR-Oxysterol-RXR-9 cis RA, NFkB (complex), NFkB (family), **NOP14**, **PDLIM1, PI3, PNPT1, PRKRIP1, RBMX2, SERPINB7, SLC2A6**, **SRSF4**, **TACSTD2, TRAPPC9**, **TRIM14, TRIM22**, **VPS41, VPS8**, Vacuolar H+ ATPase, **ZMYND11**, elastase, peptidase, tryptase	32	24	Cellular Movement, Hematological System Development and Function, Immune Cell Trafficking
12	**CA12, CLN8**, **CYP1B1**, Camk, Cytochrome bc1, **DSC2, DSP**, **ESRRA, EVPL**, Focal adhesion kinase, ITPR, **JUP, KLC3, KRT13, KRT15, KRT17**, **KRT19**, **KRT6B,** Mitochondrial complex 1, **NDUFA4L2, PTGS1**, Pde, Pka catalytic subunit, **RCOR3**, **SFN**, **SIRT1**, **SLC9A3R1, SMPDL3A**, **SPOUT1**, **TFAM**, **VAT1**, cytochrome C, cytochrome-c oxidase, estrogen receptor, succinate dehydrogenase	32	24	Cell Morphology, Embryonic Development, Hair and Skin Development and Function
13	**DDX60, DDX60L**, **DPP4**, **DTX3L**, **FAP**, GC-GCR dimer, H2AF, **HLTF**, JINK1/2, **KLK7**, N-cor, **NPC2**, **PARP14, PARP9**, **PDLIM5**, PEPCK, **PLIN2**, **PSPC1**, **RBM3**, **RNF213**, Rar, Rxr, **SAMD9L**, **SLC20A1, SLPI**, **SMCHD1**, **SPINK5**, SRC (family), STAT5a/b, SWI-SNF, Serine Protease, **TGM2, UBR7, WBP4**, growth factor	30	23	Antimicrobial Response, Inflammatory Response, Post-Translational Modification
14	**AKAP13, AKR1C1/AKR1C2, AKR1C3, ASAH1**, Aldose Reductase, **C8A, CES2**, CFB, Complement, **DSC1, DSG1, DSG3**, FUT8, GST, **GSTM2**, IgG1, Igg3, Jnk, **KRT10, KRT16, KRT23, KRT3, KRT4, KRT6A, KRT78, KRT80,** Keratin, Keratin II 6, **LGALS7/LGALS7B**, MAC, **PKP1**, PXR ligand-PXR-Retinoic acid-RXRα, T3-TR-RXR, glutathione peroxidase, transglutaminase	28	22	Dermatological Diseases and Conditions, Organismal Injury and Abnormalities, Hereditary Disorder
15	**DEK**, E2F, **GINS3, HAT1**, Hat, Hdac1/2, Histone h4, **ING1, MCM3, MCM4, MCM5, MCM6, MCM7,** Mcm, **NASP, NOC3L**, ORC, **ORC1, ORC3, ORC4, ORC5**, Pias, **RBBP7, RECQL5**, Ras, **SSRP1**, STAT-1/2, TIP60, **TONSL, TOP1, TOP3A**, Top2, Topoisomerase, histone deacetylase, thymidine kinase	26	21	DNA Replication, Recombination, and Repair, Connective Tissue Disorders, Developmental Disorder
16	**ALS2, APPL1**, CBX4, **CRABP2**, Ctbp, **DNAJC9, EPCAM**, Gsk3, **HDAC7**, HISTONE, **HMGN3**, HSP, **HTRA1**, Hdac, **MBD3**, MEF2, MTORC2, Mi2, **NSMCE2**, **PARP12**, **PML, RAB5B, RCN3, RNF114**, Rab5, **SEMA3C**, **SFRP1**, **SLBP, SMC5**, SUMO, SUMO-Ubc9 E2, **SUMO1, SUMO3**, TCF, Wnt	26	22	Cellular Assembly and Organization, DNA Replication, Recombination, and Repair, Post-Translational Modification

17	**ANGPTL4**, **ANP32B, APOL2,** ATPase, **CBS/CBSL**, **CDA**, **CSPG4**, Casein, **DCK, DHTKD1**, DUB, GOT, HDL, HDL-cholesterol, **HNRNPD**, **HNRNPH3**, HSPG2, **ICAM1**, IL23, Inflammasome (Nalp3, Asc, Casp1), LDL, LDL-cholesterol, **LDLR**, **MBD4**, Nr1h, PRKAA, SAA, **SCD, SLC16A2, SLC25A20, SLC38A7**, SP110, Srebp, VLDL-cholesterol, **VRK1**	24	20	Cardiovascular Disease, Organismal Injury and Abnormalities, Lipid Metabolism
18	**APOE**, Alpha catenin, **CD274**, **CLDN1**, **COL6A1, COL6A2**, Cg, Fgf, Growth hormone, **HMGB1**, Hsp27, IL1, **ITGAV**, Immunoglobulin, Integrin, **LGALS3BP**, **MDK, MMP9**, Mek, Mmp, NADPH oxidase, **PMAIP1, PPHLN1**, Pro-inflammatory Cytokine, **RPP25**, **S100A8, S100A9, SDC1**, **TMBIM1, TNC**, **TXNIP**, Tnf (family), **VEGFC,** c-Src, chemokine	24	20	Cancer, Organismal Injury and Abnormalities, Tumor Morphology
19	**CCNB1**, CDK4/6, **CHTOP**, Cbp/p300, Cyclin D, Cyclin E, **ERH, HMGB2**, Holo RNA polymerase II, I kappa b kinase, **IGFBP4**, IKK (complex), Ikb, Ikk (family), Importin alpha, Insulin, **KIF1C**, **NSMCE4A**, **PDLIM4**, **RBCK1, RBMX**, **RPTN**, Rb, **SMC6, SPIN1, SUPT16H**, **TCEA2, TNFAIP3**, **TNIP1, TRPV2**, Tlr, Tnf receptor, UBE2, **UHRF2**, Ubiquitin	23	19	Cell Death and Survival, Tissue Morphology, Cellular Assembly and Organization
20	26s Proteasome, **CAST, CCND2**, **COL1A1, COL1A2**, **CROT, CSTB**, **CTSK**, **CYR61**, Calcineurin protein(s), Calmodulin, Cathepsin, Collagen type I, Collagen type II, **FHL2**, Fc gamma receptor, Hif1, Hsp90, INA, IgG2b, MKI67, **MUC1, NT5E**, Nos, P glycoprotein, **P3H3, P3H4**, **SERPINB13, SERPINE2**, Tgf beta, **WNK1**, calpain, collagen, trypsin	22	19	Cancer, Organismal Injury and Abnormalities, Reproductive System Disease
21	Akt, Basc, **CDH13**, **CGAS,** Cadherin, Collagen Alpha1, Collagen type VI, DNA Polymerase, DNA-PK, DNA-directed DNA polymerase, **GPNMB**, JAK1/2, **LIG1**, **MFGE8**, MRN, **NDFIP1, OAS1, OAS2, OAS3**, Oas, **PIK3IP1**, **POLD1, POLD2, POLD3**, **POLE**, POLbeta-POLepsilon-POLgamma-XRCC1-LIGI-PARP1-PCNA-FEN1, POLbeta-POLgamma-POLepsilon-XRCC1-LIGI-PARP1, PRIM1, PRIM2, RPA, Rfc, **SCD5**, **SPRR3**, **WDHD1**, nucleotidyltransferase	22	19	Cancer, Hematological Disease, Immunological Disease
22	20s proteasome, **BST2**, C/ebp, **ERAP1**, ERK1/2, HLA Class I, **HLA-B**, HLA-B27, **HLA-C, HLA-E, HLA-F, HLA-G**, Hla-abc, Ifnar, Immunoproteasome Pa28/20s, KIR, MAP1LC3, **MAT2B**, MHC CLASS I (family), MHC Class I (complex), MHC I-α, PKC alpha/beta, **PSMB10**, **PSMB9**, **PSME1, PSME2**, **SBSN, SERPINB3**, Stat1-Stat2, **TAP1, TAP2, TAPBP, TAX1BP1**, Tap, peptide-Tap1-Tap2	20	18	Developmental Disorder, Hereditary Disorder, Immunological Disease

23	**ACOT4, ASNS, B2M, CDK1, CFAP20**, **CRYAB**, Ck2, Creb, Cyclin B, DCD, **DNAJC5**, Dynamin, **FILIP1L**, GADD45, Gcn5l, H-2db, **HSF1, HSPA2**, Histone h3, Hsp70, **LMNB1**, MAP1B, Mlc, NSD2, P-TEFb, PP1 protein complex group, RBM28, RNA polymerase II, Ras homolog, Rock, **SPAG7**, Syntaxin, **TNKS1BP1**, **TOP2A**, mediator	18	18	Post-Translational Modification, Protein Folding, Cell Death and Survival
24	ADCYAP1, **AMACR**, **ATPAF1**, Alp, BCL2, BLACAT1_NR_103783.1, **CCDC9B**, CCND1, **CCPG1, CIR1, CMTR1**, **CYB5R1**, **EFNB2**, **EZH2**, GTPase, HDAC1, HTT, Interferon alpha, MALAT1, MIR101, **MREG**, **PARP9**, POU2F3, **PRR9**, PTBP1, **RAVER2**, **SERF2**, SGSM3, **SNX18**, STAT, **SUZ12**, Smad2/3, TCHHL1, TENM2, miR-200a-5p (and other miRNAs w/seed AUCUUAC)	18	17	Cell Death and Survival, Cellular Movement, Cellular Development
25	**ARL8B**, **BTN3A2**, **BTN3A3**, CD3, **DHRS1, DUSP14, FABP5**, Gamma tubulin, Gm-csf, **HLA-A**, IL-2R, IL12 (complex), IL12 (family), IgG, IgG2a, Iga, Ige, Igm, **KIF5B**, **LAMP3**, Ldh (complex), MHC, MHC Class II (complex), **MVP**, PARP1, PLC gamma, **PLSCR1**, Pld, SCAVENGER receptor CLASS A, SERPINB5, Secretase gamma, **TUBB2A, VPS29, VPS35**, hemoglobin	18	16	Cancer, Endocrine System Disorders, Hereditary Disorder

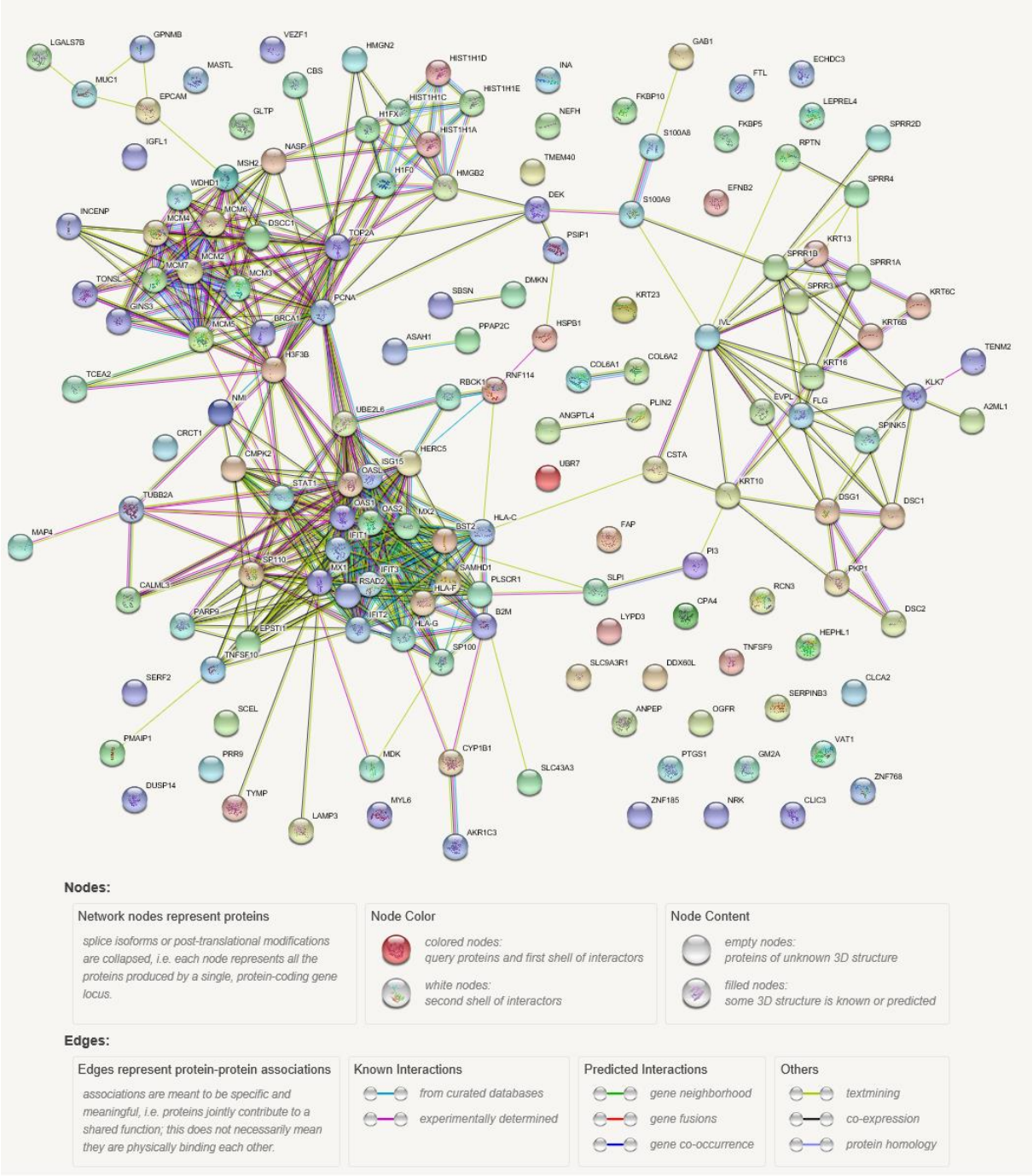

Figure 15. STRING analysis of protein-protein interactions among proteins significantly differentially abundant (p-value ≤0.05) by a minimum of ±2-fold (1.0 log2) between HEKn expressing HPV16 E6+E7 or LV-HEKn controls. The connecting lines do not indicate that the proteins are physically binding but rather that they have shared functions or relationships. Node color is insignificant.

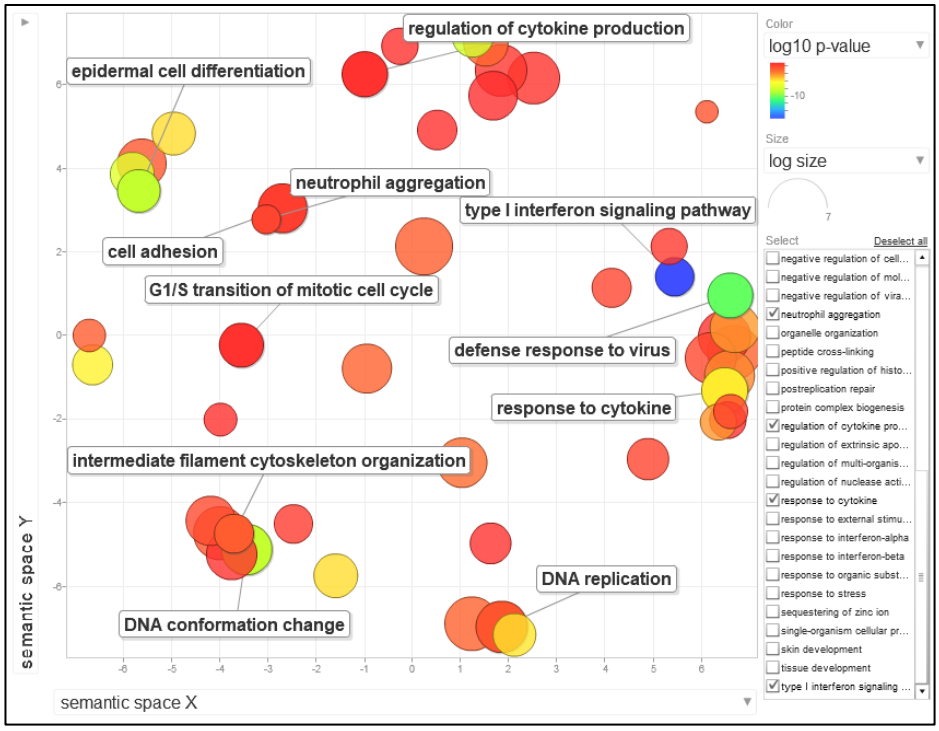

Figure 16. Revigo summary of significantly enriched biological GO terms among the proteins significantly differentially abundant by a minimum of ±2.0-fold (1.0 log2) change in keratinocytes transduced with HPV16 E6+E7 calculated by Revigo. For each class, enriched terms remaining after the redundancy reduction are represented as scatterplots in a two-dimensional space which summarize GO terms' semantic similarities. Semantically similar GO terms are close together in the plot, but the semantic space units have no intrinsic meaning. Bubble color indicates the p-value for the false discovery rates; circle size indicates the frequency of the GO term in the underlying GO database.

4.3 Summary

Of the almost 6000 proteins identified by LC/LC-MS/MS, 280 proteins were significantly differentially abundant due to the presence of the E6 PDZ binding motif. The canonical pathways predicted to be affected by the presence of the HPV16 E6 PDZ binding motif included, p53 signaling, remodeling of epithelial adherens junctions, actin nucleation by ARP-WASP complex, neuro-inflammation signaling pathway, and the antigen presentation pathway. Protein-protein network analyses revealed linkages between several proteins related to immune signaling and inflammatory responses. The second biological trend predicted to be affected by the

presence of the E6 PDZ binding motif was cellular organization and signaling. However, PDZ tight junction and polarity proteins were not among the proteins identified by LC/LC-MS/MS to be dysregulated between the cells expressing the full length or truncated HPV16 E6.

Significantly, the results of our quantitative proteomic analyses support roles for the E6 PDZ binding motif beyond the previously demonstrated role in regulating cell polarity and junctional integrity. Our experiments have resulted in a catalog of proteins which are dysregulated by the HPV16 E6 PDZ binding motif and these affected proteins and pathways may be responsible for the transformative abilities of high-risk HPV *in vivo*. Future functional studies of the significantly differentially abundant proteins will further our understanding of how the HPV16 E6 PDZ binding motif contributes to the viral life cycle.

We have also catalogued the proteomic signatures of HEKn cells expressing HPV16 E6 and E7 proteins. More than 3000 proteins were found to be dysregulated in cells expressing HPV16 E6+E7 compared to controls. Our data support previous gene expression studies linking HPV to the manipulation of the host's DNA damage response pathways, DNA replication, and interferon signaling (160, 179). For example, we have determined that several DNA damage response proteins and interferon modulating proteins including BRCA1, H2AX, SIRT1, and LAMP3 are unambiguously upregulated in primary keratinocytes expressing HPV16 E6 and E7 oncoproteins. This study also revealed proteins, such as the heparin binding protein midkine and the ubiquitinase UCHL1, which warrant further exploration regarding their relationship with HPV infection. Notably, some of these significantly differentially upregulated proteins such as LAMP3 and Midkine have potential as biomarkers or for the development of therapies.

Chapter 5: HPV16 E6 PDZ Binding Motif Effects on HEKn Tight Junction and Polarity Proteins

5.1 Introduction and Rationale

In vitro experiments have previously established the ability of high-risk HPV E6 proteins to bind and degrade PDZ proteins (92,140,180). *In vivo*, high-risk HPV E6-PDZ protein interactions have been demonstrated to degrade or mislocalize PDZ tight junction and polarity proteins (92,99,104,180,181). For example, MAGI1 has been observed to be targeted for degradation by HPV, leading to the mislocalization of ZO1, and altering the integrity of the cellular junctions (99, 180). As previously discussed, the disruption of tight junctions and cell polarity are key events associated with EMT (71).

To determine the consequences of the HPV16 E6 PDZ binding motif on expression and localization of tight junction and polarity proteins in keratinocytes, we employed immunofluorescence microscopy coupled with FIJI imaging software. Corrected total cell fluorescence calculations were made to estimate the level of PDZ proteins of interest in the cells. For this calculation, the level of protein-associated fluorescence, represented as the density of pixels in the cells after accounting for the background fluorescence, is measured using FIJI software's Particle Measurement function (170).

Quantitative immunofluorescence microscopy is highly susceptible to various sources of error which can hamper its accuracy and precision. Errors may be introduced during the preparation of the specimen, during imaging or processing of images. To mitigate sources of error from specimen preparation, biological replicates from each of the three cell lines were prepared simultaneously so that each cell line was treated with the same antibody dilution and the same incubation times.

Using a confocal microscope for these experiments prevented the capture of unfocused light. Confocal microscopes illuminate the specimen with a focused light source, using a pinhole at the image plane to block unfocused fluorescence light from the detector. Additionally, to ensure that fluorescent signals specifically associated with the proteins in our specimens were captured, the emission and detection levels were set to exclude background signal and non-specific noise. Cell controls, incubated with secondary antibodies only, were prepared in parallel with experimental cells lines and used to determine the illumination and detection settings, as well as to verify antibody specificity. Identical magnification and camera exposure times were used for all images.

To avoid bias in calculating the protein abundance from the digital images, 12 cells, per cell line, were used to calculate the level of protein of interest; six from each of two biological replicates. Each cell was measured thrice, and the average measurement was used to determine the protein-associated fluorescence in each cell. Also, the average of three background measurements from areas without any cells was used in the corrected total cell fluorescence calculation.

5.2 Results

We visualized the level and distribution of the tight junction proteins JAM1, ZO1, and MAGI1. JAM1 is a transmembrane tight junction protein which lacks a PDZ motif. ZO1 and MAGI1 are tight junction proteins, each with multiple PDZ motifs.

Although MAGI1 is classified as a tight junction protein, this protein is a cytoplasmic-plaque protein, and is distributed throughout the cytoplasm rather than concentrated at the cell junctions. This was observed in all three of the cell lines (Figure 17). Based on the calculated

corrected total cell fluorescence, the levels of MAGI1 in the keratinocytes expressing HPV16 E6+E7 were significantly lower than in HPV16 E6ΔPBM+E7 expressing cells ($p=0.024$) or LV-HEKn control cells ($p=0.002$). MAGI1 levels were not significantly different between the control cells and the HPV16 E6ΔPBM+E7 expressing cells ($p=0.08$). Although previously determined to be a target of HPV16 E6 degradation, MAGI1 was not among the proteins detected by LC/LC-MS/MS experiments (99, 180).

JAM1 was mainly distributed along the periphery of the cells, at the location of the cellular junctions with some distribution throughout the cytoplasm (Figure 17). Corrected total cell fluorescence calculations revealed that the levels of JAM1 were not significantly different among the three cell lines (ANOVA ($p=0.137$). Interestingly, the LC/LC-MS/MS experiments did not detect a difference in JAM1 levels between the HPV16 E6+E7 and HPV16 E6ΔPBM+E7 but, JAM1 levels were significantly lower in the HPV16 E6+E7 cells compared to the control cells, albeit by only 1.2-fold change. It is likely that immunofluorescence microscopy and corrected total cell fluorescence calculations lack the sensitivity to discern a 1.2-fold change difference.

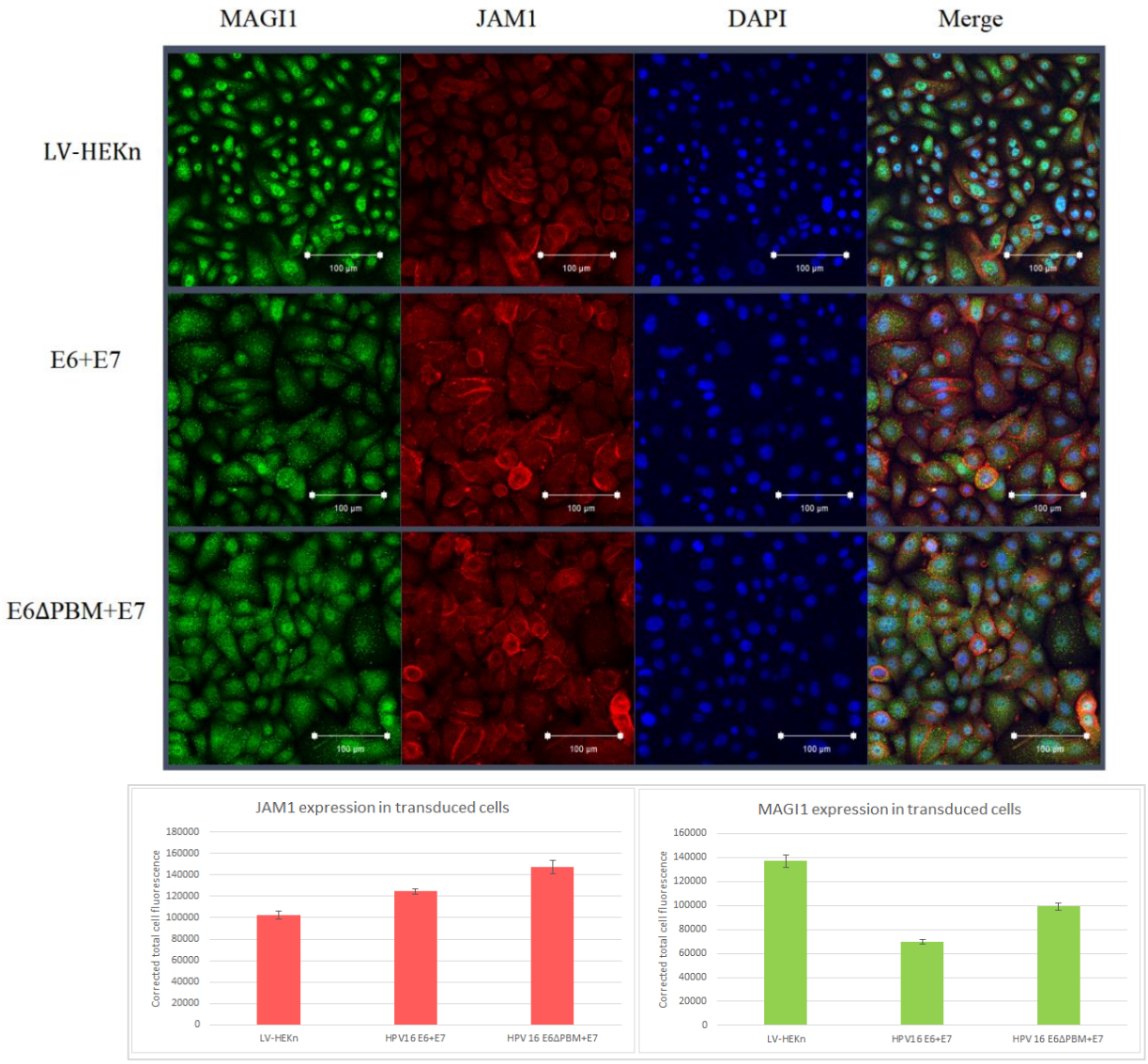

Figure 17. Immunofluorescence microscopy of MAGI1 and JAM1 tight junction proteins in the three cell lines. MAGI1 (green) is distributed throughout the cytoplasm and is not concentrated at the cellular junctions in any of the cell lines. JAM1 (red) is mainly concentrated at the periphery of the cells with some cytoplasmic distribution. The nuclei are stained blue with DAPI. The bar charts represent the corrected total cell fluorescence associated with JAM1 (red) or MAGI1 (green) in the three cell lines. The levels of JAM1 were not calculated to be significantly different among the cell lines ($p=0.137$). The levels of MAGI1 in the keratinocytes expressing HPV16 E6+E7 were significantly lower than in HPV16 E6ΔPBM+E7 expressing cells ($p=0.024$). Similarly, MAGI1 was lower in HPV16 E6+E7 expressing cells compared to LV-HEKn control cells ($p=0.002$). MAGI1 levels were not significantly different between the control cells and the HPV16 E6ΔPBM+E7 expressing cells ($p=0.08$). Scale bars =100µM.

Even though both MAGI1 and JAM1 are tight junction proteins, we observed JAM1 to be mainly localized at the cell junctions while MAGI1 was distributed throughout the cytoplasm. Therefore, we investigated whether MAGI1 colocalizes with JAM1 in HEKn cells and whether this interaction is altered by the presence of the full-length HPV16 E6 protein. To quantify the level of colocalization we used FIJI software to calculate Pearson's correlation coefficient and Mander's coefficient of overlap. (Table 12). Pearson's correlation coefficient is used to describe the intensity distribution between the two channels of interest and can range from -1.0 to 1.0. A coefficient of 1.0 means that there is 100% colocalization while a negative result indicates an absence of colocalization. Considered to be the more biologically relevant measure of colocalization, Mander's coefficient of overlap measures the overlap of fluorescent signals and can range from 0 to 1 (172). A value of 1 indicates that 100% of both channels colocalize.

As can be seen in Figure 18, there were areas of colocalization, represented by white pixels, in each of the cell lines but these were generally not located at the sites of cell to cell contact where tight junctions occur. The amount of colocalization between JAM1 and MAGI1 was highest in the control cells, and this is likely due to the higher levels of MAGI1 in the control cells, *i.e.*, there was more MAGI1 available to colocalize with JAM1. Based on Mander's coefficient calculations, the largest amount of colocalization was observed in the control cell lines with 69% of the green channel (MAGI1) overlapping with the red channel (JAM1), and alternatively 65% of the red channel (JAM1) overlapping with the green channel (MAGI1). The Pearson's coefficient in LV-HEKn cells was 0.26, indicating a low level of colocalization between JAM1 and MAGI1.

Some of the residual MAGI1 in the E6+E7 and E6ΔPBM+E7 cells does appear to colocalize with JAM1, as indicated by the white pixels in Figure 18. The cells expressing the

full-length HPV16 E6+E7 yielded a Mander's score of 50% in the MAGI1: JAM1 overlap calculation, and 40% in the JAM1: MAGI1 overlap calculation, but yielded a negative Pearson's correlation coefficient, indicating absence of correlation (-0.05). Similarly, colocalization between JAM1 and MAGI1 was reduced in HPV16 E6ΔPBM+E7 cells. The signal overlap in cells transduced with the HPV16 E6ΔPBM+E7 did not correlate very strongly (40% MAGI1: JAM1 and 17% of JAM1: MAGI1), and this was also reflected in the low Pearson's correlation coefficient score measured for these cells (0.04).

Although the Mander's coefficients of overlap were not large for any of the cells, the values were significantly different among the three groups (MAGI1:JAM1 p-value= 4.8e-05; JAM1:MAGI1 p-value= 5.3e-04). From these results it appears that JAM1:MAGI1 interactions, and ultimately tight junctions, are affected by HPV oncoproteins. The Pearson's correlation coefficient however, was not found to be significantly different among the three cell lines (p-value=0.84). Despite efforts to minimize imprecision, inconsistencies due to unequal staining, uneven illumination, or inconsistent measurements may have influenced these results.

Table 12. FIJI Colocalization Threshold between JAM1 and MAGI1 in the three experimental cell lines. LV-HEKn cells had the highest amount of colocalization. Interestingly the cells expressing HPV16 E6+E7 yielded a negative Pearson's correlation indicating an absence of correlation, but moderate overlap was indicated by Mander's coefficient calculations. Colocalization between JAM1 and MAGI1in HPV16 E6 ΔPBM+E7 cells was also very low.

		LV-HEKn	E6+E7	E6ΔPBM+E7	p-value (ANOVA)
Manders Correlation	green signal	0.69	0.5	0.39	*4.8E-05*
	red signal	0.65	0.4	0.17	*5.3E-04*
Pearson's correlation coefficient		0.26	-0.05	0.04	*0.84*

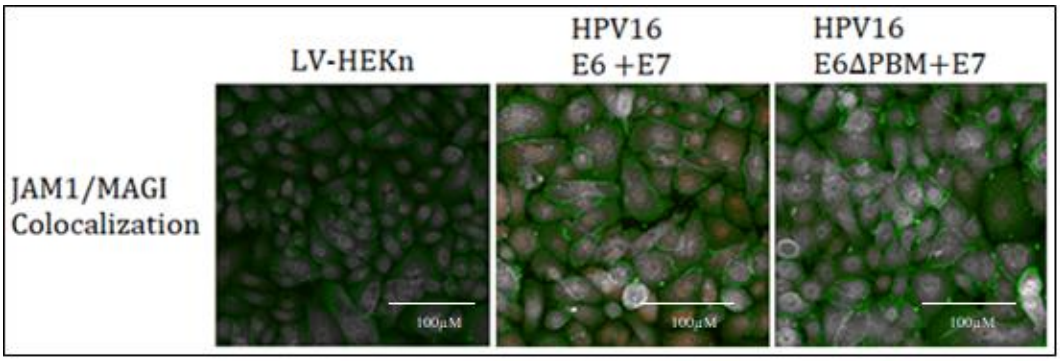

Figure 18. Colocalization of MAGI1 and JAM1 are shown in LV-HEKn, HPV16 E6+E7, and HPV16 E6ΔPBM+E7 cells. The Colocalized pixels are shown as white and non-colocalized pixels (green=JAM1 or red=MAGI; in these images the original colors are reversed by the software). These images were analyzed with FIJI software. Scale bars =100μM

The levels and distribution of the tight junction PDZ protein ZO1 and the PDZ polarity protein PAR3 were also assessed by immunofluorescence microscopy. The loss of MAGI1 from HPV16 positive cells has previously been shown to alter the location of ZO1 and PAR3 (99).

The levels of ZO1 were found to be similar among the three cell lines by immunofluorescence microscopy ($p=0.528$). In comparison, the levels of ZO1 and ZO2 were found to be lower by LC/LC-MS/MS in the HPV16 E6+E7 cells compared to the LV-HEKn cells by 1.2-fold and 1.1-fold, which may not be biologically significant. Neither ZO1 nor ZO2 were found by LC/LC-MS/MS to be significantly differentially abundant in HPV16 E6+E7 compared to HPV16 E6ΔPBM+E7 cells. Again, the lower sensitivity of immunofluorescence microscopy and corrected total cell fluorescence calculations is likely the reason for the discrepancy between LC/LC-MS/MS and the immunofluorescence microscopy results.

The distribution of ZO1 was very noticeably altered in the cells expressing the oncoproteins. As shown in Figure 19, ZO1 proteins were mainly dispersed throughout the cytoplasm rather than at the periphery of the cells in the HPV16 E6+E7 or HPV16 E6ΔPBM+E7 cells, but were highly concentrated at the cellular junctions in the LV-HEKn control cells.

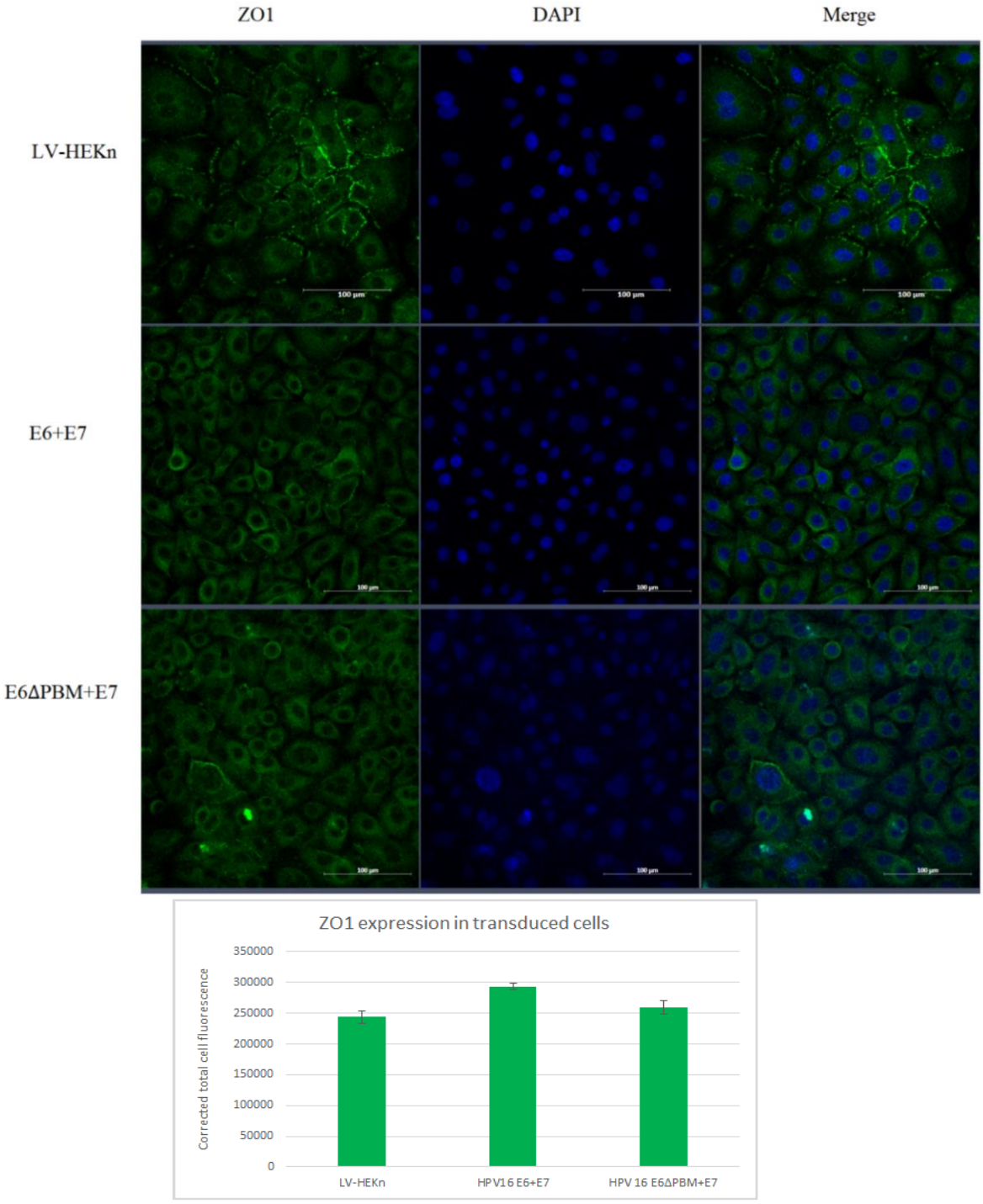

Figure 19. Immunofluorescence microscopy images of ZO1 (green) in LV-HEKn, HPV16 E6+E7, and HPV16 E6ΔPBM+E7 cells. Nuclei stained with DAPI (blue). In the cells expressing HPV16 proteins, ZO1 appears to have a more cytoplasmic distribution compared to the control cells where ZO1 stained distinctly at the cellular junctions. The overall amount of ZO1 is not significantly different among the three cell lines (ANOVA, p=0.528) Scale bars =100µM.

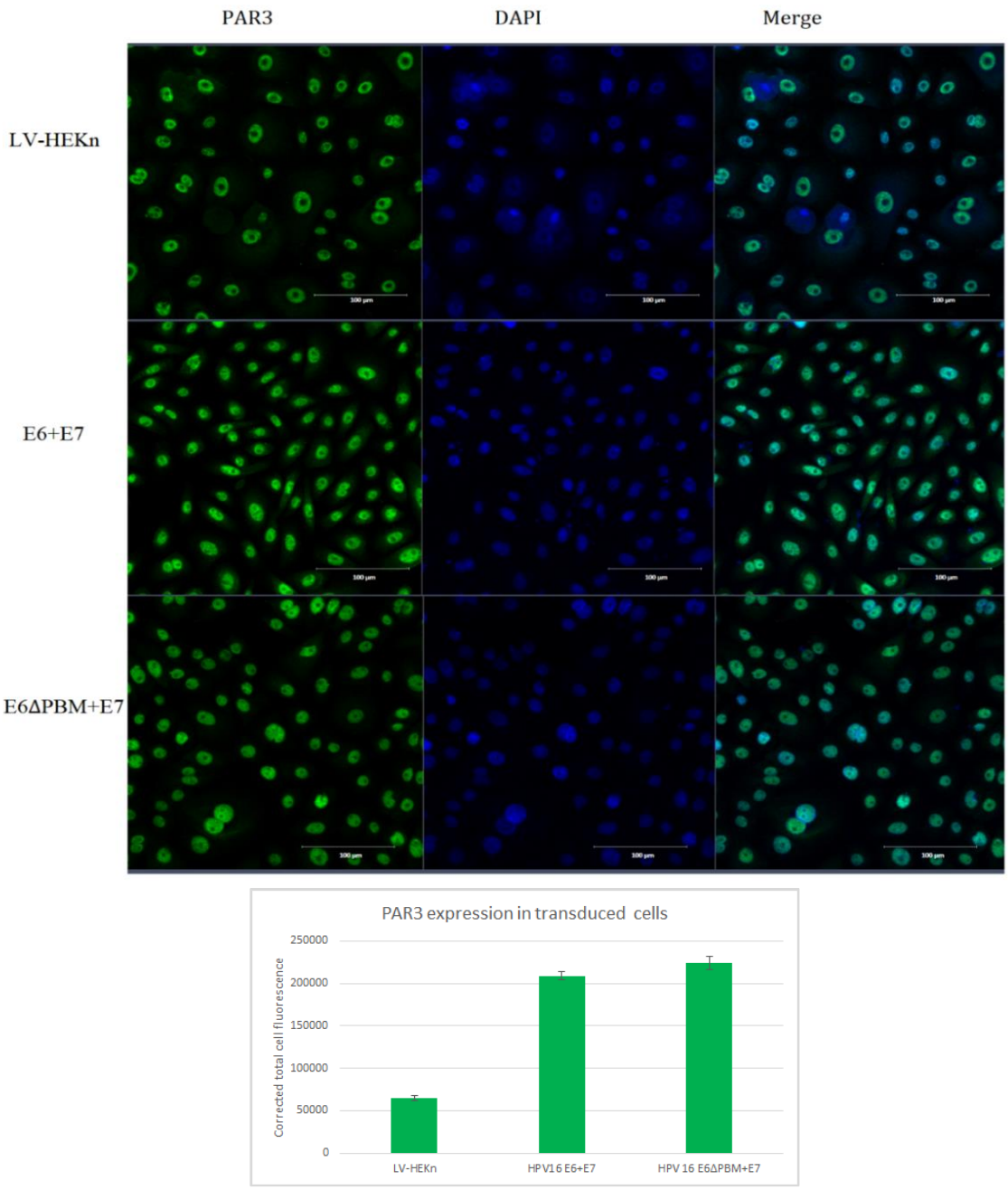

Figure 20. Immunofluorescence microscopy images of polarity protein PAR3 (green) in LV-HEKn, HPV16 E6+E7, and HPV16 E6ΔPBM+E7 cells. PAR3 has a nuclear distribution in all three cell lines. As well as some cytoplasmic distribution in HPV16 E6+E7 and LV-HEKn cells. Nuclei were stained with DAPI (blue). The levels of PAR3, based on corrected total cell fluorescence were significantly higher in the cells expressing the truncated HPV E6 oncoprotein, or the full-length E6 protein compared to the control cells (p=2.0e-04; p=8.1e-06). However, the level of PAR3 was not significantly different between the HPV oncoprotein expressing cells (p=0.586), suggesting the PDZ binding motif was not responsible for the increased PAR3 levels. Scale bars =100µM.

The polarity protein PAR3 had a nuclear or perinuclear distribution in the control cells and HPV16 E6ΔPBM+E7 cell lines. In the cells expressing the full-length HPV16 E6+E7, PAR3 was located in both cytoplasmic and perinuclear regions of the cells. Figure 20.

The levels of PAR3, based on corrected total cell fluorescence, were significantly higher in the cells expressing the truncated HPV E6 oncoprotein, or the full-length E6 protein (p=2.0e-04; p=8.1e-06) compared to the control cells. Interestingly the PAR3 levels were not significantly different between the cells expressing either the full-length or truncated HPV oncoproteins (p=0.586) suggesting the PDZ binding motif was not responsible for the increased PAR3 levels. PAR3 was not among the proteins detected by our LC/LC-MS/MS experiments.

5.3 Summary

Using immunofluorescence microscopy, we documented the level and distribution of tight junction and polarity proteins in our three transduced cell lines.

The expression of the HPV E6+E7 or E6ΔPBM+E7 did not significantly alter the levels of the non-PDZ tight junction protein JAM1. However, levels of the PDZ protein MAGI1 were found to be significantly reduced in the cells expressing the full-length HPV16 E6 compared to the cells expressing HPV16 E6ΔPBM+E7. MAGI1 has previously been shown to be a target of HPV16 E6 in a PDZ binding motif-dependent manner, and our results are in agreement with those earlier studies (104, 180).

Although JAM1 was found to be mainly located at the site of cell junctions, and MAGI1 had a cytoplasmic distribution, colocalization experiments indicated that JAM1 and MAGI1 proteins colocalize in HEKn. This interaction was reduced in the full length HPV16 E6+E7 cells and E6ΔPBM+E7 cells and this is likely due to the reduction in MAGI1 levels in these cells. It

was surprising however, that the cells expressing E6ΔPBM+E7 had the lowest levels of colocalization as calculated by the Mander's colocalization coefficient.

Future investigations into the transepithelial resistance of tight junctions in HPV oncoprotein expressing cells could be used to explore the influence of the E6 PDZ binding motif in these structures.

Levels of ZO1 were not found to be significantly different among the cell lines, but the distribution of ZO1 was noticeably altered in the cells expressing the oncoproteins compared to the controls. The ZO1 proteins were not concentrated at the site of cell junctions in the cells expressing HPV oncoproteins; evidence that the HPV oncoproteins influence cellular junctions. However, because these changes were observed in both E6+E7 and E6ΔPBM+E7 cell lines, these results suggest that the HPV16 E6 PDZ binding motif is not required for the mislocalization of ZO1.

The levels and localization of the PDZ polarity protein PAR3 were also investigated in our three cell lines. PAR3 was increased in the cells expressing HPV oncogenes regardless of the presence or absence of the E6 PDZ binding motif, suggesting that the E6 PDZ binding motif is not responsible for the elevated PAR3 levels. Interestingly, PAR3 was only observed in the nuclear and perinuclear region of the cells expressing the truncated HPV E6ΔPBM+E7, while the LV-HEKn control cells and HPV16 E6+E7 cells had both a nuclear and a diffuse cytoplasmic distribution of PAR3. It appears that the lack of the E6 PDZ binding motif in the HPV16 E6ΔPBM+E7 cells restricted PAR3 to the nucleus.

The results of the immunofluorescence microscopy experiments demonstrate that PDZ proteins associated with host tight junctions and polarity complexes were altered in HEKn cells expressing HPV oncoproteins. Due to the differences in sensitivity and precision, it is difficult

to compare immunofluorescence microscopy results to LC/LC-MS/MS results for specific proteins, especially if they are dysregulated by a very small fold change. One of the limitations associated with our immunofluorescence experiments is the challenge of comparing different experimental cell lines, particularly since the control cells were not immortalized. However, our immunofluorescence microscopy results, together with our LC/LC-MS/MS results, indicates that the HPV16 E6 and E7 proteins disrupt HEKn tight junctions.

Chapter 6: Discussion

6.1 The effects of the HPV16 E6 PDZ binding motif on HEKn cells

All high-risk HPV E6 proteins have a PDZ binding motif on their carboxyl-termini. This molecular feature is absent from all low-risk HPV types and is considered to be a marker of carcinogenic potential. Despite this carcinogenic classification, the significance of the PDZ binding motif in the cellular processes leading to transformation is unclear. This lack of clarity is due to conflicting evidence regarding the necessity of the PDZ binding motif for immortalization and transformation (66-68). There is evidence that the PDZ binding motif allows the high-risk HPV E6 proteins to bind and degrade or mislocalize PDZ tight junction and polarity proteins which can disrupt cell-cell contacts, communication, and organization, potentially promoting EMT (65, 99, 181). However, Watson *et al.* found that the E6 PDZ binding motif enhances, but is not necessary for EMT (31). Thus, the significance of the HPV16 E6 PDZ binding motif for keratinocyte immortalization and transformation requires further investigation.

Here we sought more definitive evidence of the role of the E6 PDZ binding motif in HPV transformation by the transduction of primary HEKn cells with lentiviruses carrying full-length HPV16 E6 genes or truncated HPV16 E6 genes lacking the carboxyl-terminal PDZ binding motif. This is a physiologically appropriate model and permitted the evaluation of the effects of the HPV16 E6 PDZ binding motif on growth, immortalization, transformation, and global proteomic dysregulation of keratinocytes. The effects of the E6 PDZ binding motif on tight junctions were visualized using immunofluorescence microscopy. Additionally, the effects of HPV16 E6+E7 expression on the global dysregulation of the keratinocyte proteome were explored.

6.2 Effects of the HPV16 E6 PDZ binding motif on p53

Significantly, our Western blot experiments confirmed that the E6 PDZ binding motif is not required for the degradation of the pro-apoptotic protein p53, but does significantly enhance this process. HEKn transduced with either HPV16 E6+E7 or HPV16 E6ΔPBM+E7, showed decreased p53 levels compared to LV-HEKn controls with the lowest levels observed in the cells expressing the full E6 gene. This evidence supports that the PDZ binding motif enhances anti-apoptotic mechanisms.

Notably, an earlier study by Choi *et al.* also found that the HPV16 E6 PDZ binding motif was not required for p53 degradation; however, they did not confirm whether the presence of the PDZ binding motif enhanced p53 degradation (67). In their study, keratinocytes expressing either HPV16 E6 and E7 or HPV16 E6 lacking a PDZ binding motif and E7 both had a similar reduction in p53 levels; although they did not quantify the p53 levels (67). The mutated E6 protein used by Choi *et al.* was missing only the final four amino acids at the carboxyl-terminus, while our truncated E6 protein was missing the last twelve amino acids, and this difference may account for the significant reduction in p53 levels in HPV16 E6+E7 cells compared to the HPV16 E6ΔPBM+E7 cells in our study. We chose to eliminate the amino acids upstream of the canonical four PDZ binding motif amino acids because there is evidence that these amino acids contribute to PDZ protein binding (93, 182, 183). Also, we wanted to ensure that E6-PDZ protein binding was completely impaired and excluding the carboxyl-terminus from the HPV16 E6 protein is expected to prevent the HPV16 E6ΔPBM from interacting with PDZ proteins similar to the low-risk HPV6 E6 protein.

One important way that HPV16 E6 is known to target p53 for degradation is via ubiquitination and proteasomal degradation in association with the E6AP ubiquitin ligase. The shorter carboxyl-terminus of the HPV16 E6ΔPBM protein used in our experiments, compared to that used by Choi *et al*., may have had a greater effect on the optimal E6AP-E6 heterodimer complex. Alternatively, the binding interface between the E6 protein and the target may be where the E6 carboxyl-termini has the most influence.

Recently, Martinez-Zapien *et al*. solved the crystal structure of the heterotrimer formed by HPV16 E6, E6AP, and p53 (184). They determined that the E6-E6AP heterodimer forms a cleft into which p53 can be bound. Interestingly, the authors discovered that the critical mutations which affect the E6-p53 interface and disrupt p53 degradation are in the N-terminus of E6 (184). Similarly, an earlier study found that mutations in the E6 N-terminal residues 9-13 abrogated E6-E6AP formation and p53 degradation (185). Although the carboxyl-terminal residues, Leu100 and Pro112, were noted by Martinez-Zapien *et al.*to interact with p53, the significance of the HPV16 E6 carboxyl-terminal PDZ region for the formation of the heterotrimer was not explored (184). Similarly using cross-linking mass spectrometry techniques, Sailer *et al.* verified that binding to high-risk HPV E6 proteins induces a conformational change in E6AP (186). This results in the positioning of E6-p53 in the catalytic centre of E6AP and facilitates the ubiquitination of p53 (186). These authors did not examine whether the PDZ tail influenced the interactions among these three proteins, however.

The HPV18 E6* splice transcript, which lacks the carboxyl-terminus, is unable to bind to p53 according to a study by Pim *et al.*; further evidence that the carboxyl-terminus of high-risk HPV E6 is important for p53 degradation (187). Additionally, low-risk HPV E6 proteins bind to

p53 with lower affinities than the high-risk E6 proteins *in vitro,* and do not foster proteasomal degradation of p53 (188).

HPV16 E6 is also known to promote p53 dysregulation independently of E6AP. For example, HPV16 E6 can bind to the histone acetyltransferase hADA3 and preventing the acetylation of p53 by p300/CBP (CRE-binding protein) (189-191). It is likely that the E6 PDZ binding motif does not influence every mechanism used by E6 to promote p53 degradation and this could explain why p53 levels were moderately reduced in the E6ΔPBM+E7 cells.

Because p53 levels were observed to be influenced by the presence of the E6 PDZ binding motif in Western blot experiments, it was surprising that p53 was not among the proteins detected by LC/LC-MS/MS. It is possible that p53 levels were not detected by LC/LC-MS/MS due to imprecision, leading to false negative results. Alternatively, because of the limited number of trypsin cleavage sites in p53, it is possible that there were not many usable spectra (178). Notably, p53 signaling was among the canonical pathways predicted to be affected by the presence of the HPV16 E6 PDZ binding motif. This indicates that p53 related proteins were dysregulated in these cells and supports our finding that the PDZ binding motif influences p53 degradation.

Others have also documented a relationship between E6 PDZ binding motif and p53 degradation. Brimer *et al*. found that the E6 PDZ binding motif was essential for episomal genome maintenance unless p53 levels were knocked down (70). Persistence of the HPV episomal genome is a hallmark of HPV-associated cancers.

The fact that the HPV16 E6 PDZ binding motif, a molecular feature unique to high-risk HPV, clearly enhanced the reduction in p53 levels in our study is significant because the

mutation, degradation, or functional repression of the p53 pro-apoptotic tumour suppressor is a characteristic of many types of cancer including those associated with oncogenic viruses (192).

The ability of the high-risk, but not the low-risk, HPV E6 proteins to target p53 for proteasomal degradation is well established and here we have clearly shown that the HPV E6 carboxyl-terminus influences p53 levels in keratinocytes. Important next steps will be to clarify and explore the mechanisms by which the HPV16 E6 PDZ binding motif enhances p53 degradation. It will also be crucial to investigate the effect of the truncated E6 carboxyl-terminus on the E6ΔPBM protein's stability.

6.3 Effects of the HPV16 E6 PDZ binding motif on immortalization and transformation

Immortalization, a state of indefinite cell proliferation, is one of the initial steps in the development of cancer. The expression of telomerase, an enzyme which prevents the shortening of telomeres with each cell division cycle, is regarded as the key to cell transformation as hTERT is not normally expressed in somatic cells (29). Several previous studies have found that the E6 PDZ binding motif is not required for HEKn immortalization however, only high-risk types of HPV are known to induce hTERT expression (59, 67, 68, 193). Therefore, we wanted to determine if the HPV16 E6 PDZ binding motif influences hTERT expression and immortalization.

Importantly, we discovered that when transduced with lentiviruses carrying HPV16 E6 and E7 or E6ΔPBM and E7 genes, the HEKn cells could continue to proliferate for more than twice as long as the control cells transduced with empty lentivectors. Increased longevity strongly indicated that these cells may be immortalized and that the E6 PDZ binding motif is not required to achieve this extended proliferative state. In addition to extending their longevity, both HPV16

E6+E7 and E6ΔPBM+E7 cells had increased levels hTERT compared to the control cells, as measured by Western blot. However, the cells expressing the full length HPV16 E6 had significantly higher levels of hTERT. This proved that, although the PDZ binding motif is not essential for hTERT expression, it does enhance its expression. Thus, we can conclude that the carboxyl-terminus of the HPV16 E6 protein affects hTERT; but the mechanisms associated with this still need to be determined.

The expression of hTERT requires two E box cis elements that flank the hTERT promoter, and these are normally bound by the Upstream transcription factor 1 (USF1) or c-Myc which competitively regulate hTERT expression (194-196). Several studies have shown that the E6-E6AP heterodimer binds to the E boxes and interacts with c-Myc to drive hTERT expression (197-199). It is possible that the E6 PDZ binding motif's influence on the heterotrimer (E6AP-E6-cMyc) structure may be key to this interaction as it may enhance the affinity of the E6-E6AP heterodimer for c-Myc and ultimately enhance hTERT activation.

High-risk HPV E6 proteins may also influence hTERT expression through modulation of the chromatin structure. For example, HPV16 E6 proteins have been shown to modulate histone acetyltransferase (HAT) and histone deacetylase (HDAC) recruitment to the hTERT promoter (200). NFX1-91, a transcriptional repressor of hTERT, recruits HDAC to repress hTERT transcription. However, NFX1-91 has been shown to be targeted by E6-E6AP for proteasomal degradation, increasing the HAT activity at the hTERT promoter (200). The E6-E6AP heterodimer created through the interaction of E6ΔPBM and E6AP may not be optimal for targeting NFX1-91, and permit NFX1-91 to repress hTERT expression.

The reduction in p53 and the elevation of hTERT expression, associated with the full-length E6 proteins, in our experiments show that the E6 PDZ binding motif enhances these key

effects of high-risk HPV E6 proteins. These results suggest that the presence of the E6 PDZ binding motif could be the difference between immortalization and full transformation.

Although the cells transduced with HPV oncoproteins had elevated levels of hTERT and reduced levels of p53 relative to the control cells, none of the cell lines demonstrated the capacity for anchorage-independent growth in soft agar, the phenotypic hallmark of transformed cells. Lack of growth in soft agar was not entirely surprising as previous studies have suggested that HPV-associated transformation of HEKn may also require a secondary factor such as oncogene activation or exposure to estrogen (47-49). Malignant transformation *in vivo* is a multistep process that requires accumulation of oncogenic mutations, and requires decades of progression. Likely, our *in vitro* transduction system did not run long enough for full transformation and anchorage independent growth to become apparent.

6.4 Effects of the HPV16 E6 PDZ binding motif on the HEKn proteome

We measured the global dysregulation of proteins in cells expressing the either full-length or truncated HPV16 E6 genes plus lentiviruses carrying HPV16 E7 genes. Proteomic analyses identified 280 proteins significantly dysregulated between the cell lines HPV16 E6+E7 or HPV16 E6ΔPBM+E7. Gene ontology and pathway analyses were performed using the 142 proteins significantly differentially abundant by ≥1.3-fold change. Based on these analyses, canonical pathways and downstream biological functions associated with cellular organization and immune responses were predicted.

Cellular organization

Most viruses are known to engage and modify the actin cytoskeleton at varying stages of their life cycle to promote viral entry, replication, and egress (201). Also, there is evidence that HPV16 E6 proteins dysregulate junctional and polarity proteins contributing to EMT in a PDZ binding motif-dependent manner (31, 99). Therefore it was not surprising that proteins associated with cellular organization and cytoskeletal change were found to be dysregulated in HPV E6+E7 cells compared to E6ΔPBM+E7 cells. The prediction of altered cytoskeletal organization and epithelial adherens junctions made by IPA was based on the high levels of differentially abundant intermediate filaments including Neurofilament heavy polypeptide (NFH), Neurofilament light polypeptide (NFL), CO6A2, Actin-related protein 2/3 complex (ARC1A), Actin Related *Protein* 2/3 Complex Subunit 3 (ARPC3), and reduced levels of MARE1 in HPV16 E6+E7 cells.

Intermediate filaments are cytoskeletal proteins, which include keratins, vimentins, and neurofilaments. Peculiarly, among the intermediate filaments which were dysregulated in cells expressing full-length HPV16 E6 PDZ binding motif were NFH, NFL, and AINX. These proteins are typically found in neurons, and their altered expression has been associated with the altered localization of mitochondria in neurons (202). Perhaps the upregulation of the neurofilaments is related to the upregulation of UCHL1, a deubiquitinase that is typically expressed in neurons. UCHL1 has previously been shown to associate with microtubule and cytoskeletal structures (214). The overexpression of NFH, NFL, and AINX has not been previously documented in HEKn expressing HPV16 E6 and E7 nor has their dysregulation been associated with PDZ binding motifs.

The MARE1 protein, also known as EB1, regulates microtubules, affects cell polarity, chromosomal stability and interestingly, interacts with the tumor suppressor protein

adenomatous polyposis coli (APC) (203). The dysregulation of microtubules and mitotic spindles in cells expressing the HPV16 E6 proteins has been previously documented (204). Here we have the first evidence that HPV16 E6 PDZ binding motif dysregulates the expression of MARE1 which could have implications for mitotic spindle stability. Dysregulation of mitotic spindles and chromosomal alignment could potentially introduce carcinogenic mutations.

EMT is a process during which epithelial cells lose their cell polarity, lose cell-cell contacts, and gain migratory and invasive properties as they become mesenchymal stem cells. Although a normal part of wound healing mechanisms, anomalous EMT is associated with the initiation of metastasis and cancer expression. Fittingly, since changes to cellular organization, polarity and cytoskeletal organization are part of the EMT process, the HPV E6 PDZ binding motif has previously been found to enhance EMT in keratinocytes (31, 99).

One of the first steps in the process of EMT is the loss of cellular junctions and polarity (205). While we did not observe a reduction in PDZ tight junction proteins associated with full-length E6+E7 expressing cells compared to truncated E6ΔPBM+E7 cells in our proteomic data, we did observe that the E6 PDZ binding motif was associated with altered levels and locations of PDZ proteins, such as MAGI1 and PAR3, in immunofluorescence microscopy experiments.

Notably, the diffusion of ZO1 from cell-cell contacts is a recognized attribute of EMT, and this was observed by immunofluorescence microscopy in the HPV oncoprotein expressing cells, regardless of the PDZ binding motif (206). Other hallmarks of EMT are loss of E-cadherin, and increased levels of fibronectin and N-cadherin; however none of these proteins were found to be dysregulated in HPV16 E6+E7 expressing cells compared to HPV16 E6ΔPBM+E7 by LC/LC-MS/MS (206).

The modulation of PDZ tight junction proteins observed by immunofluorescence microscopy and the prediction of changes to the cytoskeletal organization and adherens junctions by IPA supports the observation by Watson *et al.* that the E6 PDZ binding motif enhances EMT (31). However, EMT was not observed in any of our cell lines, nor did we see changes in the levels of specific EMT-associated proteins in our experimental data; thus further work is required to be able to confidently conclude that the PDZ binding motif has a role in promoting EMT.

Immune responses and inflammatory responses

Our proteomic data identified several differentially abundant proteins, canonical pathways and enriched biological GO terms associated with immune responses and inflammation in cells expressing the full-length HPV16 E6+E7 genes as compared to the cells with the truncated E6 genes, signifying that the E6 PDZ binding motif influences immune responses and inflammation. Biological downstream functions predicted to be affected in cells expressing the full-length HPV16 E6+E7 genes included, “Immune response”, “Type I interferon signaling pathway”, “Defense response to virus”, strongly indicating that the NFkB signaling pathway is affected by the E6 PDZ binding motif. Also, from the LC/LC-MS/MS experiments several NFkB related proteins, including UCHL1, BST2, and ICAM1 were identified as significantly upregulated in cells expressing the full length HPV16 E6 genes. HPV16 oncoproteins have previously been associated with increased NFkB signalling in a E6 PDZ binding motif dependent manner and the pathway analysis of our LC/LC-MS/MS data supports this (59).

NFkB

The NFkB signaling pathway is a key part of the innate immune response. Stimulated upon TLR activation, NFkB induces antiviral, inflammatory cytokines such as interferon and interferon-stimulated genes. The dysregulation of NFkB signaling is an important strategy used by many viruses to disrupt cytokine production and promote cell survival signaling (207).

The NFkB signaling pathway was identified among the top-ranked protein interaction networks affected in cells expressing the full-length HPV16 E6+E7 compared to the truncated HPV16 E6ΔPBM+E7. Previous studies have linked the HPV16 E6 proteins to the dysregulation of NFkB signaling pathways, leading to either the activation or inhibition of NFkB signaling depending upon the stage of infection (208, 209). Tilborghs *et al.* proposed that, initially HPV infection activates NFkB signaling pathways yielding an inflammatory response, and then, once the HPV infected cells become immortalized, the activity of NFkB is reduced (210). However, only activation of NFkB was associated with the E6 PDZ binding motif by James *et al*. (59). There was not enough information in our data for IPA to be able to predict whether the NFkB signaling pathway would be activated or inhibited in the cells expressing HPV16 E6+E7 compared to HPV16 E6ΔPBM+E7, so further study is required.

UCHL1

The upregulation of ubiquitin carboxyl-terminal hydrolase L1 (UCHL1) in HPV16 E6+E7 cells suggests that the E6 PDZ binding motif may downregulate NFkB signaling. UCHL1 is an enzyme that catalyzes the hydrolysis of carboxyl-terminal esters and amides of ubiquitin, and was among the significantly differentially abundant proteins upregulated in cells expressing the full-length HPV16 E6+E7 proteins. Increased levels of UCHL1 in high-risk HPV have previously been shown to permit the virus to evade the immune response by inhibiting the

polyubiquitination of tissue necrosis factor receptor-associated factor 3, promoting the degradation of the NEMO (NFkB essential modulator) and impairing NFkB signaling (211). However, NEMO was not among the differentially abundant proteins in our data, so the role of upregulated UCHL1 in the HPV16 E6+E7 cells is not clear. Importantly though, our data provides the first link between the HPV E6 PDZ binding motif and increased UCHL1 expression in HEKn cells.

HPV is not the only virus known to alter UCHL1 expression. Notably, two other oncoviruses, Epstein Barr Virus (EBV) and Kaposi's Sarcoma-associated herpesvirus (KSHV) (also known as human herpes virus 8), have been demonstrated to increase UCHL1 expression, affecting cell proliferation, adhesion, migration and inhibition of apoptosis (212-214). Bentz *et al.* determined that EBV's Latent Membrane Protein 1 (LMP1) and the KSHV Latency-associated Nuclear Protein (LANA) both activate the UCHL1 promoter via an interaction with the Notch-activated transcription factor RBP-Jk (215). The EBV EBNA2 protein also activates the UCHL1 promoter, through its interaction with the PU.1 promoter (216). The mechanism behind the HPV16 E6 PDZ binding motif's ability to upregulate UCHL1 is unknown.

Notably, UCHL1 co-localizes with microtubules in the mitotic spindle and can regulate cellular actin and microtubule networks (214). In fact, Bheda *et al*. have suggested that interactions between UCHL1 and the cytoskeleton explain this enzyme's association with tumorigenic phenotypes, such as increased cell proliferation, adhesion, and migration (214). For example, UCHL1 over-expression has been linked to EMT in prostate cancer (217). Further evidence of UCHL1 effects on the cytoskeleton came from a study by Brasseres *et al*., who found that UCHL1 alters the cytoskeleton in HeLa cells and this fosters their invasion by *Listeria monocytogenes* and *Salmonella enterica* (218). Recall that, cytoskeletal proteins were among the

proteins dysregulated in association with the expression of full-length E6+E7. Therefore, further investigations into whether there is a relationship between the upregulation of UCHL1 and altered cytoskeletal proteins or increased mitotic defects in HEKn should be considered.

BST2

The transmembrane protein, BST2, also known as tetherin, was one of the most upregulated proteins in the HEKn cells expressing full-length E6 compared to either E6ΔPBM+E7 or LV-HEKn cells. Generally, overexpression of BST2 has not been described to confer many advantages to viral life cycle. In fact, BST2 is known to inhibit the egress of several enveloped viruses from their hosts. In response, HIV1 encodes a protein, Vpu, which counteracts BST2 to permit the virions to exit their host (219). Similarly, KSHV's K5 protein, a RING-CH E3 ubiquitin ligase, targets BST2 to the proteasome for degradation to allow viral egress (220). Conversely, high levels of BST2 can enhance the entry of cytomegaloviruses (CMV) into the host (221).

BST2 is expressed in response to TLR activated interferon expression. Interestingly, BST2 acts as a negative feedback regulator to inhibit interferon production (222). It does this through an interaction with the immunoglobulin-like transcript 7 in plasmacytoid dendritic cells (222). The ability to modulate interferon levels would be beneficial for limiting the negative consequences of extended interferon exposure on the cell. BST2 was one of the most upregulated proteins in the HEKn expressing full-length E6 proteins. Perhaps the elevated levels of BST2 associated with the HPV16 E6+E7 cells could serve to counteract elevated interferon levels.

Alternatively, the increased expression of BST2 in HPV16 E6+E7 may promote host survival. BST2 targets the pro-apoptotic protein BIM (Bcl-2-like protein 11) for degradation, inhibiting anoikis (223). Mahauad-Fernandez and Okeoma recently described a mechanism by which BST2 dimerization activates ERK1/2 and phosphorylates and degrades BIM, preventing anoikis in breast cancer cells (272). However, this strategy may not be relevant to our E6+E7 expressing cells as BIM was not significantly differentially expressed in our LC/LC-MS/MS data. Verification of BIM levels in the HPV16 E6+E7 cells may clarify the feasibility of this hypothesis.

While increased levels of BST2 have been recorded in several types of cancer, including cervical cancer tissue, this is the first time the HPV16 E6 PDZ binding motif is linked to increased BST2 expression (224-226). It is unclear whether the increased BST2 expression associated with HPV16 E6+E7 expressing cells offers any advantage to HPV lifecycle, such as providing negative feedback for interferon expression, preventing anoikis, or if increased BST2 expression is simply the result of a heightened immune response.

ICAM1

The intercellular cell adhesion molecule-1 (ICAM1), also known as CD54, is a cell surface glycoprotein that is induced by interleukin-1 (IL-1) and tumor necrosis factor (TNF) as part of the immune response (227). ICAM1 binds with the Lymphocyte function-associated antigen 1 to facilitate intercellular contacts required for T helper responses, T-dependent B cell responses, antigen-induced T cell proliferation, and NK cell-mediated cytotoxicity (228). Thus, it is not surprising that several viruses have evolved mechanisms to exploit or modulate ICAM1. For example, the human-T cell Lymphoma virus (HTLV) protein p12I, and the KSHV protein K5

have been described as reducing ICAM1 expression to prevent T cell responses (229, 230). On the other hand, rhinoviruses take advantage of ICAM1 on the surface of their hosts to gain entry (231).

Since the expression of ICAM1 enhances immune responses, it is not clear how the upregulation of ICAM1 in our HEKn transfected with HPV16 E6+E7 benefits the viral lifecycle. Nevertheless, our observation that the HPV16 E6 PDZ binding motif is associated with increased ICAM1 supports a previous study by, Textor *et al.*, who observed that only high-risk and not low-risk HPV E6 proteins induce ICAM1 (232). Interestingly, Textor *et al.* also concluded that the induction of ICAM1 expression by high-risk HPV requires the activation of the NFkB signaling pathway, and this may mean that the NFkB signaling pathway is upregulated in the cells expressing HPV16 E6+E7 (232).

Clarification of the status of the NFkB signaling pathway in HPV16 E6+E7 expressing cells is required. Our LC/LC-MS/MS results strongly support the modulation of NFkB signaling and immune responses by the PDZ binding motif, but whether NFkB signaling is upregulated or repressed remains to be elucidated.

6.5 Effects of the HPV16 E6 PDZ binding motif on Tight Junction and Polarity Proteins

As previously mentioned, PDZ proteins were not among the significantly differentially abundant proteins affected by the absence of the E6 PDZ binding motif in our LC/LC-MS/MS data. This was surprising because there have been many previous studies that have described the ability of the E6 PDZ binding motif to bind and degrade PDZ proteins (87, 92, 99, 104, 233). It is possible that limitations of peptide preparation, or inaccuracy of the LC/LC-MS/MS processes,

impaired the detection of some of the PDZ proteins anticipated to be altered by HPV E6 expression.

There were a few PDZ proteins significantly decreased in the cells expressing full-length E6+E7 compared to LV-HEKn controls including GIPC, GOPC, DLG 1, 4 and 5, ZO1, ZO2, and Scribble; however, the fold changes associated with these proteins were very small, below the cut-off values set for inclusion in our gene ontology and pathway analyses. Notably, similar decreases in the expression of GIPC and DLG were observed in cells expressing HPV16 E6ΔPBM+E7 compared to the control cells, precluding the necessity of the PDZ binding motif for their dysregulation. Interestingly, Choi *et al.* also found that the presence of the full-length HPV E6 protein did not result in a reduction in endogenous PDZ proteins in keratinocytes transduced with HPV16 E6 lacking the PDZ binding motif (67).

Another possibility for the lack of dysregulated PDZ proteins could be related to the phosphorylation status of the E6 PDZ binding motif. The HPV16 E6 PDZ binding motif possesses a protein kinase A (PKA) phosphor-acceptor site, and it has previously been shown that upon phosphorylation the ability of E6 to bind PDZ proteins is abrogated (234, 235). The phosphorylation of the E6 PDZ binding motif directs the E6 proteins to interact with 14-3-3 proteins instead of PDZ proteins (234, 235). There are seven members of the 14-3-3 protein family, and these proteins influence cell signaling and cell cycle checkpoint control, and are often dysregulated in a variety of cancers, including HPV16 infected oral squamous cell carcinomas (236-239). None of the 14-3-3 proteins were observed to be differentially abundant in the cells expressing full-length E6+E7 compared to the truncated E6ΔPBM+E7 cells; but all were significantly downregulated in the E6+E7 cells compared to LV-HEKn controls.

It is unlikely that the E6 PDZ binding motif in E6+E7 cells was impaired because the E6 PDZ binding motif was shown to alter PDZ proteins in our immunofluorescence microscopy experiments. We observed that the distributions and levels of tight junction or polarity PDZ proteins in HPV16 E6+E7 cells were altered, supporting previous studies which have also shown that tight junction and polarity proteins interact with high-risk HPV E6 proteins in a PDZ binding motif-dependent manner (240-242). This is important because the loss of tight junctions and cell polarity and adhesion are traits associated with EMT and support the idea that the HPV16 E6 PDZ binding motif promotes EMT.

Tight junction proteins

MAGI1 degradation has been well documented, and so it was not surprising to observe that the level of the PDZ tight junction protein MAGI1 was significantly lower in the cell lines expressing HPV16 E6+E7 (180). Kranjec and Banks previously demonstrated the degradation of MAGI1 by high-risk HPV is detrimental to the integrity of tight junctions (180). In that study, the ablation of E6 from CaSki cells restored MAGI1 expression and relocated the tight junction protein ZO1 to the periphery of the cells at the cellular junctions (180). Similarly, in our experiments, the expression of high-risk HPVE6 was associated with lower levels of MAGI1 and an altered distribution of ZO1 compared to that of the LV-HEKn control cells. In the control cells, ZO1 was observed at the sites of cell to cell contracts, while in the cells expressing HPV16 E6+E7, ZO1 was dispersed throughout the cytoplasm. Interestingly, the loss of ZO1 from sites of cell to cell contact is a trait also observed during the initiation of EMT (206).

Remarkably, the cells expressing the truncated HPV16 E6ΔPBM+E7 also showed a reduction in MAGI1 and altered ZO1 distribution, but not to the same degree as the cells

expressing full-length E6. This enhanced degradation of MAGI1 associated with the PDZ binding motif is reminiscent of our previously discussed p53 results. Recall the E6 PDZ binding motif was not required, but enhanced p53 degradation. Notably, like p53, MAGI1 is also known to be targeted for proteasomal degradation by E6 (92, 243). This suggests that the PDZ binding motif optimizes the E6AP-E6-MAGI1 heterotrimer structure, configuring the E6 cleft and E6 interface to enhance the affinity with MAGI1. In fact, Charbonnier *et al*. examined the interaction between E6 and MAGI1 using Nuclear magnetic resonance spectrometry and they determined that residues upstream from the PDZ binding motif enhance the interaction between HPV16 E6 and MAGI1 (182).

Mislocalization of ZO1 by HPV16 E6 may stimulate cell signaling pathways, leading to cell proliferation. Previous studies have found that ZO1 forms a complex with ZONAB, and this complex is translocated to the nucleus in proliferating cells where it influences cell proliferation in a cell density-dependent manner (102). Interestingly, LC/LC-MS/MS experiments found the levels of ZO1 to be lower in the HPV16 E6+E7 cells compared to the LV-HEKn cells by 1.2-fold change (0.25log2), while ZO1 levels were not significantly different between cells expressing full length vs truncated E6+E7. When measured by corrected total cell fluorescence, the levels of ZO1 in the immunofluorescence microscopy images were not found to be significantly different among our three cell lines. However, as previously mentioned, differences in the sensitivities of these two methods make it difficult to compare their results, particularly when the fold changes in question are very small and may not be biologically significant.

Changes in JAM1 levels associated with HPV oncoproteins have not previously been reported, but an immunofluorescence microscopy study using mouse fibroblasts demonstrated

that JAM1 binds to PAR3 and ZO1 (244). We did not observe a decrease in JAM1 levels in association with the HPV16 E6 PDZ binding motif, by immunofluorescence microscopy, and this was not surprising because JAM1 is not a PDZ protein. However, like the LC/LC-MS/MS results for ZO1, there was a -1.2-fold (0.25log2) change in JAM1 levels in cells expressing HPV16 E6+E7 compared to controls. Our immunofluorescence microscopy methods were not likely able to discern this small difference in expression.

We were curious to determine whether modulation of MAGI1 by HPV16 E6 would alter the tight junction transmembrane protein JAM1. Colocalization experiments revealed that there was a moderate amount of colocalization between JAM1 and MAGI1 in LV-HEKn control cells. In comparison to the control cells, colocalization was reduced in cells expressing HPV oncoproteins, independent of the E6 PDZ binding motif. We concluded that the reduced level of colocalization in E6+E7 and E6ΔPBM+E7 cells is likely linked to the reduced levels of the PDZ protein MAGI1. Further investigations into the colocalization between JAM1 and ZO1 may provide better evidence of tight junction disruption by E6 proteins, since those protein have previously been demonstrated to interact (244). Also, future investigations into the functional integrity of the HPV16 E6+E7 cells may provide insight into the E6 PDZ binding motif's contribution to tight junction disruption and EMT.

Polarity proteins

Although classified as a polarity protein, the PDZ protein PAR3 is also involved in the formation of tight junctions and is known to interact with the tight junction proteins (244). High-risk HPV can modulate PAR3 as demonstrated by Facciuto *et al*., who found that high-risk HPV18 E6 expression was associated with a redistribution of PAR3 from cell junctions to the

cytoplasm (119). They did not observe a change in the level of PAR3 in HaCat cells expressing HPV18 E6 proteins. Conversely, Zheng *et al.* observed that PAR3 levels were reduced in cervical cancer specimens, and this reduction was associated with a poor prognosis (245). Furthermore, Zheng *et al.* determined that silencing of PAR3 in SiHa cells results in increased expression of EMT-associated genes, including N-cadherin, E-cadherin, and β-catenin (245). In our immunofluorescence microscopy experiments, the level of PAR3 was not significantly different between the cell lines expressing either full or truncated E6 proteins but was significantly increased in comparison to control cells. Thus, the PDZ binding motif may not affect the level of PAR3 expression in keratinocytes, but the expression of HPV oncoproteins increases PAR3 expression.

Increased expression of PAR3, along with its nuclear localization, may indicate that PAR3 is promoting cell proliferation in the E6+E7 and E6ΔPBM+E7 cell lines. In confluent MDCK cells PAR3 localizes to the tight junctions and in sub-confluent cells PAR3 localizes to the nucleus, where it can interact with transcriptional activators (120, 246). The role of PAR3 in the cytoplasm, as observed in our E6+E7 and control cells, is not clear. Although the PAR3 fluorescence in the cytoplasm is not strong, we don't believe that this cytoplasmic detection is noise because, in addition to the precautions taken to avoid false signals, the signal is only associated with cells and is not seen in the background areas in the absence of cells.

In summary, our experiments demonstrated that some tight junction-associated PDZ proteins are altered in association with the expression of the full length HPV16 E6 and E7 proteins, but the E6 PDZ binding motif is not essential for all of these interactions. Previous studies have demonstrated that PDZ proteins vary in their affinities for the HPV16 E6 PDZ binding motif, and this may explain the variety of interactions observed here (89, 93). The

presence of the PDZ binding motif enhanced the degradation of MAGI1 but did not appear to alter the mislocalization of ZO1. An increase in PAR3 expression was observed in both full-length and truncated E6 cell lines. Taken together with the proteomic data, these immunofluorescence microscopy results show that the HPV16 E6 PDZ binding motif alters cellular junctions and the cytoskeleton. These effects may be the key to promoting immortalization and transformation of HEKn by high-risk HPV types.

Analyses of MAGI1 and JAM1 colocalization did not provide information on whether the E6 PDZ binding motif alters the functional integrity of the HEKn tight junctions. Measurement of the transepithelial electrical resistance of cell junctions in cells expressing the HPV oncoproteins could confirm if the permeability of tight junctions is indeed altered by E6 expression.

6.6 Global dysregulation of HEKn proteome by HPV16 E6 and E7 proteins

Although not directly associated with our hypotheses, our LC/LC-MS/MS experiments provided us with an opportunity to document the HPV16 E6+E7-mediated dysregulation of proteins in HEKn cells as compared to control LV-HEKn cells. While there have been gene expression studies looking at the effects of HPV in infected tissues, our study is unique as it used a sensitive, quantitative LC/LC-MS/MS approach. We catalogued over 3000 proteins which were dysregulated in HEKn by HPV16 E6+E7, substantially adding to the current knowledge of proteins affected by HPV16. It is important to continue to investigate the cellular environment associated with persistent expression of high-risk HPV E6 and E7 proteins because how these proteins influence cell transformation is not completely understood (39, 247-250). Knowledge of the proteins and pathways altered by the E6 and E7 oncoproteins should illuminate the

mechanisms of viral persistence and the immune evasion tactics employed by HPV16 E6 and E7, leading to transformation. Additionally, the identification of proteins potentially useful for the management of persistent HPV infections are of great interest.

DNA Damage Repair and Viral Replication

The HPV proteins E1 and E2 are essential for viral replication; the E2 protein recognizes the viral origin of replication and recruits the E1 helicase to the site (16, 251). Our proteomic data confirms a supporting role for HPV 16 E6 and E7 oncoproteins in viral replication, as they modulate proteins associated with DNA damage response and repair pathways (252, 253).

DNA damage response pathways detect and repair breaks in dsDNA. Typically, when a cell's DNA is damaged one of the cellular DNA damage response pathways, ATM or ataxia-telangiectasia mutated Rad3-Related (ATR), becomes activated, arresting the cell cycle until the damage is repaired. As part of the innate immune system, members of the DNA damage repair pathway can also sense foreign DNA and initiate a response (254).

Viruses, such as HPV and polyomaviruses, have evolved mechanisms to appropriate their host's DNA repair machinery to amplify their viral genome. HPV, simian virus 40 (SV-40) and several herpesviruses, activate Ataxia-telangiectasia mutated (ATM) signaling and recruit DNA repair factors for viral replication (255-257).

A recent LC/LC-MS/MS study explored the proteomic alterations associated with various stages of cervical cancer and the authors found that DNA repair pathways were altered in the early stages of cervical cancer (162). Interestingly, ATM signaling, and DNA Double-Strand Break Repair by Homologous Recombination pathways were also among the canonical pathways predicted to be significantly activated in the cells expressing HPV16 E6+E7 in our study.

Specifically, members of the ATM pathway, Breast cancer type 1 susceptibility protein (BRCA1) and the histone H2AX, were significantly upregulated in the HPV16 E6+E7 cells.

Upon detection of DNA damage, the histone H2Ax locates to the site of damage and is phosphorylated by ATM to ɣ-H2AX. Both BRCA1 and ɣ-H2AX , together with other members of the DNA damage response system, activate cell cycle checkpoints to arrest the cell cycle and then initiate homologous recombination or non-homologous end-joining DNA repair (258, 259).

Because of BRCA1's tumour suppressive nature, it may seem peculiar that HPV E6 and E7 would promote the expression of BRCA1; however, Kudoh *et al.* have found that HPV E6 and E7 bind to BRCA1 and prevent it from repressing the estrogen-receptor-α (ER-α) transcriptional activity that inhibits c-Myc transactivation (260). The upregulation of BRCA1 in our data also supports recent study by Mehta *et al.* that described an important role for BRCA1 in HPV infections (253). Those authors found that HPV causes breaks in both cellular DNA and viral episomal DNA, and then HPV recruits the dsDNA repair enzymes, including BRCA1, to the damaged DNA to foster viral amplification (253). Mehta *et al*. found that the DNA repair enzymes BRCA1 and RAD51 were preferentially recruited to the site of damage in the viral episomes (253). The authors concluded that the damage to cellular DNA induced by HPV very likely contributes to the genetic instability, which leads to transformation (253). Either E6 or E7 oncoproteins were found to be able to induce DNA breakage, but the combination of E6 and E7-induced the most damage (253). Coincidentally, the HTLV TAX protein, which also possesses a PDZ binding motif, causes breaks in cellular DNA and its ability to do this relies on the activation of NFkB (261). Furthermore, NFkB activation is required for HTLV TAX transformation (262)

Six Mini-Chromosome Maintenance (MCM) proteins were upregulated in HEKn cells expressing HPV16 E6 and E7 compared to the controls. These MCM proteins make up an essential component of the DNA pre-replication complex. As part of that complex, six MCM proteins (MCM2 -MCM7) form a hexamer and together, with cell division cycle 6 (CDC6) and Chromatin Licensing And DNA Replication Factor 1 (CDT1), bind to a DNA origin of replication to initiate DNA replication (263). MCM protein dysregulation is strongly associated with cell proliferation and may be significant prognostic biomarkers for several types of cancer, including cervical cancer (264-266). Our results show that the HPV16 E6 and E7 proteins induce MCM dysregulation in keratinocytes and modulate DNA repair and replication mechanisms. The increase in MCM proteins observed in the cells expressing HPV16 E6+E7 is likely due to the repression of pRb by E7. pRb loss, or repression, is known to permit cyclin E1, a target of pRb, to recruit MCM proteins to pre-replication complexes (267). YAP and TAZ expression has also been cited for promoting the upregulation of MCM protein transcription leading to cell proliferation in lung cancer (268). YAP and TAZ proteins are key regulators of the HIPPO signaling pathway. However, neither of these proteins, nor the HIPPO signaling pathway were identified by IPA to be altered in HPV16 E6+E7 expressing cells compared to control cells.

Deacetylases

Histone deacetylases (HDAC) and Sirtuin (SIRT1) also known as NAD-dependent deacetylase sirtuin-1, are commonly dysregulated in cancers, including HPV-associated cancers (269-273). Via the modification of protein acetylation, HPV can evade the host's immune system and promote viral DNA replication (271, 273, 274).

Here we have proteomic evidence supporting the differential expression of protein deacetylases related to HPV16 E6 and E7 expression. Among the upregulated proteins from HEKn cells expressing HPV16 E6 and E7, there were three protein deacetylases, HDAC2 and HDAC7, and sirtuin (SIRT1) which were upregulated by 1.4, 1.5, and 1.7-fold change respectively. Notably, the expression of HDAC and SIRT1 have previously been linked to HPV immune evasion strategies. For example, HPV E7 reduces TLR9 expression by recruiting HDAC2 to the TLR9 regulatory region, and this results in the repression of interferon responses (274). Recently, So *et al.* found SIRT1 was able to repress the AIM2 (absent in melanoma inflammasome) innate immune response in HPV positive cells, promoting their survival and proliferation. However, our experiments did not identify a change in AIM1 or AIM2-associated proteins, such as interleukin-1β or caspase (272).

The upregulation of SIRT1 in the E6+E7 cells is quite interesting as this protein may have several roles in HPV infection, including immune evasion, replication, and cell survival (268, 273, 275). SIRT1 forms a complex with HPV E1and E2 proteins at the HPV origin of replication, then deacetylates E2 and recruits the DNA repair protein Werner helicase (WRN) (252, 273, 275). Fittingly, the Werner helicase interacting protein 1 was observed to be upregulated in HEKn cells expressing E6 and E7.

The fidelity of HPV replication also relies on SIRT1 expression because knockdown of SIRT1 in HPV16 infected cells fails to recruit to the E1/E2 complex and leads to a highly mutated genome (273, 275). Furthermore, SIRT1 knockdown in HPV31 infected cells diminishes the number of viral genomes in the host cells (271).

Finally, SIRT1 may also play a role in the abrogation of the p53 pro-apoptotic signaling pathway. Acetylation of p53 prevents its repression by Mdm2 by blocking the recruitment of

Mdm2 to p53-responsive promoters. Remarkably, SIRT1 deacetylates p53 (276). Thus, an increase in SIRT1 by HPV16 E6 and E7 could lead to the deacetylation of p53 by SIRT1, causing it to be repressed and promoting cell survival.

Potential Biomarkers

In our study, LAMP3 was significantly upregulated in HPV16 E6+E7 cells compared to the LV-HEKn controls. LAMP3, also known as DC-LAMP, is an integral membrane lysosomal-associated membrane protein whose role is not well defined, but previous studies have associated LAMP3 with increased levels of interferon-dependent anti-viral genes (277). There is some evidence that LAMP3 is required for cell survival during proteasomal inhibition, and there have been some recent investigations into the role of LAMP3 in different cancers (175, 176). For example, in osteosarcoma cells, LAMP3 significantly increased cell viability and abrogated apoptosis by regulating p53 expression (176). Furthermore, LAMP3 overexpression is associated with increased metastatic potential, and LAMP3 may be an important prognostic biomarker for a variety of cancers including cervical cancer (278-281). In fact, LAMP3 mRNA was found to be highly expressed in 100% of cervical cancers (278). In HeLa cells, LAMP3 was found to be associated with increased levels of interferon-dependent anti-viral genes STAT-1, IRF7, HERC5, ISG20, and OAS1 (277). Similarly, in our data, STAT-1, HERC-5, and OAS1 were upregulated in the cells expressing HPV16 E6 and E7 proteins. Whether LAMP3 expression is responsible for STAT-1, HERC-5, and OAS1 expression in HEKn remains to be determined.

Another one of the most upregulated proteins in HPV16 E6+E7 cells compared to controls was Midkine (MK). This is quite interesting because MK has previously been reported to be upregulated in cervical, bladder, esophageal and gastric cancers and increased levels of MK

are associated with poor prognosis indicating that MK may be a useful biomarker for persistent HPV (282-285).

MK, also known as neurite growth-promoting factor 2 (NEGF-2), is a heparin-binding cytokine that promotes cell survival, proliferation, and migration. For example, when MK was added to the medium of cultured neuronal cells, Owada *et al.* found that MAPK and PI3K were activated and the pro-apoptotic protein caspase-3 was inhibited (286). In Wilms tumour cells, MK was found to enhance the expression of BCL-2 survival protein (287). Also, MK promotes cell proliferation and survival by phosphorylating the ALK (anaplastic lymphoma receptor kinase) in fibroblasts leading to MAPK and PI3K activation (288). The activation of MAPK and PI3K does not fit with our data however, as IPA predicted MAPK to be strongly inhibited in the cells expressing HPV16 E6+E7.

The implications of MK upregulation in HEKn expressing HPV16 E6 and E7 remains to be explored and may be worth pursuing as MK has also received attention as a possible therapeutic target to treat malignant mesothelioma (289). The dysregulation of MK by other oncogenic viruses has not been described, but MK has been found to inhibit HIV infection (290).

Keratinized Barrier

The dysregulation of epidermal differentiation and the inhibition of the formation of the keratinized barrier was another interesting trend highlighted in our proteomic analyses of keratinocytes expressing HPV16 oncoproteins. Seven of the top ten downregulated proteins in the HPV16 E6+E7 cell line were associated with epidermal differentiation: proline-rich protein 9, elafin, repetin, keratin type II, small proline-rich protein 3, involucrin, and filaggrin. The downregulation of proteins involved in epidermal differentiation and the keratinized barrier was not unexpected because a previous gene expression study also found several genes associated

with keratinocyte differentiation to be downregulated in keratinocytes expressing high-risk E6 proteins; including elafin, small proline-rich proteins, keratins, and involucrin (291).

Elevated levels of inflammatory cytokines in HEKn expressing E6+E7 may be responsible for the downregulation of proteins of the keratinized barrier. In a proteomic analysis of cervicovaginal lavage specimens from a cohort of HIV negative sex workers, patients with elevated levels of inflammatory cytokines also had decreased levels of proteins associated with the keratinized barrier including, small proline-rich proteins, filaggrin, and involucrin (292). The keratinized envelope acts as a mechanical and permeability barrier, and so its inhibition by HPV might be essential to foster the egress of viral particles from the host.

Normally, primary keratinocytes undergo an irreversible differentiation process forming a keratinized envelope when deprived of anchorage to a semi-solid medium (293). Malignant cells, on the other hand, fail to differentiate and do not form a keratinized envelope when cultured in an anchorage-independent manner (293). The downregulation of proteins associated with the keratinized barrier suggests that the cells expressing HPV16 E6+E7 would be defective for differentiation however, when plates on soft agar there was no evidence of anchorage-independent growth observed with these cells.

Chapter 7: Conclusions and Future Directions

Our experiments have demonstrated that the HPV16 E6 PDZ binding motif enhances several processes which contribute to transformation including, p53 degradation, hTERT expression, and reduced MAGI1 expression. Remarkably, each of these processes has previously been demonstrated to involve the proteasomal degradation of the protein target, by E6 in association with E6AP (197, 294, 295). We hypothesize that, when bound with the ubiquitin ligase E6AP, the full-length HPV16 E6 protein creates an optimal interface for binding the target proteins, *i.e.*, p53, NFX1-91, or MAGI1, and promotes their ubiquitination. An important next step would be to determine if the PDZ binding motif alters the E6AP-E6 heterodimer structure and its ability to interact with these protein targets; impacting their ubiquitination and degradation. Previously, Martinez-Zapien *et al.* solved the crystal structure of HPV16 E6-E6AP-p53 (184). One could take a similar approach to solve the structure of HPV16 E6ΔPBM, E6AP, and p53 and determine how the lack of a PDZ binding motif alters the E6-p53, E6-MAGI1, or E6-NFX1-91 interfaces. If it is determined that the E6AP-E6 is the key to HPV-associated transformation, then this heterodimer might be a worthwhile therapeutic target.

Despite the enhancement of these transformation-related processes, the HPV16 E6 PDZ binding motif was not determined to be essential for increasing the longevity of HEKn; nor was it able to induce EMT or transformation. This signifies that other stimuli or factors are required for HPV-associated transformation. Work still needs to be done to determine what those other stimuli may be in natural HPV infections.

The effects of HPV16 E6+E7 or E6ΔPBM+E7 proteins on polarity and tight junction proteins in HEKn were observed by immunofluorescence microscopy, and these experiments confirmed that the levels of some PDZ proteins are reduced (MAGI1) while others are

mislocalized by HPV16 E6 (ZO1, PAR3). Our results demonstrated that the PDZ binding motif is not required for ZO1 mislocalization but appears to influence PAR3 localization, as there was a modest amount of PAR3-associated fluorescence in the cytoplasm of the E6+E7 cells but not in the cytoplasm of the E6ΔPBM+E7 cells. The HPV16 E6 PDZ binding motif appears to have the most impact on the PDZ tight junction and polarity proteins that it targets for degradation rather than mislocalization. Why some PDZ proteins are targeted for degradation rather than mislocalization may be related to their binding affinities with E6.

Despite modulating various PDZ tight junction and polarity proteins, the E6 PDZ binding motif did not affect the levels of the transmembrane protein JAM1, suggesting that tight junctions were still intact despite the expression of HPV oncoproteins. However, the functional integrity of the tight junctions was not determined. Another interesting pursuit would be to determine the permissibility of tight junctions in the cell lines expressing the truncated or full-length E6 proteins. Our results, together with previous studies, provide compelling evidence supporting a role for the high-risk HPV to abrogate the tight junctions, but it would be interesting to verify this by measuring the transepithelial resistance of the HEKn junctions in cells expressing the E6 or E6ΔPBM proteins (296).

Our study is unique in its use of LC/LC-MS/MS to quantify the effects of the HPV16 E6 PDZ binding motif on the HEKn proteome. Gene ontology and pathway analyses of our proteomic data predict roles for the E6 PDZ binding motif in the regulation of cytoskeletal organization, junctional integrity, immune signaling, and inflammatory responses.

This study data is the first to link the HPV16 E6 PDZ binding motif to the upregulation of neurofilament proteins. The role of the PDZ binding motif in modulating these intermediate filaments remains to be determined.

UCHL1, a deubiquitinase that is typically expressed in neurons has previously been shown to associate with microtubule and cytoskeletal structures (214). Although the upregulation of the deubiquitinase UCHL1 has been associated with high-risk HPV, our study is the first to describe an association between increased UCHL1 expression and the HPV16 E6 PDZ binding motif (211). Further exploration is needed to determine if elevated UCHL1 proteins in HEKn expressing HPV16 E6 proteins are involved in NFkB signaling pathway modulation, as previously described, or if they also play a role in cytoskeletal organization or episomal maintenance (211).

The presence of the HPV16 E6 PDZ binding motif also resulted in elevated levels of BST2, an association that had not previously been described. How this protein's expression is elevated in association with the E6 PDZ binding motif is not yet clear. It would be interesting to determine whether the increased BST2 expression associated with HPV16 E6+E7 expressing cells is involved in negative feedback for interferon expression or preventing anoikis, or if it is simply the result of a heightened immune response.

ICAM1 is another protein with connections to NFKB signaling that we found to be upregulated in association with the E6 PDZ binding motif. This protein has previously been shown to upregulated in response to NFkB signaling and it would be interesting to investigate whether the HPV16 E6 PDZ binding motif promotes NFkB induction of ICAM1.

Overall, our experiments exploring the significance of the HPV16 E6 PDZ binding motif prove that the carboxyl-termini of the high-risk HPV16 enhances the virus' oncogenic capacity through heightened p53 degradation, enhanced hTERT expression, modulation of immune signaling and structural reorganization. We also confirmed that the expression of HPV16 E6

together with E7 is not sufficient to induce transformation in HEKn despite the augmentation of pro-transformation processes.

Although not directly associated with our hypotheses, our LC/LC-MS/MS experiments also allowed us to explore the dysregulation of proteins in HEKn cells expressing HPV16 E6+E7 compared to control LV-HEKn cells. These results allowed us to expand the list of host proteins known to be affected by HPV16 oncoproteins. Our study is unique in that the use of quantitative LC/LC-MS/MS to investigate the global dysregulation of proteins associated with HPV16 E6 and E7 expression in HEKn has not previously been documented in the literature. Our proteomic results confirm that DNA damage response pathways, DNA replication, cytoskeletal organization, and interferon signaling are affected by HPV E6 and E7 oncoproteins. Functional studies of the differentially abundant proteins will increase our understanding of how high-risk HPV oncoproteins manipulate their hosts and could reveal therapeutic targets. The large number of proteins found to be dysregulated by HPV16 E6+E7 have the potential to generate numerous hypothesis and future studies.

Currently, there is a lack of non-surgical treatments for persistent HPV infections. Because not all persistent infections progress to cancer there is a great risk of over-treatment using invasive surgeries. Thus, the identification of prognostic biomarkers for pre-cancerous lesions is a valuable goal. In our proteomic data, there are two upregulated proteins in cells expressing the full-length HPV E6 protein and the E7 protein, which may be suitable prognostic markers: LAMP3 and MK. An investigation into the expression of these proteins in various stages of cervical lesions and cancers would verify if these proteins would be useful for the management of HPV infections.

References:

1. **Chesson HW, Dunne EF, Hariri S, Markowitz LE.** 2014. The estimated lifetime probability of acquiring human papillomavirus in the United States. Sexually transmitted diseases **41:**660-664.
2. **Serrano B, Brotons M, Bosch FX, Bruni L.** 2018. Epidemiology and burden of HPV-related disease. Best Practice & Research Clinical Obstetrics & Gynaecology **47:**14-26.
3. **Bzhalava D, Eklund C, Dillner J.** 2015. International standardization and classification of human papillomavirus types. Virology **476:**341-344.
4. **Yamada T, Wheeler CM, Halpern AL, Stewart AC, Hildesheim A, Jenison SA.** 1995. Human papillomavirus type 16 variant lineages in United States populations characterized by nucleotide sequence analysis of the E6, L2, and L1 coding segments. Journal of virology **69:**7743-7753.
5. **Belnap DM, Olson NH, Cladel NM, Newcomb WW, Brown JC, Kreider JW, Christensen ND, Baker TS.** 1996. Conserved features in papillomavirus and polyomavirus capsids. Journal of molecular biology **259:**249-263.
6. **Dillner J, Nygård M, Munk C, Hortlund M, Hansen BT, Lagheden C, Liaw K-L, Kjaer SK.** 2018. Decline of HPV infections in Scandinavian cervical screening populations after introduction of HPV vaccination programs. Vaccine.
7. **McGregor S, Saulo D, Brotherton J, Liu B, Phillips S, Skinner SR, Luey M, Oliver L, Stewart M, Tabrizi SN.** 2018. Decline in prevalence of human papillomavirus infection following vaccination among Australian Indigenous women, a population at higher risk of cervical cancer: The VIP-I study. Vaccine.
8. **Niccolai LM, Meek JI, Brackney M, Hadler JL, Sosa LE, Weinberger DM.** 2017. Declines in Human Papillomavirus (HPV)–Associated High-Grade Cervical Lesions After Introduction of HPV Vaccines in Connecticut, United States, 2008–2015. Clinical Infectious Diseases **65:**884-889.
9. **Kreimer AR.** 2014. Prospects for prevention of HPV-driven oropharynx cancer. Oral oncology **50:**555-559.
10. **Muñoz N, Méndez F, Posso H, Molano M, Van Den Brule AJ, Ronderos M, Meijer C, Muñoz Á, Group INdCHS.** 2004. Incidence, duration, and determinants of cervical human papillomavirus infection in a cohort of Colombian women with normal cytological results. The Journal of infectious diseases **190:**2077-2087.
11. **Shvetsov YB, Hernandez BY, McDuffie K, Wilkens LR, Zhu X, Ning L, Killeen J, Kamemoto L, Goodman MT.** 2009. Duration and clearance of anal human papillomavirus (HPV) infection among women: the Hawaii HPV cohort study. Clinical infectious diseases **48:**536-546.
12. **Aksoy P, Gottschalk EY, Meneses PI.** 2017. HPV entry into cells. Mutat Res Rev Mutat Res **772:**13-22.
13. **Sapp M, Bienkowska-Haba M.** 2009. Viral entry mechanisms: human papillomavirus and a long journey from extracellular matrix to the nucleus. The FEBS journal **276:**7206-7216.
14. **Doorbar J, Egawa N, Griffin H, Kranjec C, Murakami I.** 2015. Human papillomavirus molecular biology and disease association. Reviews in medical virology **25:**2-23.
15. **Fradet-Turcotte A, Bergeron-Labrecque F, Moody CA, Lehoux M, Laimins LA, Archambault J.** 2011. Nuclear accumulation of the papillomavirus E1 helicase blocks S-

phase progression and triggers an ATM-dependent DNA damage response. Journal of virology**:**JVI. 00542-00511.

16. **Hughes FJ, Romanos MA.** 1993. E1 protein of human papillomavirus is a DNA helicase/ATPase. Nucleic acids research **21:**5817-5823.
17. **Van Tine BA, Dao LD, Wu S-Y, Sonbuchner TM, Lin BY, Zou N, Chiang C-M, Broker TR, Chow LT.** 2004. Human papillomavirus (HPV) origin-binding protein associates with mitotic spindles to enable viral DNA partitioning. Proceedings of the National Academy of Sciences **101:**4030-4035.
18. **Olmedo-Nieva L, Muñoz-Bello J, Contreras-Paredes A, Lizano M.** 2018. The role of E6 spliced isoforms (E6*) in human papillomavirus-induced carcinogenesis. Viruses **10:**45.
19. **Vaeteewoottacharn K, Chamutpong S, Ponglikitmongkol M, Angeletti PC.** 2005. Differential localization of HPV16 E6 splice products with E6-associated protein. Virology journal **2:**50.
20. **Guccione E, Pim D, Banks L.** 2004. HPV-18 E6* I modulates HPV-18 full-length E6 functions in a cell cycle dependent manner. International journal of cancer **110:**928-933.
21. **Mesplède T, Gagnon D, Bergeron-Labrecque F, Azar I, Sénéchal H, Coutlée F, Archambault J.** 2012. p53 degradation activity, expression, and subcellular localization of E6 proteins from 29 human papillomavirus genotypes. Journal of virology **86:**94-107.
22. **Boyer SN, Wazer DE, Band V.** 1996. E7 protein of human papilloma virus-16 induces degradation of retinoblastoma protein through the ubiquitin-proteasome pathway. Cancer research **56:**4620-4624.
23. **Scheffner M, Werness BA, Huibregtse JM, Levine AJ, Howley PM.** 1990. The E6 oncoprotein encoded by human papillomavirus types 16 and 18 promotes the degradation of p53. Cell **63:**1129-1136.
24. **Thomas M, Banks L.** 1999. Human papillomavirus (HPV) E6 interactions with Bak are conserved amongst E6 proteins from high and low risk HPV types. Journal of General Virology **80:**1513-1517.
25. **Shimizu S, Narita M, Tsujimoto Y.** 1999. Bcl-2 family proteins regulate the release of apoptogenic cytochrome c by the mitochondrial channel VDAC. Nature **399:**483.
26. **Cordano P, Gillan V, Bratlie S, Bouvard V, Banks L, Tommasino M, Campo MS.** 2008. The E6E7 oncoproteins of cutaneous human papillomavirus type 38 interfere with the interferon pathway. Virology **377:**408-418.
27. **Nees M, Geoghegan JM, Hyman T, Frank S, Miller L, Woodworth CD.** 2001. Papillomavirus type 16 oncogenes downregulate expression of interferon-responsive genes and upregulate proliferation-associated and NF-κB-responsive genes in cervical keratinocytes. Journal of virology **75:**4283-4296.
28. **Westrich JA, Warren CJ, Pyeon D.** 2017. Evasion of host immune defenses by human papillomavirus. Virus Res **231:**21-33.
29. **Klingelhutz AJ, Foster SA, McDougall JK.** 1996. Telomerase activation by the E6 gene product of human papillomavirus type 16. Nature **380:**79.
30. **Liu X, Roberts J, Dakic A, Zhang Y, Schlegel R.** 2008. HPV E7 contributes to the telomerase activity of immortalized and tumorigenic cells and augments E6-induced hTERT promoter function. Virology **375:**611-623.
31. **Watson RA, Thomas M, Banks L, Roberts S.** 2003. Activity of the human papillomavirus E6 PDZ-binding motif correlates with an enhanced morphological

transformation of immortalized human keratinocytes. Journal of cell science **116:**4925-4934.

32. **Stubenrauch F, Hummel M, Iftner T, Laimins L.** 2000. The E8^ E2C protein, a negative regulator of viral transcription and replication, is required for extrachromosomal maintenance of human papillomavirus type 31 in keratinocytes. Journal of virology **74:**1178-1186.
33. **Straub E, Fertey J, Dreer M, Iftner T, Stubenrauch F.** 2015. Characterization of the human papillomavirus 16 E8 promoter. Journal of virology **89:**7304-7313.
34. **Kabsch K, Alonso A.** 2002. The human papillomavirus type 16 (HPV-16) E5 protein sensitizes human keratinocytes to apoptosis induced by osmotic stress. Oncogene **21:**947.
35. **Campo M, Graham S, Cortese M, Ashrafi G, Araibi E, Dornan E, Miners K, Nunes C, Man S.** 2010. HPV-16 E5 down-regulates expression of surface HLA class I and reduces recognition by CD8 T cells. Virology **407:**137-142.
36. **Pim D, Collins M, Banks L.** 1992. Human papillomavirus type 16 E5 gene stimulates the transforming activity of the epidermal growth factor receptor. Oncogene **7:**27-32.
37. **Wechsler EI, Tugizov S, Herrera R, Da Costa M, Palefsky JM.** 2018. E5 can be expressed in anal cancer and leads to epidermal growth factor receptor-induced invasion in a human papillomavirus 16-transformed anal epithelial cell line. Journal of General Virology.
38. **Wasson CW, Morgan EL, Müller M, Ross RL, Hartley M, Roberts S, Macdonald A.** 2017. Human papillomavirus type 18 E5 oncogene supports cell cycle progression and impairs epithelial differentiation by modulating growth factor receptor signalling during the virus life cycle. Oncotarget **8:**103581.
39. **Münger K, Phelps W, Bubb V, Howley P, Schlegel R.** 1989. The E6 and E7 genes of the human papillomavirus type 16 together are necessary and sufficient for transformation of primary human keratinocytes. Journal of virology **63:**4417-4421.
40. **Doorbar J.** 2013. The E4 protein; structure, function and patterns of expression. Virology **445:**80-98.
41. **Biryukov J, Myers JC, McLaughlin-Drubin ME, Griffin HM, Milici J, Doorbar J, Meyers C.** 2017. Mutations in HPV18 E1^ E4 Impact Virus Capsid Assembly, Infectivity Competence, and Maturation. Viruses **9:**385.
42. **Graham SV.** 2017. The human papillomavirus replication cycle, and its links to cancer progression: a comprehensive review. Clinical science **131:**2201-2221.
43. **Buck CB, Cheng N, Thompson CD, Lowy DR, Steven AC, Schiller JT, Trus BL.** 2008. Arrangement of L2 within the papillomavirus capsid. Journal of virology **82:**5190-5197.
44. **Mittal S, Banks L.** 2017. Molecular mechanisms underlying human papillomavirus E6 and E7 oncoprotein-induced cell transformation. Mutation Research/Reviews in Mutation Research **772:**23-35.
45. **Boshart M, Gissmann L, Ikenberg H, Kleinheinz A, Scheurlen W, zur Hausen H.** 1984. A new type of papillomavirus DNA, its presence in genital cancer biopsies and in cell lines derived from cervical cancer. The EMBO journal **3:**1151-1157.
46. **Thomas M, Pim D, Banks L.** 1999. The role of the E6-p53 interaction in the molecular pathogenesis of HPV. Oncogene **18:**7690.
47. **Arbeit JM, Howley PM, Hanahan D.** 1996. Chronic estrogen-induced cervical and vaginal squamous carcinogenesis in human papillomavirus type 16 transgenic mice. Proceedings of the National Academy of Sciences **93:**2930-2935.

48. **Pei XF, Meck JM, Greenhalgh D, Schlegel R.** 1993. Cotransfection of HPV-18 and v-fos DNA induces tumorigenicity of primary human keratinocytes. Virology **196:**855-860.
49. **Durst M, Gallahan D, Jay G, Rhim JS.** 1989. Glucocorticoid-enhanced neoplastic transformation of human keratinocytes by human papillomavirus type 16 and an activated ras oncogene. Virology **173:**767-771.
50. **Arroyo M, Bagchi S, Raychaudhuri P.** 1993. Association of the human papillomavirus type 16 E7 protein with the S-phase-specific E2F-cyclin A complex. Molecular and cellular biology **13:**6537-6546.
51. **Zhang B, Chen W, Roman A.** 2006. The E7 proteins of low- and high-risk human papillomaviruses share the ability to target the pRB family member p130 for degradation. Proc Natl Acad Sci U S A **103:**437-442.
52. **Heck DV, Yee CL, Howley PM, Münger K.** 1992. Efficiency of binding the retinoblastoma protein correlates with the transforming capacity of the E7 oncoproteins of the human papillomaviruses. Proceedings of the National Academy of Sciences **89:**4442-4446.
53. **Veldman T, Horikawa I, Barrett JC, Schlegel R.** 2001. Transcriptional activation of the telomerase hTERT gene by human papillomavirus type 16 E6 oncoprotein. Journal of virology **75:**4467-4472.
54. **Hahn WC, Stewart SA, Brooks MW, York SG, Eaton E, Kurachi A, Beijersbergen RL, Knoll JH, Meyerson M, Weinberg RA.** 1999. Inhibition of telomerase limits the growth of human cancer cells. Nature medicine **5:**1164.
55. **Aarts M, Liu Y, Liu L, Besshoh S, Arundine M, Gurd JW, Wang YT, Salter MW, Tymianski M.** 2002. Treatment of ischemic brain damage by perturbing NMDA receptor-PSD-95 protein interactions. Science **298**.
56. **Gewin L, Galloway DA.** 2001. E box-dependent activation of telomerase by human papillomavirus type 16 E6 does not require induction of c-myc. Journal of virology **75:**7198-7201.
57. **Van Doorslaer K, Burk RD.** 2012. Association between hTERT activation by HPV E6 proteins and oncogenic risk. Virology **433:**216-219.
58. **Oliveira LB, Haga IR, Villa LL.** 2018. Human papillomavirus (HPV) 16 E6 oncoprotein targets the Toll-like receptor pathway. Journal of General Virology **99:**667-675.
59. **James MA, Lee JH, Klingelhutz AJ.** 2006. Human papillomavirus type 16 E6 activates NF-kappaB, induces cIAP-2 expression, and protects against apoptosis in a PDZ binding motif-dependent manner. J Virol **80:**5301-5307.
60. **Karin M, Cao Y, Greten FR, Li Z-W.** 2002. NF-κB in cancer: from innocent bystander to major culprit. Nature reviews cancer **2:**301.
61. **Maier HJ, Schmidt-Straßburger U, Huber MA, Wiedemann EM, Beug H, Wirth T.** 2010. NF-κB promotes epithelial–mesenchymal transition, migration and invasion of pancreatic carcinoma cells. Cancer letters **295:**214-228.
62. **Romanczuk H, Howley PM.** 1992. Disruption of either the E1 or the E2 regulatory gene of human papillomavirus type 16 increases viral immortalization capacity. Proceedings of the National Academy of Sciences **89:**3159-3163.
63. **Songyang Z, Fanning A, Fu C, Xu J, Marfatia S, Chishti A, Crompton A, Chan A, Anderson J, Cantley L.** 1997. Recognition of unique carboxyl-terminal motifs by distinct PDZ domains. Science **275:**73-77.

64. **Kiyono T, Hiraiwa A, Fujita M, Hayashi Y, Akiyama T, Ishibashi M.** 1997. Binding of high-risk human papillomavirus E6 oncoproteins to the human homologue of the Drosophila discs large tumor suppressor protein. Proceedings of the National Academy of Sciences **94:**11612-11616.
65. **Nakagawa S, Huibregtse JM.** 2000. Human scribble (Vartul) is targeted for ubiquitin-mediated degradation by the high-risk papillomavirus E6 proteins and the E6AP ubiquitin-protein ligase. Molecular and cellular biology **20:**8244-8253.
66. **Lee C, Laimins LA.** 2004. Role of the PDZ domain-binding motif of the oncoprotein E6 in the pathogenesis of human papillomavirus type 31. J Virol **78:**12366-12377.
67. **Choi M, Lee S, Choi T, Lee C.** 2014. Roles of the PDZ domain-binding motif of the human papillomavirus type 16 E6 on the immortalization and differentiation of primary human foreskin keratinocytes. Virus Genes **48:**224-232.
68. **Spanos WC, Hoover A, Harris GF, Wu S, Strand GL, Anderson ME, Klingelhutz AJ, Hendriks W, Bossler AD, Lee JH.** 2008. The PDZ binding motif of human papillomavirus type 16 E6 induces PTPN13 loss, which allows anchorage-independent growth and synergizes with ras for invasive growth. J Virol **82:**2493-2500.
69. **Muench P, Hiller T, Probst S, Florea AM, Stubenrauch F, Iftner T.** 2009. Binding of PDZ proteins to HPV E6 proteins does neither correlate with epidemiological risk classification nor with the immortalization of foreskin keratinocytes. Virology **387:**380-387.
70. **Brimer N, Vande Pol SB.** 2014. Papillomavirus E6 PDZ interactions can be replaced by repression of p53 to promote episomal human papillomavirus genome maintenance. J Virol **88:**3027-3030.
71. **Kalluri R, Weinberg RA.** 2010. The basics of epithelial-mesenchymal transition. The Journal of clinical investigation **120:**1786-1786.
72. **Thiery JP.** 2002. Epithelial–mesenchymal transitions in tumour progression. Nature Reviews Cancer **2:**442.
73. **Préhaud C, Wolff N, Terrien E, Lafage M, Mégret F, Babault N, Cordier F, Tan GS, Maitrepierre E, Ménager P.** 2010. Attenuation of rabies virulence: takeover by the cytoplasmic domain of its envelope protein. Sci Signal **3:**ra5-ra5.
74. **Liu H, Golebiewski L, Dow EC, Krug RM, Javier RT, Rice AP.** 2010. The ESEV PDZ-binding motif of the avian influenza A virus NS1 protein protects infected cells from apoptosis by directly targeting Scribble. Journal of virology **84:**11164-11174.
75. **Jimenez-Guardeño JM, Nieto-Torres JL, DeDiego ML, Regla-Nava JA, Fernandez-Delgado R, Castaño-Rodriguez C, Enjuanes L.** 2014. The PDZ-binding motif of severe acute respiratory syndrome coronavirus envelope protein is a determinant of viral pathogenesis. PLoS pathogens **10:**e1004320.
76. **Kong K, Kumar M, Taruishi M, Javier RT.** 2014. The human adenovirus E4-ORF1 protein subverts discs large 1 to mediate membrane recruitment and dysregulation of phosphatidylinositol 3-kinase. PLoS pathogens **10:**e1004102.
77. **Higuchi M, Tsubata C, Kondo R, Yoshida S, Takahashi M, Oie M, Tanaka Y, Mahieux R, Matsuoka M, Fujii M.** 2007. Cooperation of NF-κB2/p100 activation and the PDZ domain binding motif signal in human T-cell leukemia virus type 1 (HTLV-1) Tax1 but not HTLV-2 Tax2 is crucial for interleukin-2-independent growth transformation of a T-cell line. Journal of virology **81:**11900-11907.

78. **Weiss RS, Javier RT.** 1997. A carboxy-terminal region required by the adenovirus type 9 E4 ORF1 oncoprotein for transformation mediates direct binding to cellular polypeptides. Journal of virology **71:**7873-7880.
79. **Kong K, Kumar M, Taruishi M, Javier RT.** 2015. Adenovirus E4-ORF1 Dysregulates Epidermal Growth Factor and Insulin/Insulin-Like Growth Factor Receptors To Mediate Constitutive Myc Expression. Journal of virology **89:**10774-10785.
80. **Glaunsinger BA, Lee SS, Thomas M, Banks L, Javier R.** 2000. Interactions of the PDZ-protein MAGI-1 with adenovirus E4-ORF1 and high-risk papillomavirus E6 oncoproteins. Oncogene **19:**5270.
81. **Lee SS, Glaunsinger B, Mantovani F, Banks L, Javier RT.** 2000. Multi-PDZ domain protein MUPP1 is a cellular target for both adenovirus E4-ORF1 and high-risk papillomavirus type 18 E6 oncoproteins. Journal of virology **74:**9680-9693.
82. **Makokha GN, Takahashi M, Higuchi M, Saito S, Tanaka Y, Fujii M.** 2013. Human T-cell leukemia virus type 1 Tax protein interacts with and mislocalizes the PDZ domain protein MAGI-1. Cancer Sci **104:**313-320.
83. **Aoyagi T, Takahashi M, Higuchi M, Oie M, Tanaka Y, Kiyono T, Aoyagi Y, Fujii M.** 2010. The PDZ domain binding motif (PBM) of human T-cell leukemia virus type 1 Tax can be substituted by heterologous PBMs from viral oncoproteins during T-cell transformation. Virus genes **40:**193-199.
84. **Cherian MA, Baydoun HH, Al-Saleem J, Shkriabai N, Kvaratskhelia M, Green P, Ratner L.** 2015. Akt Pathway Activation by Human T-cell Leukemia Virus Type 1 Tax Oncoprotein. Journal of Biological Chemistry **290:**26270-26281.
85. **Prehaud C, Wolff N, Terrien E, Lafage M, Megret F, Babault N, Cordier F, Tan GS, Maitrepierre E, Menager P.** 2010. Attenuation of rabies virulence: takeover by the cytoplasmic domain of its envelope protein. Science signaling **3:**ra5-ra5.
86. **Golebiewski L, Liu H, Javier RT, Rice AP.** 2011. The avian influenza virus NS1 ESEV PDZ binding motif associates with Dlg1 and Scribble to disrupt cellular tight junctions. Journal of virology **85:**10639-10648.
87. **Thomas M, Myers MP, Massimi P, Guarnaccia C, Banks L.** 2016. Analysis of multiple HPV E6 PDZ interactions defines type-specific PDZ fingerprints that predict oncogenic potential. PLoS pathogens **12:**e1005766.
88. **White EA, Howley PM.** 2013. Proteomic approaches to the study of papillomavirus-host interactions. Virology **435:**57-69.
89. **White EA, Kramer RE, Tan MJ, Hayes SD, Harper JW, Howley PM.** 2012. Comprehensive analysis of host cellular interactions with human papillomavirus E6 proteins identifies new E6 binding partners and reflects viral diversity. J Virol **86:**13174-13186.
90. **Subramanian N, Chinnappan S.** 2013. Prediction of promiscuous epitopes in the e6 protein of three high risk human papilloma viruses: a computational approach. Asian Pac J Cancer Prev **14:**4167-4175.
91. **Small Jr W, Bacon MA, Bajaj A, Chuang LT, Fisher BJ, Harkenrider MM, Jhingran A, Kitchener HC, Mileshkin LR, Viswanathan AN.** 2017. Cervical cancer: a global health crisis. Cancer **123:**2404-2412.
92. **Massimi P, Gammoh N, Thomas M, Banks L.** 2004. HPV E6 specifically targets different cellular pools of its PDZ domain-containing tumour suppressor substrates for proteasome-mediated degradation. Oncogene **23:**8033-8039.

93. **Thomas M, Dasgupta J, Zhang Y, Chen X, Banks L.** 2008. Analysis of specificity determinants in the interactions of different HPV E6 proteins with their PDZ domain-containing substrates. Virology **376:**371-378.
94. **Delury CP, Marsh EK, James CD, Boon SS, Banks L, Knight GL, Roberts S.** 2013. The role of protein kinase A regulation of the E6 PDZ-binding domain during the differentiation-dependent life cycle of human papillomavirus type 18. J Virol **87:**9463-9472.
95. **Boon SS, Tomaic V, Thomas M, Roberts S, Banks L.** 2015. Cancer-causing human papillomavirus E6 proteins display major differences in the phospho-regulation of their PDZ interactions. J Virol **89:**1579-1586.
96. **Takizawa S, Nagasaka K, Nakagawa S, Yano T, Nakagawa K, Yasugi T, Takeuchi T, Kanda T, Huibregtse JM, Akiyama T.** 2006. Human scribble, a novel tumor suppressor identified as a target of high-risk HPV E6 for ubiquitin-mediated degradation, interacts with adenomatous polyposis coli. Genes to Cells **11:**453-464.
97. **Zihni C, Mills C, Matter K, Balda MS.** 2016. Tight junctions: from simple barriers to multifunctional molecular gates. Nature reviews Molecular cell biology **17:**564.
98. **Van Itallie CM, Anderson JM.** 2014. Architecture of tight junctions and principles of molecular composition. Seminars in Cell & Developmental Biology **36:**157-165.
99. **Kranjec C, Massimi P, Banks L.** 2014. Restoration of MAGI-1 expression in human papillomavirus-positive tumor cells induces cell growth arrest and apoptosis. J Virol **88:**7155-7169.
100. **Gottardi CJ, Arpin M, Fanning AS, Louvard D.** 1996. The junction-associated protein, zonula occludens-1, localizes to the nucleus before the maturation and during the remodeling of cell-cell contacts. Proceedings of the National Academy of Sciences **93:**10779-10784.
101. **Balda MS, Matter K.** 2000. The tight junction protein ZO-1 and an interacting transcription factor regulate ErbB-2 expression. The EMBO journal **19:**2024-2033.
102. **Balda MS, Garrett MD, Matter K.** 2003. The ZO-1–associated Y-box factor ZONAB regulates epithelial cell proliferation and cell density. The Journal of cell biology **160:**423-432.
103. **Hernández-Monge J, Garay E, Raya-Sandino A, Vargas-Sierra O, Díaz-Chávez J, Popoca-Cuaya M, Lambert PF, González-Mariscal L, Gariglio P.** 2013. Papillomavirus E6 oncoprotein up-regulates occludin and ZO-2 expression in ovariectomized mice epidermis. Experimental cell research **319:**2588-2603.
104. **Thomas M, Glaunsinger B, Pim D, Javier R, Banks L.** 2001. HPV E6 and MAGUK protein interactions: determination of the molecular basis for specific protein recognition and degradation. Oncogene **20:**5431-5439.
105. **Thomas M, Laura R, Hepner K, Guccione E, Sawyers C, Lasky L, Banks L.** 2002. Oncogenic human papillomavirus E6 proteins target the MAGI-2 and MAGI-3 proteins for degradation. Oncogene **21:**5088.
106. **Feng X, Jia S, Martin TA, Jiang WG.** 2014. Regulation and involvement in cancer and pathological conditions of MAGI1, a tight junction protein. Anticancer Res **34:**3251-3256.
107. **Engelman JA.** 2009. Targeting PI3K signalling in cancer: opportunities, challenges and limitations. Nature Reviews Cancer **9:**550.

108. **Estévez MA, Henderson JA, Ahn D, Zhu XR, Poschmann G, Lübbert H, Marx R, Baraban JM.** 2008. The neuronal RhoA GEF, Tech, interacts with the synaptic multi-PDZ-domain-containing protein, MUPP1. Journal of neurochemistry **106:**1287-1297.
109. **Escudero-Esparza A, Jiang, W.G., Martin, T.A.** 2011. The Claudin family and its role in cancer and metastasis. Frontiers in Bioscience **16:**1069-1083.
110. **Peng J, Gassama-Diagne A.** 2016. Apicobasal polarity and Ras/Raf/MEK/ERK signalling in cancer. Gut**:**gutjnl-2016-312986.
111. **Milgrom-Hoffman M, Humbert PO.** Regulation of cellular and PCP signalling by the Scribble polarity module, p. *In* (ed), Elsevier,
112. **Humbert PO, Russell SM, Smith L, Richardson HE.** 2015. The Scribble–Dlg–Lgl Module in Cell Polarity Regulation. doi:10.1007/978-3-319-14463-4_4**:**65-111.
113. **Ellenbroek SI, Iden S, Collard JG.** Cell polarity proteins and cancer, p 208-215. *In* (ed), Elsevier,
114. **Stephens R, Lim K, Portela M, Kvansakul M, Humbert PO, Richardson HE.** 2018. The scribble cell polarity module in the regulation of cell signaling in tissue development and tumorigenesis. Journal of molecular biology.
115. **Thomas M, Banks L.** 2018. Upsetting the balance: When viruses manipulate cell polarity control. Journal of molecular biology.
116. **Joberty G, Petersen C, Gao L, Macara IG.** 2000. The cell-polarity protein Par6 links Par3 and atypical protein kinase C to Cdc42. Nature cell biology **2:**531-539.
117. **Lin D, Edwards AS, Fawcett JP, Mbamalu G, Scott JD, Pawson T.** 2000. A mammalian PAR-3–PAR-6 complex implicated in Cdc42/Rac1 and aPKC signalling and cell polarity. Nature cell biology **2:**540-547.
118. **Zihni C, Terry SJ.** 2015. RhoGTPase signalling at epithelial tight junctions: Bridging the GAP between polarity and cancer. The international journal of biochemistry & cell biology **64:**120-125.
119. **Facciuto F, Bugnon Valdano M, Marziali F, Massimi P, Banks L, Cavatorta AL, Gardiol D.** 2014. Human papillomavirus (HPV)-18 E6 oncoprotein interferes with the epithelial cell polarity Par3 protein. Mol Oncol **8:**533-543.
120. **Zhang P, Wang S, Wang S, Qiao J, Zhang L, Zhang Z, Chen Z.** 2016. Dual function of partitioning-defective 3 in the regulation of YAP phosphorylation and activation. Cell discovery **2:**16021.
121. **Guo X, Wang M, Zhao Y, Wang X, Shen M, Zhu F, Shi C, Xu M, Li X, Peng F, Zhang H, Feng Y, Xie Y, Xu X, Jia W, He R, Jiang J, Hu J, Tian R, Qin R.** 2015. Par3 regulates invasion of pancreatic cancer cells via interaction with Tiam1. Clin Exp Med doi:10.1007/s10238-015-0365-2.
122. **Ruan L, Shen Y, Lu Z, Shang D, Zhao Z, Lu Y, Wu Y, Zhang Y, Tu Z, Liu H.** 2017. Roles of partitioning-defective protein 6 (Par6) and its complexes in the proliferation, migration and invasion of cancer cells. Clinical and Experimental Pharmacology and Physiology.
123. **Nolan ME, Aranda V, Lee S, Lakshmi B, Basu S, Allred DC, Muthuswamy SK.** 2008. The polarity protein Par6 induces cell proliferation and is overexpressed in breast cancer. Cancer research **68:**8201-8209.
124. **Viloria-Petit AM, David L, Jia JY, Erdemir T, Bane AL, Pinnaduwage D, Roncari L, Narimatsu M, Bose R, Moffat J.** 2009. A role for the TGFβ-Par6 polarity pathway in

breast cancer progression. Proceedings of the National Academy of Sciences **106:**14028-14033.

125. **Mu Y, Zang G, Engström U, Busch C, Landström M.** 2015. TGFβ-induced phosphorylation of Par6 promotes migration and invasion in prostate cancer cells. British journal of cancer.
126. **Gunaratne A, Thai BL, Di Guglielmo GM.** 2013. Atypical protein kinase C phosphorylates Par6 and facilitates transforming growth factor beta-induced epithelial-to-mesenchymal transition. Mol Cell Biol **33:**874-886.
127. **Graybill C, Wee B, Atwood SX, Prehoda KE.** 2012. Partitioning-defective protein 6 (Par-6) activates atypical protein kinase C (aPKC) by pseudosubstrate displacement. Journal of Biological Chemistry **287:**21003-21011.
128. **Liu J, Li J, Ren Y, Liu P.** 2014. DLG5 in cell polarity maintenance and cancer development. Int J Biol Sci **10:**543-549.
129. **Thomas M, Massimi P, Navarro C, Borg J-P, Banks L.** 2005. The hScrib/Dlg apico-basal control complex is differentially targeted by HPV-16 and HPV-18 E6 proteins. Oncogene **24:**6222.
130. **Feigin ME, Akshinthala SD, Araki K, Rosenberg AZ, Muthuswamy LB, Martin B, Lehmann BD, Berman HK, Pietenpol JA, Cardiff RD, Muthuswamy SK.** 2014. Mislocalization of the cell polarity protein scribble promotes mammary tumorigenesis and is associated with basal breast cancer. Cancer Res **74:**3180-3194.
131. **Vaira V, Faversani A, Dohi T, Maggioni M, Nosotti M, Tosi D, Altieri DC, Bosari S.** 2011. Aberrant overexpression of the cell polarity module scribble in human cancer. Am J Pathol **178:**2478-2483.
132. **Seiki T, Nagasaka K, Kranjec C, Kawana K, Maeda D, Nakamura H, Taguchi A, Matsumoto Y, Arimoto T, Wada-Hiraike O, Oda K, Nakagawa S, Yano T, Fukayama M, Banks L, Osuga Y, Fujii T.** 2015. HPV-16 impairs the subcellular distribution and levels of expression of protein phosphatase 1gamma in cervical malignancy. BMC Cancer **15:**230.
133. **Dow L, Elsum I, King C, Kinross K, Richardson H, Humbert P.** 2008. Loss of human Scribble cooperates with H-Ras to promote cell invasion through deregulation of MAPK signalling. Oncogene **27:**5988-6001.
134. **Godde NJ, Sheridan JM, Smith LK, Pearson HB, Britt KL, Galea RC, Yates LL, Visvader JE, Humbert PO.** 2014. Scribble modulates the MAPK/Fra1 pathway to disrupt luminal and ductal integrity and suppress tumour formation in the mammary gland. PLoS Genet **10:**e1004323.
135. **Cordenonsi M, Zanconato F, Azzolin L, Forcato M, Rosato A, Frasson C, Inui M, Montagner M, Parenti AR, Poletti A.** 2011. The Hippo transducer TAZ confers cancer stem cell-related traits on breast cancer cells. Cell **147:**759-772.
136. **Sandoval GJ, Graham DB, Gmyrek GB, Akilesh HM, Fujikawa K, Sammut B, Bhattacharya D, Srivatsan S, Kim A, Shaw AS.** 2013. Novel mechanism of tumor suppression by polarity gene discs large 1 (DLG1) revealed in a murine model of pediatric B-ALL. Cancer immunology research **1:**426-437.
137. **Carr HS, Cai C, Keinänen K, Frost JA.** 2009. Interaction of the RhoA exchange factor Net1 with discs large homolog 1 protects it from proteasome-mediated degradation and potentiates Net1 activity. Journal of Biological Chemistry **284:**24269-24280.

138. **Subbaiah VK, Narayan N, Massimi P, Banks L.** 2012. Regulation of the DLG tumor suppressor by beta-catenin. Int J Cancer **131:**2223-2233.
139. **Liu L-X, Liu Z-H, Jiang H-C, Qu X, Zhang W-H, Wu L-F, Zhu A-L, Wang X-Q, Wu M.** 2002. Profiling of differentially expressed genes in human gastric carcinoma by cDNA expression array. World Journal of Gastroenterology **8:**580-585.
140. **Storrs CH, Silverstein SJ.** 2007. PATJ, a Tight Junction-Associated PDZ Protein, Is a Novel Degradation Target of High-Risk Human Papillomavirus E6 and the Alternatively Spliced Isoform 18 E6. Journal of Virology **81:**4080.
141. **Adachi M, Hamazaki Y, Kobayashi Y, Itoh M, Tsukita S, Furuse M, Tsukita S.** 2009. Similar and distinct properties of MUPP1 and Patj, two homologous PDZ domain-containing tight-junction proteins. Molecular and cellular biology **29:**2372-2389.
142. **Laplante M, Sabatini DM.** 2009. mTOR signaling at a glance. Journal of cell science **122:**3589-3594.
143. **Massey-Harroche D, Delgrossi M-H, Lane-Guermonprez L, Arsanto J-P, Borg J-P, Billaud M, Le Bivic A.** 2007. Evidence for a molecular link between the tuberous sclerosis complex and the Crumbs complex. Human molecular genetics **16:**529-536.
144. **Hoover AC, Strand GL, Nowicki PN, Anderson ME, Vermeer PD, Klingelhutz AJ, Bossler AD, Pottala JV, Hendriks WJ, Lee JH.** 2009. Impaired PTPN13 phosphatase activity in spontaneous or HPV-induced squamous cell carcinomas potentiates oncogene signaling through the MAP kinase pathway. Oncogene **28:**3960-3970.
145. **Scrima M, De Marco C, De Vita F, Fabiani F, Franco R, Pirozzi G, Rocco G, Malanga D, Viglietto G.** 2012. The Nonreceptor-Type Tyrosine Phosphatase PTPN13 Is a Tumor Suppressor Gene in Non–Small Cell Lung Cancer. The American journal of pathology **180:**1202-1214.
146. **Jing M, Bohl J, Brimer N, Kinter M, Pol SBV.** 2007. Degradation of tyrosine phosphatase PTPN3 (PTPH1) by association with oncogenic human papillomavirus E6 proteins. Journal of virology **81:**2231-2239.
147. **Thomas M, Banks L.** 2014. PDZRN3/LNX3 is a Novel Target of HPV 16 and HPV-18 E6. Journal of virology**:**JVI. 01743-01714.
148. **Favre-Bonvin A, Reynaud C, Kretz-Remy C, Jalinot P.** 2005. Human papillomavirus type 18 E6 protein binds the cellular PDZ protein TIP-2/GIPC, which is involved in transforming growth factor β signaling and triggers its degradation by the proteasome. Journal of virology **79:**4229-4237.
149. **Jeong K, Kim H, Kim S, Kim Y, Choe J.** 2007. Human papillomavirus type 16 E6 protein interacts with cystic fibrosis transmembrane regulator-associated ligand and promotes E6-associated protein-mediated ubiquitination and proteasomal degradation. Oncogene **26:**487.
150. **Accardi R, Rubino R, Scalise M, Gheit T, Shahzad N, Thomas M, Banks L, Indiveri C, Sylla BS, Cardone RA.** 2011. E6 and E7 from human papillomavirus type 16 cooperate to target the PDZ protein Na/H exchange regulatory factor 1. Journal of virology **85:**8208-8216.
151. **Katoh M.** 2013. Functional proteomics, human genetics and cancer biology of GIPC family members. Exp Mol Med **45:**e26.
152. **Hammad MM, Dunn HA, Walther C, Ferguson SS.** 2015. Role of cystic fibrosis transmembrane conductance regulator-associated ligand (CAL) in regulating the

trafficking and signaling of corticotropin-releasing factor receptor 1. Cellular signalling **27:**2120-2130.

153. **Wang Q, Qin Q, Song R, Zhao C, Liu H, Yang Y, Gu S, Zhou D, He J.** 2018. NHERF1 inhibits beta-catenin-mediated proliferation of cervical cancer cells through suppression of alpha-actinin-4 expression. Cell death & disease **9:**668.
154. **Thomas M, Banks L.** 2015. PDZRN3/LNX3 is a novel target of human papillomavirus type 16 (HPV-16) and HPV-18 E6. J Virol **89:**1439-1444.
155. **Hong S, Laimins LA.** 2013. The JAK-STAT transcriptional regulator, STAT-5, activates the ATM DNA damage pathway to induce HPV 31 genome amplification upon epithelial differentiation. PLoS pathogens **9:**e1003295.
156. **Honda T, Yamamoto H, Ishii A, Inui M.** 2010. PDZRN3 negatively regulates BMP-2–induced osteoblast differentiation through inhibition of Wnt signaling. Molecular biology of the cell **21:**3269-3277.
157. **Bae SM, Lee C-H, Cho YL, Nam KH, Kim YW, Kim CK, Han BD, Lee YJ, Chun HJ, Ahn WS.** 2005. Two-dimensional gel analysis of protein expression profile in squamous cervical cancer patients. Gynecologic oncology **99:**26-35.
158. **Merkley MA, Hildebrandt E, Podolsky RH, Arnouk H, Ferris DG, Dynan WS, Stöppler H.** 2009. Large-scale analysis of protein expression changes in human keratinocytes immortalized by human papilloma virus type 16 E6 and E7 oncogenes. Proteome science **7:**29.
159. **Rabilloud T, Chevallet M, Luche S, Lelong C.** 2010. Two-dimensional gel electrophoresis in proteomics: past, present and future. Journal of proteomics **73:**2064-2077.
160. **Ding Y, Yang M, She S, Min H, Xv X, Ran X, Wu Y, Wang W, Wang L, Yi L, Yang Y, Gao Q.** 2015. iTRAQ-based quantitative proteomic analysis of cervical cancer. Int J Oncol **46:**1748-1758.
161. **Pappa KI, Lygirou V, Kontostathi G, Zoidakis J, Makridakis M, Vougas K, Daskalakis G, Polyzos A, Anagnou NP.** 2017. Proteomic analysis of normal and cancer cervical cell lines reveals deregulation of cytoskeleton-associated proteins. Cancer Genomics-Proteomics **14:**253-266.
162. **Güzel C, Govorukhina NI, Wisman GBA, Stingl C, Dekker LJ, Klip HG, Hollema H, Guryev V, Horvatovich PL, van der Zee AG.** 2018. Proteomic alterations in early stage cervical cancer. Oncotarget **9:**18128.
163. **Kozak M.** 1986. Point mutations define a sequence flanking the AUG initiator codon that modulates translation by eukaryotic ribosomes. Cell **44:**283-292.
164. **Barczak W, Suchorska W, Rubiś B, Kulcenty K.** 2015. Universal real-time PCR-based assay for lentiviral titration. Molecular biotechnology **57:**195-200.
165. **Ma S, Dai Y.** 2011. Principal component analysis based methods in bioinformatics studies. Briefings in bioinformatics **12:**714-722.
166. **Ritchie ME, Phipson B, Wu D, Hu Y, Law CW, Shi W, Smyth GK.** 2015. limma powers differential expression analyses for RNA-sequencing and microarray studies. Nucleic acids research **43:**e47-e47.
167. **Benjamini Y, Hochberg Y.** 1995. Controlling the false discovery rate: a practical and powerful approach to multiple testing. Journal of the Royal statistical society: series B (Methodological) **57:**289-300.

168. **Supek F, Bošnjak M, Škunca N, Šmuc T.** 2011. REVIGO summarizes and visualizes long lists of gene ontology terms. PloS one **6:**e21800.
169. **Szklarczyk D, Morris JH, Cook H, Kuhn M, Wyder S, Simonovic M, Santos A, Doncheva NT, Roth A, Bork P.** 2016. The STRING database in 2017: quality-controlled protein–protein association networks, made broadly accessible. Nucleic acids research**:**gkw937.
170. **Gordon A, Colman-Lerner A, Chin TE, Benjamin KR, Richard CY, Brent R.** 2007. Single-cell quantification of molecules and rates using open-source microscope-based cytometry. Nature methods **4:**175.
171. **Costes SV, Daelemans D, Cho EH, Dobbin Z, Pavlakis G, Lockett S.** 2004. Automatic and quantitative measurement of protein-protein colocalization in live cells. Biophysical journal **86:**3993-4003.
172. **Manders E, Verbeek F, Aten J.** 1993. Measurement of co-localization of objects in dual-colour confocal images. Journal of microscopy **169:**375-382.
173. **Griffin LM, Cicchini L, Xu T, Pyeon D.** 2013. Human keratinocyte cultures in the investigation of early steps of human papillomavirus infection, p 219-238, Epidermal Cells. Springer.
174. **Crook T, Vousden KH, Tidy JA.** 1991. Degradation of p53 can be targeted by HPV E6 sequences distinct from those required for p53 binding and trans-activation. Cell **67:**547-556.
175. **Dominguez-Bautista JA, Klinkenberg M, Brehm N, Subramaniam M, Kern B, Roeper J, Auburger G, Jendrach M.** 2015. Loss of lysosome-associated membrane protein 3 (LAMP3) enhances cellular vulnerability against proteasomal inhibition. Eur J Cell Biol **94:**148-161.
176. **Liu S, Yue J, Du W, Han J, Zhang W.** 2018. LAMP3 plays an oncogenic role in osteosarcoma cells partially by inhibiting TP53. Cellular & molecular biology letters **23:**33.
177. **Michael D, Oren M.** The p53–Mdm2 module and the ubiquitin system, p 49-58. *In* (ed), Elsevier,
178. **Wang G, Fersht AR.** 2017. Multisite aggregation of p53 and implications for drug rescue. Proceedings of the National Academy of Sciences **114:**E2634-E2643.
179. **Zacapala-Gómez AE, Del Moral-Hernández O, Villegas-Sepúlveda N, Hidalgo-Miranda A, Romero-Córdoba SL, Beltrán-Anaya FO, Leyva-Vázquez MA, del Carmen Alarcón-Romero L, Illades-Aguiar B.** 2016. Changes in global gene expression profiles induced by HPV 16 E6 oncoprotein variants in cervical carcinoma C33-A cells. Virology **488:**187-195.
180. **Kranjec C, Banks L.** 2011. A systematic analysis of human papillomavirus (HPV) E6 PDZ substrates identifies MAGI-1 as a major target of HPV type 16 (HPV-16) and HPV-18 whose loss accompanies disruption of tight junctions. J Virol **85:**1757-1764.
181. **Latorre IJ, Roh MH, Frese KK, Weiss RS, Margolis B, Javier RT.** 2005. Viral oncoprotein-induced mislocalization of select PDZ proteins disrupts tight junctions and causes polarity defects in epithelial cells. Journal of cell science **118:**4283-4293.
182. **Charbonnier S, Nomine Y, Ramirez J, Luck K, Chapelle A, Stote RH, Trave G, Kieffer B, Atkinson RA.** 2011. The structural and dynamic response of MAGI-1 PDZ1 with noncanonical domain boundaries to the binding of human papillomavirus E6. J Mol Biol **406:**745-763.

183. **Zhang Y, Dasgupta J, Ma RZ, Banks L, Thomas M, Chen XS.** 2007. Structures of a human papillomavirus (HPV) E6 polypeptide bound to MAGUK proteins: mechanisms of targeting tumor suppressors by a high-risk HPV oncoprotein. J Virol **81:**3618-3626.
184. **Martinez-Zapien D, Ruiz FX, Poirson J, Mitschler A, Ramirez J, Forster A, Cousido-Siah A, Masson M, Pol SV, Podjarny A.** 2016. Structure of the E6/E6AP/p53 complex required for HPV-mediated degradation of p53. Nature **529:**541.
185. **Foster SA, Demers GW, Etscheid BG, Galloway DA.** 1994. The ability of human papillomavirus E6 proteins to target p53 for degradation in vivo correlates with their ability to abrogate actinomycin D-induced growth arrest. Journal of virology **68:**5698-5705.
186. **Sailer C, Offensperger F, Julier A, Kammer K-M, Walker-Gray R, Gold MG, Scheffner M, Stengel F.** 2018. Structural dynamics of the E6AP/UBE3A-E6-p53 enzyme-substrate complex. Nature communications **9:**4441.
187. **Pim D, Massimi P, Banks L.** 1997. Alternatively spliced HPV-18 E6* protein inhibits E6 mediated degradation of p53 and suppresses transformed cell growth. Oncogene **15:**257.
188. **Lechner MS, Laimins LA.** 1994. Inhibition of p53 DNA binding by human papillomavirus E6 proteins. Journal of virology **68:**4262-4273.
189. **Massimi P, Shai A, Lambert P, Banks L.** 2008. HPV E6 degradation of p53 and PDZ containing substrates in an E6AP null background. Oncogene **27:**1800-1804.
190. **Xie X, Piao L, Bullock BN, Smith A, Su T, Zhang M, Teknos TN, Arora PS, Pan Q.** 2014. Targeting HPV16 E6-p300 interaction reactivates p53 and inhibits the tumorigenicity of HPV-positive head and neck squamous cell carcinoma. Oncogene **33:**1037.
191. **Chand V, John R, Jaiswal N, Johar SS, Nag A.** 2014. High-risk HPV16E6 stimulates hADA3 degradation by enhancing its SUMOylation. Carcinogenesis **35:**1830-1839.
192. **Muller PA, Vousden KH.** 2013. p53 mutations in cancer. Nature cell biology **15:**2.
193. **Seo EJ, Kim HJ, Lee CJ, Kang HT, Hwang ES.** 2004. The role of HPV oncoproteins and cellular factors in maintenance of hTERT expression in cervical carcinoma cells. Gynecologic oncology **94:**40-47.
194. **Oh ST, Kyo S, Laimins LA.** 2001. Telomerase activation by human papillomavirus type 16 E6 protein: induction of human telomerase reverse transcriptase expression through Myc and GC-rich Sp1 binding sites. Journal of virology **75:**5559-5566.
195. **Chang JTC, Yang HT, Wang TCV, Cheng AJ.** 2005. Upstream stimulatory factor (USF) as a transcriptional suppressor of human telomerase reverse transcriptase (hTERT) in oral cancer cells. Molecular carcinogenesis **44:**183-192.
196. **McMurray H, McCance D.** 2003. Human papillomavirus type 16 E6 activates TERT gene transcription through induction of c-Myc and release of USF-mediated repression. Journal of virology **77:**9852-9861.
197. **James MA, Lee JH, Klingelhutz AJ.** 2006. HPV16-E6 associated hTERT promoter acetylation is E6AP dependent, increased in later passage cells and enhanced by loss of p300. International journal of cancer **119:**1878-1885.
198. **Liu X, Yuan H, Fu B, Disbrow GL, Apolinario T, Tomaić V, Kelley ML, Baker CC, Huibregtse J, Schlegel R.** 2005. The E6AP ubiquitin ligase is required for transactivation of the hTERT promoter by the human papillomavirus E6 oncoprotein. Journal of Biological Chemistry **280:**10807-10816.

199. **Kelley ML, Keiger KE, Lee CJ, Huibregtse JM.** 2005. The global transcriptional effects of the human papillomavirus E6 protein in cervical carcinoma cell lines are mediated by the E6AP ubiquitin ligase. Journal of virology **79:**3737-3747.
200. **Xu M, Luo W, Elzi DJ, Grandori C, Galloway DA.** 2008. NFX1 interacts with mSin3A/histone deacetylase to repress hTERT transcription in keratinocytes. Molecular and cellular biology **28:**4819-4828.
201. **Taylor MP, Koyuncu OO, Enquist LW.** 2011. Subversion of the actin cytoskeleton during viral infection. Nat Rev Microbiol **9:**427-439.
202. **Brownlees J, Ackerley S, Grierson AJ, Jacobsen NJ, Shea K, Anderton BH, Leigh PN, Shaw CE, Miller CC.** 2002. Charcot–Marie–Tooth disease neurofilament mutations disrupt neurofilament assembly and axonal transport. Human molecular genetics **11:**2837-2844.
203. **Tirnauer JS, Bierer BE.** 2000. EB1 proteins regulate microtubule dynamics, cell polarity, and chromosome stability. The Journal of cell biology **149:**761-766.
204. **Shirnekhi HK, Kelley EP, DeLuca JG, Herman JA.** 2017. Spindle assembly checkpoint signaling and sister chromatid cohesion are disrupted by HPV E6-mediated transformation. Molecular biology of the cell **28:**2035-2041.
205. **Lamouille S, Xu J, Derynck R.** 2014. Molecular mechanisms of epithelial–mesenchymal transition. Nature reviews Molecular cell biology **15:**178.
206. **Zeisberg M, Neilson EG.** 2009. Biomarkers for epithelial-mesenchymal transitions. The Journal of clinical investigation **119:**1429-1437.
207. **Rahman MM, McFadden G.** 2011. Modulation of NF-κB signalling by microbial pathogens. Nature Reviews Microbiology **9:**291.
208. **Vandermark ER, Deluca KA, Gardner CR, Marker DF, Schreiner CN, Strickland DA, Wilton KM, Mondal S, Woodworth CD.** 2012. Human papillomavirus type 16 E6 and E 7 proteins alter NF-kB in cultured cervical epithelial cells and inhibition of NF-kB promotes cell growth and immortalization. Virology **425:**53-60.
209. **James MA, Lee JH, Klingelhutz AJ.** 2006. Human papillomavirus type 16 E6 activates NF-κB, induces cIAP-2 expression, and protects against apoptosis in a PDZ binding motif-dependent manner. Journal of virology **80:**5301-5307.
210. **Tilborghs S, Corthouts J, Verhoeven Y, Arias D, Rolfo C, Trinh XB, Van Dam PA.** 2017. The role of nuclear factor-kappa B signaling in human cervical cancer. Critical reviews in oncology/hematology **120:**141-150.
211. **Karim R, Tummers B, Meyers C, Biryukov JL, Alam S, Backendorf C, Jha V, Offringa R, van Ommen GJ, Melief CJ, Guardavaccaro D, Boer JM, van der Burg SH.** 2013. Human papillomavirus (HPV) upregulates the cellular deubiquitinase UCHL1 to suppress the keratinocyte's innate immune response. PLoS Pathog **9:**e1003384.
212. **Zur Hausen H, Schulte-Holtausen H, Klein G, Henle G, Henle W, Clifford P, Santesson L.** 1970. Epstein-Barr virus in Burkitt's lymphoma and nasopharyngeal carcinoma.[ii] EBV DNA in biopsies of Burkitt tumours and anaplastic carcinomas of the nasopharynx. Nature **228:**1056-1058.
213. **Mesri EA, Cesarman E, Boshoff C.** 2010. Kaposi's sarcoma and its associated herpesvirus. Nature Reviews Cancer **10:**707.
214. **Bheda A, Gullapalli A, Caplow M, Pagano JS, Shackelford J.** 2010. Ubiquitin editing enzyme UCH L1 and microtubule dynamics: implication in mitosis. Cell Cycle **9:**980-994.

215. **Bentz GL, Bheda-Malge A, Wang L, Shackelford J, Damania B, Pagano JS.** 2014. KSHV LANA and EBV LMP1 induce the expression of UCH-L1 following viral transformation. Virology **448:**293-302.
216. **Bheda A, Yue W, Gullapalli A, Shackelford J, Pagano JS.** 2011. PU. 1-dependent regulation of UCH L1 expression in B-lymphoma cells. Leukemia & lymphoma **52:**1336-1347.
217. **Jang MJ, Baek SH, Kim JH.** 2011. UCH-L1 promotes cancer metastasis in prostate cancer cells through EMT induction. Cancer letters **302:**128-135.
218. **Bassères E, Coppotelli G, Pfirrmann T, Andersen JB, Masucci M, Frisan T.** 2010. The ubiquitin C-terminal hydrolase UCH-L1 promotes bacterial invasion by altering the dynamics of the actin cytoskeleton. Cellular microbiology **12:**1622-1633.
219. **Neil SJ, Zang T, Bieniasz PD.** 2008. Tetherin inhibits retrovirus release and is antagonized by HIV-1 Vpu. Nature **451:**425.
220. **Pardieu C, Vigan R, Wilson SJ, Calvi A, Zang T, Bieniasz P, Kellam P, Towers GJ, Neil SJ.** 2010. The RING-CH ligase K5 antagonizes restriction of KSHV and HIV-1 particle release by mediating ubiquitin-dependent endosomal degradation of tetherin. PLoS pathogens **6:**e1000843.
221. **Viswanathan K, Smith MS, Malouli D, Mansouri M, Nelson JA, Früh K.** 2011. BST2/Tetherin enhances entry of human cytomegalovirus. PLoS pathogens **7:**e1002332.
222. **Cao W, Bover L, Cho M, Wen X, Hanabuchi S, Bao M, Rosen DB, Wang Y-H, Shaw JL, Du Q.** 2009. Regulation of TLR7/9 responses in plasmacytoid dendritic cells by BST2 and ILT7 receptor interaction. Journal of Experimental Medicine **206:**1603-1614.
223. **Mahauad-Fernandez WD, Okeoma CM.** 2016. The role of BST-2/Tetherin in host protection and disease manifestation. Immunity, inflammation and disease **4:**4-23.
224. **Cai D, Cao J, Li Z, Zheng X, Yao Y, Li W, Yuan Z.** 2009. Up-regulation of bone marrow stromal protein 2 (BST2) in breast cancer with bone metastasis. BMC cancer **9:**102.
225. **Mukai S, Oue N, Oshima T, Mukai R, Tatsumoto Y, Sakamoto N, Sentani K, Tanabe K, Egi H, Hinoi T.** 2017. Overexpression of transmembrane protein BST2 is associated with poor survival of patients with esophageal, gastric, or colorectal cancer. Annals of surgical oncology **24:**594-602.
226. **Ahn WS, Bae SM, Lee JM, Namkoong SE, Han S-J, Cho YL, Nam GH, Seo J-S, Kim CK, Kim Y-W.** 2004. Searching for pathogenic gene functions to cervical cancer. Gynecologic oncology **93:**41-48.
227. **Albanesi C, Cavani A, Girolomoni G.** 1999. IL-17 is produced by nickel-specific T lymphocytes and regulates ICAM-1 expression and chemokine production in human keratinocytes: synergistic or antagonist effects with IFN-γ and TNF-α. The Journal of Immunology **162:**494-502.
228. **Makgoba MW, Sanders ME, Luce GEG, Dustint ML, Springer TA, Clark EA, Mannoni P, Shaw S.** 1988. ICAM-1 a ligand for LFA-1-dependent adhesion of B, T and myeloid cells. Nature **331:**86.
229. **Banerjee P, Feuer G, Barker E.** 2007. Human T-cell leukemia virus type 1 (HTLV-1) p12I down-modulates ICAM-1 and-2 and reduces adherence of natural killer cells, thereby protecting HTLV-1-infected primary CD4+ T cells from autologous natural killer cell-mediated cytotoxicity despite the reduction of major histocompatibility complex class I molecules on infected cells. Journal of virology **81:**9707-9717.

230. **Coscoy L, Ganem D.** 2001. A viral protein that selectively downregulates ICAM-1 and B7-2 and modulates T cell costimulation. The Journal of clinical investigation **107:**1599-1606.
231. **Staunton DE, Merluzzi VJ, Rothlein R, Barton R, Marlin SD, Springer TA.** 1989. A cell adhesion molecule, ICAM-1, is the major surface receptor for rhinoviruses. Cell **56:**849-853.
232. **Textor S. AR, HavlovaT., Hussain I, Sylla B.S., Gissmann L., Cerwenka A.** 2011. NF-kB-dependent upregulation of ICAM-1 by HPV16-E6/E7 facilitates NK cell/target cell interaction. International_Journal_of_Cancer **128:**1104–1113
233. **Massimi P, Narayan N, Cuenda A, Banks L.** 2006. Phosphorylation of the discs large tumour suppressor protein controls its membrane localisation and enhances its susceptibility to HPV E6-induced degradation. Oncogene **25:**4276.
234. **Boon SS, Banks L.** 2013. High-risk human papillomavirus E6 oncoproteins interact with 14-3-3zeta in a PDZ binding motif-dependent manner. J Virol **87:**1586-1595.
235. **Thatte J, Massimi P, Thomas M, Boon SS, Banks L.** 2018. The HPV E6 PDZ Binding Motif links DNA Damage Response Signaling to E6 Inhibition of p53 Transcriptional Activity. Journal of virology**:**JVI. 00465-00418.
236. **Bhawal UK, Sugiyama M, Nomura Y, Kuniyasu H, Tsukinoki K.** 2008. Loss of 14-3-3 sigma protein expression and presence of human papillomavirus type 16 E6 in oral squamous cell carcinoma. Archives of Otolaryngology–Head & Neck Surgery **134:**1055-1059.
237. **Cheng L, Pan C-X, Zhang J-T, Zhang S, Kinch MS, Li L, Baldridge LA, Wade C, Hu Z, Koch MO.** 2004. Loss of 14-3-3σ in prostate cancer and its precursors. Clinical Cancer Research **10:**3064-3068.
238. **Vercoutter-Edouart A-S, Lemoine J, Le Bourhis X, Louis H, Boilly B, Nurcombe V, Révillion F, Peyrat J-P, Hondermarck H.** 2001. Proteomic analysis reveals that 14-3-3σ is down-regulated in human breast cancer cells. Cancer research **61:**76-80.
239. **Nakanishi K, Hashizume S, Kato M, Honjoh T, Setoguchi Y, Yasumoto K.** 1997. Elevated expression levels of the 14-3-3 family of proteins in lung cancer tissues. Human antibodies **8:**189-194.
240. **Sakakibara J, Sakakibara M, Shiina N, Fujimori T, Okubo Y, Fujisaki K, Nagashima T, Sangai T, Nakatani Y, Miyazaki M.** 2017. Expression of cell polarity protein scribble differently affects prognosis in primary tumor and lymph node metastasis of breast cancer patients. Breast Cancer **24:**393-399.
241. **Xue B, Krishnamurthy K, Allred DC, Muthuswamy SK.** 2013. Loss of Par3 promotes breast cancer metastasis by compromising cell–cell cohesion. Nature cell biology **15:**189-200.
242. **Yasuko Kitagishi SM.** 2013. MAGI Scaffolding Molecules Involved in Cancer Cell Signaling. Journal of Carcinogenesis & Mutagenesis doi:10.4172/2157-2518.s7-005.
243. **Grm HS, Banks L.** 2004. Degradation of hDlg and MAGIs by human papillomavirus E6 is E6-AP-independent. J Gen Virol **85:**2815-2819.
244. **Itoh M, Sasaki H, Furuse M, Ozaki H, Kita T, Tsukita S.** 2001. Junctional adhesion molecule (JAM) binds to PAR-3: a possible mechanism for the recruitment of PAR-3 to tight junctions. J Cell Biol **154:**491-497.

245. **Zheng J, Jiao S, Na L, Zheng S, Ma Z, Wang S, Aili A, Hasim A.** 2017. Defective expression of polarity protein Par3 promotes cervical tumorigenesis and metastasis. European journal of gynaecological oncology **38:**199-206.
246. **Chen J, Zhang M.** 2013. The Par3/Par6/aPKC complex and epithelial cell polarity. Experimental cell research **319:**1357-1364.
247. **Slebos RJ, Jehmlich N, Brown B, Yin Z, Chung CH, Yarbrough WG, Liebler DC.** 2013. Proteomic analysis of oropharyngeal carcinomas reveals novel HPV-associated biological pathways. Int J Cancer **132:**568-579.
248. **Ndiaye C, Mena M, Alemany L, Arbyn M, Castellsagué X, Laporte L, Bosch FX, de Sanjosé S, Trottier H.** 2014. HPV DNA, E6/E7 mRNA, and p16INK4a detection in head and neck cancers: a systematic review and meta-analysis. The Lancet Oncology **15:**1319-1331.
249. **Moody CA, Laimins LA.** 2010. Human papillomavirus oncoproteins: pathways to transformation. Nat Rev Cancer **10:**550-560.
250. **Van Dam PA, van Dam P-JH, Rolfo C, Giallombardo M, Van Berckelaer C, Trinh XB, Altintas S, Huizing M, Papadimitriou K, Tjalma WA.** 2016. In silico pathway analysis in cervical carcinoma reveals potential new targets for treatment. Oncotarget **7:**2780.
251. **Mohr IJ, Clark R, Sun S, Androphy EJ, MacPherson P, Botchan MR.** 1990. Targeting the E1 replication protein to the papillomavirus origin of replication by complex formation with the E2 transactivator. Science **250:**1694-1699.
252. **Bristol ML, Das D, Morgan IM.** 2017. Why human papillomaviruses activate the DNA damage response (DDR) and how cellular and viral replication persists in the presence of DDR signaling. Viruses **9:**268.
253. **Mehta K, Laimins L.** 2018. Human papillomaviruses preferentially recruit DNA repair factors to viral genomes for rapid repair and amplification. MBio **9:**e00064-00018.
254. **Chatzinikolaou G, Karakasilioti I, Garinis GA.** 2014. DNA damage and innate immunity: links and trade-offs. Trends in immunology **35:**429-435.
255. **Li R, Zhu J, Xie Z, Liao G, Liu J, Chen M-R, Hu S, Woodard C, Lin J, Taverna SD.** 2011. Conserved herpesvirus kinases target the DNA damage response pathway and TIP60 histone acetyltransferase to promote virus replication. Cell host & microbe **10:**390-400.
256. **Boichuk S, Hu L, Hein J, Gjoerup OV.** 2010. Multiple DNA damage signaling and repair pathways deregulated by simian virus 40 large T antigen. Journal of virology **84:**8007-8020.
257. **Kudoh A, Iwahori S, Sato Y, Nakayama S, Isomura H, Murata T, Tsurumi T.** 2009. Homologous recombinational repair factors are recruited and loaded onto the viral DNA genome in Epstein-Barr virus replication compartments. Journal of virology **83:**6641-6651.
258. **Moynahan ME, Chiu JW, Koller BH, Jasin M.** 1999. Brca1 controls homology-directed DNA repair. Molecular cell **4:**511-518.
259. **Burma S, Chen BP, Chen DJ.** 2006. Role of non-homologous end joining (NHEJ) in maintaining genomic integrity. DNA repair **5:**1042-1048.
260. **Zhang Y, Fan S, Meng Q, Ma Y, Katiyar P, Schlegel R, Rosen EM.** 2005. BRCA1 interaction with human papillomavirus oncoproteins. Journal of Biological Chemistry **280:**33165-33177.

261. **Chaib-Mezrag H, Lemaçon D, Fontaine H, Bellon M, Bai XT, Drac M, Coquelle A, Nicot C.** 2014. Tax impairs DNA replication forks and increases DNA breaks in specific oncogenic genome regions. Molecular cancer **13:**205.
262. **Yamaoka S, Inoue H, Sakurai M, Sugiyama T, Hazama M, Yamada T, Hatanaka M.** 1996. Constitutive activation of NF-kappa B is essential for transformation of rat fibroblasts by the human T-cell leukemia virus type I Tax protein. The EMBO Journal **15:**873-887.
263. **Neves H, Kwok HF.** 2017. In sickness and in health: the many roles of the minichromosome maintenance proteins. Biochimica et Biophysica Acta (BBA)-Reviews on Cancer **1868:**295-308.
264. **Giaginis C, Vgenopoulou S, Vielh P, Theocharis S.** 2010. MCM proteins as diagnostic and prognostic tumor markers in the clinical setting. Histology and histopathology **25:**351-370.
265. **Das M, Prasad SB, Yadav SS, Govardhan H, Pandey LK, Singh S, Pradhan S, Narayan G.** 2013. Over expression of minichromosome maintenance genes is clinically correlated to cervical carcinogenesis. PloS one **8:**e69607.
266. **Li X, Tian R, Gao H, Yan F, Ying L, Yang Y, Yang P, Gao Ye.** 2018. Identification of Significant Gene Signatures and Prognostic Biomarkers for Patients With Cervical Cancer by Integrated Bioinformatic Methods. Technology in cancer research & treatment **17:**1533033818767455.
267. **Chicas A, Wang X, Zhang C, McCurrach M, Zhao Z, Mert O, Dickins RA, Narita M, Zhang M, Lowe SW.** 2010. Dissecting the unique role of the retinoblastoma tumor suppressor during cellular senescence. Cancer cell **17:**376-387.
268. **Lo Sardo F, Strano S, Blandino G.** 2018. YAP and TAZ in Lung Cancer: Oncogenic Role and Clinical Targeting. Cancers **10:**137.
269. **Weichert W, Denkert C, Noske A, Darb-Esfahani S, Dietel M, Kalloger SE, Huntsman DG, Köbel M.** 2008. Expression of class I histone deacetylases indicates poor prognosis in endometrioid subtypes of ovarian and endometrial carcinomas. Neoplasia **10:**1021-1027.
270. **Choi JH, Kwon HJ, Yoon BI, Kim JH, Han SU, Joo HJ, Kim DY.** 2001. Expression profile of histone deacetylase 1 in gastric cancer tissues. Japanese Journal of Cancer Research **92:**1300-1304.
271. **Langsfeld ES, Bodily JM, Laimins LA.** 2015. The deacetylase sirtuin 1 regulates human papillomavirus replication by modulating histone acetylation and recruitment of DNA damage factors NBS1 and Rad51 to viral genomes. PLoS pathogens **11:**e1005181.
272. **So D, Shin H-W, Kim J, Lee M, Myeong J, Chun Y-S, Park J-W.** 2018. Cervical cancer is addicted to SIRT1 disarming the AIM2 antiviral defense. Oncogene**:**1.
273. **Das D, Smith N, Wang X, Morgan IM.** 2017. The deacetylase SIRT1 regulates the replication properties of human papillomavirus 16 E1 and E2. Journal of virology**:**JVI. 00102-00117.
274. **Hasan UA, Zannetti C, Parroche P, Goutagny N, Malfroy M, Roblot G, Carreira C, Hussain I, Müller M, Taylor-Papadimitriou J.** 2013. The human papillomavirus type 16 E7 oncoprotein induces a transcriptional repressor complex on the Toll-like receptor 9 promoter. Journal of Experimental Medicine **210:**1369-1387.

275. **Morgan IM, Das D, Bristol M, Smith NW, Wang X, Pichierri P.** 2018. Werner helicase control of human papillomavirus 16 E1-E2 DNA replication is regulated by SIRT1 deacetylation. bioRxiv**:**450601.
276. **Kim E-J, Kho J-H, Kang M-R, Um S-J.** 2007. Active regulator of SIRT1 cooperates with SIRT1 and facilitates suppression of p53 activity. Molecular cell **28:**277-290.
277. **Mine KL, Shulzhenko N, Yambartsev A, Rochman M, Sanson GF, Lando M, Varma S, Skinner J, Volfovsky N, Deng T.** 2013. Gene network reconstruction reveals cell cycle and antiviral genes as major drivers of cervical cancer. Nature communications **4:**1806.
278. **Kanao H, Enomoto T, Kimura T, Fujita M, Nakashima R, Ueda Y, Ueno Y, Miyatake T, Yoshizaki T, Buzard GS, Tanigami A, Yoshino K, Murata Y.** 2005. Overexpression of LAMP3/TSC403/DC-LAMP promotes metastasis in uterine cervical cancer. Cancer Res **65:**8640-8645.
279. **Liao X, Chen Y, Liu D, Li F, Li X, Jia W.** 2015. High expression of LAMP3 is a novel biomarker of poor prognosis in patients with esophageal squamous cell carcinoma. International journal of molecular sciences **16:**17655-17667.
280. **Wang D, Cao X, Zhang Y, Liu Y, Yao C, Ge W, Xu Y.** 2017. LAMP3 expression correlated with poor clinical outcome in human ovarian cancer. Tumor Biology **39:**1010428317695014.
281. **Liao X, Song L, Zhang L, Wang H, Tong Q, Xu J, Yang G, Yang S, Zheng H.** 2017. LAMP3 regulates hepatic lipid metabolism through activating PI3K/Akt pathway. Molecular and cellular endocrinology.
282. **Moon HS, Park HM, Chung HW.** 2000. The midkine mRNA expression in invasive cervical cancer. Korean Journal of Gynecologic Oncology and Colposcopy **11:**123-130.
283. **O'Brien T, Cranston D, Fuggle S, Bicknell R, Harris AL.** 1996. The angiogenic factor midkine is expressed in bladder cancer, and overexpression correlates with a poor outcome in patients with invasive cancers. Cancer research **56:**2515-2518.
284. **Shimada H, Nabeya Y, Okazumi S-I, Matsubara H, Kadomatsu K, Muramatsu T, Ikematsu S, Sakuma S, Ochiai T.** 2003. Increased serum midkine concentration as a possible tumor marker in patients with superficial esophageal cancer. Oncology reports **10:**411-414.
285. **Zhao Z-Q, Yang S, Lu H-S.** 2012. Expression of midkine and vascular endothelial growth factor in gastric cancer and the association of high levels with poor prognosis and survival. Molecular medicine reports **5:**415-419.
286. **Owada K, Sanjo N, Kobayashi T, Mizusawa H, Muramatsu H, Muramatsu T, Michikawa M.** 1999. Midkine inhibits caspase-dependent apoptosis via the activation of mitogen-activated protein kinase and phosphatidylinositol 3-kinase in cultured neurons. Journal of neurochemistry **73:**2084-2092.
287. **Qi M, Ikematsu S, Icbihara-Tanaka K, Sakuma S, Muramatsu T, Kadomatsu K.** 2000. Midkine rescues Wilms, tumor cells from cisplatin-induced apoptosis: regulation of Bcl-2 expression by Midkine. The Journal of Biochemistry **127:**269-277.
288. **Stoica GE, Kuo A, Powers C, Bowden ET, Sale EB, Riegel AT, Wellstein A.** 2002. Midkine binds to anaplastic lymphoma kinase (ALK) and acts as a growth factor for different cell types. Journal of Biological Chemistry **277:**35990-35998.
289. **Fukazawa T, Maeda Y, Yamatsuji T, Takaoka M, Yoshida M, Ishida N, Iwai M, Yokota E, Yukawa T, Haisa M.** 2017. Development of a novel targeted therapy for malignant mesothelioma carcinoma by a midkine inhibitor. AACR.

290. **Hovanessian AG.** 2006. Midkine, a cytokine that inhibits HIV infection by binding to the cell surface expressed nucleolin. Cell research **16:**174.
291. **Duffy CL, Phillips SL, Klingelhutz AJ.** 2003. Microarray analysis identifies differentiation-associated genes regulated by human papillomavirus type 16 E6. Virology **314:**196-205.
292. **Arnold KB, Burgener A, Birse K, Romas L, Dunphy LJ, Shahabi K, Abou M, Westmacott GR, McCorrister S, Kwatampora J.** 2016. Increased levels of inflammatory cytokines in the female reproductive tract are associated with altered expression of proteases, mucosal barrier proteins, and an influx of HIV-susceptible target cells. Mucosal immunology **9:**194.
293. **Rheinwald JG, Beckett MA.** 1980. Defective terminal differentiation in culture as a consistent and selectable character of malignant human keratinocytes. Cell **22:**629-632.
294. **Thomas M, Tomaic V, Pim D, Myers MP, Tommasino M, Banks L.** 2013. Interactions between E6AP and E6 proteins from alpha and beta HPV types. Virology **435:**357-362.
295. **Cooper B, Schneider S, Bohl J, Jiang Y-h, Beaudet A, Pol SV.** 2003. Requirement of E6AP and the features of human papillomavirus E6 necessary to support degradation of p53. Virology **306:**87-99.
296. **Torres-Flores JM, Arias CF.** 2015. Tight Junctions Go Viral! Viruses **7:**5145-5154.

Appendix 1

280 Proteins dysregulated in HPV16 E6+E7 cells compared to HPV16 E6ΔPBM+E7 cells

Protein ID	Fold change	Adjusted p-value
NFH_HUMAN	4.77	1.33E-02
AINX_HUMAN	4.73	1.92E-04
BST2_HUMAN	3.05	1.83E-04
RCN3_HUMAN	2.11	2.31E-02
CO6A2_HUMAN	2.11	2.13E-03
NFL_HUMAN	2.08	2.60E-03
UCHL1_HUMAN	2.05	3.31E-04
FKB10_HUMAN	1.87	1.69E-04
RSAD2_HUMAN	1.78	1.15E-03
H1X_HUMAN	1.77	3.16E-02
GLB1L_HUMAN	1.75	4.15E-03
SMOC1_HUMAN	1.72	1.83E-04
CO6A1_HUMAN	1.71	8.56E-03
NFM_HUMAN	1.71	1.69E-04
LPP2_HUMAN	1.63	1.84E-02
SC65_HUMAN	1.63	1.69E-04
ICAM1_HUMAN	1.62	2.35E-03
TAXB1_HUMAN	1.62	6.49E-04
CBPQ_HUMAN	1.61	7.28E-03
PGH1_HUMAN	1.61	3.49E-03
AL1L2_HUMAN	1.60	1.33E-02
ECHD3_HUMAN	1.60	1.78E-02
ESIP1_HUMAN	1.56	2.12E-02
RPP25_HUMAN	1.55	1.94E-03
S39AB_HUMAN	1.55	7.02E-03
1B44_HUMAN	1.54	2.08E-02
MACD1_HUMAN	1.54	1.94E-03
IFIT2_HUMAN	1.52	3.96E-03
VLDLR_HUMAN	1.51	1.22E-02
NEST_HUMAN	1.51	2.28E-02
HSP72_HUMAN	1.51	9.90E-04
BT3A3_HUMAN	1.50	1.21E-03
CFAB_HUMAN	1.49	4.56E-02
P3H3_HUMAN	1.47	1.15E-03
1A01_HUMAN	1.47	4.15E-03
HMGN3_HUMAN	1.46	3.55E-02
OGFR_HUMAN	1.45	4.15E-03
CBX4_HUMAN	1.44	1.33E-02

CIR1_HUMAN	1.44	2.74E-02
LY75_HUMAN	1.43	9.91E-03
ASNS_HUMAN	1.43	1.33E-02
DPYL3_HUMAN	1.42	4.73E-03
ANO1_HUMAN	1.42	4.93E-02
SRSF4_HUMAN	1.42	2.40E-02
TNIP1_HUMAN	1.41	2.60E-03
DHX40_HUMAN	1.41	4.28E-02
H10_HUMAN	1.40	2.08E-02
1A02_HUMAN	1.39	5.82E-03
PCKGM_HUMAN	1.39	1.76E-02
MX2_HUMAN	1.39	1.33E-02
OASL_HUMAN	1.39	3.09E-02
CLMN_HUMAN	1.38	1.36E-02
AL1A1_HUMAN	1.37	3.00E-02
SP14L_HUMAN	1.37	1.91E-02
OAS2_HUMAN	1.36	2.98E-02
NBR1_HUMAN	1.35	1.84E-02
FKBP5_HUMAN	1.34	2.93E-02
SP100_HUMAN	1.34	1.91E-02
PSB9_HUMAN	1.32	2.28E-02
P5CR1_HUMAN	1.32	3.00E-02
DDX6L_HUMAN	1.31	2.85E-03
GDN_HUMAN	1.31	8.85E-03
MMSA_HUMAN	1.31	7.49E-03
MET17_HUMAN	1.30	1.33E-02
TNAP3_HUMAN	1.29	1.33E-02
SUMO3_HUMAN	1.29	4.35E-02
UN93B_HUMAN	1.29	4.58E-02
REXO4_HUMAN	1.29	1.91E-02
ATPF1_HUMAN	1.29	3.01E-02
WBP4_HUMAN	1.29	3.16E-02
Z280C_HUMAN	1.28	2.12E-02
UIF_HUMAN	1.28	2.13E-03
TAP2_HUMAN	1.28	4.15E-03
ALAT2_HUMAN	1.28	1.78E-02
FUT8_HUMAN	1.28	2.25E-02
THNS1_HUMAN	1.27	3.31E-02
GLPK3_HUMAN (+1)	1.27	4.23E-02
CNTP1_HUMAN	1.27	4.95E-02
KANL3_HUMAN	1.25	4.61E-02
GOGA5_HUMAN	1.25	2.60E-03
PALM2_HUMAN	1.25	4.56E-02

UBP11_HUMAN	1.25	4.65E-02
AL3A2_HUMAN	1.25	7.31E-03
DDX56_HUMAN	1.24	2.60E-02
ABCB6_HUMAN	1.24	3.53E-02
RN213_HUMAN	1.24	4.15E-03
DNJB4_HUMAN	1.24	2.60E-02
COASY_HUMAN	1.24	8.04E-03
SRRM1_HUMAN	1.24	2.93E-02
PHAR4_HUMAN	1.24	9.65E-03
KCP3_HUMAN	1.24	4.93E-02
PUR4_HUMAN	1.24	3.80E-02
SYNE1_HUMAN	1.23	1.84E-02
DCXR_HUMAN	1.22	1.33E-02
TRM1_HUMAN	1.22	2.12E-02
CROCC_HUMAN	1.22	3.46E-02
TPSN_HUMAN	1.21	4.36E-02
MECP2_HUMAN	1.21	4.56E-02
RBM26_HUMAN	1.21	1.69E-02
PPHLN_HUMAN	1.21	3.18E-02
ZKSC1_HUMAN	1.21	2.28E-02
SERPH_HUMAN	1.21	1.78E-02
SET_HUMAN	1.20	4.36E-02
HLAE_HUMAN	1.20	2.18E-02
RCN1_HUMAN	1.20	5.84E-03
HPSE_HUMAN	1.20	4.36E-02
TRM5_HUMAN	1.20	4.54E-02
MTNB_HUMAN	1.20	4.01E-02
GRIN1_HUMAN	1.20	1.80E-02
PPT1_HUMAN	1.20	2.28E-02
AGRIN_HUMAN	1.20	2.31E-02
DSRAD_HUMAN	1.20	4.56E-02
PGLT1_HUMAN	1.19	2.11E-02
TAP1_HUMAN	1.19	2.12E-02
TMED1_HUMAN	1.19	4.65E-02
CMTR1_HUMAN	1.19	2.73E-02
NOC2L_HUMAN	1.19	2.60E-02
CECR5_HUMAN	1.19	3.00E-02
TIM14_HUMAN	1.19	4.47E-02
RBM19_HUMAN	1.19	3.99E-02
K2013_HUMAN	1.19	4.36E-02
TRUA_HUMAN	1.19	4.07E-02
MORC2_HUMAN	1.18	3.60E-02
HELZ2_HUMAN	1.18	2.11E-02

TRM1L_HUMAN	1.18	3.06E-02
TRM6_HUMAN	1.18	4.23E-02
LACB2_HUMAN	1.18	3.00E-02
CATD_HUMAN	1.18	4.23E-02
TACO1_HUMAN	1.18	4.25E-02
NGDN_HUMAN	1.18	4.36E-02
PK1IP_HUMAN	1.17	1.58E-02
TIM16_HUMAN	1.17	1.91E-02
P3H2_HUMAN	1.17	4.98E-02
SART3_HUMAN	1.17	4.42E-02
SRRM2_HUMAN	1.17	2.33E-02
FERM2_HUMAN	1.16	1.01E-02
LAMC1_HUMAN	1.16	4.07E-02
TM9S1_HUMAN	1.16	4.20E-02
PYRD_HUMAN	1.16	2.52E-02
CLP1L_HUMAN	1.16	4.61E-02
DPOE4_HUMAN	1.16	4.65E-02
ARFG1_HUMAN	1.15	3.00E-02
PRC2A_HUMAN	1.15	4.93E-02
SCFD1_HUMAN	1.15	4.35E-02
NOP58_HUMAN	1.15	3.06E-02
TRIPB_HUMAN	1.15	2.74E-02
T126A_HUMAN	1.14	4.83E-02
PLOD1_HUMAN	1.14	4.28E-02
RBM8A_HUMAN	1.14	4.61E-02
PELP1_HUMAN	1.14	4.73E-02
STML2_HUMAN	1.14	4.56E-02
CN166_HUMAN	1.13	4.33E-02
ATM_HUMAN	1.13	3.80E-02
TRAP1_HUMAN	1.12	4.42E-02
GOGA3_HUMAN	1.12	4.23E-02
SPY4_HUMAN	-1.12	4.61E-02
HXK2_HUMAN	-1.13	4.23E-02
RALB_HUMAN	-1.13	4.93E-02
CQ089_HUMAN	-1.13	4.56E-02
RICTR_HUMAN	-1.13	4.20E-02
C1QT6_HUMAN	-1.14	4.36E-02
FYCO1_HUMAN	-1.14	4.44E-02
AHNK_HUMAN	-1.15	3.31E-02
FAKD5_HUMAN	-1.15	2.84E-02
DCTN4_HUMAN	-1.15	4.61E-02
CD032_HUMAN	-1.15	4.93E-02
SRC8_HUMAN	-1.15	4.93E-02

AT131_HUMAN	-1.15	4.93E-02
TMPPE_HUMAN	-1.15	3.92E-02
NT5D3_HUMAN	-1.16	4.36E-02
IDHP_HUMAN	-1.16	1.88E-02
PTN1_HUMAN	-1.16	1.96E-02
MTMR1_HUMAN	-1.16	3.25E-02
LAMB2_HUMAN	-1.17	4.01E-02
ESYT1_HUMAN	-1.17	2.60E-02
S12A4_HUMAN	-1.17	2.40E-02
IL1AP_HUMAN	-1.17	2.42E-02
NAV1_HUMAN	-1.18	2.08E-02
CYBR1_HUMAN	-1.18	4.39E-02
ACOT8_HUMAN	-1.18	4.23E-02
RHOA_HUMAN	-1.18	6.53E-03
HIP1R_HUMAN	-1.18	3.46E-02
DSC3_HUMAN	-1.19	3.06E-02
SNX33_HUMAN	-1.19	4.28E-02
CATA_HUMAN	-1.19	4.39E-02
APLP2_HUMAN	-1.19	4.73E-02
SI1L1_HUMAN	-1.20	4.15E-03
RETST_HUMAN	-1.20	1.01E-02
VAPB_HUMAN	-1.20	1.72E-02
VAMP8_HUMAN	-1.20	1.78E-02
ARPC2_HUMAN	-1.20	2.27E-02
IKIP_HUMAN	-1.20	3.80E-02
GPX1_HUMAN	-1.20	1.36E-02
DPM1_HUMAN	-1.20	1.07E-02
OXSR1_HUMAN	-1.20	3.99E-02
TMF1_HUMAN	-1.21	1.89E-02
RAB5A_HUMAN	-1.21	1.01E-02
BGAL_HUMAN	-1.21	2.64E-02
PTPRG_HUMAN	-1.21	1.96E-02
DHX30_HUMAN	-1.22	3.25E-02
SYNE2_HUMAN	-1.22	7.31E-03
CO052_HUMAN	-1.22	3.31E-02
STAU1_HUMAN	-1.22	2.74E-02
SYQ_HUMAN	-1.22	4.65E-02
NPC2_HUMAN	-1.22	1.02E-02
DC1L1_HUMAN	-1.22	4.93E-02
NUD12_HUMAN	-1.22	1.44E-02
TOP2B_HUMAN	-1.22	2.36E-02
MYO6_HUMAN	-1.22	2.08E-02
TIM8B_HUMAN	-1.23	8.20E-03

ARP3_HUMAN	-1.23	1.80E-02
SNX1_HUMAN	-1.23	4.33E-02
S39AA_HUMAN	-1.23	2.46E-03
LYRM2_HUMAN	-1.23	3.73E-02
RALY_HUMAN	-1.24	2.18E-02
RON_HUMAN	-1.24	2.18E-02
TSN14_HUMAN	-1.24	4.15E-03
PDC6I_HUMAN	-1.25	4.42E-02
KPCD_HUMAN	-1.25	2.74E-02
DNJB9_HUMAN	-1.25	4.65E-02
ES8L2_HUMAN	-1.25	4.61E-02
CHM4B_HUMAN	-1.26	2.93E-02
MBP_HUMAN	-1.26	1.73E-02
CDK4_HUMAN	-1.26	4.36E-02
SEPT9_HUMAN	-1.26	2.52E-02
C43BP_HUMAN	-1.26	4.36E-02
FAT1_HUMAN	-1.27	1.93E-02
PDE12_HUMAN	-1.27	6.35E-03
TGFR2_HUMAN	-1.27	3.48E-03
KCJ15_HUMAN	-1.27	1.53E-02
COXM1_HUMAN	-1.28	1.28E-02
ARC1A_HUMAN	-1.29	8.20E-03
ACPH_HUMAN	-1.29	2.52E-02
RABL6_HUMAN	-1.29	1.73E-02
TM7S3_HUMAN	-1.29	1.78E-02
TUSC3_HUMAN	-1.29	6.06E-03
TIGAR_HUMAN	-1.30	4.61E-02
EXOG_HUMAN	-1.30	4.22E-03
HMDH_HUMAN	-1.30	2.18E-02
MCATL_HUMAN	-1.30	2.13E-02
SSFA2_HUMAN	-1.30	2.35E-03
LANC1_HUMAN	-1.30	3.80E-02
S4A7_HUMAN	-1.31	4.58E-02
EOGT_HUMAN	-1.31	1.58E-03
TRIA1_HUMAN	-1.32	4.22E-03
AL7A1_HUMAN	-1.32	5.46E-03
TENS4_HUMAN	-1.32	5.42E-03
CLCA2_HUMAN	-1.32	3.09E-02
IMDH2_HUMAN	-1.33	1.33E-02
LTBP2_HUMAN	-1.33	4.36E-02
P5I11_HUMAN	-1.33	4.20E-02
SDHF4_HUMAN	-1.34	4.36E-02
SDC1_HUMAN	-1.35	1.64E-03

ARPC3_HUMAN	-1.35	8.20E-03
EAA1_HUMAN	-1.35	4.49E-02
DCBD2_HUMAN	-1.36	2.78E-02
TMM40_HUMAN	-1.36	7.02E-03
MARE1_HUMAN	-1.36	2.13E-03
PAI2_HUMAN	-1.36	4.80E-02
NT5D2_HUMAN	-1.37	1.78E-02
RS27L_HUMAN	-1.38	1.33E-02
CAD13_HUMAN	-1.38	1.64E-03
CTDSL_HUMAN	-1.39	8.20E-03
EFNB2_HUMAN	-1.39	1.07E-02
CP51A_HUMAN	-1.40	4.93E-02
ABC3C_HUMAN	-1.40	2.93E-02
CDN1A_HUMAN	-1.40	8.32E-03
CHM2B_HUMAN	-1.43	3.06E-02
HYAS3_HUMAN	-1.45	3.06E-02
MEGF9_HUMAN	-1.48	8.79E-03
XDH_HUMAN	-1.49	7.02E-03
TEN2_HUMAN	-1.53	4.15E-03
CAH12_HUMAN	-1.53	4.94E-02
RBM3_HUMAN	-1.54	1.36E-02
NSG1_HUMAN	-1.57	2.60E-03
ADIRF_HUMAN	-1.59	4.23E-02
GTR1_HUMAN	-1.67	1.69E-04
S10A2_HUMAN	-1.71	4.56E-02
SAP3_HUMAN	-1.73	3.42E-02
AK1C3_HUMAN	-2.53	4.28E-02

Appendix 2

3014 Proteins dysregulated in the HPV16 E6+E7 cell line compared to LV-HEKn control cells.

Protein ID	Fold change	Adjusted p-value
LAMP3_HUMAN	19.60	1.17E-02
H11_HUMAN	8.51	6.80E-04
BST2_HUMAN	6.39	4.91E-07
1B44_HUMAN	5.65	3.38E-07
S43A3_HUMAN	5.04	3.13E-04
MK_HUMAN	4.32	2.79E-04
NFH_HUMAN	4.32	1.65E-03
H13_HUMAN	4.08	1.76E-02
MX2_HUMAN	4.07	2.68E-07
TNF10_HUMAN	4.02	3.46E-06
H1X_HUMAN	3.80	1.99E-05
1B18_HUMAN	3.59	2.04E-02
UB2L6_HUMAN	3.52	9.92E-04
INCE_HUMAN	3.45	3.78E-02
SAMH1_HUMAN	3.42	4.43E-07
CO6A2_HUMAN	3.32	5.47E-06
IFIT3_HUMAN	3.26	2.91E-06
OAS2_HUMAN	3.25	6.32E-07
H10_HUMAN	3.18	7.15E-07
H12_HUMAN	3.16	1.03E-02
AINX_HUMAN	3.14	1.39E-04
RCN3_HUMAN	3.12	2.33E-04
H2AV_HUMAN (+1)	3.03	9.52E-03
CP1B1_HUMAN	3.01	2.54E-03
IFIT2_HUMAN	2.96	5.34E-07
EPCAM_HUMAN	2.91	3.46E-06
ISG15_HUMAN	2.88	3.46E-06
OAS1_HUMAN	2.84	1.13E-06
MX1_HUMAN	2.82	6.20E-06
MCM6_HUMAN	2.82	3.42E-04
BRCA1_HUMAN	2.81	7.07E-03
HLAG_HUMAN	2.75	1.16E-04
NASP_HUMAN	2.74	1.20E-05
RSAD2_HUMAN	2.64	1.95E-06
SP100_HUMAN	2.63	8.72E-07
1C07_HUMAN	2.62	9.69E-05
IFIT1_HUMAN	2.58	5.77E-06
ESIP1_HUMAN	2.56	1.99E-05
GWL_HUMAN	2.54	2.60E-06

FKB10_HUMAN	2.54	4.43E-07
OASL_HUMAN	2.42	6.66E-06
APR_HUMAN	2.35	5.76E-04
CBS_HUMAN	2.34	3.94E-04
HLAF_HUMAN	2.33	5.24E-06
LPP2_HUMAN	2.31	7.56E-05
DCC1_HUMAN	2.31	1.30E-03
MCM5_HUMAN	2.30	1.63E-04
PLS1_HUMAN	2.29	5.24E-06
CO6A1_HUMAN	2.29	5.63E-05
HERC5_HUMAN	2.28	3.38E-07
PSIP1_HUMAN	2.27	2.92E-03
SP110_HUMAN	2.26	9.18E-06
HMGN2_HUMAN	2.26	9.52E-04
DDX6L_HUMAN	2.25	3.05E-07
PSF3_HUMAN	2.24	5.50E-05
TYPH_HUMAN	2.22	1.50E-04
UBR7_HUMAN	2.22	1.03E-03
ZN768_HUMAN	2.22	1.38E-03
PCNA_HUMAN	2.18	1.28E-03
MUC1_HUMAN	2.17	9.11E-05
NMI_HUMAN	2.17	7.51E-05
NRK_HUMAN	2.15	1.22E-05
H33_HUMAN	2.15	6.66E-03
TOP2A_HUMAN	2.15	8.41E-03
RN114_HUMAN	2.14	1.77E-06
WDHD1_HUMAN	2.14	1.88E-04
OGFR_HUMAN	2.13	2.73E-06
DEK_HUMAN	2.13	2.78E-04
AMPN_HUMAN	2.11	3.46E-06
TONSL_HUMAN	2.11	1.15E-02
MCM4_HUMAN	2.09	8.88E-06
MCM7_HUMAN	2.09	1.63E-04
B2MG_HUMAN	2.05	1.77E-06
ECHD3_HUMAN	2.03	1.60E-04
1A01_HUMAN	2.02	5.51E-06
H14_HUMAN	2.02	3.84E-03
HMGB2_HUMAN	2.01	2.78E-04
MCM2_HUMAN	2.00	8.33E-04
HOIL1_HUMAN	2.00	1.67E-03
PGH1_HUMAN	1.99	2.34E-05
STAT1_HUMAN	1.99	8.66E-05
TCEA2_HUMAN	1.99	1.81E-03

PARP9_HUMAN	1.98	3.46E-06
SC65_HUMAN	1.98	9.48E-07
MCM3_HUMAN	1.98	1.87E-06
MSH2_HUMAN	1.98	2.84E-05
CMPK2_HUMAN	1.98	1.63E-05
VEZF1_HUMAN	1.96	2.78E-04
FKBP5_HUMAN	1.96	2.03E-05
IN35_HUMAN	1.95	3.36E-05
HERC6_HUMAN	1.94	7.86E-06
OAS3_HUMAN	1.94	2.52E-04
SSRP1_HUMAN	1.94	2.70E-04
BAG2_HUMAN	1.92	3.79E-04
MUC18_HUMAN	1.91	3.38E-07
HSP72_HUMAN	1.91	2.49E-06
AMPL_HUMAN	1.90	3.42E-06
UCHL1_HUMAN	1.90	5.73E-05
PSB10_HUMAN	1.90	5.04E-04
DDX58_HUMAN	1.90	8.96E-05
RPP25_HUMAN	1.89	9.18E-06
H4_HUMAN	1.89	9.63E-03
CCNB1_HUMAN	1.89	3.36E-02
PSB9_HUMAN	1.88	1.56E-05
TAP2_HUMAN	1.88	6.68E-07
DNLI1_HUMAN	1.87	3.55E-04
APOL2_HUMAN	1.86	2.08E-05
P3H3_HUMAN	1.86	2.73E-06
NEST_HUMAN	1.85	2.45E-04
HMGB1_HUMAN	1.85	9.49E-04
RFA2_HUMAN	1.85	7.62E-07
DTX3L_HUMAN	1.85	5.24E-06
TCOF_HUMAN	1.84	3.15E-04
KIF2C_HUMAN	1.84	1.04E-02
CGAS_HUMAN	1.84	8.67E-04
H2AX_HUMAN	1.84	2.36E-02
DPOD3_HUMAN	1.83	6.34E-05
RIF1_HUMAN	1.83	1.69E-03
CFAB_HUMAN	1.83	6.31E-04
LY75_HUMAN	1.82	3.55E-05
TAXB1_HUMAN	1.82	7.92E-06
UN93B_HUMAN	1.82	4.08E-05
PML_HUMAN	1.82	7.71E-05
CS066_HUMAN	1.81	7.78E-04
DDX60_HUMAN	1.81	5.43E-05

PTMA_HUMAN	1.80	3.42E-04
MIS12_HUMAN	1.79	2.93E-03
HAT1_HUMAN	1.79	3.33E-04
IF16_HUMAN	1.78	2.49E-06
CNDH2_HUMAN	1.78	1.77E-03
SP16H_HUMAN	1.77	2.87E-05
BT3A3_HUMAN	1.77	6.20E-06
TXNIP_HUMAN	1.77	2.48E-04
RN213_HUMAN	1.77	5.34E-07
1A02_HUMAN	1.77	1.36E-05
MSH6_HUMAN	1.77	3.50E-05
NRCAM_HUMAN	1.77	9.48E-07
CDK1_HUMAN	1.76	2.21E-04
SPTCS_HUMAN	1.76	3.15E-02
TRI22_HUMAN	1.76	1.18E-05
RFC4_HUMAN	1.76	8.38E-04
K0907_HUMAN	1.76	1.52E-02
HMGA1_HUMAN	1.76	3.15E-03
SIR1_HUMAN	1.75	5.56E-05
RGAP1_HUMAN	1.74	3.91E-03
DCK_HUMAN	1.74	4.88E-04
DSRAD_HUMAN	1.74	5.38E-06
CBX4_HUMAN	1.74	1.14E-04
PNPT1_HUMAN	1.74	2.71E-06
UTP23_HUMAN	1.74	5.84E-04
PKHA4_HUMAN	1.73	5.50E-04
REXO4_HUMAN	1.73	1.43E-05
FBX6_HUMAN	1.73	2.46E-03
PRI1_HUMAN	1.73	6.86E-04
ZN740_HUMAN	1.73	4.05E-03
NSE4A_HUMAN	1.72	3.97E-03
S29A1_HUMAN	1.72	1.20E-02
CSPG4_HUMAN	1.72	8.12E-04
K1C19_HUMAN	1.72	1.37E-02
BRX1_HUMAN	1.71	1.22E-04
VEGFC_HUMAN	1.71	2.02E-03
SP14L_HUMAN	1.71	8.83E-05
DNJC9_HUMAN	1.71	3.45E-05
ICAM1_HUMAN	1.71	1.02E-04
KDEL2_HUMAN	1.71	3.53E-05
SRBP1_HUMAN	1.70	2.68E-02
CATK_HUMAN	1.70	7.41E-03
NBR1_HUMAN	1.70	6.50E-05

NSE2_HUMAN	1.70	3.01E-02
TDRD7_HUMAN	1.69	5.82E-06
KIF4A_HUMAN	1.69	9.24E-04
CO1A1_HUMAN	1.69	3.15E-02
5NT3A_HUMAN	1.69	1.92E-05
EXOS5_HUMAN	1.68	1.32E-03
PD1L1_HUMAN	1.68	2.37E-04
LYAR_HUMAN	1.68	3.82E-04
SMHD1_HUMAN	1.68	1.63E-05
CAF1B_HUMAN	1.68	4.24E-03
KIF23_HUMAN	1.68	1.78E-03
LMNB1_HUMAN	1.68	7.69E-04
DHR13_HUMAN	1.68	2.13E-02
LAP2A_HUMAN	1.68	3.45E-03
SRSF4_HUMAN	1.67	2.96E-04
PMF1_HUMAN	1.67	8.66E-05
T194A_HUMAN	1.67	7.10E-05
DSN1_HUMAN	1.67	1.31E-05
SUMO1_HUMAN	1.67	5.24E-06
NFIP1_HUMAN	1.66	3.19E-03
TRFM_HUMAN	1.66	6.06E-06
GRPE2_HUMAN	1.66	3.56E-04
GBP1_HUMAN	1.66	3.91E-04
RN169_HUMAN	1.66	9.60E-04
LG3BP_HUMAN	1.66	3.74E-03
SMC2_HUMAN	1.66	5.18E-03
BT3A2_HUMAN	1.66	5.52E-04
ASNS_HUMAN	1.66	1.63E-04
RFC2_HUMAN	1.65	4.64E-04
TOP1_HUMAN	1.65	2.25E-04
RBM28_HUMAN	1.65	2.48E-04
KI67_HUMAN	1.65	1.48E-02
ANLN_HUMAN	1.65	6.08E-03
STMN1_HUMAN	1.65	1.44E-03
FANCI_HUMAN	1.65	2.72E-03
KIFC1_HUMAN	1.64	3.34E-02
EBP2_HUMAN	1.64	9.24E-05
SMOC1_HUMAN	1.64	2.55E-05
CMTR1_HUMAN	1.64	3.82E-06
CO1A2_HUMAN	1.64	6.09E-03
5NTD_HUMAN	1.64	2.04E-04
ADAM8_HUMAN	1.63	1.67E-03
RECQ5_HUMAN	1.63	7.49E-05

CFDP1_HUMAN	1.63	1.44E-03
RFA1_HUMAN	1.63	9.54E-06
RL1D1_HUMAN	1.63	1.81E-03
SPIN1_HUMAN	1.63	9.20E-03
TNIP1_HUMAN	1.63	1.99E-05
PRC1_HUMAN	1.63	2.46E-02
BRCA2_HUMAN	1.62	2.01E-02
MGME1_HUMAN	1.62	1.70E-06
DHX40_HUMAN	1.62	8.33E-04
CHTOP_HUMAN	1.61	7.46E-03
PSME2_HUMAN	1.61	8.96E-05
FEN1_HUMAN	1.61	1.01E-03
SYWC_HUMAN	1.61	4.27E-04
PAR14_HUMAN	1.60	1.68E-04
ATPF1_HUMAN	1.60	9.11E-05
E2AK2_HUMAN	1.60	2.74E-04
UHRF2_HUMAN	1.60	2.74E-03
HELZ2_HUMAN	1.60	2.81E-06
DNMT1_HUMAN	1.60	3.52E-03
FHL1_HUMAN	1.59	1.47E-03
PARP1_HUMAN	1.59	1.24E-03
IFIH1_HUMAN	1.59	4.37E-05
EXOS8_HUMAN	1.59	1.83E-04
CA174_HUMAN	1.59	4.18E-02
PDIA4_HUMAN	1.59	5.99E-04
CBX1_HUMAN	1.59	1.91E-03
BAZ1B_HUMAN	1.58	1.67E-03
ERR1_HUMAN	1.58	2.29E-02
FLNC_HUMAN	1.58	1.77E-04
PAR12_HUMAN	1.58	3.53E-05
LIN54_HUMAN	1.58	8.51E-03
N4BP1_HUMAN	1.57	6.50E-05
RFC5_HUMAN	1.57	1.45E-03
DDX49_HUMAN	1.57	7.38E-04
ORC4_HUMAN	1.57	5.39E-03
UBP11_HUMAN	1.57	1.16E-04
PPM1G_HUMAN	1.57	1.84E-04
DPOD1_HUMAN	1.57	1.66E-03
ACOT4_HUMAN	1.57	4.09E-04
ARI5B_HUMAN	1.57	2.02E-03
SPB1_HUMAN	1.57	2.37E-03
RBMX2_HUMAN	1.57	3.55E-03
DHTK1_HUMAN	1.57	5.82E-06

ING1_HUMAN	1.57	1.38E-03
AN32E_HUMAN	1.57	6.95E-04
HNRH3_HUMAN	1.56	6.71E-04
FBLN1_HUMAN	1.56	5.79E-04
VLDLR_HUMAN	1.56	6.50E-04
NUMA1_HUMAN	1.56	8.12E-04
SMC4_HUMAN	1.56	6.27E-03
SERA_HUMAN	1.56	1.46E-03
SMC1A_HUMAN	1.56	1.72E-03
ARGL1_HUMAN	1.56	3.55E-04
GLB1L_HUMAN	1.56	1.28E-03
CIR1_HUMAN	1.56	9.65E-04
RU17_HUMAN	1.56	2.09E-03
PKRI1_HUMAN	1.56	2.25E-03
RRS1_HUMAN	1.56	2.21E-03
DPOE3_HUMAN	1.56	1.14E-04
TRI14_HUMAN	1.56	1.79E-05
PARP2_HUMAN	1.56	1.39E-02
HLAE_HUMAN	1.55	9.18E-06
TFAM_HUMAN	1.55	2.20E-04
DCD_HUMAN	1.55	1.84E-02
ERAP1_HUMAN	1.55	1.47E-04
SLBP_HUMAN	1.55	1.66E-03
ING2_HUMAN	1.54	3.22E-04
CCPG1_HUMAN	1.54	3.09E-03
SUMO3_HUMAN	1.54	2.79E-04
TPA_HUMAN	1.54	3.55E-05
CAF1A_HUMAN	1.54	8.58E-03
TPSN_HUMAN	1.54	5.49E-05
TAP1_HUMAN	1.54	7.22E-06
HNRPD_HUMAN	1.53	1.83E-04
S2535_HUMAN	1.53	1.69E-03
IRF9_HUMAN	1.53	1.39E-04
RBMX_HUMAN	1.53	5.20E-04
LAP2B_HUMAN	1.53	1.89E-03
MPH6_HUMAN	1.53	3.49E-04
MBD3_HUMAN	1.53	3.81E-03
NSD2_HUMAN	1.53	3.93E-02
MACD1_HUMAN	1.53	1.58E-04
TNAP3_HUMAN	1.53	6.43E-05
CBX5_HUMAN	1.53	2.67E-03
LBR_HUMAN	1.53	4.24E-03
UBF1_HUMAN	1.53	7.77E-04

RFC1_HUMAN	1.53	7.80E-04
FUT8_HUMAN	1.52	1.02E-04
MAT2B_HUMAN	1.52	5.28E-04
SAM9L_HUMAN	1.52	4.18E-04
MMP9_HUMAN	1.52	5.80E-03
DPOD2_HUMAN	1.52	1.44E-04
ERH_HUMAN	1.52	2.18E-03
NUB1_HUMAN	1.52	2.89E-03
CMS1_HUMAN	1.52	2.48E-04
PDS5B_HUMAN	1.51	8.12E-04
ORC3_HUMAN	1.51	7.58E-04
DDX50_HUMAN	1.51	8.63E-04
ATF1_HUMAN	1.51	4.24E-03
UHRF1_HUMAN	1.51	1.31E-02
NOC3L_HUMAN	1.51	1.64E-03
VRK1_HUMAN	1.51	5.27E-03
TGM2_HUMAN	1.51	1.60E-03
NUSAP_HUMAN	1.51	3.34E-02
HNRPU_HUMAN	1.51	7.03E-04
EXOS3_HUMAN	1.51	1.63E-03
EXOS9_HUMAN	1.51	5.66E-04
SRSF9_HUMAN	1.51	2.43E-04
DDX21_HUMAN	1.51	4.78E-03
SMC5_HUMAN	1.50	1.93E-04
CTRO_HUMAN	1.50	4.12E-03
SMC3_HUMAN	1.50	3.76E-04
RBBP7_HUMAN	1.50	3.33E-03
VPS72_HUMAN	1.50	6.43E-04
PSME1_HUMAN	1.49	2.43E-04
HDAC7_HUMAN	1.49	1.98E-02
HMGN3_HUMAN	1.49	3.20E-03
RNPS1_HUMAN	1.49	3.33E-03
MTDC_HUMAN	1.49	7.91E-03
CTF18_HUMAN	1.49	2.03E-05
PPHLN_HUMAN	1.49	5.07E-05
WBP4_HUMAN	1.49	2.73E-04
FACD2_HUMAN	1.49	1.18E-02
MDC1_HUMAN	1.49	1.66E-04
MYEF2_HUMAN	1.49	7.69E-04
TTF1_HUMAN	1.49	5.25E-03
TRPV2_HUMAN	1.49	2.48E-04
UBP28_HUMAN	1.49	4.66E-04
EXOS6_HUMAN	1.49	2.69E-04

MLH1_HUMAN	1.49	6.05E-04
TREX1_HUMAN	1.48	9.40E-04
HP1B3_HUMAN	1.48	1.61E-04
HSF1_HUMAN	1.48	5.76E-04
PRI2_HUMAN	1.48	8.97E-04
LEG9_HUMAN	1.48	3.30E-02
SURF6_HUMAN	1.48	1.09E-03
CNDG2_HUMAN	1.48	1.33E-04
BARD1_HUMAN	1.48	2.53E-02
ORC5_HUMAN	1.48	5.57E-03
ZC3H4_HUMAN	1.48	3.25E-04
RAVR1_HUMAN	1.48	3.33E-04
NOP14_HUMAN	1.48	2.50E-03
ADCY3_HUMAN	1.48	1.19E-02
RCOR3_HUMAN	1.48	1.40E-02
BGLR_HUMAN	1.47	7.03E-04
CC137_HUMAN	1.47	1.84E-03
GUAA_HUMAN	1.47	3.22E-04
TLK1_HUMAN	1.47	4.19E-03
AAAT_HUMAN	1.47	1.97E-02
MINA_HUMAN	1.47	1.28E-03
CBX3_HUMAN	1.47	1.28E-03
DPOE1_HUMAN	1.47	1.98E-02
ORC1_HUMAN	1.47	4.00E-02
RBM39_HUMAN	1.47	3.39E-03
NOLC1_HUMAN	1.47	3.58E-03
EZH2_HUMAN	1.47	2.45E-02
PRP19_HUMAN	1.46	6.73E-04
EXOS2_HUMAN	1.46	8.64E-05
SSF1_HUMAN	1.46	8.36E-03
HNRPC_HUMAN	1.46	3.87E-04
HLTF_HUMAN	1.46	5.99E-04
SPAG7_HUMAN	1.46	5.66E-04
DDX27_HUMAN	1.46	7.92E-04
CI114_HUMAN	1.46	1.81E-03
IBP4_HUMAN	1.46	6.26E-03
PSPC1_HUMAN	1.46	9.39E-04
RAVR2_HUMAN	1.46	4.20E-04
ZCHC8_HUMAN	1.46	5.28E-04
ZMY11_HUMAN	1.46	5.92E-04
NBN_HUMAN	1.46	6.34E-05
SUZ12_HUMAN	1.46	3.58E-03
MSLN_HUMAN	1.46	3.89E-03

CFA20_HUMAN	1.46	2.31E-03
WRIP1_HUMAN	1.46	8.48E-06
LSM8_HUMAN	1.46	2.67E-03
SMC6_HUMAN	1.46	2.49E-04
MBD4_HUMAN	1.45	1.19E-03
AN32B_HUMAN	1.45	3.46E-03
I2BPL_HUMAN	1.45	6.16E-05
TOP3A_HUMAN	1.45	4.28E-04
BUD13_HUMAN	1.45	2.54E-03
RPA34_HUMAN	1.45	9.10E-04
HNRPR_HUMAN	1.45	1.38E-03
KIF14_HUMAN	1.45	3.97E-03
DDX56_HUMAN	1.45	1.44E-04
GOLM1_HUMAN	1.45	5.20E-04
RED_HUMAN	1.45	9.23E-04
DDX10_HUMAN	1.45	3.21E-03
LRWD1_HUMAN	1.45	2.04E-04
BAP18_HUMAN	1.45	1.26E-03
MCMBP_HUMAN	1.45	6.19E-04
SP3_HUMAN	1.45	4.87E-03
DJC14_HUMAN	1.45	8.78E-03
RAB3B_HUMAN	1.45	2.14E-02
TOE1_HUMAN	1.45	3.05E-03
SAFB1_HUMAN	1.45	4.36E-04
SDS3_HUMAN	1.45	4.66E-03
TF3C3_HUMAN	1.45	9.75E-03
SMCA5_HUMAN	1.44	5.81E-04
ZN451_HUMAN	1.44	1.65E-02
RFC3_HUMAN	1.44	7.77E-04
KIN17_HUMAN	1.44	3.05E-03
TNR5_HUMAN	1.44	4.12E-04
ECM1_HUMAN	1.44	1.44E-04
CND2_HUMAN	1.44	9.95E-03
SRSF3_HUMAN	1.44	1.34E-03
MRM1_HUMAN	1.44	9.61E-04
RRP1_HUMAN	1.44	6.28E-04
PININ_HUMAN	1.44	6.86E-04
SODM_HUMAN	1.44	4.64E-02
SLD5_HUMAN	1.43	1.24E-02
POGK_HUMAN	1.43	5.46E-03
DAXX_HUMAN	1.43	2.46E-04
ROAA_HUMAN	1.43	8.00E-04
CEBPZ_HUMAN	1.43	2.18E-04

RBM22_HUMAN	1.43	2.79E-04
CENPB_HUMAN	1.43	5.11E-04
RBM7_HUMAN	1.43	1.66E-02
I20L2_HUMAN	1.43	1.93E-04
NUCL_HUMAN	1.43	9.10E-04
KMT2A_HUMAN	1.43	5.66E-04
JUNB_HUMAN	1.43	1.39E-03
WDR83_HUMAN	1.43	8.42E-03
MRE11_HUMAN	1.43	6.64E-06
MD2L1_HUMAN	1.43	5.07E-05
NR2C2_HUMAN	1.42	1.21E-02
ECSIT_HUMAN	1.42	3.41E-02
RFX5_HUMAN	1.42	1.59E-03
TRA2B_HUMAN	1.42	1.77E-03
PHC2_HUMAN	1.42	3.90E-02
F208A_HUMAN	1.42	7.69E-04
EPCR_HUMAN	1.42	2.13E-03
SATT_HUMAN	1.42	6.09E-03
CYBP_HUMAN	1.42	8.19E-03
CENPH_HUMAN	1.42	6.13E-03
CD11B_HUMAN	1.42	4.03E-04
SLFN5_HUMAN	1.42	2.21E-03
ESF1_HUMAN	1.42	2.38E-03
TM209_HUMAN	1.42	2.48E-04
CDC5L_HUMAN	1.42	3.42E-04
ZN326_HUMAN	1.42	3.44E-04
GPTC4_HUMAN	1.42	2.88E-03
S27A3_HUMAN	1.41	1.94E-03
PCKGM_HUMAN	1.41	1.28E-03
AL1L2_HUMAN	1.41	6.57E-03
RSRC1_HUMAN	1.41	1.05E-02
XRCC6_HUMAN	1.41	1.09E-03
NSRP1_HUMAN	1.41	1.56E-03
PMYT1_HUMAN	1.41	1.55E-03
CND1_HUMAN	1.41	1.18E-02
CI078_HUMAN	1.41	1.42E-03
SAFB2_HUMAN	1.41	2.69E-04
NUDC_HUMAN	1.40	3.12E-03
KHNYN_HUMAN	1.40	1.81E-02
MPZL2_HUMAN	1.40	1.93E-04
MBB1A_HUMAN	1.40	8.34E-04
MRGBP_HUMAN	1.40	5.94E-03
SRSF7_HUMAN	1.40	9.88E-04

P2RX4_HUMAN	1.40	1.14E-02
NOP2_HUMAN	1.40	1.28E-03
SARNP_HUMAN	1.40	1.94E-02
ANO1_HUMAN	1.40	8.98E-03
EXOSX_HUMAN	1.40	4.46E-04
SR140_HUMAN	1.40	3.05E-03
WDR12_HUMAN	1.40	9.99E-05
SNW1_HUMAN	1.40	8.88E-04
LA_HUMAN	1.40	9.67E-04
RIR2_HUMAN	1.40	1.53E-03
NRM_HUMAN	1.40	1.10E-02
ENTP6_HUMAN	1.40	1.73E-04
NSE1_HUMAN	1.40	7.29E-04
DJC17_HUMAN	1.40	5.39E-03
ACINU_HUMAN	1.40	1.81E-03
CPSM_HUMAN	1.40	2.87E-03
RAD50_HUMAN	1.40	1.92E-05
PUR4_HUMAN	1.40	3.50E-04
BCLF1_HUMAN	1.40	4.52E-04
KCP3_HUMAN	1.40	5.84E-04
PMS1_HUMAN	1.40	7.02E-04
RAD21_HUMAN	1.39	4.70E-04
RU2B_HUMAN	1.39	2.48E-03
DHSO_HUMAN	1.39	3.92E-03
HDGR2_HUMAN	1.39	5.72E-04
DX39A_HUMAN	1.39	6.41E-03
RLP24_HUMAN	1.39	1.01E-02
DPY30_HUMAN	1.39	1.08E-02
RBM25_HUMAN	1.39	2.88E-04
DPOE4_HUMAN	1.39	6.66E-05
PPIG_HUMAN	1.39	2.62E-04
TF2AA_HUMAN	1.39	3.03E-03
PPIL4_HUMAN	1.39	6.07E-04
SNR27_HUMAN	1.39	6.09E-03
NAT10_HUMAN	1.39	6.63E-04
TPX2_HUMAN	1.39	7.74E-03
SP1_HUMAN	1.39	2.02E-03
SYNE3_HUMAN	1.39	3.23E-03
BRD8_HUMAN	1.39	7.53E-03
BCAT1_HUMAN	1.39	1.18E-02
DAF_HUMAN	1.39	1.90E-02
RPR1B_HUMAN	1.39	1.03E-04
LEO1_HUMAN	1.39	8.67E-04

PAXI1_HUMAN	1.39	3.43E-02
CWC15_HUMAN	1.39	4.18E-03
INO80_HUMAN	1.39	9.58E-03
ROA2_HUMAN	1.39	1.51E-03
BUD31_HUMAN	1.39	1.54E-03
THOC6_HUMAN	1.39	2.58E-04
STAT2_HUMAN	1.38	3.36E-04
MMTA2_HUMAN	1.38	2.06E-03
HNRPL_HUMAN	1.38	1.53E-04
C2AIL_HUMAN	1.38	1.16E-03
SRSF1_HUMAN	1.38	1.03E-03
NHEJ1_HUMAN	1.38	7.96E-03
HPRT_HUMAN	1.38	3.16E-03
TRM6_HUMAN	1.38	1.24E-04
WBP11_HUMAN	1.38	8.89E-04
PABP2_HUMAN	1.38	1.54E-04
PLRG1_HUMAN	1.38	7.49E-04
SRRT_HUMAN	1.38	9.95E-04
MET16_HUMAN	1.38	1.03E-03
BAZ1A_HUMAN	1.38	1.66E-03
CHAP1_HUMAN	1.38	5.75E-03
MCE1_HUMAN	1.38	6.40E-03
IFIT5_HUMAN	1.38	1.30E-03
P20L1_HUMAN	1.38	1.65E-02
CLMN_HUMAN	1.38	1.25E-03
FBRL_HUMAN	1.38	3.51E-04
TBP_HUMAN	1.38	3.10E-02
TACO1_HUMAN	1.38	1.16E-04
PAXB1_HUMAN	1.38	2.22E-03
RXRB_HUMAN	1.38	2.35E-02
HDAC2_HUMAN	1.37	1.77E-03
ITA1_HUMAN	1.37	4.22E-03
FGFP1_HUMAN	1.37	4.90E-03
RPP40_HUMAN	1.37	2.19E-02
HINT2_HUMAN	1.37	2.46E-05
SAP18_HUMAN	1.37	1.51E-04
RCC1_HUMAN	1.37	1.65E-04
NOC2L_HUMAN	1.37	9.69E-05
ARP5_HUMAN	1.37	6.10E-03
SMU1_HUMAN	1.37	4.47E-04
PHF3_HUMAN	1.37	2.37E-03
TASP1_HUMAN	1.37	1.06E-02
SENP2_HUMAN	1.37	2.58E-03

THOC1_HUMAN	1.37	2.16E-04
CTBL1_HUMAN	1.37	1.09E-03
DDX54_HUMAN	1.37	1.27E-02
CUL4B_HUMAN	1.37	2.74E-04
CHD4_HUMAN	1.37	4.00E-04
STAG1_HUMAN	1.37	1.39E-03
NUP62_HUMAN	1.37	2.10E-03
DDX18_HUMAN	1.37	2.23E-03
PDS5A_HUMAN	1.37	9.10E-04
PRP4B_HUMAN	1.37	4.51E-03
C19L2_HUMAN	1.37	5.08E-03
ZCH18_HUMAN	1.37	1.56E-04
RBM15_HUMAN	1.37	3.68E-04
H2AY_HUMAN	1.37	1.03E-03
MFAP1_HUMAN	1.37	1.19E-03
DDB2_HUMAN	1.37	2.73E-02
RP9_HUMAN	1.37	4.30E-02
FA98B_HUMAN	1.37	1.04E-03
DMAP1_HUMAN	1.37	3.17E-03
MAFF_HUMAN	1.37	6.84E-03
FRG1_HUMAN	1.37	7.10E-03
S19A1_HUMAN	1.36	2.89E-03
SUMO2_HUMAN	1.36	1.26E-03
SF3B4_HUMAN	1.36	5.84E-04
SAE2_HUMAN	1.36	8.07E-04
CABIN_HUMAN	1.36	4.72E-02
MPP8_HUMAN	1.36	1.26E-03
SAE1_HUMAN	1.36	1.01E-03
RBM26_HUMAN	1.36	1.01E-04
LACB2_HUMAN	1.36	1.01E-04
DDX52_HUMAN	1.36	3.36E-04
RPP30_HUMAN	1.36	6.16E-04
NOL7_HUMAN	1.36	1.80E-03
MEPCE_HUMAN	1.36	9.23E-05
DDX47_HUMAN	1.36	4.70E-04
CIB1_HUMAN	1.36	4.60E-03
RANG_HUMAN	1.36	2.31E-02
SMD2_HUMAN	1.35	5.82E-04
THOC3_HUMAN	1.35	3.54E-04
MAK16_HUMAN	1.35	5.50E-04
MATR3_HUMAN	1.35	1.25E-03
REQU_HUMAN	1.35	3.13E-04
SK2L2_HUMAN	1.35	5.77E-03

LSM6_HUMAN	1.35	5.40E-04
NDC1_HUMAN	1.35	7.10E-05
SENP3_HUMAN	1.35	3.83E-04
RBBP4_HUMAN	1.35	9.09E-04
F192A_HUMAN	1.35	6.04E-03
TR150_HUMAN	1.35	2.73E-04
ZMAT2_HUMAN	1.35	7.25E-04
CHK2_HUMAN	1.35	6.38E-03
RPP29_HUMAN	1.35	9.37E-03
POGZ_HUMAN	1.35	9.52E-03
SLU7_HUMAN	1.35	1.00E-03
DPOLA_HUMAN	1.35	1.19E-03
EXOS7_HUMAN	1.35	8.61E-05
NCBP2_HUMAN	1.35	3.34E-04
RBP2_HUMAN	1.35	3.69E-04
CDK8_HUMAN	1.35	4.17E-03
HELLS_HUMAN	1.35	7.59E-03
ABT1_HUMAN	1.35	4.01E-03
RCN1_HUMAN	1.35	2.03E-05
GLYM_HUMAN	1.35	3.23E-03
THOC4_HUMAN	1.35	8.00E-03
SELH_HUMAN	1.35	1.75E-02
FMR1_HUMAN	1.35	2.64E-05
ADCK4_HUMAN	1.35	2.68E-04
PP1RA_HUMAN	1.35	1.00E-03
ZMYM1_HUMAN	1.35	8.39E-03
RECQ1_HUMAN	1.35	3.24E-03
ASH2L_HUMAN	1.35	2.16E-03
ZMYM4_HUMAN	1.35	3.75E-04
SRS11_HUMAN	1.35	3.50E-03
UBC9_HUMAN	1.35	2.47E-04
BRD4_HUMAN	1.35	1.14E-02
B4GA1_HUMAN	1.34	1.67E-03
SMRC2_HUMAN	1.34	6.93E-04
SDE2_HUMAN	1.34	5.10E-04
SPG20_HUMAN	1.34	3.64E-03
HNRPF_HUMAN	1.34	1.44E-03
8ODP_HUMAN	1.34	1.54E-02
RBM19_HUMAN	1.34	2.28E-04
DHX9_HUMAN	1.34	3.41E-03
RSF1_HUMAN	1.34	1.51E-04
ALAT2_HUMAN	1.34	6.20E-04
TAF2_HUMAN	1.34	2.00E-02

SERC_HUMAN	1.34	9.78E-03
PSB8_HUMAN	1.34	1.31E-04
Z280C_HUMAN	1.34	8.89E-04
MED6_HUMAN	1.34	1.61E-03
FUS_HUMAN	1.34	1.10E-02
RHOB_HUMAN	1.34	5.99E-04
P5CR1_HUMAN	1.34	2.54E-03
XRCC1_HUMAN	1.34	3.24E-03
U520_HUMAN	1.34	1.75E-03
SGMR1_HUMAN	1.34	1.32E-04
ISY1_HUMAN	1.34	4.11E-03
U2AF2_HUMAN	1.34	1.07E-03
NU153_HUMAN	1.34	2.43E-03
ACL6A_HUMAN	1.34	8.57E-04
GAR1_HUMAN	1.34	1.23E-03
NUDC1_HUMAN	1.34	4.27E-04
CWC22_HUMAN	1.34	9.10E-04
TF2H1_HUMAN	1.34	1.06E-03
P52K_HUMAN	1.34	3.51E-03
CACO2_HUMAN	1.34	2.67E-03
NOL8_HUMAN	1.34	8.63E-04
AEBP1_HUMAN	1.33	4.02E-03
ZN516_HUMAN	1.33	4.27E-04
ROA0_HUMAN	1.33	5.99E-04
DHX16_HUMAN	1.33	3.34E-03
HACD3_HUMAN	1.33	7.03E-04
DDX24_HUMAN	1.33	2.70E-03
FKBP4_HUMAN	1.33	3.12E-03
ELYS_HUMAN	1.33	3.41E-03
QSER1_HUMAN	1.33	1.03E-03
TNF6B_HUMAN	1.33	2.20E-03
TLR3_HUMAN	1.33	5.79E-04
RALY_HUMAN	1.33	4.51E-04
ZN787_HUMAN	1.33	3.17E-03
NCBP1_HUMAN	1.33	3.36E-04
NPM_HUMAN	1.33	1.57E-03
SRSF6_HUMAN	1.33	3.62E-04
CTR9_HUMAN	1.33	1.03E-03
MBD1_HUMAN	1.33	4.19E-03
PTMS_HUMAN	1.33	1.24E-02
DPOA2_HUMAN	1.33	2.45E-02
PRKDC_HUMAN	1.33	1.46E-04
PNKP_HUMAN	1.33	4.67E-03

THOC7_HUMAN	1.33	1.09E-03
PCNT_HUMAN	1.33	5.06E-03
SRBD1_HUMAN	1.33	4.47E-04
SFR15_HUMAN	1.33	5.95E-04
COM1_HUMAN	1.33	9.56E-04
MICB_HUMAN	1.33	4.90E-02
MORC2_HUMAN	1.33	2.24E-04
UTP18_HUMAN	1.33	2.44E-03
ARI4A_HUMAN	1.33	4.41E-02
BRD7_HUMAN	1.33	4.93E-02
ERI1_HUMAN	1.33	1.68E-03
RSBNL_HUMAN	1.33	3.86E-03
NOG1_HUMAN	1.33	1.82E-02
PHC3_HUMAN	1.33	1.94E-02
TF3B_HUMAN	1.33	3.85E-02
CISD1_HUMAN	1.33	7.49E-04
RU2A_HUMAN	1.33	1.67E-03
ZFR_HUMAN	1.33	1.70E-03
PSMG2_HUMAN	1.33	5.31E-04
NOL11_HUMAN	1.33	1.81E-03
SRS10_HUMAN	1.33	2.74E-03
ELAV1_HUMAN	1.32	1.81E-03
CEP85_HUMAN	1.32	7.16E-03
LDHB_HUMAN	1.32	9.42E-03
RING1_HUMAN	1.32	1.38E-02
BT2A1_HUMAN	1.32	9.09E-04
SF3B6_HUMAN	1.32	1.47E-03
EMSY_HUMAN	1.32	7.19E-03
ZHX1_HUMAN	1.32	3.32E-02
RPP38_HUMAN	1.32	5.50E-04
PQBP1_HUMAN	1.32	6.02E-03
SRRM1_HUMAN	1.32	7.25E-04
ELOA1_HUMAN	1.32	1.60E-02
TPSNR_HUMAN	1.32	6.74E-03
NSD3_HUMAN	1.32	2.77E-02
PAF1_HUMAN	1.32	5.93E-03
THOC5_HUMAN	1.32	5.30E-04
PHIP_HUMAN	1.32	1.92E-03
ELAV2_HUMAN	1.32	3.40E-02
NC2A_HUMAN	1.32	9.46E-04
TFPT_HUMAN	1.32	4.68E-02
CATS_HUMAN	1.32	4.27E-04
KS6A5_HUMAN	1.32	1.26E-03

RU1C_HUMAN	1.32	1.81E-03
GLPK3_HUMAN (+1)	1.32	2.28E-03
TMM97_HUMAN	1.32	1.87E-02
CNTP1_HUMAN	1.32	3.03E-03
BAF_HUMAN	1.32	2.25E-04
KRR1_HUMAN	1.32	6.86E-04
NT5D1_HUMAN	1.32	1.10E-02
HNRPK_HUMAN	1.32	1.68E-03
SREK1_HUMAN	1.32	5.33E-03
I2BP1_HUMAN	1.32	3.62E-04
RRP1B_HUMAN	1.32	5.53E-04
PR38A_HUMAN	1.32	6.13E-03
ZNRF2_HUMAN	1.32	1.60E-02
TRAP1_HUMAN	1.31	3.18E-05
DHX15_HUMAN	1.31	1.36E-03
BBX_HUMAN	1.31	5.41E-03
TF3C2_HUMAN	1.31	1.48E-03
RPC6_HUMAN	1.31	1.54E-03
RRP15_HUMAN	1.31	4.44E-03
ADNP_HUMAN	1.31	3.77E-03
C560_HUMAN	1.31	6.77E-04
SDPR_HUMAN	1.31	8.34E-04
SF3B2_HUMAN	1.31	1.38E-03
RB33B_HUMAN	1.31	3.08E-03
GP180_HUMAN	1.31	1.26E-02
SMD1_HUMAN	1.31	3.91E-04
PR40A_HUMAN	1.31	8.88E-04
CIR1A_HUMAN	1.31	9.24E-04
XRCC5_HUMAN	1.31	1.75E-03
EXOS1_HUMAN	1.31	1.81E-03
CDKA1_HUMAN	1.31	8.05E-03
WDR43_HUMAN	1.31	3.15E-03
SFPQ_HUMAN	1.31	6.23E-03
RT24_HUMAN	1.31	1.37E-03
WDR36_HUMAN	1.31	1.44E-03
RB12B_HUMAN	1.31	1.63E-03
SF01_HUMAN	1.31	1.76E-03
TPR_HUMAN	1.31	4.83E-04
KAT7_HUMAN	1.31	9.63E-03
SF3A3_HUMAN	1.31	1.39E-03
SON_HUMAN	1.31	1.43E-03
YTDC1_HUMAN	1.31	3.56E-04
GLT14_HUMAN	1.31	6.96E-03

NUP54_HUMAN	1.31	7.14E-05
CB047_HUMAN	1.31	9.66E-05
PP1G_HUMAN	1.31	1.28E-02
ECE1_HUMAN	1.30	2.93E-04
CECR5_HUMAN	1.30	3.36E-04
CCNL1_HUMAN	1.30	2.39E-03
NEP_HUMAN	1.30	5.10E-03
SOX15_HUMAN	1.30	3.73E-03
DCPS_HUMAN	1.30	5.38E-03
RAD9A_HUMAN	1.30	1.49E-02
TR61B_HUMAN	1.30	3.87E-03
WDR3_HUMAN	1.30	8.67E-04
ZC3HE_HUMAN	1.30	2.31E-03
BCL7C_HUMAN	1.30	1.96E-02
U5S1_HUMAN	1.30	1.10E-03
PRP8_HUMAN	1.30	1.17E-03
GRIN1_HUMAN	1.30	1.89E-04
UBP7_HUMAN	1.30	5.43E-04
ILF2_HUMAN	1.30	5.80E-04
DCNL5_HUMAN	1.30	3.77E-03
CHD1_HUMAN	1.30	5.56E-04
TBL3_HUMAN	1.30	1.03E-03
ZN318_HUMAN	1.30	9.88E-04
PHAR4_HUMAN	1.30	2.69E-04
IF4A3_HUMAN	1.30	4.09E-04
FKB11_HUMAN	1.30	2.09E-02
MOT4_HUMAN	1.30	1.42E-03
CENPC_HUMAN	1.30	2.65E-03
NUPL2_HUMAN	1.30	1.28E-03
MOV10_HUMAN	1.30	1.39E-04
ADCK3_HUMAN	1.30	8.00E-03
THOC2_HUMAN	1.30	4.27E-04
UBN2_HUMAN	1.30	1.03E-02
PHF14_HUMAN	1.30	2.02E-03
THYN1_HUMAN	1.30	7.84E-03
DIM1_HUMAN	1.30	2.10E-02
MO4L1_HUMAN	1.30	1.25E-02
EXOS4_HUMAN	1.29	1.83E-03
SMD3_HUMAN	1.29	4.34E-04
UBP48_HUMAN	1.29	3.14E-04
CHD3_HUMAN	1.29	4.39E-03
SMRD1_HUMAN	1.29	2.22E-03
NU133_HUMAN	1.29	8.34E-04

CN37_HUMAN	1.29	9.95E-04
WDR18_HUMAN	1.29	1.46E-04
PPT1_HUMAN	1.29	3.08E-04
TFP11_HUMAN	1.29	3.03E-03
NOP9_HUMAN	1.29	6.05E-04
TSAP1_HUMAN	1.29	3.74E-03
GOT1B_HUMAN	1.29	1.67E-03
CD320_HUMAN	1.29	9.53E-03
SAAL1_HUMAN	1.29	2.61E-03
NQO1_HUMAN	1.29	1.34E-02
SE6L2_HUMAN	1.29	7.75E-03
EHMT2_HUMAN	1.29	8.15E-03
MED28_HUMAN	1.29	3.63E-04
PSMG1_HUMAN	1.29	7.03E-04
ABHDA_HUMAN	1.29	3.16E-04
SENP1_HUMAN	1.29	4.87E-03
PAPD5_HUMAN	1.29	5.47E-03
ZMYM2_HUMAN	1.29	2.20E-04
NELFE_HUMAN	1.29	5.26E-03
TCRG1_HUMAN	1.29	9.97E-04
K0020_HUMAN	1.29	3.21E-03
PODXL_HUMAN	1.29	4.87E-03
U2AF1_HUMAN	1.29	4.99E-03
BMS1_HUMAN	1.29	4.42E-03
DVL2_HUMAN	1.29	1.65E-02
CCAR2_HUMAN	1.29	5.38E-03
TRM1L_HUMAN	1.29	3.57E-04
CROCC_HUMAN	1.29	9.73E-04
DNJC8_HUMAN	1.29	3.62E-03
XRCC4_HUMAN	1.29	1.03E-02
PAI1_HUMAN	1.29	8.89E-04
TRUA_HUMAN	1.29	5.28E-04
PHF5A_HUMAN	1.29	6.27E-04
RPF2_HUMAN	1.29	1.40E-03
DDX51_HUMAN	1.29	1.05E-03
SIN3A_HUMAN	1.29	1.56E-03
TERF2_HUMAN	1.29	2.28E-02
HNRH1_HUMAN	1.29	1.49E-03
SART3_HUMAN	1.29	3.82E-04
GPTC1_HUMAN	1.29	2.95E-03
TMUB1_HUMAN	1.29	6.84E-04
API5_HUMAN	1.29	9.49E-04
RIOK3_HUMAN	1.29	3.03E-02

SPF27_HUMAN	1.29	6.75E-04
SPF45_HUMAN	1.29	3.08E-03
PELP1_HUMAN	1.29	1.80E-04
NOL10_HUMAN	1.29	2.78E-04
TF3C4_HUMAN	1.29	4.24E-04
ZC3H1_HUMAN	1.29	8.93E-04
MIER1_HUMAN	1.29	1.47E-03
EREG_HUMAN	1.29	5.08E-03
CWC27_HUMAN	1.28	9.02E-04
CC134_HUMAN	1.28	2.92E-03
CHERP_HUMAN	1.28	1.46E-03
CHD1L_HUMAN	1.28	1.16E-03
RCAS1_HUMAN	1.28	1.92E-03
FUBP1_HUMAN	1.28	4.73E-03
ILKAP_HUMAN	1.28	7.49E-04
CDYL1_HUMAN	1.28	1.06E-02
ZN207_HUMAN	1.28	1.47E-03
XRN2_HUMAN	1.28	6.50E-04
RRP12_HUMAN	1.28	7.55E-03
CSTF3_HUMAN	1.28	1.07E-04
CL043_HUMAN	1.28	1.16E-02
NU205_HUMAN	1.28	6.21E-04
UPAR_HUMAN	1.28	5.60E-03
SIN3B_HUMAN	1.28	4.26E-02
RFA3_HUMAN	1.28	4.52E-04
SNRPA_HUMAN	1.28	2.47E-03
MTHFS_HUMAN	1.28	6.23E-03
GSH0_HUMAN	1.28	2.00E-02
DNJA1_HUMAN	1.28	1.03E-03
WDR5_HUMAN	1.28	1.37E-03
BOP1_HUMAN	1.28	3.19E-03
EED_HUMAN	1.28	6.72E-03
PROF2_HUMAN	1.28	4.58E-02
MAT1_HUMAN	1.28	7.61E-04
RBM10_HUMAN	1.28	4.63E-03
INT9_HUMAN	1.27	1.70E-03
NUPL1_HUMAN	1.27	3.14E-03
QCR6_HUMAN	1.27	1.25E-02
NGDN_HUMAN	1.27	6.21E-04
CPSF6_HUMAN	1.27	6.45E-04
RSMB_HUMAN	1.27	1.15E-03
KDM1A_HUMAN	1.27	3.21E-04
NUP88_HUMAN	1.27	5.11E-04

GPKOW_HUMAN	1.27	7.84E-04
TEBP_HUMAN	1.27	2.50E-02
WAPL_HUMAN	1.27	1.26E-03
IWS1_HUMAN	1.27	1.66E-03
NPM3_HUMAN	1.27	3.07E-03
RBM14_HUMAN	1.27	3.93E-03
HEAT1_HUMAN	1.27	2.73E-03
GLYC_HUMAN	1.27	9.74E-03
HNRPM_HUMAN	1.27	1.25E-03
METK2_HUMAN	1.27	1.44E-03
ZFPL1_HUMAN	1.27	6.05E-03
ASPH_HUMAN	1.27	7.37E-03
ATF6A_HUMAN	1.27	4.18E-02
RBBP6_HUMAN	1.27	6.31E-04
MED22_HUMAN	1.27	8.08E-04
NFXL1_HUMAN	1.27	8.64E-04
COQ3_HUMAN	1.27	3.34E-03
ENL_HUMAN	1.27	1.05E-02
CISD2_HUMAN	1.27	1.70E-02
GABPA_HUMAN	1.27	1.20E-02
SDCB1_HUMAN	1.27	1.81E-02
NUP85_HUMAN	1.27	4.04E-04
PRP6_HUMAN	1.27	1.03E-03
ILF3_HUMAN	1.27	1.25E-03
NONO_HUMAN	1.27	2.70E-03
PXMP2_HUMAN	1.27	7.82E-03
PP1R8_HUMAN	1.27	2.21E-03
AGRIN_HUMAN	1.27	5.00E-04
NIP7_HUMAN	1.27	3.51E-03
SNUT1_HUMAN	1.27	3.82E-03
FIP1_HUMAN	1.27	3.88E-03
PNISR_HUMAN	1.27	4.07E-03
CING_HUMAN	1.27	3.33E-02
RBM8A_HUMAN	1.27	2.37E-04
DDX23_HUMAN	1.27	1.35E-03
RPR1A_HUMAN	1.27	2.17E-03
RUXE_HUMAN	1.27	8.94E-04
LENG8_HUMAN	1.27	1.34E-03
MKLN1_HUMAN	1.27	3.13E-02
ATF2_HUMAN	1.27	4.14E-02
UTP15_HUMAN	1.27	6.44E-04
RPA49_HUMAN	1.27	2.70E-03
SMRCD_HUMAN	1.27	3.74E-03

AGR2_HUMAN	1.26	1.03E-02
QKI_HUMAN	1.26	6.28E-03
PISD_HUMAN	1.26	5.89E-03
GGH_HUMAN	1.26	2.36E-03
ZC11A_HUMAN	1.26	8.74E-03
MORC3_HUMAN	1.26	3.77E-04
GRB7_HUMAN	1.26	1.16E-03
ZN687_HUMAN	1.26	1.17E-03
RT18A_HUMAN	1.26	1.81E-03
TCF20_HUMAN	1.26	4.32E-03
SF3A2_HUMAN	1.26	3.36E-04
NU160_HUMAN	1.26	7.03E-04
GHDC_HUMAN	1.26	2.60E-02
RAB31_HUMAN	1.26	4.21E-04
PRP17_HUMAN	1.26	5.43E-03
CO4A1_HUMAN	1.26	1.76E-02
SRPR_HUMAN	1.26	5.52E-03
CG050_HUMAN	1.26	1.54E-02
ATG4B_HUMAN	1.26	2.89E-02
NALP1_HUMAN	1.26	6.86E-04
HNRLL_HUMAN	1.26	1.92E-03
NR2F6_HUMAN	1.26	2.82E-02
RO52_HUMAN	1.26	1.68E-02
LARP7_HUMAN	1.26	6.50E-04
RBM34_HUMAN	1.26	5.33E-03
B3GT6_HUMAN	1.26	3.33E-04
PTN2_HUMAN	1.26	3.68E-03
NUP50_HUMAN	1.26	8.15E-03
CSTF1_HUMAN	1.26	6.05E-04
ICMT_HUMAN	1.26	4.42E-03
SRSF2_HUMAN	1.26	1.43E-02
ROA1_HUMAN	1.26	3.67E-02
SFR19_HUMAN	1.26	2.36E-02
INT8_HUMAN	1.26	1.42E-03
WDR82_HUMAN	1.26	1.71E-03
PUS7_HUMAN	1.26	3.24E-03
NUP93_HUMAN	1.26	5.24E-04
GTPB2_HUMAN	1.26	3.04E-03
CTBP2_HUMAN	1.26	2.78E-02
ATN1_HUMAN	1.26	3.84E-02
UBP36_HUMAN	1.26	3.80E-02
SF3A1_HUMAN	1.26	5.31E-03
MAOM_HUMAN	1.26	4.00E-04

CDC73_HUMAN	1.25	4.24E-03
GPX8_HUMAN	1.25	5.08E-03
MET14_HUMAN	1.25	5.43E-03
LMNB2_HUMAN	1.25	8.99E-04
C19L1_HUMAN	1.25	2.27E-03
STAG2_HUMAN	1.25	2.28E-03
SAS10_HUMAN	1.25	3.18E-03
UTP6_HUMAN	1.25	4.77E-03
PAPS2_HUMAN	1.25	3.94E-02
AATF_HUMAN	1.25	1.43E-03
GSDMD_HUMAN	1.25	2.68E-03
GBB4_HUMAN	1.25	1.02E-02
SPF30_HUMAN	1.25	8.60E-04
CIP2A_HUMAN	1.25	5.08E-03
AQR_HUMAN	1.25	1.23E-02
S39AE_HUMAN	1.25	2.31E-02
VWA9_HUMAN	1.25	6.67E-03
LSM3_HUMAN	1.25	1.15E-02
TSR1_HUMAN	1.25	1.03E-03
NUP98_HUMAN	1.25	1.23E-03
PRPF3_HUMAN	1.25	3.61E-03
RUS1_HUMAN	1.25	3.62E-03
CHM4A_HUMAN	1.25	5.34E-03
RCL1_HUMAN	1.25	5.46E-03
AK17A_HUMAN	1.25	1.65E-02
SERPH_HUMAN	1.25	6.04E-04
PUF60_HUMAN	1.25	7.80E-04
PCID2_HUMAN	1.25	2.86E-03
WDR75_HUMAN	1.25	4.17E-03
STML2_HUMAN	1.25	2.78E-04
GPTC8_HUMAN	1.25	9.18E-04
ENPL_HUMAN	1.25	2.99E-02
SQSTM_HUMAN	1.25	8.07E-03
TRM1_HUMAN	1.25	1.31E-03
EDC4_HUMAN	1.25	1.53E-03
SYAC_HUMAN	1.25	2.31E-02
RM42_HUMAN	1.25	5.21E-04
ZC3HD_HUMAN	1.25	1.37E-02
UIF_HUMAN	1.25	3.26E-04
FXRD1_HUMAN	1.25	4.18E-04
CAND1_HUMAN	1.25	1.47E-03
LGMN_HUMAN	1.25	2.82E-02
FST_HUMAN	1.25	3.47E-02

KDM3B_HUMAN	1.25	8.60E-04
COIA1_HUMAN	1.25	3.13E-03
T2EB_HUMAN	1.25	2.56E-02
NHP2_HUMAN	1.25	2.18E-04
NUP37_HUMAN	1.25	1.29E-03
NVL_HUMAN	1.25	3.50E-03
NFIC_HUMAN	1.25	8.74E-03
DKC1_HUMAN	1.25	3.94E-04
LRC42_HUMAN	1.25	4.87E-03
SFXN1_HUMAN	1.25	2.39E-04
SG196_HUMAN	1.25	1.22E-03
LSM2_HUMAN	1.25	1.97E-03
WDR46_HUMAN	1.25	8.19E-03
CTCF_HUMAN	1.25	1.35E-02
CPSF5_HUMAN	1.25	5.93E-03
NCOA5_HUMAN	1.25	1.08E-02
TLR2_HUMAN	1.25	1.35E-02
CRNL1_HUMAN	1.25	6.13E-03
HNRL2_HUMAN	1.25	6.21E-04
ZN638_HUMAN	1.24	3.36E-03
PRP31_HUMAN	1.24	1.45E-03
ZCRB1_HUMAN	1.24	3.28E-02
CDK12_HUMAN	1.24	3.04E-04
BRD1_HUMAN	1.24	1.22E-03
KHDR1_HUMAN	1.24	5.31E-03
TAF6L_HUMAN	1.24	7.43E-03
NOP58_HUMAN	1.24	2.62E-04
BRE1A_HUMAN	1.24	2.30E-03
MAGG1_HUMAN	1.24	6.15E-03
RIR1_HUMAN	1.24	1.46E-02
RCOR1_HUMAN	1.24	1.38E-03
PPIH_HUMAN	1.24	1.83E-03
FOXK1_HUMAN	1.24	2.86E-03
BRE1B_HUMAN	1.24	2.25E-03
UBXN7_HUMAN	1.24	2.58E-03
MRM3_HUMAN	1.24	7.91E-03
AIP_HUMAN	1.24	4.62E-03
ZCHC9_HUMAN	1.24	4.04E-03
NELFA_HUMAN	1.24	5.39E-03
PTCD2_HUMAN	1.24	3.41E-04
MED27_HUMAN	1.24	6.00E-03
RB27A_HUMAN	1.24	3.11E-03
ABD12_HUMAN	1.24	1.21E-03

RRP7A_HUMAN	1.24	1.54E-03
RALA_HUMAN	1.24	1.78E-03
EPHA2_HUMAN	1.24	1.14E-02
TLK2_HUMAN	1.24	1.82E-02
KNOP1_HUMAN	1.24	2.31E-02
RPAB3_HUMAN	1.24	4.62E-03
CWC25_HUMAN	1.24	3.70E-02
PWP2_HUMAN	1.24	7.03E-04
GLU2B_HUMAN	1.24	1.67E-03
RPC3_HUMAN	1.24	1.05E-02
SFSWA_HUMAN	1.24	1.23E-03
TIF1B_HUMAN	1.24	2.47E-03
PK1IP_HUMAN	1.24	2.98E-04
RTF1_HUMAN	1.24	1.73E-03
TEX10_HUMAN	1.24	2.92E-03
FND3A_HUMAN	1.24	9.61E-03
LSM4_HUMAN	1.24	1.73E-02
PRCC_HUMAN	1.24	2.16E-02
PESC_HUMAN	1.24	1.73E-02
IAH1_HUMAN	1.24	2.10E-02
PDIP3_HUMAN	1.24	1.78E-02
QCR9_HUMAN	1.24	1.25E-03
TAP26_HUMAN	1.24	5.55E-03
TAF6_HUMAN	1.24	1.77E-02
SPSY_HUMAN	1.24	3.79E-02
P4HA1_HUMAN	1.24	3.44E-03
GSHR_HUMAN	1.24	1.04E-02
R113A_HUMAN	1.24	4.02E-02
SYF1_HUMAN	1.24	5.46E-03
KMT2D_HUMAN	1.24	2.82E-02
AN32A_HUMAN	1.24	4.54E-02
NU107_HUMAN	1.23	1.42E-03
RAGP1_HUMAN	1.23	1.05E-03
SPT6H_HUMAN	1.23	1.40E-03
BRI3B_HUMAN	1.23	2.04E-02
NIPA_HUMAN	1.23	1.62E-03
TRM61_HUMAN	1.23	5.42E-03
ZN609_HUMAN	1.23	8.73E-03
NELFB_HUMAN	1.23	2.33E-03
PBX2_HUMAN	1.23	1.35E-02
URB2_HUMAN	1.23	2.99E-03
LSM7_HUMAN	1.23	3.08E-03
TF3C5_HUMAN	1.23	3.32E-03

ERLN1_HUMAN	1.23	3.78E-04
CPNE1_HUMAN	1.23	4.00E-02
MD1L1_HUMAN	1.23	1.11E-03
WDR55_HUMAN	1.23	8.12E-04
WIZ_HUMAN	1.23	1.81E-02
RBM27_HUMAN	1.23	4.70E-03
DDX55_HUMAN	1.23	5.37E-03
HCFC1_HUMAN	1.23	2.67E-03
PKCB1_HUMAN	1.23	6.86E-04
DHX33_HUMAN	1.23	1.22E-02
CSTF2_HUMAN	1.23	1.90E-03
SF3B1_HUMAN	1.23	2.54E-03
TADA3_HUMAN	1.23	7.40E-03
CCAR1_HUMAN	1.23	5.80E-04
CELF1_HUMAN	1.23	1.33E-02
SMCA4_HUMAN	1.23	9.68E-04
APC7_HUMAN	1.23	9.50E-03
COQ9_HUMAN	1.23	2.72E-02
TM9S1_HUMAN	1.23	9.23E-04
LARG2_HUMAN	1.23	6.50E-03
SMCE1_HUMAN	1.23	4.96E-03
MTA2_HUMAN	1.23	6.99E-03
MTFP1_HUMAN	1.23	1.68E-02
CAND2_HUMAN	1.23	4.16E-02
MTNB_HUMAN	1.23	2.43E-03
F136A_HUMAN	1.23	4.02E-04
SEN34_HUMAN	1.23	1.41E-03
TRI33_HUMAN	1.23	2.21E-03
TDIF1_HUMAN	1.23	1.45E-02
ANGE2_HUMAN	1.23	2.08E-02
CYB5_HUMAN	1.23	3.64E-02
MED29_HUMAN	1.22	8.88E-04
TAF10_HUMAN	1.22	4.08E-02
RT14_HUMAN	1.22	1.18E-03
NOC4L_HUMAN	1.22	1.57E-03
SHCBP_HUMAN	1.22	1.53E-02
CTBP1_HUMAN	1.22	9.61E-04
FUBP2_HUMAN	1.22	1.78E-03
MED17_HUMAN	1.22	7.21E-03
MARC2_HUMAN	1.22	1.13E-02
ACS2L_HUMAN	1.22	1.63E-02
NOP56_HUMAN	1.22	5.40E-04
FAH2A_HUMAN	1.22	6.45E-03

SCOT1_HUMAN	1.22	6.62E-04
HIRA_HUMAN	1.22	1.22E-03
CCYL1_HUMAN	1.22	7.75E-03
TAF5L_HUMAN	1.22	1.62E-02
BD1L1_HUMAN	1.22	2.63E-03
MED20_HUMAN	1.22	9.74E-03
RM30_HUMAN	1.22	1.31E-02
DLG3_HUMAN	1.22	2.13E-02
CH60_HUMAN	1.22	9.32E-04
PIGT_HUMAN	1.22	3.55E-03
RT33_HUMAN	1.22	2.02E-03
SCPDL_HUMAN	1.22	7.96E-03
ORC2_HUMAN	1.22	1.25E-02
NOL9_HUMAN	1.22	6.38E-04
SF3B3_HUMAN	1.22	2.18E-03
OSMR_HUMAN	1.22	4.33E-03
FBRS_HUMAN	1.22	1.38E-02
SET1A_HUMAN	1.22	2.65E-03
HNRL1_HUMAN	1.22	3.89E-03
NUP53_HUMAN	1.22	3.21E-03
TCEA1_HUMAN	1.22	8.41E-03
BPTF_HUMAN	1.22	3.56E-04
NIPS2_HUMAN	1.22	1.89E-03
T2FB_HUMAN	1.22	9.84E-03
BUB3_HUMAN	1.22	1.59E-03
E41L2_HUMAN	1.22	1.79E-02
RAE1L_HUMAN	1.22	1.11E-03
SYMPK_HUMAN	1.22	3.03E-03
MET17_HUMAN	1.22	6.04E-03
UBL5_HUMAN	1.22	5.56E-04
RPRD2_HUMAN	1.22	3.36E-03
CAAP1_HUMAN	1.22	7.72E-03
NOP16_HUMAN	1.22	2.39E-02
SRSF5_HUMAN	1.22	1.73E-02
P4R3A_HUMAN	1.22	1.49E-02
SLTM_HUMAN	1.22	3.33E-03
ZDHC6_HUMAN	1.22	1.71E-02
LSR_HUMAN	1.22	8.33E-04
TP53B_HUMAN	1.22	1.04E-03
RM46_HUMAN	1.22	1.31E-03
FL2D_HUMAN	1.22	2.06E-03
CNDD3_HUMAN	1.22	2.74E-02
COASY_HUMAN	1.22	1.22E-03

TACC1_HUMAN	1.22	3.53E-03
STX17_HUMAN	1.22	7.75E-03
DCTP1_HUMAN	1.22	3.78E-02
ZCHC7_HUMAN	1.22	5.80E-03
LUC7L_HUMAN	1.21	4.55E-02
RAB23_HUMAN	1.21	1.40E-03
ZN512_HUMAN	1.21	6.57E-03
CIC_HUMAN	1.21	6.67E-03
WDR89_HUMAN	1.21	1.32E-03
GXLT1_HUMAN	1.21	3.14E-02
NU155_HUMAN	1.21	1.87E-03
WDR33_HUMAN	1.21	3.50E-03
CMC4_HUMAN	1.21	1.53E-02
NFYA_HUMAN	1.21	2.65E-02
NSA2_HUMAN	1.21	1.53E-02
ROA3_HUMAN	1.21	5.80E-03
AFF4_HUMAN	1.21	1.77E-02
CP131_HUMAN	1.21	1.75E-03
GNL3_HUMAN	1.21	3.12E-02
ZN217_HUMAN	1.21	1.81E-03
VIR_HUMAN	1.21	8.99E-03
MTA1_HUMAN	1.21	1.86E-02
PINX1_HUMAN	1.21	1.04E-02
SNUT2_HUMAN	1.21	1.22E-02
PIGU_HUMAN	1.21	9.64E-04
PPIL1_HUMAN	1.21	3.59E-03
JPH1_HUMAN	1.21	7.16E-03
CLP1_HUMAN	1.21	6.18E-03
BCS1_HUMAN	1.21	7.05E-03
TADBP_HUMAN	1.21	9.37E-03
F178A_HUMAN	1.21	2.92E-02
T2FA_HUMAN	1.21	9.41E-03
KANL3_HUMAN	1.21	1.68E-02
CSTFT_HUMAN	1.21	1.15E-03
DNLI3_HUMAN	1.21	1.81E-02
DDX28_HUMAN	1.21	1.95E-02
EFTS_HUMAN	1.21	1.34E-03
CCNT1_HUMAN	1.21	2.19E-02
NH2L1_HUMAN	1.21	9.02E-04
CPSF7_HUMAN	1.21	6.81E-03
TLN2_HUMAN	1.21	2.86E-02
PLOD3_HUMAN	1.21	1.57E-03
C1TC_HUMAN	1.20	4.60E-02

SNIP1_HUMAN	1.20	7.42E-03
CYTC_HUMAN	1.20	4.15E-02
ERCC1_HUMAN	1.20	3.44E-03
NUDT9_HUMAN	1.20	7.21E-03
PYRD_HUMAN	1.20	8.57E-04
RPB4_HUMAN	1.20	1.97E-03
ERCC3_HUMAN	1.20	3.93E-03
RPA2_HUMAN	1.20	5.95E-03
PUSL1_HUMAN	1.20	4.62E-02
SCAFB_HUMAN	1.20	9.19E-03
AAR2_HUMAN	1.20	3.42E-02
PUR6_HUMAN	1.20	3.69E-02
DDX31_HUMAN	1.20	3.05E-03
IDH3B_HUMAN	1.20	6.38E-03
BRE_HUMAN	1.20	9.82E-03
TOR4A_HUMAN	1.20	1.99E-02
IMP4_HUMAN	1.20	9.02E-04
ECI1_HUMAN	1.20	8.77E-03
UBL4A_HUMAN	1.20	3.44E-02
LIPS_HUMAN	1.20	2.30E-02
GPX7_HUMAN	1.20	4.62E-03
SCAF8_HUMAN	1.20	2.88E-03
TGFB1_HUMAN	1.20	6.40E-03
FAAA_HUMAN	1.20	4.26E-02
CLK1_HUMAN	1.20	4.75E-02
INT4_HUMAN	1.20	9.84E-04
PHB_HUMAN	1.20	1.26E-03
SNR40_HUMAN	1.20	2.96E-03
BACH1_HUMAN	1.20	4.78E-03
TMA16_HUMAN	1.20	6.50E-03
EWS_HUMAN	1.20	2.30E-02
CDCA2_HUMAN	1.20	3.00E-02
DEFM_HUMAN	1.20	1.92E-03
TSNAX_HUMAN	1.20	4.05E-03
NU214_HUMAN	1.20	9.24E-04
TMX1_HUMAN	1.20	1.28E-03
K2013_HUMAN	1.20	4.39E-03
RPAB1_HUMAN	1.20	4.63E-03
MED23_HUMAN	1.20	2.00E-02
CCNK_HUMAN	1.20	4.72E-03
NPA1P_HUMAN	1.20	9.00E-04
INT10_HUMAN	1.20	5.50E-03
PSA7_HUMAN	1.20	8.13E-04

TRIPC_HUMAN	1.20	1.29E-03
ACSA_HUMAN	1.20	1.51E-02
NSUN5_HUMAN	1.20	1.12E-03
BRM1L_HUMAN	1.20	1.00E-02
CJ012_HUMAN	1.20	2.77E-02
CSN3_HUMAN	1.20	2.64E-03
YIPF4_HUMAN	1.20	1.20E-02
DNJC1_HUMAN	1.20	2.34E-02
VRK2_HUMAN	1.20	8.73E-03
PUR8_HUMAN	1.20	2.31E-02
RASN_HUMAN	1.19	2.81E-02
ZFP91_HUMAN	1.19	3.87E-02
IDHP_HUMAN	1.19	6.46E-04
CP2J2_HUMAN	1.19	4.12E-02
HTSF1_HUMAN	1.19	7.28E-03
LAS1L_HUMAN	1.19	8.89E-04
RBM40_HUMAN	1.19	4.53E-02
FLOT1_HUMAN	1.19	2.95E-02
TIM16_HUMAN	1.19	1.03E-03
MEN1_HUMAN	1.19	1.18E-02
PHF2_HUMAN	1.19	7.70E-03
TGFR1_HUMAN	1.19	4.19E-03
DIC_HUMAN	1.19	1.77E-03
TXD12_HUMAN	1.19	1.47E-02
MED1_HUMAN	1.19	1.20E-02
CSN8_HUMAN	1.19	8.10E-03
RT35_HUMAN	1.19	1.61E-03
RRP8_HUMAN	1.19	1.47E-02
ATD3A_HUMAN	1.19	8.71E-04
RPB1_HUMAN	1.19	1.47E-03
RM20_HUMAN	1.19	4.67E-03
RAP2C_HUMAN	1.19	7.17E-03
SRPRB_HUMAN	1.19	1.96E-02
HS90B_HUMAN	1.19	2.86E-02
ELL_HUMAN	1.19	3.38E-02
MTA70_HUMAN	1.19	2.48E-02
MDN1_HUMAN	1.19	5.37E-03
RM01_HUMAN	1.19	7.33E-03
RAI1_HUMAN	1.19	5.97E-03
BCCIP_HUMAN	1.19	2.37E-03
RBBP5_HUMAN	1.19	7.71E-03
ATX1L_HUMAN	1.19	2.31E-02
CPSF1_HUMAN	1.19	5.37E-03

MRRP3_HUMAN	1.19	2.36E-03
TRRAP_HUMAN	1.19	2.37E-03
SCFD1_HUMAN	1.19	1.68E-03
SFXN2_HUMAN	1.19	1.11E-02
ABCB6_HUMAN	1.19	1.59E-02
CL065_HUMAN	1.19	4.29E-02
VPP2_HUMAN	1.19	1.07E-02
COX15_HUMAN	1.19	1.89E-03
STX5_HUMAN	1.19	8.16E-03
CHD8_HUMAN	1.19	2.86E-03
NFYB_HUMAN	1.19	1.35E-02
CTL1_HUMAN	1.19	2.72E-02
LTMD1_HUMAN	1.19	3.31E-02
TSN13_HUMAN	1.19	7.17E-03
NFIP2_HUMAN	1.19	1.26E-02
BRD3_HUMAN	1.19	1.27E-02
PUR1_HUMAN	1.19	1.83E-02
GTF2I_HUMAN	1.19	2.13E-02
ZN668_HUMAN	1.19	2.19E-02
TIM44_HUMAN	1.18	2.68E-03
AP2A_HUMAN	1.18	8.59E-03
PGRC1_HUMAN	1.18	7.11E-03
RM23_HUMAN	1.18	4.87E-02
TXN4A_HUMAN	1.18	9.56E-03
DHX35_HUMAN	1.18	2.73E-02
PAR16_HUMAN	1.18	4.62E-02
GPAA1_HUMAN	1.18	1.87E-03
TF2H3_HUMAN	1.18	5.83E-03
RM53_HUMAN	1.18	4.34E-03
DDB1_HUMAN	1.18	7.65E-03
SURF1_HUMAN	1.18	1.34E-02
MSH3_HUMAN	1.18	3.13E-02
CHD2_HUMAN	1.18	1.65E-03
SEC63_HUMAN	1.18	2.96E-03
PHAG1_HUMAN	1.18	1.90E-02
DDX46_HUMAN	1.18	5.39E-03
RM41_HUMAN	1.18	1.38E-02
CD2B2_HUMAN	1.18	1.20E-02
RM17_HUMAN	1.18	5.52E-03
CK5P1_HUMAN	1.18	4.86E-02
LAMC1_HUMAN	1.18	3.26E-03
3HIDH_HUMAN	1.18	3.83E-03
TIM14_HUMAN	1.18	7.52E-03

ZN462_HUMAN	1.18	3.37E-02
RRP5_HUMAN	1.18	7.67E-03
PRP4_HUMAN	1.18	1.03E-03
TAF4_HUMAN	1.18	6.54E-03
CSN1_HUMAN	1.18	2.15E-03
MINT_HUMAN	1.18	5.88E-03
QSOX2_HUMAN	1.18	9.57E-03
RING2_HUMAN	1.18	2.34E-03
INT2_HUMAN	1.18	3.94E-03
SPT5H_HUMAN	1.18	7.03E-03
RBM12_HUMAN	1.18	2.31E-02
NOL6_HUMAN	1.18	1.44E-02
ARI1A_HUMAN	1.17	5.30E-03
RAB34_HUMAN	1.17	2.64E-03
ERCC2_HUMAN	1.17	2.20E-03
KS6A4_HUMAN	1.17	7.96E-03
OFD1_HUMAN	1.17	3.46E-02
NRDE2_HUMAN	1.17	2.23E-02
CACO1_HUMAN	1.17	9.22E-03
RM24_HUMAN	1.17	4.07E-03
RT10_HUMAN	1.17	5.78E-03
CASC4_HUMAN	1.17	7.31E-03
LEG8_HUMAN	1.17	4.30E-03
RREB1_HUMAN	1.17	1.82E-03
LAMB1_HUMAN	1.17	3.28E-03
NU188_HUMAN	1.17	4.19E-03
IDH3A_HUMAN	1.17	8.51E-03
PF21A_HUMAN	1.17	1.39E-02
DUT_HUMAN	1.17	2.96E-03
IF2M_HUMAN	1.17	6.70E-03
AGAL_HUMAN	1.17	4.75E-02
CSN2_HUMAN	1.17	9.41E-03
RD23A_HUMAN	1.17	4.65E-02
SYDM_HUMAN	1.17	8.11E-03
UBR5_HUMAN	1.17	9.44E-03
BRD2_HUMAN	1.17	1.43E-02
MPP10_HUMAN	1.17	2.23E-02
PHF6_HUMAN	1.17	2.72E-02
INT1_HUMAN	1.17	1.84E-03
CEBPB_HUMAN	1.17	4.53E-02
COR2A_HUMAN	1.17	1.29E-02
GPDM_HUMAN	1.17	2.75E-03
CSN7A_HUMAN	1.17	1.63E-02

THEM6_HUMAN	1.17	2.25E-02
CCD58_HUMAN	1.17	5.48E-03
PARN_HUMAN	1.17	1.43E-02
DDX42_HUMAN	1.17	2.02E-02
SEM4B_HUMAN	1.16	1.14E-03
MED12_HUMAN	1.16	7.10E-03
NDUS4_HUMAN	1.16	1.05E-02
BCL7A_HUMAN	1.16	3.31E-02
BOLA3_HUMAN	1.16	3.05E-02
MTEF3_HUMAN	1.16	5.17E-03
SRFB1_HUMAN	1.16	7.04E-03
MMS19_HUMAN	1.16	9.19E-03
SETX_HUMAN	1.16	4.68E-02
XRN1_HUMAN	1.16	3.90E-03
NUP43_HUMAN	1.16	1.31E-02
GOGA3_HUMAN	1.16	8.13E-04
SSBP_HUMAN	1.16	2.84E-02
MYO19_HUMAN	1.16	2.86E-02
YLPM1_HUMAN	1.16	4.23E-03
BTAF1_HUMAN	1.16	5.85E-03
NFYC_HUMAN	1.16	8.16E-03
ATRIP_HUMAN	1.16	2.71E-02
KDEL1_HUMAN	1.16	2.96E-03
GPI8_HUMAN	1.16	2.02E-03
RM10_HUMAN	1.16	1.01E-02
MRT4_HUMAN	1.16	2.86E-02
PLRKT_HUMAN	1.16	2.54E-03
DCAF7_HUMAN	1.16	8.36E-03
RFOX2_HUMAN	1.16	1.96E-02
AKP8L_HUMAN	1.16	3.80E-03
PIGS_HUMAN	1.16	6.75E-03
RM18_HUMAN	1.16	7.33E-03
SEC20_HUMAN	1.16	3.89E-03
FNBP4_HUMAN	1.16	7.21E-03
RN149_HUMAN	1.16	2.25E-02
TRM5_HUMAN	1.16	1.72E-02
NDUV2_HUMAN	1.16	3.41E-03
PPWD1_HUMAN	1.16	9.58E-03
CQ085_HUMAN	1.16	1.45E-02
P3H1_HUMAN	1.16	5.36E-03
RPC1_HUMAN	1.16	6.95E-03
SUGP1_HUMAN	1.16	7.45E-03
RPAC1_HUMAN	1.16	8.17E-03

KDM2A_HUMAN	1.16	1.30E-02
PRDX4_HUMAN	1.16	3.31E-03
RPB2_HUMAN	1.16	2.25E-03
NELFD_HUMAN	1.16	5.33E-03
CPSF4_HUMAN	1.16	8.41E-03
PDIA3_HUMAN	1.16	4.24E-02
INT3_HUMAN	1.16	1.68E-02
UTP20_HUMAN	1.16	1.41E-02
PTBP1_HUMAN	1.16	1.83E-02
LYN_HUMAN	1.16	3.96E-03
TMCO1_HUMAN	1.16	7.00E-03
HEAT3_HUMAN	1.16	1.61E-02
NAKD2_HUMAN	1.16	7.48E-03
TF3C1_HUMAN	1.16	9.05E-03
HIAL1_HUMAN	1.16	2.64E-02
HDAC1_HUMAN	1.16	3.76E-02
MIMIT_HUMAN	1.16	2.18E-03
PSA4_HUMAN	1.16	3.02E-03
ODP2_HUMAN	1.16	3.58E-03
TIM21_HUMAN	1.16	3.58E-03
PSA1_HUMAN	1.16	6.81E-03
PIMT_HUMAN	1.16	9.78E-03
RM02_HUMAN	1.15	9.21E-03
SYSM_HUMAN	1.15	6.40E-03
ADPGK_HUMAN	1.15	1.44E-02
NUDT8_HUMAN	1.15	3.67E-02
UBN1_HUMAN	1.15	1.65E-02
K1C18_HUMAN	1.15	3.96E-03
VKOR1_HUMAN	1.15	4.04E-03
RAB43_HUMAN	1.15	1.71E-02
H2AW_HUMAN	1.15	1.61E-02
D19L4_HUMAN	1.15	1.31E-02
CTDS1_HUMAN	1.15	1.15E-02
TRUB1_HUMAN	1.15	3.80E-02
ERCC6_HUMAN	1.15	2.07E-02
NXF1_HUMAN	1.15	4.74E-03
RO60_HUMAN	1.15	2.77E-02
PHB2_HUMAN	1.15	5.64E-03
SRCAP_HUMAN	1.15	6.58E-03
SP130_HUMAN	1.15	4.00E-02
GLE1_HUMAN	1.15	5.89E-03
RM43_HUMAN	1.15	7.31E-03
CLP1L_HUMAN	1.15	8.97E-03

DAZP1_HUMAN	1.15	3.14E-02
PLOD2_HUMAN	1.15	6.17E-03
NCOR1_HUMAN	1.15	8.65E-03
NIPBL_HUMAN	1.15	5.81E-03
NDUA9_HUMAN	1.15	3.17E-03
HAX1_HUMAN	1.15	5.74E-03
TDIF2_HUMAN	1.15	1.68E-02
EHD4_HUMAN	1.15	1.52E-02
RM11_HUMAN	1.15	1.81E-02
REEP4_HUMAN	1.15	4.73E-02
ATM_HUMAN	1.15	2.35E-03
STT3A_HUMAN	1.15	5.87E-03
PB1_HUMAN	1.15	2.05E-02
CNPY3_HUMAN	1.15	2.10E-02
SUMF2_HUMAN	1.15	2.62E-02
DNJA3_HUMAN	1.15	5.37E-03
SYAM_HUMAN	1.15	6.00E-03
DPOLB_HUMAN	1.15	1.44E-02
CDC27_HUMAN	1.15	4.75E-02
ANFY1_HUMAN	1.15	2.24E-03
GRHL2_HUMAN	1.15	3.13E-02
TE2IP_HUMAN	1.15	4.01E-03
GTPB3_HUMAN	1.15	4.85E-02
CCNH_HUMAN	1.14	8.13E-03
MCUR1_HUMAN	1.14	1.25E-02
FLOT2_HUMAN	1.14	1.79E-02
NEP1_HUMAN	1.14	6.11E-03
UTP11_HUMAN	1.14	1.15E-02
VKORL_HUMAN	1.14	4.99E-02
S30BP_HUMAN	1.14	1.41E-02
CS047_HUMAN	1.14	3.43E-02
RPOM_HUMAN	1.14	2.45E-02
CRLF3_HUMAN	1.14	3.35E-02
TOM40_HUMAN	1.14	4.11E-03
TIM50_HUMAN	1.14	7.02E-03
HS90A_HUMAN	1.14	4.19E-02
DUS3L_HUMAN	1.14	8.58E-03
SUV3_HUMAN	1.14	6.72E-03
ABCBA_HUMAN	1.14	4.87E-03
MED16_HUMAN	1.14	7.19E-03
PPIC_HUMAN	1.14	2.79E-02
CDK7_HUMAN	1.14	2.99E-03
ERAP2_HUMAN	1.14	6.50E-03

CBP_HUMAN	1.14	3.95E-02
GANAB_HUMAN	1.14	4.59E-03
CSN7B_HUMAN	1.14	1.85E-02
APC5_HUMAN	1.14	3.14E-02
CF089_HUMAN	1.14	4.39E-02
DHC24_HUMAN	1.14	2.69E-02
PRPK_HUMAN	1.14	4.24E-02
RM16_HUMAN	1.14	3.15E-03
QCR8_HUMAN	1.14	1.10E-02
RBM45_HUMAN	1.14	3.64E-02
ATAD1_HUMAN	1.14	8.96E-03
RCC2_HUMAN	1.14	1.66E-02
RM47_HUMAN	1.14	2.03E-02
RPB7_HUMAN	1.14	3.93E-02
RM12_HUMAN	1.14	7.12E-03
DCA13_HUMAN	1.14	2.51E-02
CR021_HUMAN	1.14	4.83E-02
CSN4_HUMAN	1.14	1.18E-02
RPC2_HUMAN	1.14	2.63E-02
CD97_HUMAN	1.14	2.67E-02
SYTM_HUMAN	1.14	2.33E-02
UQCC2_HUMAN	1.14	3.99E-02
CPSF3_HUMAN	1.14	6.73E-03
RM32_HUMAN	1.14	7.36E-03
M2OM_HUMAN	1.14	7.98E-03
INT6_HUMAN	1.14	2.67E-02
FCF1_HUMAN	1.14	4.26E-02
RM40_HUMAN	1.14	4.39E-03
S35B2_HUMAN	1.14	1.54E-02
RT06_HUMAN	1.14	7.43E-03
LAMA5_HUMAN	1.14	2.91E-02
S38AA_HUMAN	1.14	1.20E-02
BORG5_HUMAN	1.14	3.77E-02
ATD3B_HUMAN	1.13	8.75E-03
ZN592_HUMAN	1.13	1.25E-02
NDUC2_HUMAN	1.13	3.65E-02
SRRM2_HUMAN	1.13	7.48E-03
MBD2_HUMAN	1.13	1.02E-02
DX39B_HUMAN	1.13	6.03E-03
IPRI_HUMAN	1.13	2.03E-02
NSUN2_HUMAN	1.13	2.56E-02
GRP75_HUMAN	1.13	4.81E-03
SNF5_HUMAN	1.13	2.44E-02

D19L1_HUMAN	1.13	3.79E-02
RUVB2_HUMAN	1.13	2.33E-02
TRA2A_HUMAN	1.13	4.38E-02
NDUA6_HUMAN	1.13	1.26E-02
COIL_HUMAN	1.13	2.33E-02
AAAS_HUMAN	1.13	1.65E-02
RDH14_HUMAN	1.13	3.17E-02
ACBD5_HUMAN	1.13	1.27E-02
ISCA2_HUMAN	1.13	3.67E-02
CDK9_HUMAN	1.13	7.70E-03
RT18B_HUMAN	1.13	9.37E-03
FABD_HUMAN	1.13	1.78E-02
PSA3_HUMAN	1.13	1.52E-02
TPBG_HUMAN	1.13	1.18E-02
RM04_HUMAN	1.13	1.63E-02
RM03_HUMAN	1.13	1.79E-02
SDHA_HUMAN	1.13	1.23E-02
STIM2_HUMAN	1.13	1.96E-02
ARL10_HUMAN	1.13	2.04E-02
RBM33_HUMAN	1.13	2.27E-02
DNPEP_HUMAN	1.13	3.11E-02
RL7L_HUMAN	1.13	3.52E-02
RM14_HUMAN	1.13	1.99E-02
PLCB_HUMAN	1.13	1.72E-02
RRP44_HUMAN	1.13	3.63E-02
MTX1_HUMAN	1.13	9.19E-03
MESD_HUMAN	1.13	1.44E-02
RBFA_HUMAN	1.13	5.14E-03
GEMI8_HUMAN	1.13	2.01E-02
DCNL1_HUMAN	1.13	4.78E-02
CUL1_HUMAN	1.13	3.71E-02
LRC59_HUMAN	1.13	3.71E-02
MTA3_HUMAN	1.13	3.37E-02
DJC11_HUMAN	1.13	3.69E-02
PSA6_HUMAN	1.13	8.73E-03
MIC19_HUMAN	1.13	2.25E-02
MYH6_HUMAN	1.13	2.65E-02
DDX41_HUMAN	1.13	3.45E-02
TSN_HUMAN	1.13	4.98E-02
RPC5_HUMAN	1.13	1.70E-02
LMNA_HUMAN	1.13	3.11E-02
VAPA_HUMAN	1.13	9.57E-03
EFTU_HUMAN	1.13	2.67E-02

AASS_HUMAN	1.13	3.28E-02
MPRD_HUMAN	1.13	3.28E-02
CARM1_HUMAN	1.12	9.88E-03
SC11A_HUMAN	1.12	4.53E-02
JAK1_HUMAN	1.12	1.34E-02
FKBP8_HUMAN	1.12	4.78E-02
CALU_HUMAN	1.12	4.87E-02
FERM2_HUMAN	1.12	4.18E-03
RT05_HUMAN	1.12	2.28E-02
ALG5_HUMAN	1.12	1.18E-02
ASUN_HUMAN	1.12	3.52E-02
MED24_HUMAN	1.12	1.38E-02
PSA5_HUMAN	1.12	9.39E-03
LONM_HUMAN	1.12	1.26E-02
CNPY2_HUMAN	1.12	1.83E-02
AUHM_HUMAN	1.12	2.63E-02
COG6_HUMAN	1.12	9.74E-03
GRPE1_HUMAN	1.12	1.10E-02
IMP3_HUMAN	1.12	2.28E-02
ALG6_HUMAN	1.12	4.64E-02
GANP_HUMAN	1.12	3.00E-02
PCF11_HUMAN	1.12	2.79E-02
RHDF2_HUMAN	1.12	1.55E-02
BET1L_HUMAN	1.12	3.07E-02
FA49B_HUMAN	1.12	3.33E-02
SCO1_HUMAN	1.12	2.39E-02
CCD47_HUMAN	1.12	2.54E-02
ARFP2_HUMAN	1.12	3.01E-02
RT21_HUMAN	1.12	4.09E-02
PLCC_HUMAN	1.12	4.06E-02
COG5_HUMAN	1.12	1.13E-02
QCR7_HUMAN	1.11	1.38E-02
P66B_HUMAN	1.11	1.78E-02
CPSF2_HUMAN	1.11	2.23E-02
PGAM5_HUMAN	1.11	1.05E-02
CSN5_HUMAN	1.11	3.53E-02
RRAS2_HUMAN	1.11	3.64E-02
CUL4A_HUMAN	1.11	4.33E-02
RM50_HUMAN	1.11	2.04E-02
CCD12_HUMAN	1.11	4.20E-02
TM109_HUMAN	1.11	2.16E-02
MED4_HUMAN	1.11	4.61E-02
TTL12_HUMAN	1.11	1.69E-02

TOM22_HUMAN	1.11	4.77E-02
RM48_HUMAN	1.11	1.29E-02
SF3B5_HUMAN	1.11	4.11E-02
GRAM4_HUMAN	1.11	4.26E-02
RPC4_HUMAN	1.11	1.18E-02
RT31_HUMAN	1.11	1.83E-02
CARF_HUMAN	1.11	3.60E-02
ACADM_HUMAN	1.11	3.07E-02
PPIE_HUMAN	1.11	1.88E-02
DNJA2_HUMAN	1.11	2.67E-02
ACPM_HUMAN	1.11	2.34E-02
CS025_HUMAN	1.11	2.84E-02
FAF1_HUMAN	1.11	2.91E-02
MFN2_HUMAN	1.11	3.81E-02
RT12_HUMAN	1.11	3.63E-02
PSB4_HUMAN	1.11	3.87E-02
TF2H4_HUMAN	1.11	2.62E-02
CTSL2_HUMAN	1.11	3.07E-02
RM49_HUMAN	1.11	2.55E-02
RT11_HUMAN	1.11	2.84E-02
CQ062_HUMAN	1.11	2.70E-02
RAB12_HUMAN	1.11	1.65E-02
OFUT1_HUMAN	1.11	3.52E-02
COA7_HUMAN	1.11	3.43E-02
NSUN4_HUMAN	1.10	4.19E-02
SGPP1_HUMAN	1.10	4.98E-02
RM27_HUMAN	1.10	4.89E-02
DCXR_HUMAN	1.10	4.87E-02
NKRF_HUMAN	1.10	1.76E-02
CUL2_HUMAN	1.10	4.40E-02
LMF2_HUMAN	1.10	2.22E-02
SYNE2_HUMAN	1.10	2.68E-02
RM39_HUMAN	1.10	4.04E-02
RER1_HUMAN	1.10	4.81E-02
RRF2M_HUMAN	1.10	4.98E-02
PSB1_HUMAN	1.10	2.56E-02
ISCU_HUMAN	1.10	3.72E-02
WDR74_HUMAN	1.10	3.84E-02
ICT1_HUMAN	1.10	1.74E-02
PREB_HUMAN	1.10	3.73E-02
HM13_HUMAN	1.10	3.80E-02
UFSP2_HUMAN	1.10	3.78E-02
NDUA2_HUMAN	1.10	3.91E-02

I2BP2_HUMAN	1.10	2.91E-02
UCHL5_HUMAN	1.10	3.39E-02
BIG2_HUMAN	1.10	3.63E-02
SSU72_HUMAN	1.10	3.81E-02
SUN1_HUMAN	1.09	4.38E-02
G45IP_HUMAN	1.09	2.44E-02
MRRP1_HUMAN	1.09	3.21E-02
UCRI_HUMAN	1.09	2.52E-02
DIEXF_HUMAN	1.09	4.54E-02
VDAC3_HUMAN	1.09	4.27E-02
RT09_HUMAN	1.09	4.72E-02
CSK2B_HUMAN	1.09	3.16E-02
AGK_HUMAN	1.08	4.80E-02
PTCD3_HUMAN	1.08	3.04E-02
THIL_HUMAN	1.08	3.30E-02
ECI2_HUMAN	1.08	3.57E-02
SYNM_HUMAN	1.08	3.88E-02
PRS8_HUMAN	-1.08	3.13E-02
PSB6_HUMAN	-1.08	4.33E-02
VAS1_HUMAN	-1.08	4.68E-02
PSMD1_HUMAN	-1.09	3.36E-02
T106B_HUMAN	-1.09	3.77E-02
FAKD5_HUMAN	-1.09	3.88E-02
PSMD3_HUMAN	-1.09	2.77E-02
FYCO1_HUMAN	-1.09	4.88E-02
CNOT1_HUMAN	-1.09	3.77E-02
RASH_HUMAN	-1.09	4.12E-02
VPS45_HUMAN	-1.09	2.47E-02
GSLG1_HUMAN	-1.10	3.32E-02
SCRIB_HUMAN	-1.10	2.92E-02
RB3GP_HUMAN	-1.10	3.38E-02
TMED9_HUMAN	-1.10	1.55E-02
AHDC1_HUMAN	-1.10	3.34E-02
NPTN_HUMAN	-1.10	4.68E-02
PDIA1_HUMAN	-1.10	2.50E-02
TCF25_HUMAN	-1.10	2.36E-02
PP2BA_HUMAN	-1.10	2.47E-02
PSMD8_HUMAN	-1.10	2.61E-02
MRCKA_HUMAN	-1.10	4.14E-02
TANC1_HUMAN	-1.10	3.91E-02
ERGI2_HUMAN	-1.10	1.73E-02
CTGE5_HUMAN	-1.10	4.40E-02
PSD13_HUMAN	-1.10	2.26E-02

HTAI2_HUMAN	-1.10	3.93E-02
DCAF6_HUMAN	-1.10	4.55E-02
AP1G1_HUMAN	-1.10	2.04E-02
DLG5_HUMAN	-1.10	2.53E-02
S39AA_HUMAN	-1.10	1.29E-02
TEX2_HUMAN	-1.10	2.74E-02
RT36_HUMAN	-1.10	1.18E-02
NUMB_HUMAN	-1.10	1.18E-02
KAPCB_HUMAN	-1.10	2.19E-02
TEN3_HUMAN	-1.11	3.11E-02
PYC_HUMAN	-1.11	1.36E-02
F91A1_HUMAN	-1.11	3.81E-02
HNRH2_HUMAN	-1.11	3.18E-02
ERG28_HUMAN	-1.11	1.84E-02
RAP1B_HUMAN	-1.11	1.81E-02
MIC25_HUMAN	-1.11	2.06E-02
CTR1_HUMAN	-1.11	1.18E-02
PKHA5_HUMAN	-1.11	6.51E-03
PTRF_HUMAN	-1.11	2.89E-02
SPRY7_HUMAN	-1.11	3.25E-02
EHD1_HUMAN	-1.11	4.94E-02
DGLB_HUMAN	-1.11	3.04E-02
TPP1_HUMAN	-1.11	4.88E-02
FPRP_HUMAN	-1.11	4.11E-02
MIC1_HUMAN	-1.12	2.15E-02
CTND1_HUMAN	-1.12	1.92E-02
NNTM_HUMAN	-1.12	2.06E-02
CAMLG_HUMAN	-1.12	2.49E-02
VPS52_HUMAN	-1.12	3.51E-02
NEK9_HUMAN	-1.12	2.56E-02
PAK4_HUMAN	-1.12	2.32E-02
WFS1_HUMAN	-1.12	2.73E-02
SIM12_HUMAN	-1.12	3.49E-02
PSN1_HUMAN	-1.12	3.88E-02
K1671_HUMAN	-1.12	2.77E-02
MON2_HUMAN	-1.12	3.79E-02
ATPB_HUMAN	-1.12	2.66E-02
C27C1_HUMAN	-1.12	3.39E-02
UBAC2_HUMAN	-1.12	3.74E-02
ACON_HUMAN	-1.12	2.25E-02
KC1D_HUMAN	-1.12	1.98E-02
PICAL_HUMAN	-1.12	9.89E-03
PVRL1_HUMAN	-1.12	4.62E-02

EFR3A_HUMAN	-1.12	4.21E-02
WDFY1_HUMAN	-1.12	9.98E-03
TR10B_HUMAN	-1.12	4.84E-02
PI4KA_HUMAN	-1.12	4.96E-03
CCHL_HUMAN	-1.12	4.19E-02
AP1S1_HUMAN	-1.13	1.99E-02
NEB2_HUMAN	-1.13	8.63E-03
SPY4_HUMAN	-1.13	5.20E-03
2AAA_HUMAN	-1.13	1.74E-02
RCD1_HUMAN	-1.13	1.90E-02
VWA8_HUMAN	-1.13	1.98E-02
TMED7_HUMAN	-1.13	1.12E-02
MARK2_HUMAN	-1.13	2.44E-02
ATPA_HUMAN	-1.13	3.52E-02
ODPA_HUMAN	-1.13	6.94E-03
FGOP2_HUMAN	-1.13	3.61E-02
HXK2_HUMAN	-1.13	4.91E-03
TTC19_HUMAN	-1.13	2.14E-02
ATPO_HUMAN	-1.13	3.50E-02
HERC4_HUMAN	-1.13	2.04E-02
RAB1B_HUMAN	-1.13	6.51E-03
CD59_HUMAN	-1.13	9.23E-03
MCU_HUMAN	-1.13	4.00E-02
UBE4A_HUMAN	-1.13	6.05E-03
RAB13_HUMAN	-1.13	1.59E-02
MA7D1_HUMAN	-1.13	2.54E-02
ADT3_HUMAN	-1.13	8.83E-03
BAP31_HUMAN	-1.13	1.64E-02
SH3B4_HUMAN	-1.13	2.33E-02
SPIT2_HUMAN	-1.13	3.43E-02
QSOX1_HUMAN	-1.13	4.11E-02
PCAT2_HUMAN	-1.13	3.08E-02
L2GL2_HUMAN	-1.13	4.86E-02
AP2B1_HUMAN	-1.13	3.21E-03
RAB1A_HUMAN	-1.13	2.03E-02
PSMD6_HUMAN	-1.13	3.88E-03
MCCA_HUMAN	-1.13	4.05E-02
LRRC1_HUMAN	-1.13	1.19E-02
MYO1B_HUMAN	-1.13	1.01E-02
AP2A1_HUMAN	-1.13	3.62E-03
PDC10_HUMAN	-1.13	1.68E-02
ATP5H_HUMAN	-1.13	2.53E-02
AT2C1_HUMAN	-1.14	6.89E-03

SCFD2_HUMAN	-1.14	2.97E-02
PKD2_HUMAN	-1.14	2.31E-02
ODPB_HUMAN	-1.14	8.65E-03
SPNS1_HUMAN	-1.14	4.83E-02
SEN54_HUMAN	-1.14	2.88E-02
PLEC_HUMAN	-1.14	5.88E-03
OCAD2_HUMAN	-1.14	1.50E-02
GALT2_HUMAN	-1.14	1.77E-02
PHLB2_HUMAN	-1.14	7.42E-03
ANKH1_HUMAN	-1.14	2.11E-02
LRC57_HUMAN	-1.14	3.41E-02
AP2A2_HUMAN	-1.14	3.31E-03
DHB12_HUMAN	-1.14	6.87E-03
ATPG_HUMAN	-1.14	2.12E-02
EPHB4_HUMAN	-1.14	5.16E-03
RBP1_HUMAN	-1.14	1.64E-02
MICU2_HUMAN	-1.14	7.19E-03
MMAA_HUMAN	-1.14	3.17E-02
COX20_HUMAN	-1.14	3.61E-03
RBM5_HUMAN	-1.14	4.77E-02
RAB8A_HUMAN	-1.14	1.20E-02
YLAT2_HUMAN	-1.14	1.99E-02
GBG12_HUMAN	-1.14	9.98E-03
TM55B_HUMAN	-1.14	2.36E-02
TMX2_HUMAN	-1.14	2.79E-02
DHRS7_HUMAN	-1.14	1.60E-02
SRPK1_HUMAN	-1.14	6.50E-03
TARA_HUMAN	-1.14	5.64E-03
KTN1_HUMAN	-1.14	6.38E-03
AP2S1_HUMAN	-1.14	9.96E-03
AP2M1_HUMAN	-1.14	1.62E-03
MPZL1_HUMAN	-1.14	1.85E-02
UBAP1_HUMAN	-1.15	3.64E-02
SEC13_HUMAN	-1.15	1.86E-02
PP1B_HUMAN	-1.15	2.10E-02
HCD2_HUMAN	-1.15	3.87E-02
DPM3_HUMAN	-1.15	4.81E-02
MBOA5_HUMAN	-1.15	9.41E-03
CTL2_HUMAN	-1.15	3.09E-02
GORS2_HUMAN	-1.15	3.38E-02
FKB14_HUMAN	-1.15	4.62E-02
EMC3_HUMAN	-1.15	7.47E-03
RL30_HUMAN	-1.15	2.48E-02

HCDH_HUMAN	-1.15	4.93E-02
CLH1_HUMAN	-1.15	3.58E-03
CYFP1_HUMAN	-1.15	4.33E-03
PTN23_HUMAN	-1.15	3.26E-03
TSC2_HUMAN	-1.15	4.30E-02
CASP_HUMAN	-1.15	5.57E-03
GDPD1_HUMAN	-1.15	3.58E-02
PTN12_HUMAN	-1.15	3.32E-02
UBR1_HUMAN	-1.15	2.46E-02
RBGPR_HUMAN	-1.15	6.68E-03
FUCT1_HUMAN	-1.15	1.18E-02
SHOC2_HUMAN	-1.15	1.98E-02
TMF1_HUMAN	-1.15	7.84E-03
RHOD_HUMAN	-1.15	1.92E-02
FERM1_HUMAN	-1.15	2.15E-02
PRDBP_HUMAN	-1.15	1.38E-02
UXS1_HUMAN	-1.16	4.81E-02
41_HUMAN	-1.16	4.67E-03
ASCC2_HUMAN	-1.16	1.72E-02
B4GT1_HUMAN	-1.16	3.07E-02
REEP5_HUMAN	-1.16	3.55E-03
EI24_HUMAN	-1.16	1.01E-02
SKT_HUMAN	-1.16	2.08E-03
FAK1_HUMAN	-1.16	1.12E-02
AL7A1_HUMAN	-1.16	1.59E-02
CC50A_HUMAN	-1.16	3.34E-03
CTNB1_HUMAN	-1.16	1.39E-03
ANO6_HUMAN	-1.16	1.37E-03
AT10D_HUMAN	-1.16	2.76E-02
LRP1_HUMAN	-1.16	3.15E-02
BMP1_HUMAN	-1.16	2.01E-02
PTPRF_HUMAN	-1.16	1.28E-03
DHX29_HUMAN	-1.16	2.81E-03
TOIP2_HUMAN	-1.16	3.21E-03
HELZ_HUMAN	-1.16	2.23E-02
VAC14_HUMAN	-1.16	2.43E-03
GNL3L_HUMAN	-1.16	4.31E-03
FRYL_HUMAN	-1.16	1.26E-02
5NTC_HUMAN	-1.16	2.91E-02
LCAP_HUMAN	-1.16	1.47E-03
CHP1_HUMAN	-1.16	7.16E-03
STAM1_HUMAN	-1.16	1.59E-02
TM7S3_HUMAN	-1.16	2.84E-02

EFC14_HUMAN	-1.16	8.41E-03
DNS2A_HUMAN	-1.16	3.88E-02
LIPE_HUMAN	-1.16	1.37E-02
ISOC2_HUMAN	-1.16	1.99E-02
GPC1_HUMAN	-1.16	4.48E-02
DICER_HUMAN	-1.16	3.52E-02
PDZD8_HUMAN	-1.16	5.44E-03
S23IP_HUMAN	-1.16	2.00E-02
MCA3_HUMAN	-1.16	3.48E-02
COPE_HUMAN	-1.16	3.90E-02
MBRL_HUMAN	-1.16	1.89E-03
PEX19_HUMAN	-1.16	2.71E-02
GNAI2_HUMAN	-1.16	2.78E-03
TRIO_HUMAN	-1.16	1.58E-02
PPP6_HUMAN	-1.17	1.83E-02
PP2AA_HUMAN	-1.17	2.48E-03
TWF2_HUMAN	-1.17	1.63E-02
2A5G_HUMAN	-1.17	2.53E-03
ITPR3_HUMAN	-1.17	2.30E-02
SI1L3_HUMAN	-1.17	4.96E-02
ADRO_HUMAN	-1.17	1.48E-02
FA83F_HUMAN	-1.17	4.21E-03
DHB4_HUMAN	-1.17	2.86E-03
VPP3_HUMAN	-1.17	4.07E-03
ERG7_HUMAN	-1.17	4.94E-03
STK24_HUMAN	-1.17	4.10E-02
ACATN_HUMAN	-1.17	2.92E-02
EGFR_HUMAN	-1.17	4.39E-03
MACOI_HUMAN	-1.17	4.38E-02
DLP1_HUMAN	-1.17	2.61E-02
VPS11_HUMAN	-1.17	1.08E-02
NAV1_HUMAN	-1.17	2.36E-03
LIPB1_HUMAN	-1.17	2.37E-03
ZDHC5_HUMAN	-1.17	3.02E-03
CPT1A_HUMAN	-1.17	6.59E-03
ELMD2_HUMAN	-1.17	3.47E-02
WDR11_HUMAN	-1.17	2.42E-03
SCAM1_HUMAN	-1.17	3.33E-03
NDUF4_HUMAN	-1.17	9.56E-03
CD63_HUMAN	-1.17	2.73E-02
IMA3_HUMAN	-1.17	8.15E-03
SRC_HUMAN	-1.17	1.22E-03
LIMA1_HUMAN	-1.17	3.26E-02

RHG10_HUMAN	-1.17	1.30E-02
C1QT6_HUMAN	-1.17	1.83E-03
TM9S2_HUMAN	-1.17	3.09E-03
MYOME_HUMAN	-1.17	3.33E-03
PRRC1_HUMAN	-1.17	4.00E-02
CYBR1_HUMAN	-1.17	6.27E-03
MYO1D_HUMAN	-1.17	4.27E-03
NGAP_HUMAN	-1.17	1.45E-02
RTKN_HUMAN	-1.17	1.94E-02
DPYL2_HUMAN	-1.18	3.77E-02
DGKA_HUMAN	-1.18	9.42E-03
MLF2_HUMAN	-1.18	5.16E-03
TMM17_HUMAN	-1.18	6.25E-03
CDC42_HUMAN	-1.18	7.36E-03
ARHG5_HUMAN	-1.18	7.41E-03
MAGT1_HUMAN	-1.18	1.45E-02
F162A_HUMAN	-1.18	3.94E-02
CLAP1_HUMAN	-1.18	2.29E-02
DPM1_HUMAN	-1.18	2.00E-03
S38A5_HUMAN	-1.18	1.60E-02
PSB5_HUMAN	-1.18	1.56E-03
GLGB_HUMAN	-1.18	1.67E-02
GLO2_HUMAN	-1.18	4.15E-02
EIF3K_HUMAN	-1.18	1.09E-02
SELB_HUMAN	-1.18	4.20E-02
CALM_HUMAN	-1.18	2.64E-03
GIPC1_HUMAN	-1.18	8.70E-03
ARMX3_HUMAN	-1.18	1.77E-03
MLEC_HUMAN	-1.18	5.93E-03
COPG1_HUMAN	-1.18	2.17E-02
PURB_HUMAN	-1.18	7.02E-03
IRGQ_HUMAN	-1.18	1.41E-02
INP4B_HUMAN	-1.18	2.28E-02
ERF1_HUMAN	-1.18	4.12E-02
GSTK1_HUMAN	-1.18	2.49E-02
STX8_HUMAN	-1.18	3.61E-03
ATPD_HUMAN	-1.18	2.86E-02
CMC2_HUMAN	-1.18	2.87E-02
GPAT4_HUMAN	-1.18	5.06E-03
LTOR1_HUMAN	-1.18	2.23E-03
MSI2H_HUMAN	-1.18	2.02E-02
RENT2_HUMAN	-1.18	9.01E-03
OSTM1_HUMAN	-1.18	1.29E-02

SAC1_HUMAN	-1.18	1.11E-03
CAZA1_HUMAN	-1.18	5.48E-03
GDE_HUMAN	-1.18	1.74E-02
LEG3_HUMAN	-1.18	1.20E-02
GNAQ_HUMAN	-1.18	1.86E-02
SYNPO_HUMAN	-1.19	1.81E-02
ORML2_HUMAN	-1.19	1.04E-02
BORG2_HUMAN	-1.19	4.70E-03
APLP2_HUMAN	-1.19	8.39E-03
RISC_HUMAN	-1.19	2.99E-02
BIN3_HUMAN	-1.19	2.66E-03
METL8_HUMAN	-1.19	7.79E-03
BMP2K_HUMAN	-1.19	5.64E-03
ARL4C_HUMAN	-1.19	3.87E-02
SI1L1_HUMAN	-1.19	4.63E-04
ABCF1_HUMAN	-1.19	9.55E-03
COPB2_HUMAN	-1.19	1.39E-02
LYRM2_HUMAN	-1.19	1.29E-02
EIF3B_HUMAN	-1.19	3.07E-02
UBQL2_HUMAN	-1.19	4.25E-02
COBL1_HUMAN	-1.19	1.75E-02
CX6B1_HUMAN	-1.19	3.03E-03
RAB4A_HUMAN	-1.19	1.63E-02
TMM43_HUMAN	-1.19	1.25E-03
NF1_HUMAN	-1.19	2.43E-03
GNPAT_HUMAN	-1.19	1.96E-02
RAI14_HUMAN	-1.19	5.87E-04
TM189_HUMAN	-1.19	2.61E-02
CSKI2_HUMAN	-1.19	3.41E-02
ANR17_HUMAN	-1.19	5.60E-03
CHIP_HUMAN	-1.19	7.95E-03
K1522_HUMAN	-1.19	8.12E-04
MRP1_HUMAN	-1.19	1.13E-02
ARHG7_HUMAN	-1.19	3.01E-02
PKP3_HUMAN	-1.19	2.01E-02
S10AG_HUMAN	-1.19	5.18E-03
AF1L2_HUMAN	-1.19	1.91E-02
TBB6_HUMAN	-1.19	4.73E-02
PDE12_HUMAN	-1.19	3.20E-03
CQ089_HUMAN	-1.19	9.61E-04
GPX4_HUMAN	-1.19	2.44E-02
PAXI_HUMAN	-1.19	2.88E-02
JAM1_HUMAN	-1.19	1.69E-03

HSBP1_HUMAN	-1.19	7.34E-03
SUCB2_HUMAN	-1.19	1.98E-03
RDH13_HUMAN	-1.19	2.00E-02
CAMP2_HUMAN	-1.20	2.88E-02
PI42B_HUMAN	-1.20	3.03E-03
TIGAR_HUMAN	-1.20	3.95E-02
UN45A_HUMAN	-1.20	1.84E-03
MYOF_HUMAN	-1.20	2.80E-03
G3BP2_HUMAN	-1.20	3.94E-02
SPTC3_HUMAN	-1.20	6.30E-03
TJAP1_HUMAN	-1.20	2.00E-02
AKAP2_HUMAN	-1.20	2.31E-02
CTNA1_HUMAN	-1.20	2.08E-03
ZFY16_HUMAN	-1.20	6.72E-03
UBR4_HUMAN	-1.20	1.41E-02
RPTOR_HUMAN	-1.20	1.94E-02
RASK_HUMAN	-1.20	2.16E-03
ORN_HUMAN	-1.20	2.95E-02
ZO1_HUMAN	-1.20	1.45E-02
ARG28_HUMAN	-1.20	1.20E-02
ZC3HF_HUMAN	-1.20	4.13E-02
TSN6_HUMAN	-1.20	4.92E-02
TWF1_HUMAN	-1.20	4.94E-03
DBNL_HUMAN	-1.20	6.67E-03
BECN1_HUMAN	-1.20	2.12E-02
MPRIP_HUMAN	-1.20	5.55E-03
RFTN1_HUMAN	-1.20	6.96E-04
VAMP7_HUMAN	-1.20	2.48E-03
GRN_HUMAN	-1.20	3.75E-02
TSPOA_HUMAN	-1.20	1.43E-02
ECHA_HUMAN	-1.20	2.51E-02
MSMO1_HUMAN	-1.20	3.57E-02
RAB7A_HUMAN	-1.20	4.95E-04
TPRA1_HUMAN	-1.20	7.72E-03
STK38_HUMAN	-1.20	5.89E-03
AT132_HUMAN	-1.20	1.47E-02
EPN4_HUMAN	-1.20	1.16E-03
DYN2_HUMAN	-1.20	1.01E-02
CLCB_HUMAN	-1.20	1.81E-03
S12A9_HUMAN	-1.20	2.53E-03
PGM2_HUMAN	-1.20	2.38E-02
4ET_HUMAN	-1.20	2.66E-02
MYPT1_HUMAN	-1.20	5.00E-03

PKHO2_HUMAN	-1.20	4.37E-02
SC5D_HUMAN	-1.20	1.51E-02
ITB5_HUMAN	-1.20	3.06E-03
WDR91_HUMAN	-1.20	1.74E-02
RFIP5_HUMAN	-1.20	2.07E-03
NDE1_HUMAN	-1.20	2.95E-03
RLA0_HUMAN	-1.20	4.28E-02
NCS1_HUMAN	-1.20	2.29E-03
MGST1_HUMAN	-1.20	1.62E-02
LYPA1_HUMAN	-1.20	4.15E-02
LTOR5_HUMAN	-1.21	4.94E-03
PKN2_HUMAN	-1.21	1.03E-03
SNX4_HUMAN	-1.21	8.15E-03
CDCP1_HUMAN	-1.21	1.32E-02
MXRA7_HUMAN	-1.21	1.07E-02
NBEL2_HUMAN	-1.21	3.54E-02
CC120_HUMAN	-1.21	8.73E-03
STRN4_HUMAN	-1.21	8.60E-04
EH1L1_HUMAN	-1.21	2.07E-03
MPRI_HUMAN	-1.21	5.24E-04
NHSL1_HUMAN	-1.21	1.65E-02
XDH_HUMAN	-1.21	3.12E-02
KC1A_HUMAN	-1.21	9.75E-03
OCRL_HUMAN	-1.21	1.46E-02
SHPS1_HUMAN	-1.21	1.97E-03
RDHE2_HUMAN	-1.21	1.35E-02
ECHB_HUMAN	-1.21	3.64E-02
NLRX1_HUMAN	-1.21	3.90E-02
SYDC_HUMAN	-1.21	1.98E-02
ABI1_HUMAN	-1.21	7.03E-04
FA65A_HUMAN	-1.21	5.46E-03
SHRM2_HUMAN	-1.21	7.19E-03
SSH1_HUMAN	-1.21	1.17E-02
LSM12_HUMAN	-1.21	2.09E-03
IDE_HUMAN	-1.21	3.05E-03
EI2BG_HUMAN	-1.21	1.66E-02
HEXB_HUMAN	-1.21	3.09E-02
EFNB1_HUMAN	-1.21	2.18E-02
STRN3_HUMAN	-1.21	1.44E-03
PDCD4_HUMAN	-1.21	1.33E-02
NPL4_HUMAN	-1.21	2.36E-03
AP1B1_HUMAN	-1.21	2.94E-03
CQ059_HUMAN	-1.21	3.24E-03

USO1_HUMAN	-1.21	3.34E-03
PKHA1_HUMAN	-1.21	1.52E-02
EIF3M_HUMAN	-1.21	2.20E-02
RTN4_HUMAN	-1.21	1.75E-03
CSCL2_HUMAN	-1.21	1.03E-03
CLAP2_HUMAN	-1.21	3.10E-03
PTSS2_HUMAN	-1.21	5.48E-03
D2HDH_HUMAN	-1.21	2.40E-02
STRN_HUMAN	-1.21	4.00E-04
EHBP1_HUMAN	-1.21	3.21E-03
GAK_HUMAN	-1.21	1.07E-02
MA7D3_HUMAN	-1.22	7.75E-03
OPA3_HUMAN	-1.22	1.84E-02
STRP1_HUMAN	-1.22	3.74E-03
TPC6B_HUMAN	-1.22	1.09E-02
LNP_HUMAN	-1.22	3.26E-03
ATP5J_HUMAN	-1.22	3.79E-03
PERQ2_HUMAN	-1.22	8.56E-03
SC24B_HUMAN	-1.22	1.09E-02
GCP2_HUMAN	-1.22	2.45E-02
SC23B_HUMAN	-1.22	4.74E-02
F1142_HUMAN	-1.22	1.69E-02
ETHE1_HUMAN	-1.22	4.18E-03
EZRI_HUMAN	-1.22	3.69E-02
CSKP_HUMAN	-1.22	1.10E-02
PEA15_HUMAN	-1.22	3.77E-02
CAV1_HUMAN	-1.22	1.22E-03
RENT1_HUMAN	-1.22	1.60E-03
DAAM1_HUMAN	-1.22	3.41E-03
IF2P_HUMAN	-1.22	9.32E-03
Z3H7A_HUMAN	-1.22	3.78E-02
STX12_HUMAN	-1.22	1.01E-02
MIC27_HUMAN	-1.22	9.61E-04
HECD1_HUMAN	-1.22	3.91E-02
ARF6_HUMAN	-1.22	2.13E-03
AP3D1_HUMAN	-1.22	3.64E-03
L1CAM_HUMAN	-1.22	5.43E-03
PTN14_HUMAN	-1.22	2.24E-02
BNIP2_HUMAN	-1.22	4.23E-02
TRPM4_HUMAN	-1.22	3.41E-03
DOCK5_HUMAN	-1.22	1.67E-02
MYO1E_HUMAN	-1.22	1.00E-02
TRI13_HUMAN	-1.22	2.19E-02

AT8B1_HUMAN	-1.22	4.28E-02
STRP2_HUMAN	-1.22	1.17E-02
CAN2_HUMAN	-1.22	2.58E-02
VPS53_HUMAN	-1.22	5.74E-03
DCMC_HUMAN	-1.22	6.69E-03
ARVC_HUMAN	-1.22	1.50E-02
BASP1_HUMAN	-1.22	2.54E-03
SYTL1_HUMAN	-1.22	1.99E-03
ZNT1_HUMAN	-1.22	2.00E-03
PREP_HUMAN	-1.22	3.15E-03
TMOD2_HUMAN	-1.22	5.84E-03
CACP_HUMAN	-1.22	1.99E-02
ACACA_HUMAN	-1.22	5.64E-03
DNJB6_HUMAN	-1.22	7.19E-04
CYTSA_HUMAN	-1.23	1.72E-02
REEP6_HUMAN	-1.23	4.36E-02
CRBG3_HUMAN	-1.23	3.66E-03
IMDH2_HUMAN	-1.23	6.99E-03
LRBA_HUMAN	-1.23	4.88E-02
PTRD1_HUMAN	-1.23	1.32E-02
DNJB9_HUMAN	-1.23	1.06E-02
ARP2_HUMAN	-1.23	1.56E-03
ITSN1_HUMAN	-1.23	6.97E-03
BACD3_HUMAN	-1.23	2.16E-02
PP2AB_HUMAN	-1.23	1.09E-03
TPD54_HUMAN	-1.23	6.69E-03
TPC10_HUMAN	-1.23	1.08E-02
SIKE1_HUMAN	-1.23	3.58E-03
ROCK1_HUMAN	-1.23	9.97E-03
LTOR3_HUMAN	-1.23	3.26E-03
CPT2_HUMAN	-1.23	1.29E-02
TLDC1_HUMAN	-1.23	6.73E-03
CATC_HUMAN	-1.23	2.59E-02
PARP4_HUMAN	-1.23	9.96E-03
CD44_HUMAN	-1.23	4.36E-04
SNX17_HUMAN	-1.23	5.48E-03
SCAP_HUMAN	-1.23	8.75E-03
SEPT7_HUMAN	-1.23	1.22E-02
GSK3B_HUMAN	-1.23	4.19E-02
EP15R_HUMAN	-1.23	1.69E-03
SNX12_HUMAN	-1.23	1.18E-02
ITPR2_HUMAN	-1.23	2.82E-03
SNX6_HUMAN	-1.23	9.61E-04

NUFP2_HUMAN	-1.24	3.33E-03
FA83G_HUMAN	-1.24	4.49E-03
TPPC3_HUMAN	-1.24	2.59E-03
RN170_HUMAN	-1.24	1.76E-02
DJC13_HUMAN	-1.24	3.15E-04
VTI1B_HUMAN	-1.24	1.44E-03
SFXN3_HUMAN	-1.24	2.67E-03
MGST3_HUMAN	-1.24	2.13E-02
SNX2_HUMAN	-1.24	2.25E-03
DLGP4_HUMAN	-1.24	8.38E-03
DNJB2_HUMAN	-1.24	1.32E-02
UFD1_HUMAN	-1.24	4.72E-04
RHOA_HUMAN	-1.24	1.24E-04
OXSM_HUMAN	-1.24	3.12E-02
MEMO1_HUMAN	-1.24	3.89E-02
DREB_HUMAN	-1.24	3.33E-03
S12A4_HUMAN	-1.24	5.17E-04
RRAGC_HUMAN	-1.24	3.05E-03
STX7_HUMAN	-1.24	1.87E-04
STXB2_HUMAN	-1.24	1.32E-03
SVIL_HUMAN	-1.24	1.07E-02
FA98A_HUMAN	-1.24	4.12E-03
TUFT1_HUMAN	-1.24	1.76E-02
NUD12_HUMAN	-1.24	8.73E-04
DLG1_HUMAN	-1.24	3.11E-03
SCYL2_HUMAN	-1.24	4.07E-03
CD81_HUMAN	-1.24	8.59E-03
TBCD5_HUMAN	-1.24	1.18E-02
1433B_HUMAN	-1.24	3.60E-02
RNBP6_HUMAN	-1.24	7.67E-03
REPS1_HUMAN	-1.24	1.31E-02
AL1A1_HUMAN	-1.24	2.30E-02
NBEL1_HUMAN	-1.24	2.20E-02
FAS_HUMAN	-1.24	1.90E-02
RAB3A_HUMAN	-1.24	2.39E-02
GOPC_HUMAN	-1.25	2.86E-03
ESYT1_HUMAN	-1.25	4.27E-04
CP062_HUMAN	-1.25	7.97E-03
SIR2_HUMAN	-1.25	2.68E-02
TSN14_HUMAN	-1.25	2.89E-04
RHG01_HUMAN	-1.25	1.61E-02
MPP7_HUMAN	-1.25	1.79E-02
GDE1_HUMAN	-1.25	5.78E-04

ERMP1_HUMAN	-1.25	1.72E-03
PTN3_HUMAN	-1.25	2.04E-03
CTDSL_HUMAN	-1.25	6.64E-03
XRP2_HUMAN	-1.25	2.62E-03
MGLL_HUMAN	-1.25	3.52E-03
SEPT2_HUMAN	-1.25	3.18E-03
IL1RA_HUMAN	-1.25	3.19E-02
ARMX1_HUMAN	-1.25	1.80E-03
DKK3_HUMAN	-1.25	1.37E-02
STRAP_HUMAN	-1.25	1.48E-02
SC16A_HUMAN	-1.25	1.47E-03
NIBL1_HUMAN	-1.25	9.95E-03
SYUA_HUMAN	-1.25	1.37E-02
S35F6_HUMAN	-1.25	1.17E-02
EXOC3_HUMAN	-1.25	4.82E-04
MRCKB_HUMAN	-1.25	2.65E-03
JAG1_HUMAN	-1.25	2.70E-03
CCD22_HUMAN	-1.25	3.88E-02
STAU2_HUMAN	-1.25	5.25E-03
OSBP1_HUMAN	-1.25	3.33E-03
COR1C_HUMAN	-1.25	3.98E-03
STIM1_HUMAN	-1.25	6.75E-03
SPD2A_HUMAN	-1.26	4.21E-04
MBP_HUMAN	-1.26	1.65E-03
ARF4_HUMAN	-1.26	3.87E-04
TPPC4_HUMAN	-1.26	6.45E-03
ITSN2_HUMAN	-1.26	6.44E-04
POTEJ_HUMAN	-1.26	6.26E-03
JAGN1_HUMAN	-1.26	1.44E-02
GP108_HUMAN	-1.26	2.38E-02
UBXN6_HUMAN	-1.26	1.56E-03
NOTC2_HUMAN	-1.26	1.56E-03
RL22_HUMAN	-1.26	8.59E-03
BAIP2_HUMAN	-1.26	1.67E-04
RLA2_HUMAN	-1.26	5.25E-03
INADL_HUMAN	-1.26	5.84E-04
STRUM_HUMAN	-1.26	2.61E-03
FGD4_HUMAN	-1.26	4.67E-03
BI2L1_HUMAN	-1.26	1.39E-03
RABX5_HUMAN	-1.26	7.26E-03
SND1_HUMAN	-1.26	1.20E-02
WASH7_HUMAN	-1.26	3.23E-02
SLMAP_HUMAN	-1.26	2.78E-04

EPS15_HUMAN	-1.26	9.09E-04
CD2AP_HUMAN	-1.26	5.74E-03
ACOX3_HUMAN	-1.26	5.56E-03
LMBR1_HUMAN	-1.26	1.65E-02
RGS12_HUMAN	-1.26	2.27E-03
AT2B4_HUMAN	-1.26	6.13E-03
OFUT2_HUMAN	-1.26	6.49E-04
LRCH3_HUMAN	-1.26	1.07E-02
SPX2_HUMAN	-1.26	2.28E-02
TERA_HUMAN	-1.26	9.24E-04
NEXN_HUMAN	-1.26	1.38E-02
DC1L2_HUMAN	-1.26	8.59E-03
BCR_HUMAN	-1.27	6.69E-03
SC23A_HUMAN	-1.27	3.29E-02
FA83B_HUMAN	-1.27	1.14E-03
DHDDS_HUMAN	-1.27	1.39E-03
RB_HUMAN	-1.27	1.03E-02
ATG7_HUMAN	-1.27	4.47E-03
FACR1_HUMAN	-1.27	6.45E-04
TXND9_HUMAN	-1.27	9.29E-03
KPCD_HUMAN	-1.27	2.02E-03
S27A1_HUMAN	-1.27	4.30E-04
ACSL1_HUMAN	-1.27	1.12E-02
MYADM_HUMAN	-1.27	2.00E-03
MARK3_HUMAN	-1.27	6.70E-03
SUMF1_HUMAN	-1.27	1.44E-02
PACN2_HUMAN	-1.27	1.67E-03
BOK_HUMAN	-1.27	3.11E-02
MCATL_HUMAN	-1.27	3.65E-03
ACAD8_HUMAN	-1.27	2.80E-03
MGRN1_HUMAN	-1.27	3.33E-03
LICH_HUMAN	-1.27	6.59E-03
HMOX1_HUMAN	-1.27	1.12E-02
TPM2_HUMAN	-1.27	1.29E-02
FBN2_HUMAN	-1.27	4.52E-02
LAMA3_HUMAN	-1.27	4.55E-02
IF4A2_HUMAN	-1.27	4.60E-02
RABL6_HUMAN	-1.27	2.15E-03
TPC11_HUMAN	-1.27	9.10E-04
ZO2_HUMAN	-1.27	2.92E-03
ARC1B_HUMAN	-1.27	4.52E-04
GAPR1_HUMAN	-1.27	2.26E-02
EHD2_HUMAN	-1.27	3.13E-04

SYEP_HUMAN	-1.27	1.07E-02
F110C_HUMAN	-1.28	8.71E-03
TIM8A_HUMAN	-1.28	9.23E-03
CLN3_HUMAN	-1.28	1.65E-02
FCHO2_HUMAN	-1.28	5.97E-03
SUCO_HUMAN	-1.28	8.07E-03
ANR46_HUMAN	-1.28	1.14E-02
TBA1C_HUMAN	-1.28	1.81E-02
AGFG1_HUMAN	-1.28	3.15E-03
STXB5_HUMAN	-1.28	7.70E-03
TIM13_HUMAN	-1.28	3.58E-04
PAI2_HUMAN	-1.28	2.23E-02
UGPA_HUMAN	-1.28	1.24E-02
RABE1_HUMAN	-1.28	2.54E-03
TNR6B_HUMAN	-1.28	5.06E-04
K1C14_HUMAN	-1.28	1.91E-02
ABC3C_HUMAN	-1.28	1.75E-02
LYAG_HUMAN	-1.28	2.82E-02
UBP2L_HUMAN	-1.28	7.96E-03
EIF3L_HUMAN	-1.28	1.88E-02
NACAM_HUMAN	-1.28	4.88E-02
RB6I2_HUMAN	-1.28	4.00E-04
PX11B_HUMAN	-1.28	8.64E-04
SEPT6_HUMAN	-1.28	4.64E-03
CD82_HUMAN	-1.28	5.55E-03
RAB10_HUMAN	-1.28	9.58E-03
RS21_HUMAN	-1.28	3.10E-02
CRIM1_HUMAN	-1.28	4.38E-02
PHOCN_HUMAN	-1.28	1.93E-04
AIMP1_HUMAN	-1.28	6.51E-03
TSN1_HUMAN	-1.28	2.18E-03
RGS20_HUMAN	-1.28	4.62E-02
SBDS_HUMAN	-1.28	1.03E-02
MERL_HUMAN	-1.28	7.40E-04
MFSD6_HUMAN	-1.28	3.42E-02
FUCO_HUMAN	-1.28	3.64E-02
2A5E_HUMAN	-1.28	9.23E-04
MTMR1_HUMAN	-1.29	2.01E-04
SEPT8_HUMAN	-1.29	1.91E-03
AP3M1_HUMAN	-1.29	4.33E-03
DCTN4_HUMAN	-1.29	2.48E-04
NCKP1_HUMAN	-1.29	5.97E-04
MTM1_HUMAN	-1.29	1.99E-03

RL38_HUMAN	-1.29	7.00E-03
TIP_HUMAN	-1.29	9.52E-03
MARCS_HUMAN	-1.29	6.31E-04
THSD4_HUMAN	-1.29	1.06E-02
ARPC5_HUMAN	-1.29	9.00E-04
DDR1_HUMAN	-1.29	4.01E-04
TIM8B_HUMAN	-1.29	2.25E-04
LRRF1_HUMAN	-1.29	1.11E-03
PPR21_HUMAN	-1.29	3.10E-03
PITM1_HUMAN	-1.29	5.37E-03
VATF_HUMAN	-1.29	2.78E-04
AIMP2_HUMAN	-1.29	8.72E-03
VAMP3_HUMAN	-1.29	2.81E-03
MPP5_HUMAN	-1.29	4.52E-04
FAHD1_HUMAN	-1.29	5.55E-03
TMPPE_HUMAN	-1.29	1.87E-04
BSDC1_HUMAN	-1.29	7.07E-04
AP3S1_HUMAN	-1.29	2.67E-03
GIT2_HUMAN	-1.29	1.66E-03
DRG1_HUMAN	-1.29	6.89E-03
FBX2_HUMAN	-1.29	1.06E-02
PKHM2_HUMAN	-1.29	1.20E-02
HD_HUMAN	-1.29	2.67E-03
JIP4_HUMAN	-1.29	5.27E-03
NSF_HUMAN	-1.29	7.52E-05
CATA_HUMAN	-1.29	7.28E-04
ZNF48_HUMAN	-1.29	1.94E-02
TMOD3_HUMAN	-1.29	5.45E-04
ERG1_HUMAN	-1.29	3.94E-04
IF4G3_HUMAN	-1.29	1.25E-03
OXSR1_HUMAN	-1.29	7.81E-04
S11IP_HUMAN	-1.29	3.30E-04
TOM1_HUMAN	-1.29	6.86E-04
CHMP3_HUMAN	-1.29	2.56E-03
T120B_HUMAN	-1.30	2.08E-03
THEM4_HUMAN	-1.30	1.59E-02
GCN1L_HUMAN	-1.30	9.34E-03
KITM_HUMAN	-1.30	2.67E-03
RB22A_HUMAN	-1.30	2.06E-03
DEST_HUMAN	-1.30	5.60E-03
P4K2A_HUMAN	-1.30	3.63E-04
SPTN2_HUMAN	-1.30	2.87E-02
EXOC4_HUMAN	-1.30	1.25E-03

PHLA2_HUMAN	-1.30	1.18E-02
CHM2B_HUMAN	-1.30	1.75E-02
CATL2_HUMAN	-1.30	3.55E-02
VPS16_HUMAN	-1.30	2.18E-04
SRC8_HUMAN	-1.30	2.20E-04
SYNC_HUMAN	-1.30	3.92E-02
LASP1_HUMAN	-1.30	3.16E-02
WASF2_HUMAN	-1.31	1.56E-04
FARP2_HUMAN	-1.31	2.13E-02
SYFB_HUMAN	-1.31	3.52E-03
TENS4_HUMAN	-1.31	5.84E-04
PDLI7_HUMAN	-1.31	4.48E-02
TPPC5_HUMAN	-1.31	2.83E-04
TM127_HUMAN	-1.31	9.87E-05
H1BP3_HUMAN	-1.31	1.26E-03
SYVC_HUMAN	-1.31	1.61E-03
IF4E_HUMAN	-1.31	3.05E-03
GPX1_HUMAN	-1.31	1.46E-04
HIP1R_HUMAN	-1.31	2.78E-04
SNX33_HUMAN	-1.31	4.05E-04
MAST4_HUMAN	-1.31	1.47E-03
LUZP1_HUMAN	-1.31	1.78E-03
NLTP_HUMAN	-1.31	1.90E-03
IF4E2_HUMAN	-1.31	7.85E-03
UBE4B_HUMAN	-1.31	1.28E-02
FA21C_HUMAN	-1.31	2.14E-02
SH3L1_HUMAN	-1.31	2.64E-02
ASCC3_HUMAN	-1.31	6.71E-04
FGFR3_HUMAN	-1.31	6.51E-03
S27A4_HUMAN	-1.31	6.05E-04
PP4R1_HUMAN	-1.31	7.38E-03
K2C5_HUMAN	-1.31	1.14E-02
CDV3_HUMAN	-1.31	9.15E-03
ATRN_HUMAN	-1.31	1.39E-04
K1161_HUMAN	-1.31	3.23E-03
ARMX2_HUMAN	-1.31	3.66E-04
SORL_HUMAN	-1.31	1.60E-04
AT131_HUMAN	-1.32	1.86E-04
VCIP1_HUMAN	-1.32	1.52E-03
EF1A1_HUMAN (+1)	-1.32	4.02E-03
L12R1_HUMAN	-1.32	5.19E-03
CXA1_HUMAN	-1.32	1.10E-02
VPS39_HUMAN	-1.32	1.42E-03

LAMB3_HUMAN	-1.32	2.39E-02
CADH1_HUMAN	-1.32	3.62E-04
TPPC8_HUMAN	-1.32	6.05E-04
VP26B_HUMAN	-1.32	6.46E-04
MAP7_HUMAN	-1.32	1.29E-03
F213A_HUMAN	-1.32	2.52E-02
WDR1_HUMAN	-1.32	4.22E-03
PLPL6_HUMAN	-1.32	2.18E-04
PLS3_HUMAN	-1.32	8.67E-04
SC31A_HUMAN	-1.32	8.06E-03
ARP3_HUMAN	-1.32	3.15E-04
OSB10_HUMAN	-1.32	7.82E-03
SPRE_HUMAN	-1.32	7.12E-03
SULF2_HUMAN	-1.32	1.54E-02
CT2NL_HUMAN	-1.32	1.79E-02
LIMK2_HUMAN	-1.32	5.44E-03
TFG_HUMAN	-1.32	8.58E-03
CERS3_HUMAN	-1.32	2.19E-02
HOOK2_HUMAN	-1.32	1.17E-03
TAGL2_HUMAN	-1.33	1.53E-02
VP13C_HUMAN	-1.33	7.52E-03
CF132_HUMAN	-1.33	3.61E-04
SNX5_HUMAN	-1.33	2.27E-03
KANK1_HUMAN	-1.33	5.40E-04
SC11C_HUMAN	-1.33	4.74E-02
NUCB1_HUMAN	-1.33	2.73E-04
CNTN1_HUMAN	-1.33	2.29E-02
ARL15_HUMAN	-1.33	1.97E-03
PDK2_HUMAN	-1.33	3.29E-02
SEP11_HUMAN	-1.33	2.10E-03
VP33A_HUMAN	-1.33	2.01E-04
CAN1_HUMAN	-1.33	1.28E-02
TFR1_HUMAN	-1.33	1.39E-03
TTC37_HUMAN	-1.33	2.04E-02
FLII_HUMAN	-1.33	2.18E-04
CIP4_HUMAN	-1.33	2.14E-03
PHLA1_HUMAN	-1.33	5.35E-03
GOGA4_HUMAN	-1.33	1.73E-04
SYIC_HUMAN	-1.33	1.93E-03
PPR18_HUMAN	-1.33	7.52E-04
PROD_HUMAN	-1.33	9.94E-05
TTYH3_HUMAN	-1.33	2.75E-04
AP1M2_HUMAN	-1.33	3.13E-04

SPB6_HUMAN	-1.33	3.61E-02
PRKRA_HUMAN	-1.33	1.92E-03
EF1D_HUMAN	-1.33	4.37E-03
ARPC2_HUMAN	-1.33	1.58E-04
MACF1_HUMAN	-1.33	3.91E-04
COF1_HUMAN	-1.34	1.22E-02
C170B_HUMAN	-1.34	2.21E-04
LTOR2_HUMAN	-1.34	4.00E-04
SETD3_HUMAN	-1.34	2.21E-02
GSTP1_HUMAN	-1.34	4.97E-02
IASPP_HUMAN	-1.34	3.32E-04
RHG12_HUMAN	-1.34	3.68E-02
ERBB2_HUMAN	-1.34	2.13E-03
EXC6B_HUMAN	-1.34	3.14E-03
WNT5A_HUMAN	-1.34	1.57E-02
WDFY2_HUMAN	-1.34	1.16E-04
ARC1A_HUMAN	-1.34	3.30E-04
DSC3_HUMAN	-1.34	1.61E-04
STXB1_HUMAN	-1.34	1.53E-03
SYLC_HUMAN	-1.34	1.45E-03
GDAP2_HUMAN	-1.34	2.21E-04
NEMF_HUMAN	-1.34	1.42E-03
DAG1_HUMAN	-1.34	8.49E-05
TX1B3_HUMAN	-1.34	3.74E-04
MPCP_HUMAN	-1.34	5.24E-04
1433T_HUMAN	-1.34	4.66E-03
ASC_HUMAN	-1.34	3.57E-02
PTPRG_HUMAN	-1.34	1.59E-04
ACPH_HUMAN	-1.34	1.23E-03
RMD2_HUMAN	-1.34	7.38E-04
AL4A1_HUMAN	-1.34	9.24E-04
T184C_HUMAN	-1.35	4.00E-04
DYHC1_HUMAN	-1.35	6.31E-04
KC1G1_HUMAN	-1.35	6.89E-03
MAGD1_HUMAN	-1.35	2.53E-02
CPEB2_HUMAN	-1.35	5.39E-04
DAPK3_HUMAN	-1.35	1.93E-03
HAP28_HUMAN	-1.35	4.95E-02
S10AE_HUMAN	-1.35	1.85E-03
C43BP_HUMAN	-1.35	1.40E-03
GAS6_HUMAN	-1.35	1.66E-02
TDRP_HUMAN	-1.35	2.54E-02
ATX2_HUMAN	-1.35	5.17E-04

EXOC8_HUMAN	-1.35	8.99E-04
CDK6_HUMAN	-1.35	2.61E-02
TTC7B_HUMAN	-1.36	1.75E-04
LAMP1_HUMAN	-1.36	7.96E-04
ATPK_HUMAN	-1.36	6.33E-03
HGNAT_HUMAN	-1.36	5.66E-04
RAB5A_HUMAN	-1.36	4.37E-05
BZW1_HUMAN	-1.36	2.19E-03
HXK1_HUMAN	-1.36	4.11E-04
EEA1_HUMAN	-1.36	1.84E-04
BRK1_HUMAN	-1.36	4.54E-04
NECP2_HUMAN	-1.36	4.04E-03
PP14B_HUMAN	-1.36	2.65E-02
AAK1_HUMAN	-1.36	2.27E-03
EXOC2_HUMAN	-1.36	5.28E-04
PDC6I_HUMAN	-1.36	9.00E-04
CASZ1_HUMAN	-1.36	4.17E-02
RFIP1_HUMAN	-1.36	6.69E-03
NT5D3_HUMAN	-1.37	7.10E-05
PCY1A_HUMAN	-1.37	1.03E-03
FA21B_HUMAN	-1.37	4.33E-02
SPG21_HUMAN	-1.37	2.11E-04
CD151_HUMAN	-1.37	3.80E-05
EI2BB_HUMAN	-1.37	2.17E-03
IF4G1_HUMAN	-1.37	1.60E-03
VATH_HUMAN	-1.37	1.44E-04
TBB3_HUMAN	-1.37	2.43E-03
LPP_HUMAN	-1.37	3.62E-04
KLC1_HUMAN	-1.37	1.23E-03
GLCM_HUMAN	-1.37	1.92E-03
WIBG_HUMAN	-1.37	4.78E-03
SYFA_HUMAN	-1.37	1.68E-03
VATD_HUMAN	-1.37	4.62E-04
TRIP4_HUMAN	-1.37	4.00E-04
RAB9A_HUMAN	-1.37	6.33E-03
ARP10_HUMAN	-1.37	8.50E-04
ZFYV9_HUMAN	-1.37	1.58E-04
GTR1_HUMAN	-1.38	2.35E-04
NSDHL_HUMAN	-1.38	1.63E-04
TINAL_HUMAN	-1.38	4.22E-03
TGFR2_HUMAN	-1.38	4.91E-05
SAP_HUMAN	-1.38	5.84E-03
VP26A_HUMAN	-1.38	1.25E-03

RS10_HUMAN	-1.38	2.43E-02
MY18A_HUMAN	-1.38	4.36E-04
ACOX1_HUMAN	-1.38	1.24E-03
SC24C_HUMAN	-1.38	1.82E-02
1433Z_HUMAN	-1.38	2.62E-03
TM192_HUMAN	-1.38	1.91E-04
AP3B1_HUMAN	-1.38	1.10E-04
DCTN5_HUMAN	-1.38	8.60E-04
PYGL_HUMAN	-1.38	1.04E-02
MROH1_HUMAN	-1.38	3.65E-04
IQGA1_HUMAN	-1.38	5.78E-04
SYRC_HUMAN	-1.38	1.01E-03
CU025_HUMAN	-1.38	9.57E-03
MTMR5_HUMAN	-1.38	1.42E-04
XPP3_HUMAN	-1.38	2.34E-04
CSTN1_HUMAN	-1.38	3.98E-03
UBE3A_HUMAN	-1.38	2.67E-04
T120A_HUMAN	-1.39	1.05E-03
ATS19_HUMAN	-1.39	3.58E-02
CLIC4_HUMAN	-1.39	3.44E-03
SNX3_HUMAN	-1.39	1.09E-03
KLC2_HUMAN	-1.39	1.93E-03
PEPL_HUMAN	-1.39	4.46E-02
VATC1_HUMAN	-1.39	3.91E-04
SEPT9_HUMAN	-1.39	4.04E-04
ATS1_HUMAN	-1.39	1.72E-04
ES8L2_HUMAN	-1.39	7.78E-04
ABCF3_HUMAN	-1.39	2.48E-03
VATA_HUMAN	-1.39	8.83E-05
PLXB1_HUMAN	-1.39	8.88E-04
LPP1_HUMAN	-1.39	6.73E-04
STX3_HUMAN	-1.39	2.45E-02
ALDH2_HUMAN	-1.39	1.18E-05
S26A6_HUMAN	-1.39	1.07E-03
ACTBL_HUMAN	-1.39	7.30E-03
ANXA2_HUMAN	-1.40	8.33E-04
ASPC1_HUMAN	-1.40	1.57E-03
AGAP3_HUMAN	-1.40	1.21E-03
SNX1_HUMAN	-1.40	3.65E-04
PI42C_HUMAN	-1.40	1.22E-05
SCO2_HUMAN	-1.40	4.30E-04
FLRT2_HUMAN	-1.40	6.40E-03
GLSK_HUMAN	-1.40	9.94E-05

DIRC2_HUMAN	-1.40	3.41E-03
MAVS_HUMAN	-1.40	4.78E-05
ARPC4_HUMAN	-1.40	8.05E-04
UBAP2_HUMAN	-1.40	1.03E-03
VINC_HUMAN	-1.40	1.41E-03
VA0D1_HUMAN	-1.40	7.24E-04
HOOK1_HUMAN	-1.40	1.66E-03
RB11A_HUMAN	-1.41	2.17E-03
PROM2_HUMAN	-1.41	6.97E-03
DDX3X_HUMAN	-1.41	1.54E-02
TSP2_HUMAN	-1.41	9.62E-03
LRRF2_HUMAN	-1.41	5.93E-03
ARP5L_HUMAN	-1.41	1.07E-03
ENDD1_HUMAN	-1.41	1.52E-03
PPGB_HUMAN	-1.41	9.00E-04
CCD93_HUMAN	-1.41	9.19E-03
ARP19_HUMAN	-1.41	6.28E-03
VAMP8_HUMAN	-1.41	2.70E-05
STON2_HUMAN	-1.41	4.27E-04
SYCM_HUMAN	-1.42	2.74E-04
ANXA8_HUMAN	-1.42	1.98E-02
CC124_HUMAN	-1.42	3.58E-04
EXOG_HUMAN	-1.42	6.42E-05
PLST_HUMAN	-1.42	2.56E-03
DMD_HUMAN	-1.42	1.20E-02
VATE1_HUMAN	-1.42	6.82E-05
CXAR_HUMAN	-1.42	2.59E-04
BICD2_HUMAN	-1.42	3.76E-04
KRT34_HUMAN	-1.42	3.78E-04
CASPE_HUMAN	-1.42	9.90E-04
HERP1_HUMAN	-1.42	1.68E-02
PCYOX_HUMAN	-1.42	1.44E-03
BGAL_HUMAN	-1.42	8.34E-05
VPS18_HUMAN	-1.42	1.73E-03
ETFD_HUMAN	-1.42	5.75E-03
USP9X_HUMAN	-1.42	4.03E-04
CC132_HUMAN	-1.42	2.93E-02
EXOC5_HUMAN	-1.42	1.89E-04
GNS_HUMAN	-1.42	1.37E-03
ARSA_HUMAN	-1.43	1.30E-02
FLRT3_HUMAN	-1.43	2.55E-05
DC1L1_HUMAN	-1.43	2.69E-04
RHG29_HUMAN	-1.43	9.09E-04

PTTG_HUMAN	-1.43	3.42E-03
CCD53_HUMAN	-1.43	7.85E-03
EXOC1_HUMAN	-1.43	8.78E-05
GYS1_HUMAN	-1.43	1.50E-03
MET7A_HUMAN	-1.43	1.17E-02
ABLM1_HUMAN	-1.43	4.03E-03
GABT_HUMAN	-1.43	3.94E-03
ARHGC_HUMAN	-1.43	3.41E-03
PAG15_HUMAN	-1.43	6.73E-04
GSDMA_HUMAN	-1.43	9.38E-03
SEPT5_HUMAN	-1.44	1.47E-04
FIS1_HUMAN	-1.44	1.38E-03
PRS23_HUMAN	-1.44	1.68E-03
RAB3D_HUMAN	-1.44	3.45E-03
ANXA4_HUMAN	-1.44	1.71E-02
RAB7B_HUMAN	-1.44	3.61E-03
EDF1_HUMAN	-1.44	1.73E-02
VASP_HUMAN	-1.44	4.18E-04
TOLIP_HUMAN	-1.44	1.20E-04
ACADV_HUMAN	-1.44	1.46E-03
SYQ_HUMAN	-1.44	2.02E-04
RBNS5_HUMAN	-1.44	4.86E-02
DYL1_HUMAN	-1.45	2.02E-03
AXA82_HUMAN	-1.45	2.11E-02
ZYX_HUMAN	-1.45	1.23E-03
LX15B_HUMAN	-1.45	3.69E-02
MYO6_HUMAN	-1.45	5.81E-05
TACD2_HUMAN	-1.45	3.27E-02
S10A2_HUMAN	-1.45	3.73E-02
VPS8_HUMAN	-1.45	2.74E-04
LAD1_HUMAN	-1.45	1.00E-03
AHNK_HUMAN	-1.45	7.27E-06
OCTC_HUMAN	-1.45	2.15E-03
VATB2_HUMAN	-1.45	1.54E-04
DCTN1_HUMAN	-1.45	1.16E-04
KAP2_HUMAN	-1.46	3.42E-05
HOME3_HUMAN	-1.46	1.86E-04
EPN3_HUMAN	-1.46	4.27E-03
S10A4_HUMAN	-1.46	4.10E-02
DYSF_HUMAN	-1.46	1.46E-04
RAB5B_HUMAN	-1.46	5.07E-04
DCTN3_HUMAN	-1.46	7.61E-04
DOCK9_HUMAN	-1.46	9.24E-04

TPPC9_HUMAN	-1.46	7.74E-03
NSG1_HUMAN	-1.46	5.92E-04
K1C17_HUMAN	-1.46	2.31E-02
KI13A_HUMAN	-1.46	1.56E-04
TPRGL_HUMAN	-1.46	1.58E-03
PYGB_HUMAN	-1.46	3.27E-03
HOOK3_HUMAN	-1.46	1.18E-05
KIF1C_HUMAN	-1.47	1.93E-04
FIL1L_HUMAN	-1.47	4.65E-03
RLA1_HUMAN	-1.47	1.20E-02
K2C3_HUMAN	-1.47	1.46E-02
PGBM_HUMAN	-1.47	1.17E-03
LDLR_HUMAN	-1.47	2.13E-03
SFRP1_HUMAN	-1.47	1.34E-03
MILK2_HUMAN	-1.47	6.45E-04
FILA2_HUMAN	-1.47	1.83E-02
MA2B2_HUMAN	-1.47	7.70E-04
VPS29_HUMAN	-1.47	9.09E-04
GDN_HUMAN	-1.48	9.75E-05
PLD1_HUMAN	-1.48	2.28E-04
DCTN2_HUMAN	-1.48	2.69E-04
TRIA1_HUMAN	-1.48	4.08E-05
ALS2_HUMAN	-1.48	9.90E-03
PPA5_HUMAN	-1.48	1.27E-02
GSDMC_HUMAN	-1.48	1.51E-02
TRI29_HUMAN	-1.49	6.31E-04
LR16A_HUMAN	-1.49	2.48E-03
TENA_HUMAN	-1.49	7.15E-03
DPP4_HUMAN	-1.49	1.23E-02
MOT8_HUMAN	-1.49	5.44E-03
MREG_HUMAN	-1.49	6.54E-05
AHNK2_HUMAN	-1.49	5.24E-06
CYR61_HUMAN	-1.49	6.84E-04
AL2CL_HUMAN	-1.50	1.26E-03
OSBL9_HUMAN	-1.50	3.84E-03
CLN8_HUMAN	-1.50	1.16E-04
DP13A_HUMAN	-1.50	4.00E-04
EOGT_HUMAN	-1.50	5.77E-06
FAT1_HUMAN	-1.50	8.86E-05
BAG3_HUMAN	-1.50	6.24E-05
EF1G_HUMAN	-1.50	2.26E-03
ALG13_HUMAN	-1.50	2.47E-02
GELS_HUMAN	-1.50	3.13E-02

KINH_HUMAN	-1.50	4.00E-04
MYO5A_HUMAN	-1.50	2.16E-04
DC1I2_HUMAN	-1.50	3.08E-04
CAP1_HUMAN	-1.51	4.00E-03
FRIH_HUMAN	-1.51	1.16E-04
SSFA2_HUMAN	-1.51	7.27E-06
ACTZ_HUMAN	-1.51	2.64E-04
PLAK_HUMAN	-1.52	5.32E-03
VPS41_HUMAN	-1.52	7.52E-04
DHRS1_HUMAN	-1.52	5.55E-03
ARPC3_HUMAN	-1.52	1.01E-04
FLNB_HUMAN	-1.53	6.71E-04
LACTB_HUMAN	-1.53	1.28E-03
COR1A_HUMAN	-1.53	6.67E-03
K2C4_HUMAN	-1.53	3.83E-02
MA2B1_HUMAN	-1.53	1.87E-03
MANBA_HUMAN	-1.53	1.75E-04
EXOC7_HUMAN	-1.54	1.93E-04
S20A1_HUMAN	-1.54	9.54E-04
RETST_HUMAN	-1.54	2.71E-06
FBLI1_HUMAN	-1.54	5.78E-04
SNX30_HUMAN	-1.55	2.17E-03
LAMP2_HUMAN	-1.55	6.50E-03
VATG1_HUMAN	-1.55	1.44E-04
SARG_HUMAN	-1.55	1.58E-04
ASM3A_HUMAN	-1.55	8.20E-04
TM39B_HUMAN	-1.55	7.01E-04
CAH12_HUMAN	-1.55	6.31E-03
VPS35_HUMAN	-1.55	1.71E-03
QORX_HUMAN	-1.56	9.09E-04
N2DL2_HUMAN	-1.56	5.83E-03
MARE3_HUMAN	-1.56	4.01E-03
KLC3_HUMAN	-1.56	1.39E-04
THIK_HUMAN	-1.56	4.22E-04
KCC2G_HUMAN	-1.56	6.19E-03
COR1B_HUMAN	-1.56	7.10E-03
SIAE_HUMAN	-1.56	5.93E-04
TM159_HUMAN	-1.56	3.43E-02
ACOD_HUMAN	-1.57	6.89E-03
LEGL_HUMAN	-1.57	9.27E-03
DNJC5_HUMAN	-1.57	3.08E-04
DCBD2_HUMAN	-1.57	3.35E-04
ANK3_HUMAN	-1.58	1.32E-04

AKP13_HUMAN	-1.58	2.10E-04
TB182_HUMAN	-1.58	3.36E-04
GTR6_HUMAN	-1.58	7.62E-05
CSDE1_HUMAN	-1.58	5.66E-04
S10AA_HUMAN	-1.58	1.01E-03
EST2_HUMAN	-1.58	1.24E-02
GSTM2_HUMAN	-1.58	1.42E-02
M17L2_HUMAN	-1.59	9.56E-04
UB2E3_HUMAN	-1.59	4.00E-04
SDK2_HUMAN	-1.59	8.89E-04
TPM1_HUMAN	-1.59	3.38E-03
EF1B_HUMAN	-1.59	2.72E-03
HMDH_HUMAN	-1.59	8.05E-05
MAP1B_HUMAN	-1.60	2.97E-04
PDDC1_HUMAN	-1.60	7.03E-04
CLIP1_HUMAN	-1.60	5.21E-04
PLCD1_HUMAN	-1.60	2.20E-04
PRAF3_HUMAN	-1.60	9.94E-05
HTRA1_HUMAN	-1.61	6.30E-03
RNT2_HUMAN	-1.62	1.67E-03
NDEL1_HUMAN	-1.62	1.71E-03
HYAS3_HUMAN	-1.63	8.00E-04
PAFA2_HUMAN	-1.63	6.03E-04
SPHM_HUMAN	-1.63	2.69E-04
NB5R1_HUMAN	-1.63	6.38E-04
PDLI5_HUMAN	-1.63	2.04E-03
ENAH_HUMAN	-1.64	6.75E-04
CC167_HUMAN	-1.64	2.33E-03
CDD_HUMAN	-1.64	7.13E-04
SH3L3_HUMAN	-1.64	5.27E-03
CATB_HUMAN	-1.64	2.73E-02
SPB13_HUMAN	-1.64	2.79E-03
1433G_HUMAN	-1.64	4.90E-04
K2C80_HUMAN	-1.65	2.40E-03
TPM3_HUMAN	-1.65	7.99E-04
S38A7_HUMAN	-1.65	3.99E-05
SCD5_HUMAN	-1.65	1.65E-03
WNK1_HUMAN	-1.66	5.56E-04
NPC2_HUMAN	-1.66	1.87E-06
PPIP2_HUMAN	-1.66	3.83E-04
MFGM_HUMAN	-1.66	2.14E-05
ITAV_HUMAN	-1.66	3.36E-04
LFG3_HUMAN	-1.66	1.93E-04

AL1A3_HUMAN	-1.67	3.66E-03
FHL2_HUMAN	-1.67	2.18E-04
MTAP2_HUMAN	-1.67	3.82E-03
ITB6_HUMAN	-1.68	3.78E-04
GAN_HUMAN	-1.68	4.39E-04
FLNA_HUMAN	-1.68	4.02E-04
PDLI4_HUMAN	-1.68	3.03E-03
RS27L_HUMAN	-1.69	6.34E-05
AMD_HUMAN	-1.69	9.46E-04
LY6D_HUMAN	-1.70	4.67E-02
UPK3L_HUMAN	-1.70	4.28E-02
S10A7_HUMAN (+1)	-1.71	4.43E-03
ROBO1_HUMAN	-1.71	1.29E-04
TM1L2_HUMAN	-1.72	2.68E-05
CCND2_HUMAN	-1.72	8.91E-03
IGSF3_HUMAN	-1.72	2.69E-04
ACTN1_HUMAN	-1.73	2.49E-03
AK1C1_HUMAN	-1.73	1.91E-03
PAWR_HUMAN	-1.73	2.42E-03
VPP1_HUMAN	-1.74	8.83E-05
TBA4A_HUMAN	-1.74	4.22E-03
CO052_HUMAN	-1.74	5.47E-06
CAMP3_HUMAN	-1.74	4.47E-04
MVP_HUMAN	-1.75	2.10E-04
A4_HUMAN	-1.76	1.14E-04
DSG3_HUMAN	-1.76	3.18E-03
KCNK6_HUMAN	-1.77	1.67E-03
TPM4_HUMAN	-1.77	5.24E-04
EAA1_HUMAN	-1.78	1.60E-04
SDC1_HUMAN	-1.78	1.13E-06
CNN2_HUMAN	-1.79	1.51E-04
PLBL2_HUMAN	-1.79	3.62E-04
SNX18_HUMAN	-1.79	1.43E-05
RNAS7_HUMAN	-1.80	1.75E-03
ANO10_HUMAN	-1.80	5.24E-06
SEM3C_HUMAN	-1.80	6.03E-06
AMACR_HUMAN	-1.80	3.93E-04
CALD1_HUMAN	-1.82	2.00E-03
MCAT_HUMAN	-1.82	9.94E-05
K2C6A_HUMAN	-1.82	1.21E-02
CRYAB_HUMAN	-1.82	2.79E-04
NUA4L_HUMAN	-1.83	5.38E-03
APOE_HUMAN	-1.83	1.33E-02

ARL8B_HUMAN	-1.83	3.13E-04
K2C78_HUMAN	-1.83	2.02E-03
CLN5_HUMAN	-1.84	7.56E-05
MFAP5_HUMAN	-1.85	3.10E-03
CAD13_HUMAN	-1.85	1.29E-06
CO8A_HUMAN	-1.85	9.96E-03
ACTN4_HUMAN	-1.86	2.18E-03
FABP5_HUMAN	-1.86	1.76E-02
ML12A_HUMAN	-1.87	8.05E-04
SPB5_HUMAN	-1.87	3.77E-03
PDLI1_HUMAN	-1.88	7.47E-04
ICAL_HUMAN	-1.89	6.36E-04
K0930_HUMAN	-1.89	3.66E-04
RBM3_HUMAN	-1.89	1.47E-04
CALL5_HUMAN	-1.89	5.54E-03
CYTB_HUMAN	-1.89	2.82E-02
P3IP1_HUMAN	-1.89	7.04E-03
MYH9_HUMAN	-1.90	7.03E-04
ABCAC_HUMAN	-1.91	8.08E-04
K1C15_HUMAN	-1.91	2.70E-05
PALLD_HUMAN	-1.92	3.45E-04
RABP2_HUMAN	-1.92	4.37E-02
SPB7_HUMAN	-1.92	8.50E-04
DESP_HUMAN	-1.93	1.45E-03
1433S_HUMAN	-1.93	3.75E-04
MEGF9_HUMAN	-1.93	2.84E-05
CLD1_HUMAN	-1.94	1.52E-02
F16A1_HUMAN	-1.94	3.55E-05
POF1B_HUMAN	-1.95	3.39E-03
EFNB2_HUMAN	-1.95	9.18E-06
TNFL9_HUMAN	-1.98	2.77E-02
FRIL_HUMAN	-1.99	1.41E-04
TEN2_HUMAN	-2.00	1.40E-05
PKP1_HUMAN	-2.00	4.42E-03
S10A8_HUMAN	-2.01	1.39E-02
SPB3_HUMAN	-2.02	1.83E-03
EVPL_HUMAN	-2.02	2.52E-03
MYL6_HUMAN	-2.09	5.33E-04
DUS14_HUMAN	-2.09	2.92E-03
VAT1_HUMAN	-2.10	2.70E-05
K2C6C_HUMAN	-2.13	3.21E-04
ASAH1_HUMAN	-2.14	7.96E-04
PLIN2_HUMAN	-2.14	1.14E-02

SERF2_HUMAN	-2.15	1.81E-03
SPR1B_HUMAN	-2.22	2.67E-03
TMM40_HUMAN	-2.23	9.48E-07
LEG7_HUMAN	-2.25	2.84E-03
DSC1_HUMAN	-2.25	6.86E-04
SBSN_HUMAN	-2.26	5.04E-04
CLCA2_HUMAN	-2.30	3.46E-06
GPNMB_HUMAN	-2.30	4.91E-04
SCEL_HUMAN	-2.31	2.16E-03
DSC2_HUMAN	-2.33	1.91E-03
TBB2A_HUMAN	-2.35	2.56E-03
SPR1A_HUMAN	-2.35	2.70E-03
MAP4_HUMAN	-2.37	2.34E-05
CBPA4_HUMAN	-2.37	4.00E-04
ZN185_HUMAN	-2.39	1.74E-03
K1C10_HUMAN	-2.44	9.22E-03
CLIC3_HUMAN	-2.45	9.47E-04
SPR2D_HUMAN	-2.48	7.43E-03
KLK7_HUMAN	-2.49	1.53E-04
S10A9_HUMAN	-2.51	1.18E-02
GLTP_HUMAN	-2.56	1.37E-03
HPHL1_HUMAN	-2.60	6.66E-05
CYTA_HUMAN	-2.63	4.18E-03
GAB1_HUMAN	-2.64	4.67E-03
CALL3_HUMAN	-2.69	2.86E-03
NHRF1_HUMAN	-2.69	1.91E-04
ANGL4_HUMAN	-2.72	2.34E-04
K1C13_HUMAN	-2.73	5.65E-03
HSPB1_HUMAN	-2.73	1.53E-03
DSG1_HUMAN	-2.85	9.11E-04
DMKN_HUMAN	-2.88	2.16E-05
K1C23_HUMAN	-2.89	5.19E-04
SEPR_HUMAN	-2.96	1.71E-05
FM25A_HUMAN (+3)	-3.01	2.99E-03
LYPD3_HUMAN	-3.03	4.04E-03
CRCT1_HUMAN	-3.25	1.92E-03
SAP3_HUMAN	-3.51	2.55E-05
SLPI_HUMAN	-3.61	9.73E-04
K1C16_HUMAN	-3.65	1.22E-03
SPRR4_HUMAN	-3.84	1.40E-05
ISK5_HUMAN	-3.90	1.89E-04
A2ML1_HUMAN	-3.99	5.40E-04
FILA_HUMAN	-4.14	1.56E-05

INVO_HUMAN	-4.24	1.51E-04
AK1C3_HUMAN	-4.43	3.82E-04
SPRR3_HUMAN	-4.53	1.80E-05
IGFL1_HUMAN	-5.21	1.10E-03
K2C6B_HUMAN	-6.03	7.78E-04
RPTN_HUMAN	-6.80	7.44E-03
ELAF_HUMAN	-8.10	1.38E-03
PRR9_HUMAN	-12.79	2.14E-03